UNIVERZITA KARLOVA V PRAZE

PŘÍRODOVĚDECKÁ FAKULTA

STUDIJNÍ PROGRAM: KARTOGRAFIE, GEOINFORMATIKA A DÁLKOVÝ PRŮZKUM ZEMĚ

RNDr. Jan MIŠUREC

VYUŽITÍ OBRAZOVÉ SPEKTROSKOPIE PRO MONITORING ZÁTĚŽE VEGETACE POLUTANTY OBSAŽENÝMI V PŮDNÍM SUBSTRÁTU SOKOLOVSKÉ HNĚDOUHELNÉ PÁNVE

APPLICATION OF IMAGING SPECTROSCOPY IN MONITORING OF VEGETATION STRESS CAUSED BY SOIL POLLUTANTS IN THE SOKOLOV LIGNITE BASIN

DIZERTAČNÍ PRÁCE

VEDOUCÍ PRÁCE: RNDr. Lucie Kupková Ph.D.

Praha 2017

Disclaimer

I declare that this thesis has been worked up and compiled independently using the referenced literature and other sources. Neither the thesis nor its substantial parts have been used to obtain either the same or another academic degree.

Some parts of the thesis are based on data acquired in team cooperation of several people and organizations. Forest needle sampling was conducted by the team of the Faculty of Sciences, Charles University in Prague (PřF UK) led by Prof. Jana Albrechtová Ph.D. and Mgr. Zuzana Lhotáková Ph.D. with active participation of the author. Further processing of the collected needle samples was performed as follows: needle foliar pigments and water content (PřF UK, Prof. Jana Albrechtová, Dr. Z. Lhotáková), calculation of needle projection and total area (Czechglobe, Dr. P. Lukeš), measurements of the collected needle spectra (PřF UK, Prof. Jana Albrechtová, Dr. Z. Lhotáková), needle chemical elements analysis (laboratory of the Czech Geological Survey). Soil sampling and further processing was performed under the leading and supervision of Mgr. Veronika kopačková Ph.D. (Czech Geological Survey). The collected samples were analysed in the laboratory of the Czech Geological Survey. Field reference specstrosopy data (used for calibration of the airborne hyperspectral imagery) were collected by the Czechglobe team (2009) and DLR team (2010) with active participation of the author. HyMap airborne hyperspectral data pre-processing was performed by Czechglobe team (2009) and DLR team (2010). Further cross-track illumination correction of the data was applied by Dr. Jörg Weyermann (University of Zürich). All other parts of the thesis were worked up by the author.

The thesis is based on data acquired and analysed within the framework of the projects GA ČR 205/09/1989 (HypSo) and FP7 244242 (EO-Miners).

Prohlášení

Prohlašuji, že jsem tuto práci zpracoval a sestavil samostatně s využitím informačních zdrojů a literatury, na které odkazuji. Tato práce ani její podstatní část nebyla předložena k získání stejného nebo jiného akademického titulu.

Některé dílčí části této práce jsou výledkem týmové spolupráce několika lidí nebo institucí. Sběr vzorků smrkových jehlic byl organizován týmem Prof. Jany Albrechtové a Dr. Zuzany Lhotákové (PřF UK) s aktivní účastí autora práce. Další zpracování odebraných vzorků bylo realizováno následovně: analýza obsahu listových pigmentů a vody (PřF UK, Prof. J. Albrechtová, Dr. Z. Lhotáková), výpočet projekční a celkové plochy jehlic (Czechglobe, Dr. P. Lukeš), měření spektrálních charakteristik jehlic (PřF UK, Prof. J. Albrechtová, Dr. Z. Lhotáková), analýza obsahu vybraných chemických prvků (laboratoř České geologické služby). Odběry vzorků půdního substrátu a jejich další zpracování byly relizovány pod vedením a odborným dohledem Dr. Veroniky Kopačkové (Česká geologická služba), vzorky byly zpracovány v laboratoří České geologické služby. Měření spektrálních charakteristik referenčních ploch (použitých ke kalibraci leteckých hyperspektrálních dat) byly provedeny týmy Czechglobe (2009) a DLR (2010) za aktivní účasti autora. Základní zpracování leteckých hyperspektrálních dat HyMap (kalibrace, geometrická a atmosférická korekce) byly provedeny týmy Czechglobe (2009) a DLR (2010). Následnou aplikaci cross-track illumination korekce dat provedl Dr. Jörg Weyermann (University of Zürich). Ostatní části práce byly vypracovány autorem práce.

Práce byla zpracována na podkladě dat pořízených v rámci projektů GA ČR 205/09/1989 (HypSo) a FP7 244242 (EO-Miners).

RNDr. Jan Mišurec

Prague, 27.8. 2017

Acknowledgements

Finalization of this thesis would not be possible without support of several people who directly or indirectly provided their assistance and guidance during the entire period from preparation to completion of this study.

First and foremost I would like to express my appreciation to **Ing. Petr Lukeš Ph.D.** for providing guidance in the scope of hyperspectral remote sensing of vegetation and especially for his help with development of procedure used for parameterization of both PROSPECT-5 and FRT radiative transfer models. My thanks goes also to the rest of the Remote sensing group of the Global Change Research Center of the Czech Academy of Sciences (Czechglobe) for pre-processing and atmospheric correction of the HyMap airborne hyperspectral data used within this study.

I would like to thank **Mgr. Veronika Kopačková Ph.D.**, leader of the research projects within which the basics of the study described in this thesis have been established. I am very grateful not only for providing the HyMap hyperspectral imagery and other data which were crucial for this thesis, but also for many ideas and inspiration that have improved quality of my research.

I am extremely thankful to the research team of the Department of Experimental Plant Biology of the Charles University in Prague, namely **Prof. Jana Albrechtová Ph.D.** and **Mgr. Zuzana Lhotáková, Ph.D.**, for organizing of Norway spruce needle sampling and laboratory analysis of the collected samples as well as for help with interpretation of the observed results and many others useful and inspiring ideas related to plant physiology.

My special thanks goes to **Dr. Andres Kuusk DSc.** from Department of Remote Sensing of Tartu observatory for providing the FRT canopy level radiative transfer model and for helping with setting this model for the further use.

I want also appreciate **Dr. Jörg Weyermann Ph.D.** from Geographic Institute of University of Zürich for BRDF correction of the HyMap hyperspectral data.

The deepest appreciation goes to the supervisor of this thesis **RNDr. Lucie Kupková, Ph.D.** from the Department of Applied Geoinformatics and Cartography of the Charles University in Prague for creative guidance, constructive feedback and many suggestions that helped me to improve my work.

Finally, last but not least, I want to express my heartfelt gratitude to my family, namely to my parents **Jan** and **Helena Mišurcovi** and to my sister **Hana Šídová** and brother-in-law **Petr Šída**, for their support and words of encouragement during the whole period of my study.

Abstract

Forests can be considered as one of the most important Earth's ecosystems not only because of oxygen production and carbon sequestration via photosynthesis, but also as a source of many natural resources (such as wood) and as a habitat of many specific plants and animals. Monitoring of forest health status is thus crucial activity for keeping all production and ecosystem functions of forests.

The main aim of the thesis is development of an alternative approach for forest health status based on airborne hyperspectral data (HyMap) analysis supported by field sampling. The proposed approach tries to use similar vegetation parameters which are used in case of the current methods of forest health status assessment based on field inspections. It is believed that importance of such new methods will significantly increase in the time when the planned satellite hyperspectral missions (e.g. EnMap) will move into operational phase. The developed forest health monitoring approach is practically demonstrated on mature Norway spruce (*Picea abies L. Karst*) forests of the Sokolov lignite basin which were affected by long-term coal mining and heavy industry and therefore high variability of forest health status was assumed in this case.

Two leaf level radiative transfer models were used for simulating spectral signatures of Norway spruce needles: PROSPECT-5 and LIBERTY taking into account two concepts of models parameterization considering the measured reference needle spectra as either single leaf reflectance (R) or infinite reflectance (R_∞). Slightly better results were obtained in case of the PROSPECT-5 model using the R_∞ parameterization approach. The leaf level simulations were further up-scaled to shoot level using spectral invariants theory and then to canopy level using the FRT radiative transfer model.

The FRT canopy level radiative transfer model was parameterized first using description of crowns and canopy geometrical and optical characteristics from various sources such as digital hemispherical photography, allometric relationships and in-situ expert estimations. The simulated canopy level spectra obtained from couplings of PROSPECT-5 and LIBERTY models with the FRT model were compared with the HyMap image-extracted spectra of the reference stands with better results obtained in case of using the PROSPECT-5 model. This PRO-FRT model coupling was thus used for the further analysis.

Absolute estimations of Leaf Area Index (LAI) and chlorophyll content (C_{ab}) were performed using the PRO-FRT simulations. Although the obtained results of LAI estimations (based on D_{733}/D_{805} and D_{748}/D_{805} vegetation indices) were found not as very good (RMSE 0.77 – 0.81), C_{ab} estimation (based on N_{718} index) was considered as successful (RMSE 4.83 μg/cm^2 (2009) and 4.53 μg/cm^2 (2010)).

Functional relationships between various vegetation indices and the vegetation variables of interest were modelled using the PRO-FRT coupling. Three indices with the tightest relationships to the variables of interest ($N_{718} - C_{ab}$, $R_{558}/R_{529} - C_x/(C_x+C_{ab})$, NMDI - C_w) were then used as the inputs to the statistical health classification model classifying forests into five classes without using any fixed threshold values.

Further assessment of the obtained results showed good agreement between spatial patterns of the forest health classification and foliar biochemistry. Influence of other factors such as stand elevation, age or topographic orientation was also tested showing possible influence only in case of stand age and elevation. Links between the results of the forest health classification and soil substrate characteristics were studied as well. Observed differences in forest health status corresponds mainly with the soil parameters related to soil acidity such as exchangeable pH or Base Exchangeable Cations (BSE) further related to deficiency in alkaline elements (such as Calcium) in forest foliage. On the other hand, influence of soil heavy metals content (such as copper or zinc) remained unclear.

Due to its high temporal stability and ability to describe spatial patterns of forest vegetation status the proposed approach can be further considered as potential extension of the current forest monitoring methods bringing the possibility of spatially continuous observations as the main benefit. Integrating of such remote sensing based approach into the current forest monitoring workflow would be a logical consequence of this work.

Abstrakt

Lesy mohou být považovány za jeden z nejdůležitějších ekosystémů Země nejen kvůli produkci kyslíku a ukládání uhlíku prostřednictvím fotosyntézy, ale současně jako zdroj mnoha přírodních surovin (např. dřeva) a jako životní prostor mnoha specifických druhů rostlin a živočichů. Monitoring stavu lesa je proto naprosto zásadní činností k udržení všech ekologických a produkčních funkcí lesních ekosystémů.

Hlavním cíle práce je vývoj alternativního přístupu k monitoringu zdravotního stavu lesa založeného na analýze leteckých hyperspektrálních dat (HyMap) s podporou pozemního průzkumu. Navrhovaný postup se snaží využívat obdobné parametry vegetace jako současné klasické metody hodnocení stavu lesa založené na terénním průzkumu. Význam navrhovaných metod pravděpodobně významně vzroste v době, kdy plánované družicové hyperspektrální mise (např. EnMap) dosáhnou operační fáze. Vyvíjený přístup k monitoringu stavu lesa je prakticky demonstrován na příklad dospělých porostů smrku ztepilého (*Picea abies L. Karst*) v oblasti Sokolovské hnědouhelné pánve, které byly dlouhodobě ovlivňovány těžbou uhlí a přítomností těžkého průmyslu a u kterých byla tudíž předpokládána značná variabilita zdravotního stavu.

Dvojice modelů přenosu záření byla použita pro simulaci spektrálních signatur na úrovni jehlic: PROSPECT-5 a LIBERTY, pro jejichž parametrizaci byly uvažovány dva přístupy považující naměřená referenční spektra smrkových jehlic za tzv. single leaf (R) nebo infinite (R_∞) reflektanci. Lepších výsledků bylo dosaženo v případě použití modelu PROSPECT-5 s využitím konceptu infinite reflektance. Simulace byly poté transformovány na úroveň výhonů pomocí teorie spektrálních invariant a poté na úroveň korun/porostů pomocí modelu přenosu záření FRT.

Parametrizace modelu FRT byla založena na popisu geometrických a optických charakteristik korun na podkladě digitálních hemisférických fotografií, alometrického modelování a in-situ expertního odhadu. Spektra na úrovni porostů získaná kombinací modelů PROSPECT-5 a LIBERTY s modelem FRT byla srovnána se spektry referenčních porostů extrahovanými z leteckých hyperspektrálních dat HyMap, kdy lepších výsledků bylo dosaženo v případě použití modelu PROSPECT-5. Tato kombinace (PRO-FRT) byla pak nadále využita pro další analýzy.

Absolutní odhady indexu listový plochy (LAI) a obsahu chlorofylu byly následně provedeny na podkladě simulací PRO-FRT. Přestože výsledky odhadu LAI (na podkladě vegetačních indexů D_{733}/D_{805} a D_{748}/D_{805}) nemohly být považovány za uspokojivé (RMSE 0.77 – 0.81), odhad chlorofylu (založený na indexu N_{718}) je možné považovat za úspěšný (RMSE 4.83 $\mu g/cm^2$ (2009), 4.53 $\mu g/cm^2$ (2010)).

Funkční závislosti mezi různými vegetačními indexy a zájmovými parametry vegetace byly následně modelovány pomocí kombinace modelů PRO-FRT. Tři z těchto vegetačních indexů s nejtěsnější vazbou na zájmové parametry (N_{718} – $C_{ab,}$ R_{558}/R_{529} – $C_x/(C_x + C_{ab})$, NMDI - C_w) byly dále použity jako vstup pro vyvíjený statistický klasifikační model stavu lesa rozdělující porosty do pěti tříd bez použití jakýchkoliv pevných prahových hodnot.

Další analýza výsledků ukázala dobrou shodu mezi prostorovými gradienty stavu lesa dle uvedeného klasifikačního modelu a biochemickou charakteristikou listoví. Následně byl hodnocen vliv dalších faktorů jako např. nadmořská výška, topografická orientace nebo stáří porostu, kdy významný vliv na dosažené výsledky byl shledán pouze v případě věku a nadmořské výšky. Současně byla studována spojitost výsledků klasifikace stavu lesa s charakterem půdního substrátu, kdy rozdíly pozorované na referenčních stanovištích odpovídaly zejména parametrům souvisejícím s kyselostí půdy (např. výměnné pH, obsah zásadotvorných kationtů apod.), které byly dále spojeny např. s nedostatkem zásadotvorných prvků (např. vápníku) v listoví. Naproti tomu vliv přítomnosti těžkých kovů (např. mědi a zinku) zůstal nejasný.

Vzhledem ke své temporální stabilitě a schopnosti popisu prostorových gradientů stavu lesa může být navrhovaný postup dále považován za možné rozšíření současných metod hodnocení stavu lesa, přinášející zejména možnost plošně souvislého monitoringu. Integrace metod založených na zpracování dat dálkového průzkumu Země do metodik lesního monitoringu by tak byl logickým důsledkem této práce.

Contents

Disclaimer/Prohlášení **1**

Acknowledgements **2**

Abstract **3**

Abstrakt **4**

Contents **5**

List of Figures **7**

List of Tables **10**

List of Abbreviations and Symbols **11**

Chapter 1: Introduction **18**

1.1 General background 18

1.2 Forest health and forest damage 19

1.3 Imaging spectroscopy and its applications in forest health assessment 22

1.4 Purpose of this study 32

Chapter 2: Study site **34**

2.1 Sokolov lignite basin 34

2.2 Sampling localities 38

Chapter 3: Data acquisition **41**

3.1 Foliage needle sampling 41

3.2 Estimation of biophysical and structural parameters of Norway spruce forest stand using digital hemispherical photography 45

3.3 Soil sampling and sample processing 49

3.4 Acquisition of reference field spectroscopy data 50

3.5 Acquisition and pre-processing of HyMap airborne hyperspectral data 50

Chapter 4: Performance of PROSPECT and LIBERTY leaf level radiative transfer models for coniferous tree species **53**

4.1 Introduction of PROSPECT and LIBERTY leaf level radiative transfer models 53

4.2 Parameterization of PROSPECT model 54

4.3 Parameterization of LIBERTY model 55

4.4 Forward simulations using PROSPECT and LIBERTY models 56

4.5 Up-scaling to shoot level 57

Chapter 5: Simulating spectral properties of Norway spruce coniferous forests using radiative transfer approach 59

5.1 Introduction of FRT canopy level radiative transfer model 60

5.2 Parameterization of the FRT model 60

5.3 Forward FRT simulations 65

Chapter 6: Retrieval of semi-quantitative indices of Norway spruce forests from HyMap airborne hyperspectral data 66

6.1 Classification of the HyMap airborne data 66

6.2 Sensitivity analysis 68

6.3 Leaf Area Index (LAI) 69

6.4 Total chlorophyll content (C_{ab}) 72

6.5 Relative carotenois content ((C_x/C_x+C_{ab})) 76

6.6 Total water content (C_w) 79

6.7 Forest health classification model 83

Chapter 7: Results 87

7.1 Leaf biochemical parameters assessment and its relationship to soil chemistry 87

7.2 Leaf level radiative transfer simulations 99

7.3 Canopy level radiative transfer simulations 104

7.4 Retrieval of semi-quantitative indices 107

7.5 Classification of forest health status using statistical model 119

Chapter 8: Discussion 125

8.1 Comparison of local conditions of the Norway spruce stands of interest 125

8.2 Leaf level spectra modelling 127

8.3 Canopy level spectra modelling 130

8.4 Retrieval of semi-quantitative indicators of forest health status and its classification 131

8.5 Statistical forest health classification model 134

Chapter 9: Synthesis and Conclusions 137

References 141

List of Figures

Chapter 1: Introduction

Figure 1.1 19
Figure 1.2 22
Figure 1.3 24
Figure 1.4 24
Figure 1.5 25
Figure 1.6 27
Figure 1.7 28
Figure 1.8 29

Chapter 2: Study site

Figure 2.1 35
Figure 2.2 36
Figure 2.3 37
Figure 2.4 38
Figure 2.5 40
Figure 2.6 40

Chapter 3: Data acquisition

Figure 3.1 42
Figure 3.2 44
Figure 3.3 45
Figure 3.4 46
Figure 3.5 47
Figure 3.6 48
Figure 3.7 48
Figure 3.8 49
Figure 3.9 52

Chapter 4: Performance of PROSPECT and LIBERTY leaf level radiative transfer models for coniferous tree species

Figure 4.1 54
Figure 4.2 56
Figure 4.3 57
Figure 4.4 58

Chapter 5: Simulating spectral properties of Norway spruce coniferous forests using radiative transfer approach

Figure 5.1 59
Figure 5.2 61
Figure 5.3 62
Figure 5.4 63
Figure 5.5 64
Figure 5.6 64

Chapter 6: Retrieval of semi-quantitative indices of Norway spruce forests from HyMap airborne hyperspectral data

Figure 6.1 67
Figure 6.2 68
Figure 6.3 70
Figure 6.4 70
Figure 6.5 71
Figure 6.6 72
Figure 6.7 74
Figure 6.8 75
Figure 6.9 76
Figure 6.10 77
Figure 6.11 78
Figure 6.12 79
Figure 6.13 79
Figure 6.14 81
Figure 6.15 82
Figure 6.16 83
Figure 6.17 85
Figure 6.18 86

Chapter 7: Results

Figure 7.1 90
Figure 7.2 92
Figure 7.3 93
Figure 7.4 94

Figure 7.5 95
Figure 7.6 96
Figure 7.7 96
Figure 7.8 103
Figure 7.9 103
Figure 7.10 104
Figure 7.11 106
Figure 7.12 106
Figure 7.13 107
Figure 7.14 108
Figure 7.15 108
Figure 7.16 110
Figure 7.17 112
Figure 7.18 113
Figure 7.19 113
Figure 7.20 114
Figure 7.21 116
Figure 7.22 118
Figure 7.23 120
Figure 7.24 121
Figure 7.25 122
Figure 7.26 123
Figure 7.27 124

Chapter 8: Discussion

Figure 8.1 129

List of Tables

Chapter 1: Introduction

Table 1.1 21
Table 1.2 22

Chapter 2: Study site

Table 2.1 39

Chapter 5: Simulating spectral properties of Norway spruce coniferous forests using radiative transfer approach

Table 5.1 65

Chapter 6: Retrieval of semi-quantitative indices of Norway spruce forests from HyMap airborne hyperspectral data

Table 6.1 69

Chapter 7: Results

Table 7.1 89
Table 7.2 92
Table 7.3 97
Table 7.4 98
Table 7.5 100
Table 7.6 100
Table 7.7 101
Table 7.8 105
Table 7.9 108
Table 7.10 111
Table 7.11 112
Table 7.12 115
Table 7.13 117

Chapter 8: Discussion

Table 8.1 128
Table 8.2 130

List of Abbreviations and Symbols

A

A ..... Sun azimuth

Al/Al^{3+} ..... Aluminium; Aluminium cation

ALA ..... Average Leaf inclination Angle

AN ..... Anthroposols

AMA ..... Advanced Mercury Analyser

ANN ..... Artificial Neural Network

ANN-BP-GA ..... ANN classifier with backpropagation learning and Gaussian activation

ANN-BP-SS ..... ANN classifier with backpropagation learning and Symetrical Sigmoid activation

ANN-RPROP-SS ..... ANN classifier with RPROP training and Symetrical Sigmoid activation

$ANCB_{650-720}$ Area under curve Normalized by max. Chlorophyll absorption Between 650 – 720 nm

ANOVA ..... Analysis of Variance

As ..... Arsenic

B

BAI/LAI ..... Branch Area Index/Leaf Area Index ratio

BC ..... Biochemistry

BCE ..... Base Exchangeable Cations

BD ..... Band depth

BP ..... Biophysics

BRDF ..... Bi-directional Reflectance Distribution Function

BS ..... Base Saturation

C

C ..... Carbon

C_{ab} ..... Chlorophyll a+b content

C_b ..... Brown pigments content

C_w ..... Water content (equivalent water thickness)

C_x ..... Total carotenoids content

$C_x/(C_x+C_{ab})$ ..... Carotenoids to foliar pigments ratio

C/N ..... Organic carbon to organic nitrogen ratio

Ca, Ca^{2+} ..... Calcium; Calcium kation

CAC ..... Canopy closure

CCD ..... Charge Coupled Device

Cd ..... Cadmium

CEC ..... Cation Exchange Capacity
CENIA ..... Czech Environmental Information Agency
CEST ..... Central European Summar Time
CL ..... Clays
C_m ..... Dry matter content
CO_2 ..... Carbon dioxide
COg ..... Colluvium of acid granite
COmp ..... Colluvium of mica schist and phyllite
CP ..... Contact probe
CR; nCR ..... Continuum removal; normalized Continuum removal
CRC ..... Crown closure
Cu ..... Copper
ČGS ..... Czech Geological Survey
ČHMÚ ..... Czech Hydrometeorological Institute
ČZU ..... Czech University of Life Sciences

D

D_λ ..... 1st derivative of reflectance at wavelength λ
DBH ..... Diameter at breast height
DC ..... Damage class
DEM ..... Digital Elevation Model
DEN ..... Stand tree density
DHP ..... Digital Hemispherical Photography
DLR ..... Deutches Luft- und Raumfahrt (German Space Agency)
DLW ..... Dry leaf weight
DMU-25 ..... Digital Landscape Model 1: 25 000
DN ..... Digital Number
DT ..... Decision Tree
DW ..... Dry needle weight

E

E, H, M, S ..... Erika, Habartov, Mezihorská and Studenec forest sites
E_1, E_2, E_3, E_4, E_6 ..... Norway spruce stands at Erika locality
EAP ..... Equisolid Angle Projection
EPF ..... Empirical Projection Function
ESU ..... Elementary Sampling Unit
EVI ..... Enhanced Vegetation Index

F

FA.....Absorption feature area

FA/BD..... Absorption feature area normalized by absorption feature depth

FAAS.....Flameless Atomic Absorption Spectroscopy

fAPAR..... Fraction of Absorbed Photosynthetic Active Radiation

fCOVER.....Fraction of Canopy Cover

FL..... Fluvisols

FOV.....Field of view

FRT.....Forest Reflectance and Transmittance

FW..... Fresh needle weight

G

G200..... Geological map 1: 200 000

GBT..... Gradient Boosted Tree

GCPs.....Ground Control Points

GI.....Fisher's Grouping Index

GPS..... Global Positioning System

H

H^+.....Hydrogen cation

H_3..... Norway spruce stand at Habartov locality

h.....Tree height

h_c.....Crown height

h_1, h_2, h_3, h_4..... upper organic, lower organic, upper mineral, lower mineral soil horizon

HCRF.....Hemispherical-Conical Reflectance Factor

Hg..... Mercury

HGAAS..... Hydride Generation Atomic Absorption Spectroscopy

CH

CH7..... Cold climatic zone

I

ICP..... International Co-operative Programme

IMU..... Inertial Measurement Unit

IS..... Integration sphere

K

K; K^+ ..... Potassium; Potassium cation

KAa ..... Dystric cambisol

KAd ..... Hyperdystric cambisol

KNN ..... K-nearest Neighbours classifier

L

λ ..... wavelength

L_1 ..... Current year needle samples collected from transitional part of the crown

L_3 ..... Current + 2 years old needle samples collected from transitional part of the crown

LAD ..... Leaf Angle Distribution

LAP ..... Needle projection area

LAT ..... Needle total area

LAI; LAI_e ..... Leaf Area Index, effective Leaf Area Index

LAI_{DHP} ..... LAI extracted from digital hemispherical photography

LAI_{HYMAP} ..... LAI extracted from HyMap imagery

LIB-FRT ..... PROSPECT-5 and FRT radiative transfer models coupling

LUT ..... Look-up table

M

μ ..... Mean

M_1, M_2, M_3, M_4, M_{5a}, M_{5b}, M_6 ..... Norway spruce stands at Merzihorská locality

MCARI ..... Modified Chlorophyll Absorption Reflectance Index

Mg; Mg^{2+} ..... Magnesium; Magnesium cation

MLC ..... Maximum Likelihood Classifier

Mn ..... Manganese

Mo ..... Molybdenum

MPLSR ..... Multiple Partial Least Squared Regression

mRENDVI ..... Modified Red Edge Normalized Difference Vegetation Index

mRESR ..... Modified Red Edge Simple Ratio

MSI ..... Moisture Stress Index

MT3 – MT4 ..... Moderate-warm climatic zone

MZ ČR ..... Ministry of Agriculture of the Czech Republic

N

N (chemical element) ..... Nitrogen

N ..... Leaf structural parameter (PROSPECT-5 model)

N_{718} ..... Normalized reflectance at 718 nm

Na/Na^+ ..... Sodium; Sodium cation

NB ..... Normal Bayes classifier

$ND_{925-710}$ ..... Normalized difference of reflectance at 925 and 710 nm

NDII ..... Normalized Difference Infrared Index

NDVI ..... Normalized Difference Vegetation Index

NDWI ..... Normalized Difference Water Index

Ni ..... Nickel

NIR ..... Near infrared radiation

NMDI ..... Normalized Multiband Drought Index

NO_x ..... Nitrogen oxides

O

O_2 ..... Molecular oxygen

O_3 ..... Ozone

OSAVI ..... Optimized Soil Adjusted Vegetation Index

P

P ..... Phosphorus

p ..... Recollision probability or p-value

PAI ..... Plant Area Index

Pb ..... Lead

PC ..... Principal Component

PCA ..... Principal Components Analysis

PEga ..... Pelosols

PGm ..... Haptic stagnosols

PL ..... Polygenetic loams

PLSR ..... Partial Least Squared Regression

PM_{10} ..... Particulate matter up to 10μ

PRO-FRT ..... PROSPECT-5 and FRT radiative transfer models coupling

PřF UK ..... Faculty of Sciences of the Charles University in Prague

PVI ..... Perpendicular Vegetation Index

R

R; R_λ ..... Reflectance; Reflectance at wavelength λ

R_∞ ..... Infinite reflectance

R^2 ..... Coefficient of determination

R_{ASD} ..... Reflectance measured by ASD Fieldspec radiometer

R_c ..... Crown diameter

r_P ..... Pearson's correlation coefficient

RF ..... Random Forest classifier

RMSE ..... Root Mean Squared Error

$RMSE_S$ ..... systematic component of RMSE

$RMSE_R$ ..... random component of RMSE

RRMSE ..... Relative Root Mean Squared Error

rSE ..... Relative sensitivity index

RTM ..... Radiative Transfer Model

RVI ..... Ratio Vegetation Index

S

σ ..... Standard Deviation

S ..... Sulphur

S_1, S_2, S_3, S_4, S_5, S_6 ..... Norway spruce stands at Studenec locality

SAM ..... Spectral Angle Mapper

SAVI, SAVI2 ..... Soil Adjusted Vegetation Index (ver. 2)

SE ..... Sensitivity index

Si ..... Silicon

SHL ..... Shoot length

SISWI ..... Shot-wave Infrared Water Stress Index

SLA ..... Specific Leaf Area

SLW ..... Specific Leaf Weight

SMLR ..... Stepwise Multiple Linear Regression

SO ..... Soil sampling

SO_2 ..... Sulphur dioxide

SO_4^{2-} ..... Sulphate anion

$SR_{750/710}$ ..... Simple ratio of reflectance at 750 and 710 nm

SRWI ..... Simple Ratio Water Index

SSC ..... Shoot Shading Coefficient

SVM-L ..... Support Vector Machine classifier with linear kernel

SVM-P ..... Support Vector Machine classifier with polynomial kernel

SWIR ..... Short-wave infrared radiation

T

T, T_λ ..... Transmittance, Transmittance at wavelength λ

TCARI ..... Transformed Chlorophyll Absorption Reflectance Index
TDP ..... Tree Distribution Parameter
TEA ..... Total Exchangeable Acidity
TIR ..... Thermal infrared radiation
TOC ..... Top of Canopy
TSAVI ..... Transformed Soil Adjusted Vegetation Index

U

U_1 ..... Current year needle samples collected from sunlit part of the crown
U_3 ..... Current + 2 years old needle samples collected from sunlit part of the crown
UN/ECE ..... United Nations Economic Commission for Europe
UTC ..... Universal Time Coordinated
UTM 33N ..... Universal Transverse Mercator projection (zone 33N)

V

VIS ..... Visible radiation
VIS-B ..... Blue part of the visible radiation
VIS-G ..... Green part of the visible radiation
VIS-R ..... Red part of the visible radiation
VOG_1 ..... Vogelmann Red Edge Index (ver. 1)
VÚLHM ..... Forestry and Game Management Research Institute

W

W_I ..... Water absorption feature between 920 – 1040 nm
W_{II} ..... Water absorption feature between 1120 – 1270 nm
W_{III} ..... Water absorption feature between 1300 – 1650 nm
W_{IV} ..... Water absorption feature between 1800 – 2230 nm
WAI ..... Wood Area Index
WBI ..... Water Band Index
WGS-84 ..... World Geodetic System 1984

Z

Z ..... Sun zenith angle
Zn ..... Zinc

Chapter 1: Introduction

The chapter provides general introduction to the current methods of forest health status assessment focusing especially on issues where potential methodical improvement might be achieved by the use of hyperspectral remote sensing and imaging spectroscopy workflows. The chapter also notes the problematics of definition of the basic terms "forest health" and "forest damage", which are crucial for understanding of the further analyses. Spectral characteristics of vegetation and their links to vegetation biochemistry and biophysics are briefly summarized as well as some of the biochemical and biophysical vegetation parameters are further used as indicators of vegetation health status. In addition, two basic concepts of retrieving biochemical/biophysical vegetation parameters (empirical and radiative transfer modelling) from hyperspectral imagery are introduced in the next part of the chapter. Finally, research objectives and goals of the thesis are summarized at the end of the chapter.

1.1 General background

Forests have an irreplaceable role in regulation of the global Earth's climate vie their important functions in the global carbon cycle as CO_2 sinks and O_2 sources (Jackson et al. 2008; Bonan 2008). In the global scale, forests cover approximately 40 % of ice-free surface (Waring and Running 2010). One of the most important forest biomes are temperate evergreen coniferous forests of the boreal climate region as they consist of approximately 20 % of the whole green biomass of the world (Walker and Kenkel 2000). Norway spruce (*Picea abies* L. *Karst.*) and Scots pine (*Pinus Sylvestris* L.) are two of the most abundant tree species in this biome and thus play the predominant role in boreal coniferous forest ecosystems. Norway spruce has currently approximately 51 % abundance in all tree species in the Czech Republic. The abundance of Scots pine is approximately 17 % (MZ ČR, 2012).

Unfortunately, forest have been recently seriously threatened by anthropogenic activities and their consequences including air pollution (e.g. SO_2 and NO_x emissions), acid rains and soil contamination (e.g. Ore Mountains or Giant Mountains during 1970s – 1980s) or pests invasions (e.g. bark-beetle outbreaks in Šumava Mountains). All these influences can lead to decline of forest ecosystems health status, which can consequently results either in decrease of their productive capacity or in their total collapse. Forest health status assessment and its methods on the all levels are in the forefront of the interest of many scientists and forest managers.

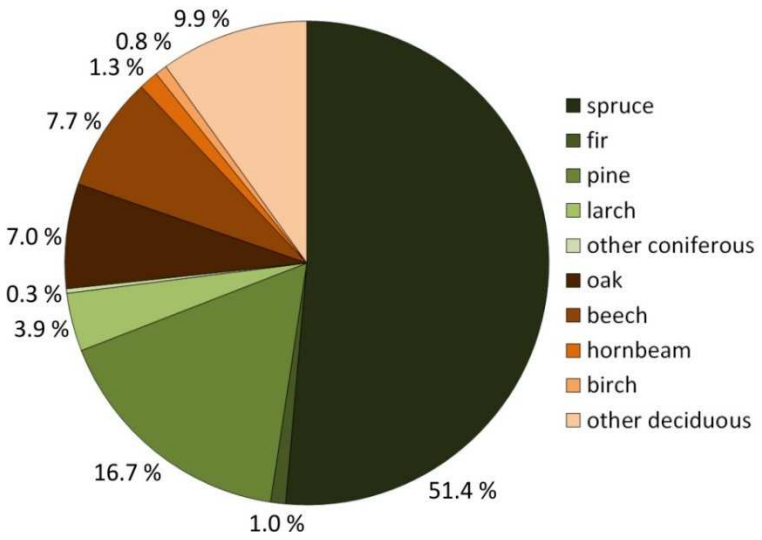

Figure 1.1: *Proportional abundance of the main forest tree species in the Czech Republic in 2012 (MZ ČR, 2012)*

1.2 Forest health and forest damage

1.2.1 Forest health, forest damage and vegetation stress definition

Despite its widespread use, the definition of the term "forest health" is not as clear as it seems to be. In fact the definition is quite vague (Kolb et al. 1994). The conditions of the given forest stand can be therefore classified as healthy as well as unhealthy depending on the point of view (Tuominen et al. 2009). One of the first definitions of the forest health was used by Leopold (1949): *"health is the capacity of the land for self-renewal"*. Monning and Byller (1992) consider the forest health as: *"a condition of forest ecosystems that sustains their complexity while providing for human needs"*. Finally Kolb et al. (1994) suggest that: *"the term forest health should be restricted to the examination of the role of biotic and abiotic agents in ecosystem processes"*.

At this point it is necessary to highlight the fact that in terms of the above definitions the forest health cannot be limited only to the conditions of trees as they are only one part of more complex forest ecosystem. In broader sense is thus forest health used synonymously with forest ecosystem health (Coulson and Stephen 2008). However, due to high complexity of forest ecosystems is the term forest health usually limited to the status of trees in more restricted sense (Wulff 2011).

Nevertheless, the definition of healthy and unhealthy tree is far from straightforward. According to Solberg (1999) healthy tree is *"a tree without symptoms or malfunctions due to biotic and abiotic stresses at present or in the past; it performs well in growth rate; has good chance to further survival and has certain ability to defend itself against, to tolerate and recover from stress"*. This raises the question whether the forest health and tree status can be somehow precisely and exactly measured. According to O'Laughlin et al. (1994) it is possible to find objective indicators of tree/forest status which can be clearly specified and exactly measured, but the final decision of the forest health is a result of a subjective judgement.

Regarding to the above described vague definition will be the term *"Norway spruce forest health status"* considered as the status of Norway spruce trees described by exact biochemical, biophysical and structural indicators having close relationship to their basic life functions.

Similarly as in case of the forest health, it is firstly necessary to find the definition of forest damage and vegetation stress. Lichtenthaler (1988) defined vegetation stress as: *"a state of plant under the condition of a force applied"* and vegetation damage as: *"a result of too high stress which can no longer be compensated for"*. Larsen (1995) defines vegetation stress as: *"a significant deviation from the optimal living conditions which negatively affects functions, growth or development of the plant mechanisms"*. However, this definition can be found as problematics in some aspects as the "optimal living conditions" are not exactly defined and may be site a species specific. In other words, plant species can grow also in the areas where the conditions are not optimal which results into for example lower growing rate, but even so they cannot be considered as stressed. Thus it is very difficult to clearly define any absolute threshold values of the given forest health status indicators to separate the values indicating normal conditions from those indicating vegetation stress.

Different causes of forest damage and vegetation stress have been studied for last decades. Manion (1991) defines three basic groups of factors that may result in vegetation stress and forest damages. These are: 1) biotic diseases, 2) abiotic diseases and 3) decline. Biotic stress factors includes fungi (i.e. *Armillaria*) and virus infections as well as outbreaks of pest insects (i.e. *Ips typographus*, *Choristoneura fumiferata*, *Epirrita autumnata* etc.) and damage caused by deer roe and elk.

Abiotic stress factors are mainly related to air, water and soil pollution. Air pollution is usually considered as the most crucial factor as it causes damage to trees through the direct effect of gaseous pollutants as well as indirectly through it effects to soil. The main concern is related to acidifying sulphur (SO_2) and nitrogen (NO_X) deposits as well as to concentration of ground-level ozone (O_3) having direct effect on plant foliage and metabolism (Caldwell et al. 1997). According to Pfanz and Beyschlag (1993) and Slovik et al. (1995), K^+ and Mg^{2+} cations are consumed for change balance of SO_4^{2-} anions and thus they are not available for growth which results in reducing tree vitality and photosynthetic capacity. Other concerning factors related to soil conditions are acidification and potential contamination by toxic agents (e.g. heavy metals like Pb, As, Cd etc.). Acid inputs are neutralized and buffered within the soil as a result of weathering and cation exchange. However, in most acidic forest soils the weathering of silicate minerals is too low to be able to compensate the elevated acidic deposits (Chadwick and Hutton 1991). According Ardö (1998) the acid input decreases the base saturation, increases exchangeable acidity and decrease soil pH. This results in higher mobility of base cations which are leaching to lower soil horizons before they are removed by runoff. The low pH may be also linked with the effects of toxic Al^{3+} cations due to Al solubility at low pH (Mossor-Pietraszawska 2001). The toxic aluminium forces fine root development to soil horizons with higher pH leading to dieback of water conductive tissue from lower horizons. This results in water stress, vulnerability to drought, decrease of photosynthetic capacity and deficiencies of Mg, Ca, P, Mo and Si (Ulrich 1991; Hüttl and Schaaf 1997, Ardö 1998, Mossor-Pietraszewska 2001). Acidification also increases the solubility of harmful metals such as Cd, Pb, Cu, Mn and Zn in the soil (Ardö 1998). Except of air and soil

pollution, other events as storms, frost, drought or forest fires may be also considered as abiotic stress factors causing forest damage.

1.2.1 Current methodology of forest health assessment

The presence of vegetation stress is usually leading to activation of plant responses which give raise to some stress symptoms. Unfortunately, many different types of vegetation stress can result in very similar (or the same) symptoms. Therefore it is usually very difficult to diagnose the exact causes of the observed plant responses (Jones and Vaughan 2010).

The current classical methods of forest health/damage monitoring are based mainly on visual in-situ assessment of crown conditions and classification of trees into several (usually five) damage classes. In the next step, the crown characteristics are summarized to classify whole stands into the damage classes. According to Campbell et al. (2004) the primary factors for field damage class assessment include: 1) crown type, form and shape, 2) percentage of foliar loss (defoliation), 3) presence or absence of chlorosis and 4) foliar retention (see Table 1.1).

The most intensive and systematic forest health monitoring activities are currently being undertaken within the framework of the International Co-operative Programme on Assessment and Monitoring of Air Pollution Effects on Forests (ICP Forests; http://icp-forests.net) established by the United Nations Economic Comission for Europe (UN/ECE) in 1985. The program was adopted by the European Union one year later and today it involves 41 European states as well as the United States of America and Canada. The methodology used within the ICP Forest programme is thus considered as the international standard and is described in "*The Manual on methods and criteria for harmonized sampling, assessment, monitoring and analysis of the effects of air pollution on forests*" (in short the ICP Manual; http://icp-forests.net/page/icp-forests-manual). The methodology for tree condition classification is based on defoliation and discolouration assessment and is described in the Part IV of the ICP Forests Manual: "*Visual assessment of crown condition and damage analysis*" (see Table 1.2.).

In the Czech Republic, the forest condition monitoring is systematically performed by the Forestry and Game Management Research Institute (Výzkumný ústav lesního hospodářství a myslivosti – VÚLHM; http://www.vulhm.cz).

Table 1.1: *Forest damage classification criteria by Campbell et al. (2004).*

Damage Class (DC)	Ecosystem vitality	Canopy defoliation	
		Chlorosis absent	Chlorosis present
DC_0	Healthy	0-10 %	X
DC_1	Initial damage	11-25 %	0-10%
DC_2	Medium damage	26-60%	11-25%
DC_3	Heavy damage	61-80%	26-60%
DC_4	Ecosystem collapse	81-100%	61-100%

Table 1.2: *Crown condition classification in terms of defoliation and discolouration by UN-ECE (1992)*

Defoliation class	Discolouration class	Crown damage	Defoliation	Discolouration
DC_0	DC_0	None or slight	0-10 %	0-10 %
DC_1	DC_1	Moderate	11-25 %	11-25 %
DC_2	DC_2	Strong	26-60 %	26-60 %
DC_3	DC_3	Very strong	61-99 %	more than 60 %
DC_4	DC_4	Dead tree	100 %	X

Figure 1.2: *Symptoms of vegetation stress: healthy non-chlorotic (a) and chlorotic (b) Norway spruce shoot, healthy shoot with no signs of defoliation (c), shoot with high degree of defoliation (d).*

1.3 Imaging spectroscopy and its applications in forest health assessment

Imaging spectroscopy (also known as hyperspectral remote sensing) is relatively new field of science developed during the last decades. It is based on the combination of spectroscopy (as the method for obtaining and analysing spectra of different materials) and remote sensing (as the tool for acquiring image data of the Earth's surface without direct contact). Hyperspectral image datasets are usually consisting of tens to hundreds very narrow (usually 3 – 15 nm) continuous (no gaps between the adjacent bands) spectral bands. Therefore it allows to study surface spectral properties at much detailed level in compare with the classical multispectral imagery. Detailed study of the surface spectral properties then enables determining various physical and chemical variables of the surface which are closely related to spectral properties. Different materials and components absorb electromagnetic radiation of specific wavelengths

forming so called absorption features, which can be finally used for identification of the given material and estimation of its relative concentration or abundance. This workflow is generally called as “spectral analysis”.

Imaging spectroscopy is currently applied mostly in the reflected solar radiation domain including the visible domain VIS (400 – 750 nm), near-infrared domain NIR (750 – 1200 nm) and shortwave-infrared domain SWIR (1200 – 2500 nm). Most recently, new high spectral resolution sensors operating in the thermal domain TIR (8 – 14 μm) have been developed.

1.3.1 Spectral properties of vegetation and its scaling

Interaction of light with vegetation is very complex process. One of the first studies of vegetation spectral characteristics was performed by Gates et al. (1965) which was followed later by Allen et al. (1970), Thomas (1971), Wooley (1971), Gausman and Allen (1973) and others. These studies proved that leaf optical properties are closely linked to the content of photosynthetic pigments and other biochemical elements, water content and leaf structure.

The influence of foliar pigments (chlorophylls, carotenoids, anthocyanins etc.) is significant in the VIS domain where the main part of the incoming radiation is absorbed by these pigments and reflectance is thus very low. The strongest absorption occurs between ca. 300 – 500 nm (chlorophylls and carotenoids) and 650 – 720 nm (chlorophylls). On the other hand, absorption of pigments is lower between 500 – 600 nm and thus so called green peak can be observed in vegetation spectra. Decrease in pigments concentration (visually detectable as chlorosis) therefore leads to increase of VIS-B and VIS-R reflectance (Hogue et al. 1988; Koch et al. 1990; Rock et al. 1993). On the other hand foliar loss leads to higher exposure of understory and wooden parts of trees resulting in increase of reflectance (Guyot et al., 1989; Rock et al. 1988; Koch et al. 1990).

The NIR reflectance is affected mainly by the internal leaf structure and vegetation biophysical/structural characteristics including vegetation density and canopy closure. The foliar loss thus leads to decrease of NIR reflectance as it increase the exposure of wooden parts which have usually lower NIR reflectance than foliage (Guyot et al. 1989; Koch et al. 1990). A water absorption feature can be observed in the NIR domain at approx. 970 nm.

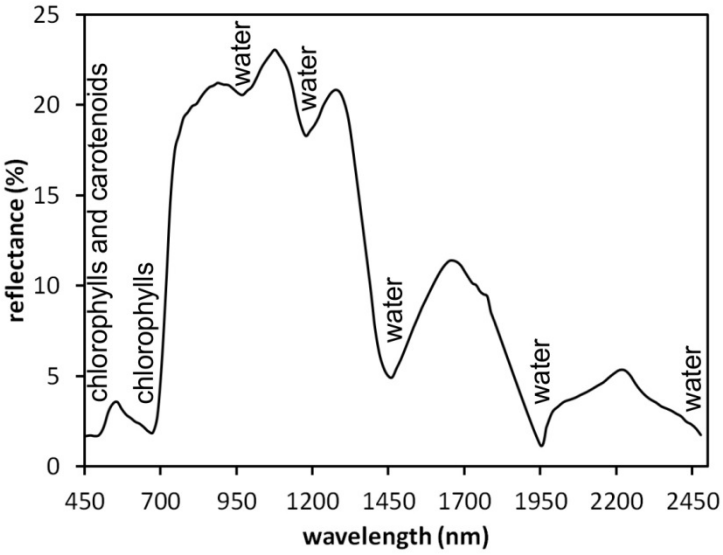

Figure 1.3: *Spectral properties of vegetation with main absorption features.*

The optical properties of vegetation in the SWIR domain are affected mainly by water absorption. The main water absorption features are located at approx. 1200, 1450 and 1940 nm. As the vegetation water content decreases, the SWIR reflectance generally increases. Decrease in leaf pigments content has no direct effect on the SWIR reflectance. However, brown or yellow chlorotic (or dead) leaves/needles are drier than the fresh ones and therefore it is possible to observe the influence of chlorosis indirectly in the SWIR region (Guyot et al. 1989; Koch et al. 1990). The influence of other biochemical components as well as structural parameters are described in high details in Asner (1998), Rautiainen et al. (2004) and Kokaly et al. (2009).

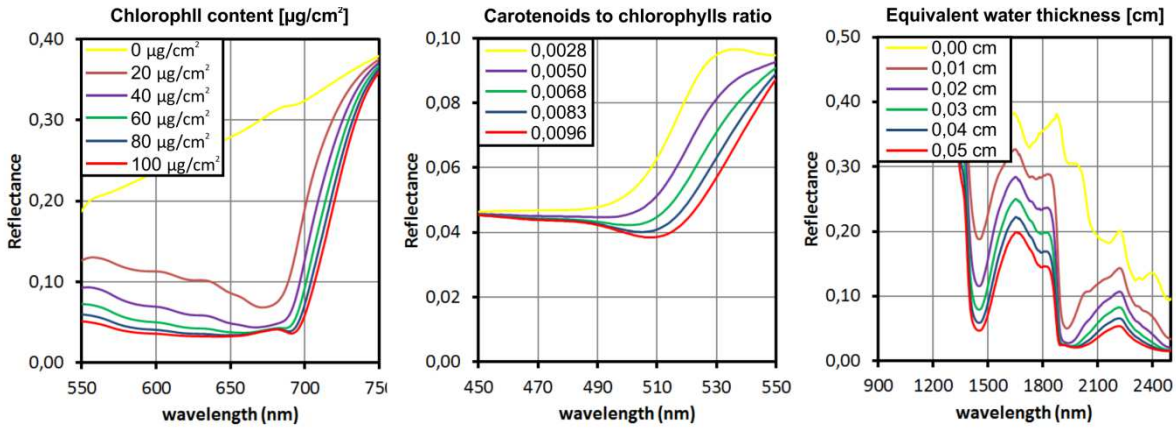

Figure 1.4: *Relationship of vegetation biochemical and spectral properties simulated by the PROSPECT-5 leaf level radiative transfer model.*

In general point of view, the VIS, NIR and SWIR reflectance generally decreases with vegetation age, biomass, LAI and canopy closure (Butera 1986; Kleman 1986; Poso et al. 1987; Koch et al. 1990; Spanner et al. 1990; Brockhaus and Khorram 1992). It is also necessary to take into account the influence of understory and soil, which is closely connected with vegetation density and canopy closure (Butera 1986).

The spectral properties of vegetation are not determined only by the optical properties of individual leaves, but they are also significantly affected by vegetation structure, state, spatial pattern and canopy composition (Asner 1998). Therefore it is not possible to simply use the leaf level vegetation spectra to characterize vegetation at the canopy level. Nevertheless, the leaf level spectra can be up-scaled from leaf to canopy level using either empirical (statistical) approach or by physical radiative transfer modelling (Malenovský et al. 2007).

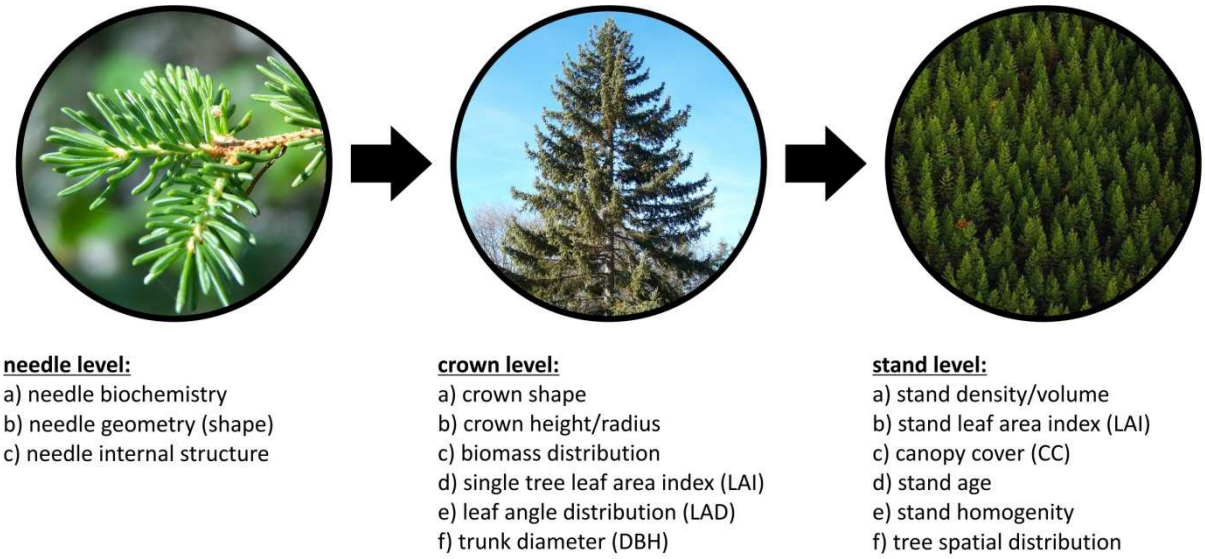

Figure 1.5: *Scaling levels in vegetation studies.*

1.3.2 Biophysical and structural parameters of forest stands and their estimation

Scaling of the leaf level spectral properties to canopy level is closely connected with the biophysical and structural parameters of modelled canopies. Note that only those parameters used within this thesis are described in this section.

Leaf Area Index (LAI)

Leaf Are Index (LAI) is one of the most common vegetation biophysical parameter originally defined by Watson (1947) as: "total one-sided leaf area per unit ground surface". However, this definition is not suitable for coniferous tree species whose needles have approximately cylindrical shape and calculation of one-sided leaf area is rather problematic. Therefore alternative definitions of LAI were developed:

- Half of the total leaf area per unit ground surface (Lang, et al. 1991; Chen and Black 1992)
- Projected area per unit ground surface (Bolstad and Gower 1990, Smith 1991)

Regarding these definitions LAI defines the area of active interaction between plants and atmosphere (Bréda, 2003). Therefore it is closely linked with the intensity of evapotranspiration, energy and gas exchange. In case of forest stands consisting of individual tree crowns it is also necessary to distinguish between single tree LAI (determined by amount of biomass in the crown)

and stand LAI (determined both by amount of biomass and stand tree density). The physical unit of LAI is [m^2/m^2] and thus it is usually considered as dimensionless parameter.

Except of LAI there is also another biophysical parameter called Plant Area Index (PAI) which is defined as the total area of plant per unit area of ground (Neumann et al. 1989). PAI thus takes into account the leaf area as well as the area of the other parts of plant bodies (stem, branches etc.). The physical unit of PAI is the same as in case of LAI [m^2/m^2].

Canopy closure (CAC) and crown closure (CRC)

There are two parameters describing amount of light which is able to penetrate through vegetation to the forest floor: canopy closure (CAC) and crown closure (CRC). Although the names of these parameters are similar, their definitions are different. On top of that the definitions of these parameters slightly differ in case of different authors.

Canopy closure (CAC): is proportion of sky hemisphere obscured by vegetation when viewed from a single point (Jennings et al. 1999). It can be measured either by a spherical densitometer or by digital hemispherical photography. On the other hand Kuusk (personal communication) defines canopy closure as the proportion of sky obscured by vegetation in zenith.

Crown closure (CRC): is proportion of ground area covered by vertical projection of tree crown perimeters (Jennings et al. 1999). However, some authors call this concept as "**canopy cover**" (Jennings et al. 1999; Korhonen et al. 2006; Paletto and Tossi 2009).

Regarding these definitions canopy closure might be equal to crown closure in case of non-overlapping sparse stands, whereas in case of dense stands with overlapping crowns crown closure is always higher than canopy closure. The maximal canopy closure is 1.0 (or 100 %), whereas crown closure can exceed 1.0 (100 %) in case of overlapping crowns (see Figure 1.6).

Methods for biophysical parameters estimation

The biophysical and structural parameters can be estimated either directly or indirectly. Very detailed review of both direct and indirect methods including their advantages and disadvantages provide Chen et al. (1997), Gower et al. (1999), Jonckheere et al. (2004) and Seidel et al. (2012).

Direct methods are generally based on foliage collection (either destructive or using leaf traps during the leaf fall) and calculation of its area (so called planimetric approach) or dry mass (so called gravimetric approach) (Jonckheere et al. 2004). Direct LAI measurement is the most precise, however it is also extremely time and labour consuming. Therefore indirect methods of LAI estimation have been developed. Currently the most common and most often used indirect methods are based on the study of light extinction during its transmission through vegetation canopies that are known as gap fraction methods. These methods include measuring of LAI (and other parameters) using special plant canopy analysers like LAI-2200, AccuPAR, TRAC etc. as well as using digital hemispherical photography of the studied canopy (Rich 1990; Chen et al. 1991; Welles and Norman 1991; Welles and Cohen 1996). Both of these approaches are generally based

on the calculation of the ratio of sky to plant area (gap fraction) in the upward (zenith) direction. The most up-to-date method of indirect LAI estimation is based on the use of ground LIDAR (Zhao et al. 2011).

One of the problematic issues of using the gap fraction methods is that the models for biophysical parameters estimation are based on the Poisson law assuming random distribution of leaves which is not true in case of crops and forest plantations (Demarez et al. 2008). The calculated LAI is therefore underestimated up to 40 % (van Gardingen et al. 1999; Demarez et al. 2008). This so called effective LAI (LAI_e) should be corrected using the clumping index to estimate true LAI (Demarez et al. 2008, Gonsamo and Pelikka, 2009). It is also necessary to acquire a sequence of measurements to sample canopy heterogeneity to remove local abnormalities from the gap fraction estimations (Garrigues et al. 2008). Garrigues et al. (2008) performed an intercomparison of LAI retrieval using canopy analysers (LAI-2000 and AccuPAR) and digital hemispherical photography (DHP). They highlighted the fact that the DHP method is the most robust in terms of its sensitivity to illumination conditions. Another advantage over the LAI-meters is the ability to estimate the clumping index and to calculate with it. On the other hand Zhang et al. 2005 pointed out that the performance of DHP method is influenced by the exposure of the photographs as the higher exposure results in more gaps and thus lower LAI. The problematics of image exposure were discussed also in Guevara-Escobar et al. (2005); Garrigues et al. (2008); Paletto and Tossi (2009) and Chianucci and Cuttini (2013) but with no clear conclusions.

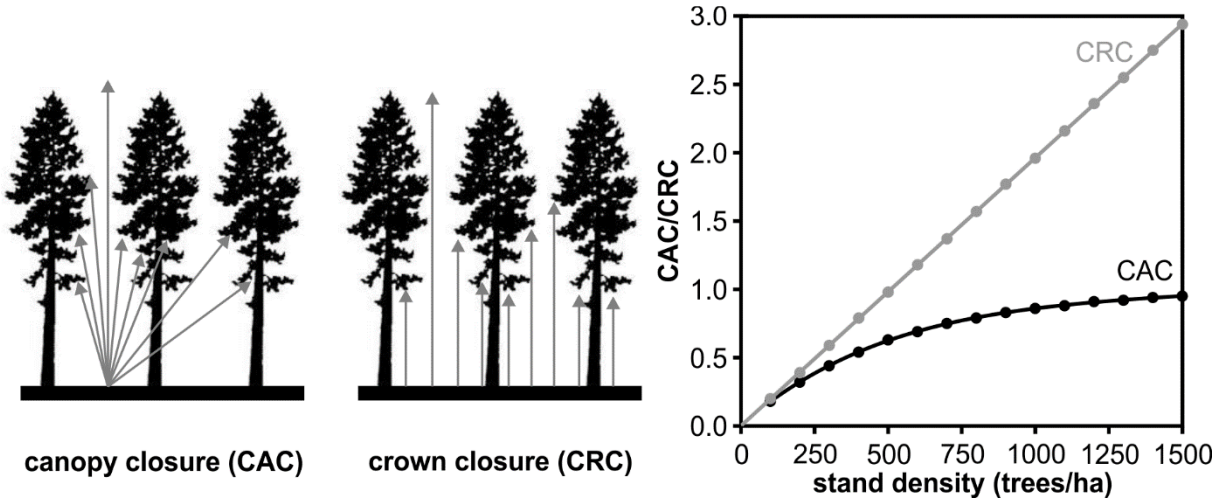

Figure 1.6: *Definition of canopy closure (CAC) and crown closure (CRC). Relationship between forest density and CAC resp. CRC modelled by forest canopy geometrical model. Tree crown diameter is fixed to 2.5 m and tree distribution is random. CRC is continually rising with increasing tree density, whereas CAC is rising up to its maximal value of 1.0.*

1.3.3 Retrieval of forest parameters using high spectral resolution image data

Retrieval of vegetation biochemical and biophysical parameters using high spectral resolution image data can be carried out by two basic approaches: 1) empirical modelling and 2) radiative transfer approach.

Empirical models are generally based on direct correlations between received vegetation spectral properties (usually transformed into the form of e.g. vegetation indices) and the in-situ measured data on vegetation biochemical/biophysical characteristics. The obtained regression formula is then applied inversely on the rest of the data. This approach offers fast and simple retrieval of vegetation parameters and can establish important correlations, but its use is limited by several facts. Empirical models are generally site, species and structure specific due to strong angular anisotropy of vegetation reflectance and the influence of vegetation understory (Asner 1998, Broge and Leblanc 2000, Rautiainen et al. 2004). Since the vegetation spectral properties change in time due to plant phenology, they are also inevitably time specific (Wang 2005, Nagai et al. 2014). Moreover, it is necessary to have sufficient number of ground-sampled values of biochemical/biophysical parameter to obtain strong and reliable statistical relationship. The principles of empirical modelling see in Figure 1.7.

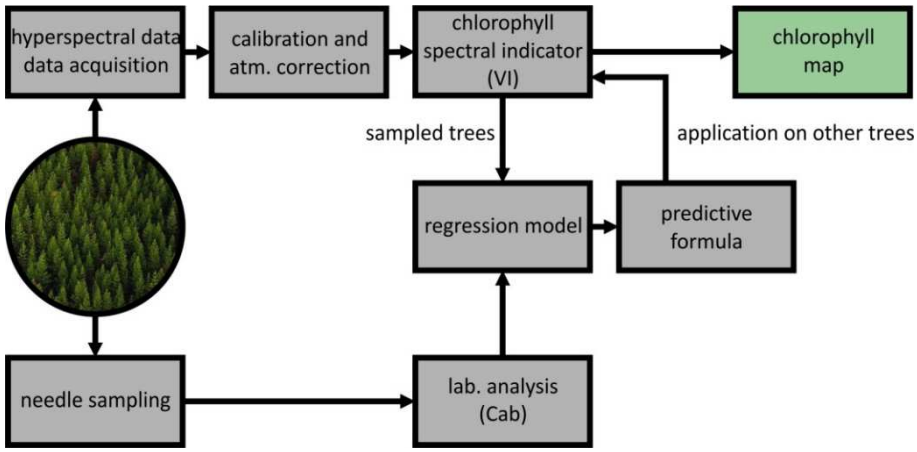

Figure 1.7: *Principle of the retrieval of vegetation chlorophyll content using empirical modelling approach.*

A solution to overcome the site-, species- and time specificity is to apply physical modelling approaches where the spectral properties of foliage as well as whole vegetation canopies are simulated via the radiative transfer theory describing propagation and interaction of light with vegetation. Typically, leaf/needle internal structure (e.g. thickness, mesophyll structure etc.) and biochemistry (chlorophylls, carotenoids, water etc.) are used as inputs in leaf level radiative transfer models for forward simulation of leaf spectral properties. PROSPECT (Jacquemoud and Baret 1990), LIBERTY (Dawson et al. 1998), RAYTRAN (Govaerts et al. 1996), LEAFMOD (Ganapol et al. 1998) or SLOP (Maier et al. 1999) can be mentioned as typical examples of the current leaf level models.

Similarly to leaf level, information on vegetation structure (tree height, canopy shape, leaf area index etc.), understory and optical properties of leaves can be used as inputs for canopy level radiative transfer modelling. Many of the model inputs related to forest structure are either easily

measurable or can be taken from forest inventory databases. In contrast, information about leaf optical properties are rare since they vary with both species and phonological stage. Some of the models (called 1-D) assume vegetation as homogenous turbid medium with randomly distributed leaves – e.g. SAIL (Verhoef 1984). These models can be successfully used for simulation the canopy spectra of grass or agricultural crops, but they are not applicable in case of heterogenous and discontinuous canopies with individual crowns (typically for forest ecosystems). Therefore 3-D canopy level models have been developed taking into account the influence of crown geometry – e.g. GeoSAIL (Huemmrich 2001), DART (Gastellu-Etchegorry et al. 2004), SPRINT (Goel and Thompson 2000), FLIGHT (North 1996) or FRT (Kuusk and Nilson 2000).

The coupled leaf and canopy level models can be used to simulate the spectral properties of vegetation for various combinations of the input parameters. These simulations are then linked with the values of biochemical and biophysical parameters via a retrieval algorithm (e.g. one-dimensional or multiple regression, artificial neural network etc.) to find the predictive equations. These equations are then applied inversely on the real hyperspectral image data to retrieve the required values of the biochemical and biophysical parameters. The principles of radiative transfer modelling see in Figure 1.8.

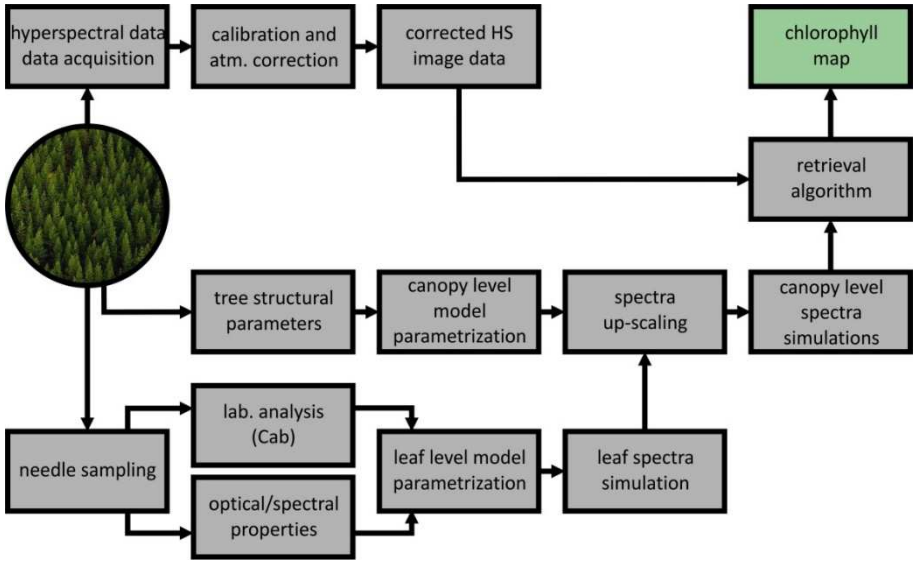

Figure 1.8: *Principle of the retrieval of vegetation chlorophyll content using radiative transfer approach.*

The use of radiative transfer models has several advantages against the empirical modelling. It is based on well-defined physical laws which are not site and time specific. On the other hand the development of such models is very complex and time demanding process. Moreover, each model represents some degree of generalization and thus the simulated vegetation spectra might not correspond with the real spectra in case of inappropriate model or wrong model parameterization.

Retrieval of vegetation biochemical and biophysical parameters from the spectral information has been the subject of many studies in the past decades. Retrieval of leaf chlorophyll and carotenoids content based on the statistical relationship to spectral information (vegetation indices) was described in details by Datt et al. (1998), Gitelson et al. (2002), Sims and Gamon

(2002) and others. Schlerf et al. (2010) used an empirical relationship between the spectra (at both leaf and canopy levels) and chlorophyll and nitrogen concentration. The empirical relationship was established using Stepwise Multiple Linear Regression (SMLR) on the 1st derivative, continuum removal (CR) and normalized continuum removal (nCR) vegetation spectra. The obtained predictive formulas were applied on HyMap airborne hyperspectral data acquired over homogenous Norway spruce forests. Zarco-Tejada et al. (2004) coupled the PROSPECT and SPRINT radiative transfer models to estimate chlorophyll content of Jack pine (*Pinus banksiana*) forest stands using CASI airborne hyperspectral data. Moorthy et al. (2008) used the simulations of Jack pine needles spectral properties performed by the PROSPECT and LIBERTY models. The needle level simulations were then up-scaled using the SAILH canopy level model and chlorophyll content estimation was performed by the regression with R_{750}/R_{710} ratio (calculated from model simulations). Zhang et al. (2008) performed retrieval of chlorophyll content both per unit leaf area as well as per unit ground surface based on coupling the PROSPECT and 4-SCALE models and CASI hyperspectral data acquired over Black spruce (*Picea mariana*) forest stands. Hernández-Clemente et al. (2012) estimated chlorophyll and carotenoids content in heterogenous conifer forest stands using the coupling of PROSPECT and DART radiative transfer models simulations at 500 – 600 nm domain. Malenovský et al. (2013) presented a sophisticated method of canopy chlorophyll content retrieval based on coupling of the PROSPECT and DART models to simulate Norway spruce canopy reflectance. The chlorophyll content estimation was estimated using artificial neural network (ANN) and newly developed $ANCB_{650\text{-}720}$ vegetation index. The results were compared with the performance of several others vegetation indices ($ND_{925\text{-}710}$, $SR_{750/710}$, TCARI/OSAVI). The study was practically performed on the AISA-Eagle hyperspectral dataset acquired over homogeneous Norway spruce stands at Moravia-Silezian Beskyds.

Canopy water content was estimated by Clevers et al. (2010) by the means of linear relationship with the 1st derivative of vegetation spectra simulations obtained from the PROSAIL (PROSPECT+SAIL) model. The application was performed on grazed fen meadows. Canopy water retrieval was performed also by Cheng et al. (2006) by the use of PROSPECT-SAILH, PROSPECT-rowMCRM and PROSPECT-FLIM models couplings. The study was using AVIRIS airborne hyperspectral data which were then used to assess the behaviour of vegetation water content retrieval based on NDVI, EVI, NDWI and SISWI vegetation indices calculated from MODIS data.

Huang et al. (2004) used direct empirical application of various multidimensional models including ANN, PLSR, MPLSR and SMLR to estimate foliar nitrogen content of Eucalyptus canopies using continuum removed spectra, 1st and 2nd derivatives as well as log(1/R) spectra. Huber et al. (2008) performed estimation of nitrogen, carbon and water content by direct empirical application of SMLR multidimensional model on the canopy level spectra obtained from HyMap hyperspectral image dataset acquired over mixed forest in Switzerland. Kokaly and Clark (1999) and Kokaly et al. (2009) determined nitrogen, lignin and cellulose content using SMLR applied on continuum removed spectra as well as on 1st and 2nd derivatives of log(1/R) spectra. The established relationships were then applied on AVIRIS airborne hyperspectral dataset. The

quantitative modelling of nitrogen content was performed also on the level of satellite data by Lu et al. (2009) who applied SMLR model on Hyperion hyperspectral imagery.

As for biophysical and structural parameters, most authors have focused on LAI estimation. Gong et al. (2003) estimated forest LAI using direct statistical relationship to 12 different vegetation indices calculated from a Hyperion hyperspectral dataset. Retrievals of LAI for various agricultural crops were performed by D'Urso et al. (2004), who used CHRIS/PROBA satellite hyperspectral data, and by Haboudane et al. (2004), who used CASI airborne hyperspectral data. Both teams were using spectral simulations performed in the PROSAIL radiative transfer model. Darvishzadeh et al. (2007) evaluated direct relationships of different vegetation indices (RVI, NDVI, PVI, TSAVI and SAVI2) to LAI for various vegetation species by the means of linear and exponential regression. Schlerf et al. (2005) established a statistical relationship between LAI and other biophysical parameters such as stem density, canopy cover, perimeter at breast height, stand height and crown volume and vegetation indices calculated from HyMap airborne hyperspectral data acquired over homogeneous Norway spruce stands. Unfortunately, statistically reliable regression was found only in case of LAI and crown volume using linear regression model. Verrelst et al. (2012) proposed a method of LAI and fCOVER retrieval as well as chlorophyll content retrieval based on the use of Gaussian process technique providing non-linear regression as a linear combination of spectra mapped to high-dimensional space.

1.3.4 Potentials of imaging spectroscopy and remote sensing in forest management

Many of the vegetation stress symptoms (e.g. discolouration, defoliation etc.) are closely linked with the changes of the biophysical and biochemical parameters values and thus they are generally detectable by remote sensing tools. However, remote sensing techniques are always monitoring symptoms and not the causes of the vegetation stress, so the vegetation stress can be detected only indirectly (e.g. stress → chlorophyll decrease → spectral response). On the other hand, some of the variables observable by remote sensing tools can be directly linked to the parameters used in classical in-situ forest health assessment methods (e.g. discoloration/chlorosis – leaf pigments content, growth vitality/defoliation – LAI, presence of dry/dead leaves – canopy water content etc.). Moreover, imaging spectroscopy is capable to detect not only visual symptoms of stress (which the classical methods are based on), but also the pre-visual ones indicating very early stages of vegetation stress. Remote sensing tools provide continual information in contrast with the classical assessment methods which are always discrete.

The main disadvantage of the hyperspectral remote sensing applications is their high cost which is limiting their broad use. Hyperspectral imaging is also strongly weather-dependent as airborne/satellite data acquisition can be performed only in case of clear (cloud-free) weather only. Therefore it can be concluded that imaging spectroscopy applications will not totally replace the classical in-situ assessment methods in the near future, but they have a great potential to be combined with the current methodologies to study vegetation health status in more complex view.

1.4 Purpose of this study

Although imaging spectroscopy has been used in the field of vegetation studies for at least two decades, utilization of hyperspectral imagery has been mostly focused on quantitative retrieval of several parameters (like chlorophyll content, LAI etc.). On the other hand, only very few studies have used it to build-up a complex models describing forest stand health status, which might be a new challenge and opportunity for further research.

As it mentioned above, the current forest health status classifications are designed mostly for in-situ assessment based on very limited number of visually detectable parameters which are not very suitable for remote sensing applications. The main reason is that the used parameters have mostly qualitative character (e.g. presence X absence of chlorosis, presence X absence of defoliation etc.), whereas hyperspectral remote sensing products have mostly quantitative character (e.g. chlorophyll content, water content, LAI etc.). The classical methods are also based on discrete point measurements, whereas remote sensing products provide continuous estimations of the selected vegetation parameters. Therefore the main motivation is to find common link between the current classical forest health status assessment methodologies and the capabilities of hyperspectral remote sensing technologies. The main goal is thus not to replace the current forest health status assessment methodologies, but to enrich them with new approaches and perspectives.

1.4.1 Research assumptions and hypothesis

Assumption 1: Presence of vegetation stress has a direct effect on the values of vegetation biochemical and biophysical parameters.

Assumption 2: Spectral properties of vegetation are directly determined by biochemical and biophysical parameters.

Assumption 3: Spectral properties of vegetation can be simulated accurately for wide range values of the given biochemical and biophysical parameters using the combination of radiative transfer approach and empirical modelling.

Hypothesis 1: Based on the assumptions 1 and 2, vegetation stress results in a change of vegetation spectral properties and thus its presence is detectable by the stadium of vegetation spectral properties on very detailed level provided by imaging and field (laboratory) spectroscopy tools.

Hypothesis 2: Based on the assumptions 1, 2 and 3, combination of radiative transfer simulations and field (laboratory) spectroscopy data allows constructing a vegetation health classification model which is able to classify vegetation health conditions using the spectral features linked to four basic biochemical/biophysical parameters: chlorophyll content, carotenoids-to-total pigments ratio, water content and vegetation structure (represented by leaf area index).

1.4.2 Goals and Objectives

The main goal of this thesis is to develop a semi-empirical semi-quantitative model for forest health status assessment based on utilization of the HyMap hypersapectral image data in combination with in-situ and laboratory measurements of foliage biochemical and spectral properties as well as biophysical and structural parameters of forest stands. The proposed model will be demonstrated at Sokolov lignite basin test locality where the main factor of vegetation stress is soil acidification and air pollution.

semi-empirical: means that the model is combining radiative transfer approach and empirical modelling. The use of radiative transfer modelling allows simulating vegetation spectral properties for wide range values of the given biochemical/biophysical/structural parameters. This is therefore used to find the general relationships between the spectral information and the parameters of interest. On the other hand, radiative transfer models cannot take into account specificities of the particular localities where they are practically applied. Therefore the general radiative transfer simulations may be empirically fitted to the real data using several ground-truth points.

semi-quantitative: means that the model is based on estimation of quantitative parameters, but the interest is paid to their spatial patterns, trends and gradients rather than to their absolute values. It was also demonstrated that there are no "global" threshold values of the biochemical/biophysical parameters separating healthy and damaged vegetation. In fact these threshold values are site-specific. The forest health status classification proposed in this study is thus not based on any fixed absolute threshold values, but on the statistical distribution of the given forest health status indicators values.

There are several particular sub-objectives that need to be solved within the workflow of the proposed model development:

1) To parameterize the selected leaf level radiative transfer model and simulate the spectral properties of Norway spruce needles for sufficient range of the particular biochemical parameters values.
2) To parameterize the selected canopy level radiative transfer model using the in-situ digital hemispherical photography to up-scale the needle level simulations to the canopy level taking into account vegetation structure.
3) To perform sensitivity analyses on the simulated canopy level spectra to find the most appropriate spectral indicator of the biochemical/biophysical parameters of interest optimized to the used airborne hyperspectral image data.
4) To extract the spatial patterns, gradients and trends of the proposed spectral indicators using complex contextual classification model.
5) To validate the obtained results by the validation ground-truth dataset.

Chapter 2: Study site

The chapter provides general description of the Sokolov lignite basin – the study site related to the analyses presented within this study. Characteristics related to geology, pedology, climate and air quality are briefly summarized as all these factors are assumed to be influencing forest vegetation characteristics in this area. In addition, detailed description of the Norway spruce stands where needle sampling and other field measurements were conducted is also provided at the end of the chapter.

2.1 Sokolov lignite basin

2.1.1 General characteristics

The study was carried out in the area of Sokolov lignite basin located in the North-west part of the Czech Republic, west of the town Karlovy Vary. Sokolov basin is a part of the Eger rift system boarded by the Ore Mountains (Krušné hory) in the north and by Slavkov Forest (Slavkovský les) in the south. The area covers approximately 200 km^2 (9 × 36 km). Elevation is ranging between approx. 400 – 750 meters above the sea level. The natural axes of Sokolov basin are the rivers Eger (Ohře) and Svatava (the main branch of the Eger river in this area).

Sokolov basin area has been affected by long-term intensive brown coal mining. As the mining activities have been conducted in open-pit mines, they have changed the local landscape and environment significantly. Actually (2017), brown coal is exploited in the last active coal mine Jiří. Mining activities were temporarily interrupted in the Družba mine in 2012, but they are planned to be restored in the future. In addition there are also several non-active (closed) open-pit coal mines (Medard, Lomnice, Marie, Vilém, Silvestr). Coal mining is closely linked to electricity production realized in two coal powerplants (Tisová and Vřesová). The mine waste material as well as poweplant fly ash have been stored at several dumps. Some of them are still active (e.g. Smolnice dump) whereas others were reclaimed in the past (Lítov dump, Antonín dump, Podkrušnohorská dump etc.). The Sokolov basin is also rich in resources of caolinite which has been used for traditional porcelain production (e.g. in Nová Role and Chodov).

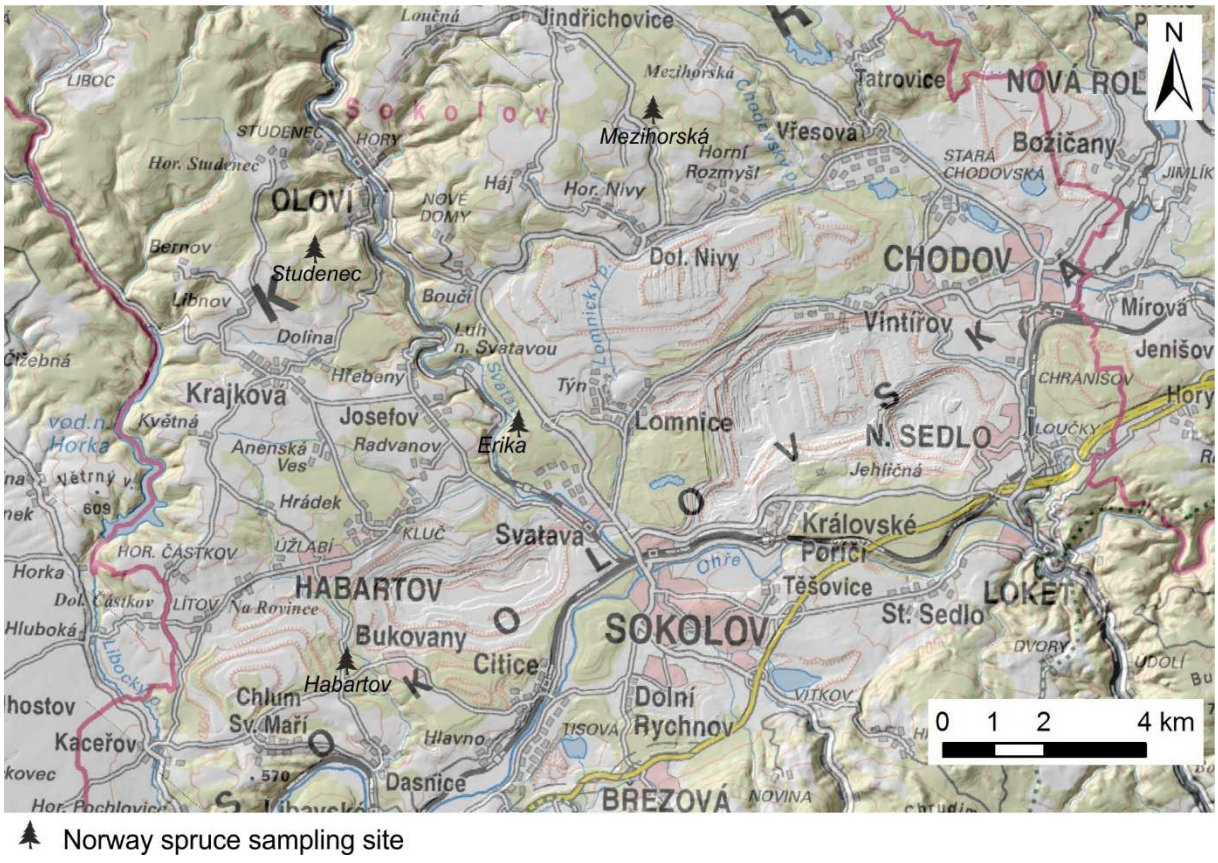

Figure 2.1: *Topographic map ZM200 of the Sokolov lignite basin area with the positions of Norway spruce sampling sites.*

2.1.2 Geology

The Sokolov lignite basin is a part of the Eger river rift and is bordered by a complex of faults running in SW – NE direction and cut by NW – SW direction faults. The basement is formed by Variscan and pre-Variscan complexes of the Eger, Erzgebirge (Ore Mountains), Slavkov Forest and Thuring-Vogtland crystalline units and Karlovy Vary pluton. The basal late Eocene Staré Sedlo formation (formed by sandstones, quartzites and conglomerates) is overlain by up to 350 m thick volcano-sedimentary complex formed by a cypris clay formation, volcanoclastics (tuffs) and three brown coal seams (Josef, Anežka and Antonín) (Rojík 2003). Brown coal contains 5 – 8 % of sulfur (S) and is enriched by heavy metals such as As, Cd, Ni, Cu, Zn and Pb (Bouška and Pešek, 1999; Yudovich and Ketris, 2005). The basin is bordered by the slopes of the Ore Mountains and Slavkov Forest composed of granites, granodiorites, paragneiss and mica schist rocks of Proterozoic and Paleozoic age. The general geological map of the Sokolov basin see in Figure 2.2.

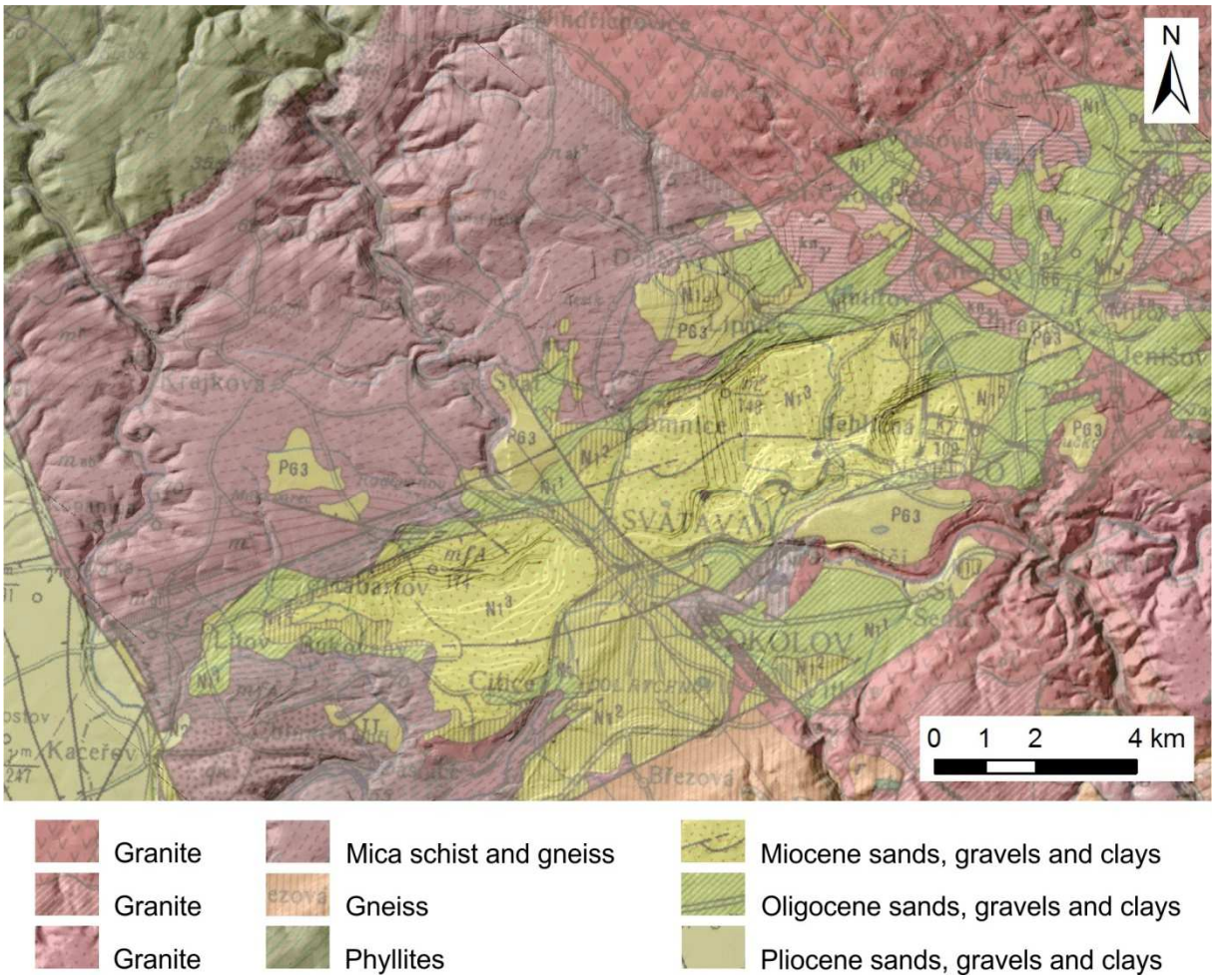

Figure 2.2: *Geological map (G200) of the Sokolov lignite basin area (ČGS)*

2.1.3 Soils

The soil cover is formed mainly by acid Dystric Cambisols (KAa) transforming into Hyperdystric Cambisols (KAd) at higher elevations. The parent rock of these soil types is colluvium of mica schist, phyllite and acid granite. Lower situated areas are covered typically by Haptic Stagnosols (PGm) formed mainly from glacial polygenetic loams. The areas along the streams and rivers are formed by fluvisols (FL). The area located to the west of the Jiří open pit mine is characteristic by the presence of gleyed acid Pelosols (PEga) formed from various clays. As the area has been affected by long-term mining activities, anthroposols (AN) are very common. All the information regarding the soil cover of the Sokolov lignite basin were extracted from the Soil map of the Czech Republic provided by the Czech University of Life Sciences (ČZU) via the geoportal of Czech National Geoportal (CENIA) – see Figure 2.3 .

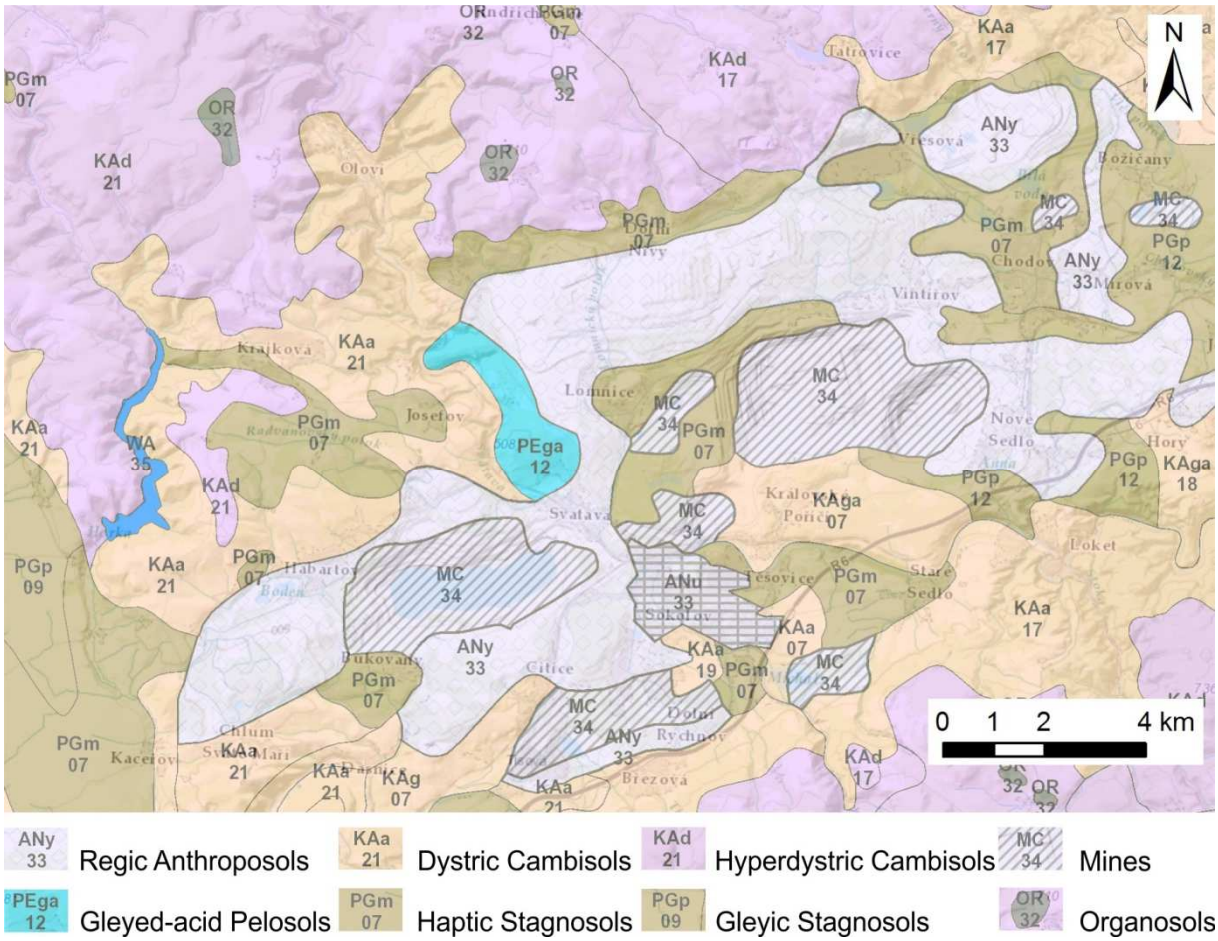

Figure 2.3: *Map of the basic soil types in the Sokolov lignite basin.*

2.1.4 Climate and air quality

The Sokolov lignite basin is situated on the border of moderate-warm (MT3-MT4) and cold climate (CH7) zones regarding the classification by Quitt (1971). The long-term average temperature is 6 to 7°C: -2°C to -3 °C (January) and 16 to 17 °C (July) in lower situated areas resp. -3° to -4°C (January) and 15 to 16 °C (July) in higher situated areas. The long-term average rainfall is 600 – 700 mm. There are 110 – 120 precipitation days with 300 – 350 mm rainfall during the vegetation season and 60 – 100 day with snow cover in the lower situated areas. Climate of the higher situated areas is slightly wetter with 120 – 130 precipitation days with 500 – 600 mm rainfall during the vegetation season and 100 – 120 days with snow cover.

The Sokolov lignite basin area has suffered by serious air pollution due to the intensive heavy industry. The air pollution gives rise to acid rains leading finally to soil acidification. Figure 2.4 shows annual imissions of SO_2, NO_x, PM_{10} and tropospheric O_3 measured between 1997 and 2012 at the meteorological station in Sokolov. There was a significant decrease of SO_2 imissions at the end of 1990s dropping from 27 µg/m³ to approx. 10 µg/m³. The values are stable since that. There is also steady decrease of NO_x imissions dropping from approx. 40 µg/m³ in 1997 to less than 20 µg/m³ in 2012. The PM_{10} and O_3 values seems to be relatively stable ranging between 15 – 25 µg/m³ (PM_{10}) and 40 – 60 µg/m³ (O_3). The values of SO_2, NO_x, PM_{10} and

tropospheric O_3 were obtained from publicly available annual yearbooks of the Czech Hydrometeorological Institute (ČHMÚ):

http://portal.chmi.cz/files/portal/docs/uoco/isko/tab_roc/tab_roc_CZ.html

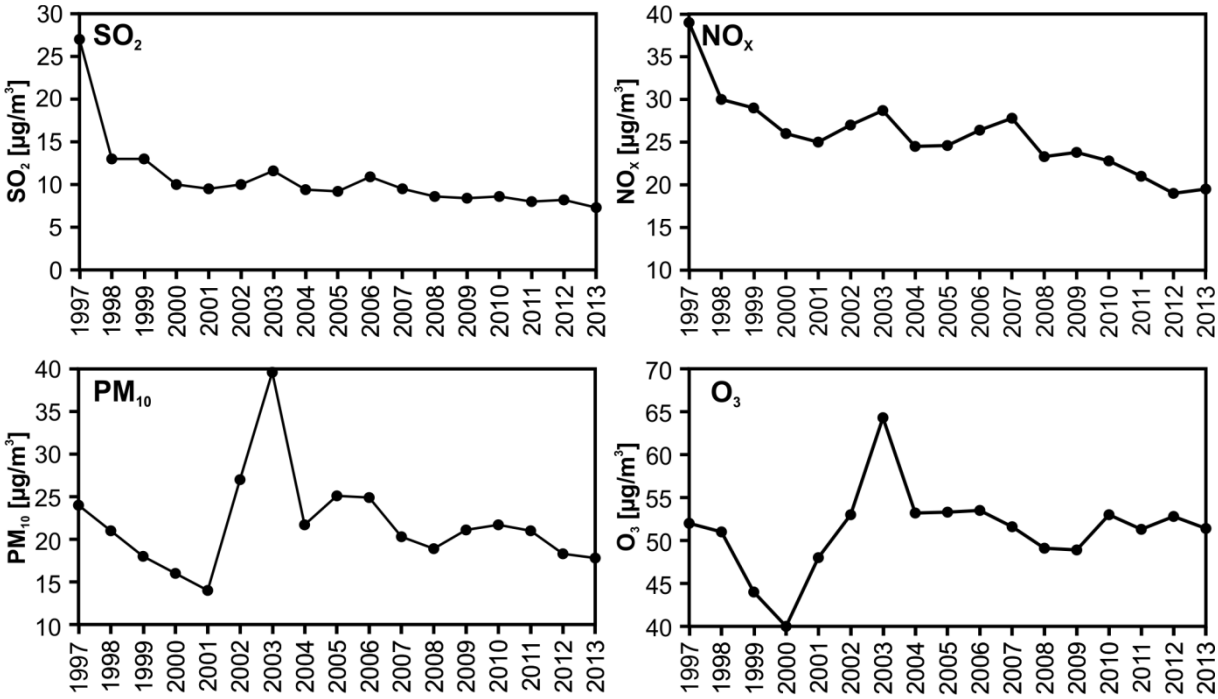

Figure 2.4: *Imissions of SO_2, NO_x, PM_{10} and tropospheric O_3 measured between 1997 – 2013 at the meteorological station in Sokolov*

2.2 Sampling localities

2.2.1 Norway spruce stands

Norway spruce forest stands health status assessment was conducted at four test localities called Erika, Habartov, Mezihorská and Studenec. One primary mature Norway spruce stand was selected at each locality where needle and soil sampling as well as the biophysical and structural parameters measurements was conducted during the field campaigns. None of this stand exhibited any symptoms of visual macroscopic damage with total crown defoliation less than 25 % and average needle retention of 8 – 10 needle age classes. These stands were therefore classified as initially damaged (damage class DC1).

The primary stands were selected to be as most similar and comparable as possible. Due to that no significant differences in the values of the biophysical and structural parameters were expected between the primary stands. Several additional (secondary) stands were therefore selected at each locality to cover as wide range of biophysical/structural parameters values as possible. The secondary stands were selected regarding the forest management maps. The chosen secondary stands were selected as the representative examples of homogeneous Norway spruce stands of all age classes. Note, that no stands representing the age classes 7 (120 – 140 years) and 8 (140+ years) were included in this study as there are no homogenous Norway spruce stands of these age classes in the area of interest. The measurements of biophysical/structural parameters

were performed at the secondary stands, but neither needle nor soil sampling was conducted there. In total, 19 Norway spruce stands were included in this study. The complete list of these stands see in Table 2.1. Note that the Norway spruce stands have never been affected by the mining activities directly, but they are located in the neighbourhood of the open-pit coal mines and thus they have been affected indirectly via the air pollution, dust fallout and soil acidification.

Table 2.1: *Norway spruce sampling stands*

Stand	Locality	Age	Northing (WGS-84)	Easting (WGS-84)	Elevation (m)	Aspect	Slope	Soil	Parent rock	Sampling
E_1	Erika	1-20	50.2065	12.6044	502	50	1.8	PEga	CL	BP
E_2	Erika	21-40	50.2034	12.6037	494	159	6.9	PEga	CL	BP
E_3	Erika	41-60	50.2069	12.6044	501	118	2.8	PEga	CL	BP, BC, SO
E_4	Erika	61-80	50.2054	12.6089	492	148	3.0	PEga	CL	BP
E_6	Erika	101-120	50.2085	12.6063	486	101	3.8	PEga	CL	BP
H_3	Habartov	41-60	50.1629	12.5596	459	43	3.7	PGm	PL	BP, BC, SO
M_1	Mezihorská	1-20	50.2661	12.6382	701	195	8.9	KAd	COg	BP
M_2	Mezihorská	21-40	50.2648	12.6383	684	181	6.7	KAd	COg, COmp	BP
M_3	Mezihorská	41-60	50.2676	12.6414	704	150	1.2	KAd	COg	BP
M_4	Mezihorská	61-80	50.2657	12.6362	692	179	5.0	KAd	COg, COmp	BP
M_{5a}	Mezihorská	81-100	50.2640	12.6382	674	175	7.8	KAd	COmp	BP, BC, SO
M_{5b}	Mezihorská	81-100	50.2656	12.6341	691	207	4.1	KAd	COmp	BP
M_6	Mezihorská	101-120	50.2675	12.6390	706	46	1.8	KAd	COg	BP
S_1	Studenec	1-20	50.2361	12.5559	654	78	1.9	KAd	COmp	BP
S_2	Studenec	21-40	50.2343	12.5546	630	148	17.8	KAd	COmp	BP
S_3	Studenec	41-60	50.2357	12.5501	662	121	1.6	KAd	COmp	BP, BC, SO
S_4	Studenec	61-80	50.2374	12.5548	655	27	8.1	KAd	COmp	BP
S_5	Studenec	81-100	50.2367	12.5513	648	37	11.0	KAd	COmp	BP
S_6	Studenec	101-120	50.2351	12.5535	652	157	6.2	KAd	COmp	BP

PEga – gleyed acid Pelosols; KAa – dystric Cambisols; KAa – hyperdystric Cambisols; PGm – haptic Stagnosols
CL – clays; PL – polygenetic loams; COmp – colluvium of mica schist and phyllite; COg – colluvium of acid granite
BP – biophysical measurements; BC – biochemical needle sampling; SO – soil sampling

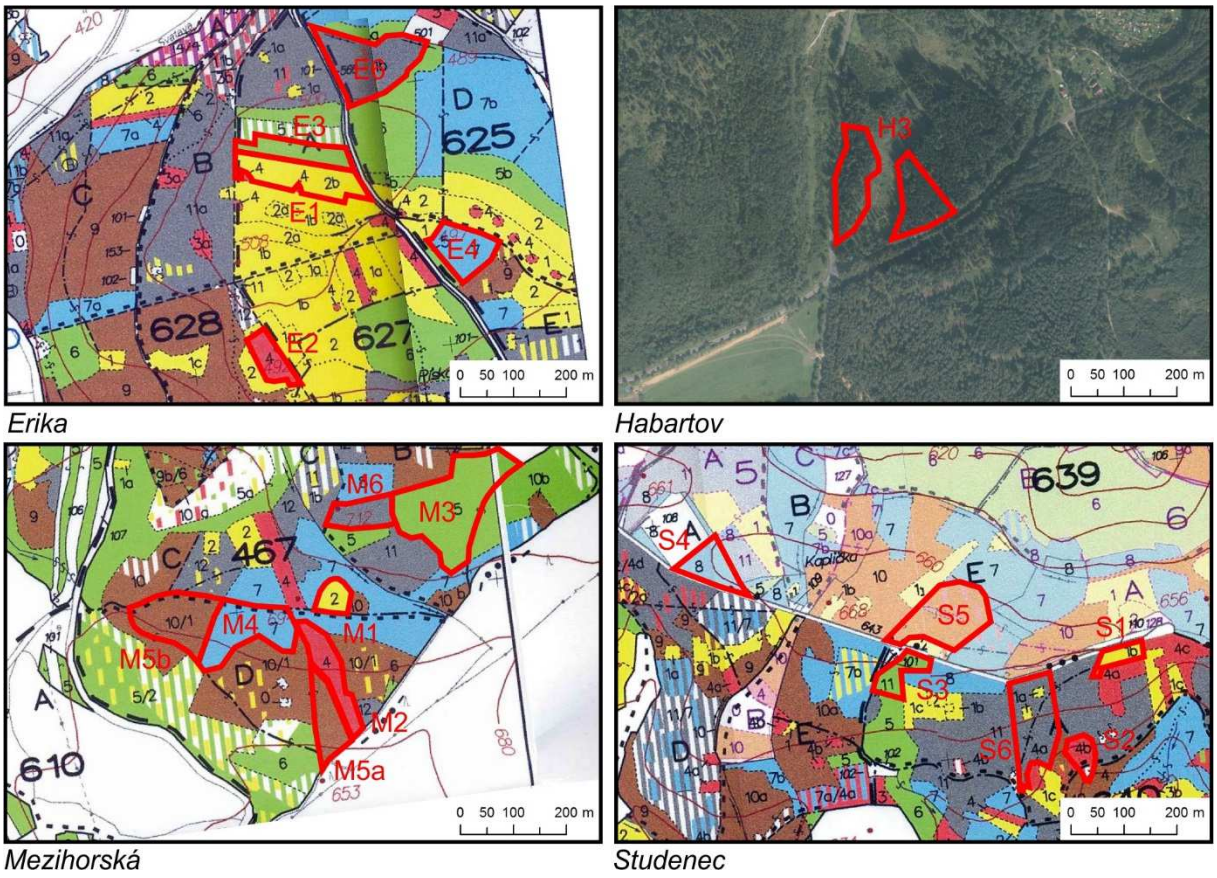

Figure 2.5: *Norway spruce sampling stands at Erika, Habartov, Mezihorská and Studenec sites (no forestry management map available for Habartov site).*

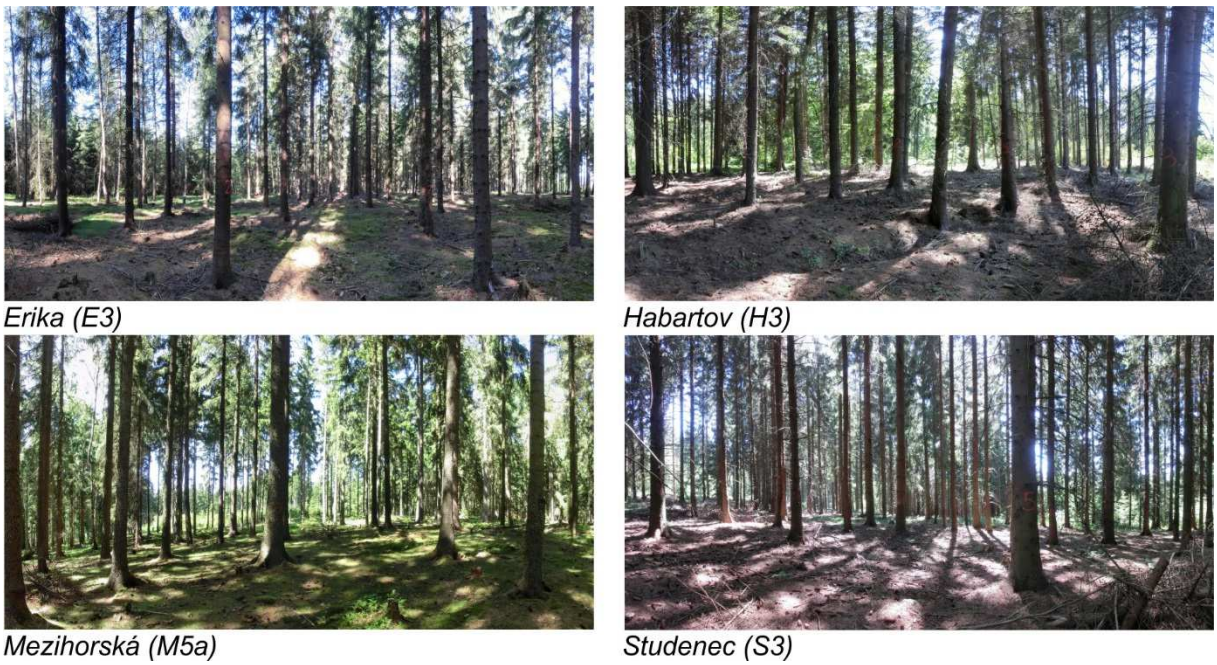

Figure2.6: *Panoramic photos taken at the primary Norway spruce stands at Erika (E3), Habartov (H3), Mezihorská (M5a) and Studenec (S3).* ***Author:*** *Jan Mišurec.*

Chapter 3: Data acquisition

The chapter provides detailed description of data acquisition. Norway spruce foliage sampling and its further laboratory analysis is described first including estimation of the basic biochemical parameters such as foliar pigments (chlorophylls and carotenoids), water and dry matter contents, specific leaf area and content of the selected chemical elements having potential linkage to actual environmental conditions the forest stands of interest. Workflow used for estimation of forest canopy structure (including for example leaf are index) using acquisition and analysis of digital hemispherical photography is described in the next part of the chapter. In addition, description of soil sampling and laboratory analysis of the collected soil samples are described as well including also calculation of the basic soil characteristics such as total exchangeable acidity, basic exchangeable cations, cation exchange capacity and base saturation. Finally, detailed description of the HyMap airborne hyperspectral imagery acqusition is provided including also all steps of the data pre-processing (i.e. calibration, geometric, topographic and atmospheric correction).

3.1 Foliage needle sampling

3.1.1 Collection of foliage samples

The reference needle samples were collected from 50 mature Norway spruce trees from 4 different stands: Erika (E_3) – 10 trees, Habartov (H_3) – 15 trees, Mezihorská (M_{5a}) – 15 trees and Studenec (S_3) – 10 trees. In 2009, the needle sampling campaign was organized in the day of the HyMap data acquisition and the following day (27th and 28th July 2009). In 2010, the needle sampling campaign was organized 12 days after the HyMap data acquisition due to heavy rains in the area of interest (2nd September 2010).

The branches from upper and lower part of the sunlit crowns were cut off by tree climbers and the representative samples of current and current + 2 years age class needles were collected. Therefore the current and current + 2 years needles taken from the upper level of the crown are referred as U_1 and U_3 respectively, whereas the current and current + 2 years needles taken from lower level of crown are referred as L_1 and L_3 respectively. The sampling using is demonstrated at Figure 3.1. In total, 200 Norway spruce needle samples were taken during the each sampling campaign. The collected needle samples were placed into cold and dark portable freezer and transported within 2 hours for further laboratory processing.

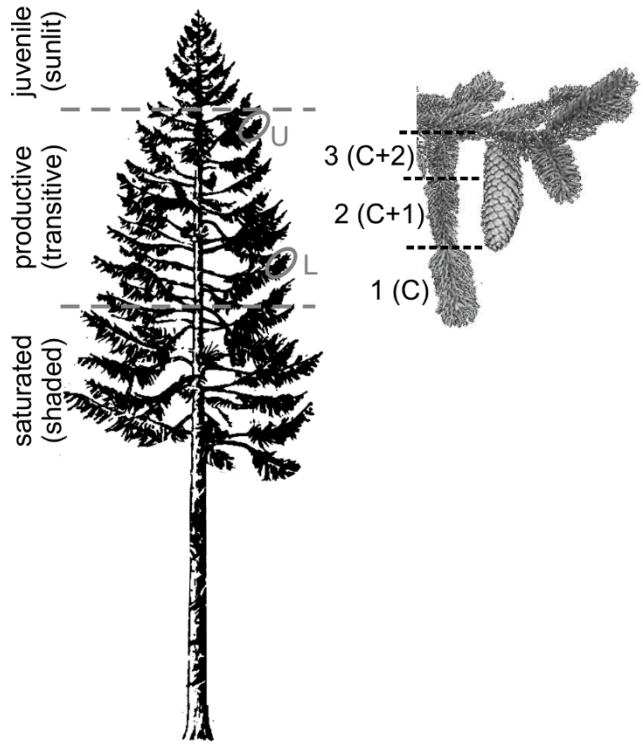

Figure 3.1: *Norway spruce needles sampling design. The Norway spruce crown is usually divided into three parts: juvenile (sunlit for whole day), productive (sunlit for a part of the day) and saturated (shaded for whole day). The samples were collected from upper (U) and lower (L) level of the productive crown. 1st (current - C) and 3rd (current + 3 years – C+2) age class needles were taken during the field sampling.*

3.1.2 Laboratory analyses of foliage samples

The Norway spruce needle samples collected in 2009 were divided into two parallel sub-datasets (NS_1 and NS_2). The NS_1 dataset was used to estimate the water (C_w) and dry matter content (C_m) and needle projection area (LAP). The fresh weight (FW) of the needles were measured first. Then the samples were scanned using a table scanner to determine their projection area. Finally they were dried for 48 hours at 80°C in an electric oven to determine their dry weight (DW), water and dry matter content.

The NS_2 dataset was used to determine the photosynthetic pigments content (C_{ab}: chlorophyll-a+b and C_x: total carotenoids). Photosynthetic pigments were extracted in dimehylforamide (DMF) for 7 days at 4°C in dark conditions following the procedure described in Porra at al. (1989). The foliar pigments content was then determined spectrophotometrically using equations of Wellburn (1994). The photosynthetic pigments content was expressed in the units normalized to the dry weight of the sample [mg/g].

In addition to determination of plant pigments, water and dry matter content, the content of several trace elements, macronutrients and heavy metals was performed. The content of Zn, Pb, Cu, Cd, Al, Mg, Ca, Na and K was determined using the Flameless Atomic Absorption Spectroscopy (FAAS). The content of arsenic (As) was determined using Hydride Generation Atomic Absorption

Spectroscopy (HGAAS) and the Hg content was measured by the Advanced Mercury Analyzer (AMA). The laboratory analyses were performed by the Central laboratory of the Czech Geological Survey. For more details see Kopačková et al. (2014a).

The processing workflow was the same in 2010, but no Norway spruce needle projection area was measured that time.

3.1.3 Total needle area calculation

The Norway spruce total needle area (LAT) was calculated from the measured needle projection area (LAP) by the method described in Homolová et al. (2013). The total needle area was then used to determine specific leaf area (SLA) describing the ratio of needle total area and dry mass:

$$SLA = \frac{LAT}{DW}$$

where: SLA…specific leaf area; LAT…needle total area; DW…needle dry mass

The contents of chlorophylls, carotenoids, water and dry matter were then transformed from the units normalized by the sample dry weight to the units normalized by the sample area using the calculated SLA values:

$$C_{ab}[\mu g \cdot cm^{-2}] = \frac{C_{ab}[mg \cdot g^{-1}]}{SLA} \cdot 1000$$

$$C_x[\mu g \cdot cm^{-2}] = \frac{C_x[mg \cdot g^{-1}]}{SLA} \cdot 1000$$

$$C_w[cm] = \frac{FW - DW}{LAT}$$

$$C_m[g \cdot cm^{-2}] = \frac{1}{SLA}$$

where: C_{ab}…total chlorophylls content; C_x…total carotenoids content; C_w…water content – equivalent water thickness; C_m…dry matter content; SLA…specific leaf area; LAT…needle total area; FW…needle fresh weight; DW…needle dry weight.

In case of the samples collected in 2010 no LAP measurements were performed and thus the direct determination of SLA was not possible. Therefore the transformation of units normalized by sample dry weight to the units normalized by sample area had to be performed by an alternative way using the indirect estimation of LAP. The statistical regression between DW and LAP was constructed separately for each U_1, U_3, L_1 and L_3 needle samples using the data from 2009 campaign (see Figure 3.2). The obtained predictive equations were then applied to the DW values from 2010 dataset to estimate their LAP. The further workflow was then the same as in case of the samples collected in 2009.

The processing of the collected needle samples was realized by both PřF UK and CzechGlobe teams. The collection of the samples was realized by the PřF UK team with active

contribution of the author. The extraction of photosynthetic pigments was performed by the PřF UK team too. The needle projection and total area and SLA calculation was performed by the CzechGlobe team for the samples collected in 2009. The indirect LAP estimation was conducted by the author for the samples collected in 2010.

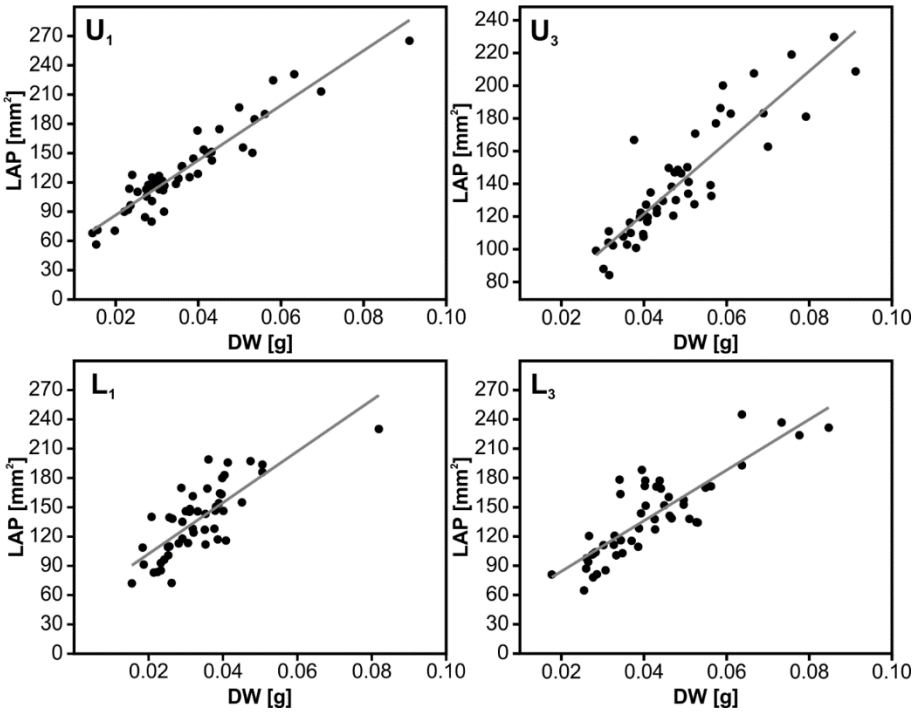

Figure 3.2: *Statistical regression between the needle dry weight (DW) and projection area (LAP) calculated from the needle samples collected in 2009.*

3.1.4 Measurement of spectral properties of foliage samples

Spectral properties of the Norway spruce (U_1, L_1) needle samples collected in 2010 were performed using ASD Fieldpec-3 spectroradiometer equipped by High-intensity contact probe. The sampled needles were placed on a surface coated by matt-black colour with constant reflectance across the studied spectral range and near-lambertian behaviour. The contact probe was placed on the top of a needle layer so that full field of view was filled by the needles. The measured radiance was normalized against the white reference Spectralon target to produce relative reflectance values. Each sample was measured five times on different places of needle layer. The scan average time was reduced to 15 to avoid overheating of the needle samples. Individual measurements were further processed using the ViewSpecPro software and stacked using median stacking method resulting in one spectrum for each needle sample. The spectral characteristics of the needle samples see in Figure 3.3.

The acquisition of the foliage spectra was performed by the PřF UK team. The processing of the acquired spectra was performed by the author.

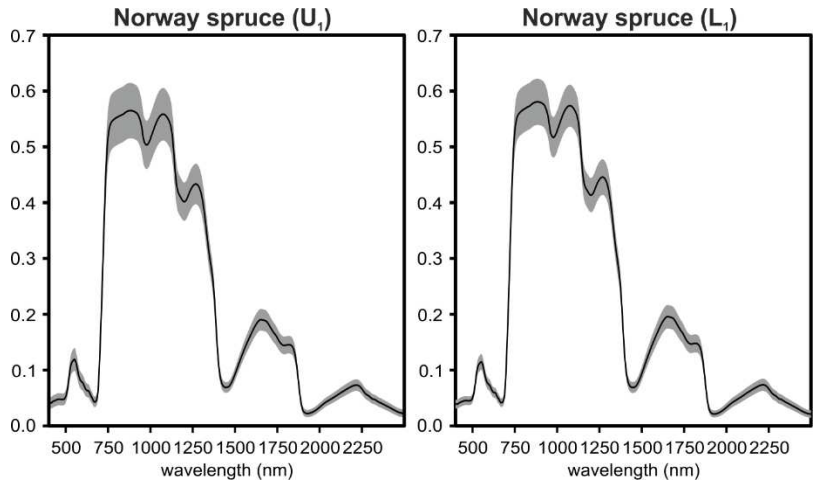

Figure 3.3: *Spectral properties of the Norway spruce U_1 and L_1 needle samples collected in 2010.*

3.2 Estimation of biophysical and structural parameters of Norway spruce forest stands using digital hemispherical photography

3.2.1 Optical centre and projection function calibration

Real optical systems are not perfect at least in terms of two parameters affecting their optical characteristics. These two parameters are:

1) Coordinates of optical centre
2) Projection function

The optical centre defined as the point where the optical axis is projected on to the CCD matrix should be identical to the geometrical centre of the output image in case of an ideal optical system. However, this is not true in case of real lenses. Therefore the coordinates of the optical centre are not identical to the coordinates of the geometric centre. Projection function describes the relationship between the angular distance of the object from the optical axis and radial distance of the corresponding pixel on the image plane.

The CanEye user manual proposes simple methods to estimate the coordinates of the optical centre as well as the projection function. In case of the optical centre it is suggested to drill several small holes into the plastic cap of the fisheye lens. A sequence of photographs is then taken with the fisheye lens while rotating the cap around the optical axis. The positions of the holes are measured in terms of row/column for each image. From these coordinates it is possible to calculate the coordinates of hypothetical point around which the images of the holes rotates. This point is the required optical centre (see Figure 3.4).

In fact, the proposed method is complicated by several factors. First, it is a bit destructive as it requires drilling the holes into the lens cap. Therefore a new substitute cap was made using hard paper. The holes were drilled using a very thin needle. However, it was found that the holes are still too big despite using the thinnest available needle. Due to that it was not possible to measure the coordinates of the holes with the required accuracy. Therefore an alternative method

was developed. The cap was made using white hard paper again. However, three crosses were printed to its front part using the very thin lines instead of drilling holes. The cap was then put on the lens and the camera was pointed to the strong light source. As the paper is partially transparent, the crosses printed onto the front part of the cap are clearly and sharply visible on the taken photographs so they can substitute the holes.

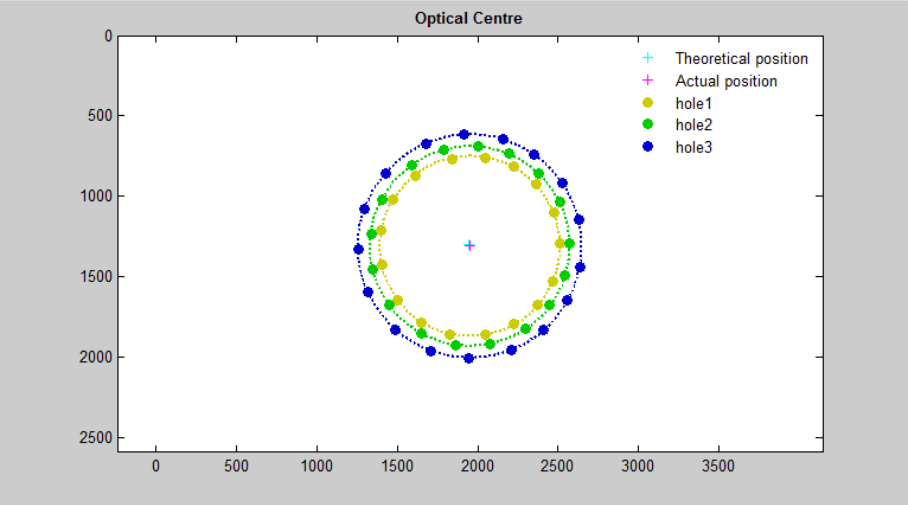

Figure 3.4: *Determination of the optical centre*

The projection function is estimated using a special design consisting of three rulers – one oriented across the optical axis (perpendicular) and two oriented along the optical axis (lateral). For detailed information see the CanEye User's manual (p. 46). The measurement was performed twice to estimate so called empirical projection functions EPF_1 and EPF_2. However, there were significant discrepancies between the results of these two measurements resulting in differences between these two functions. From the original technical documentation it is known that the used Sigma 4.5 mm F 2.8 DC HSM fisheye lens provides Equisolid Angle Projection (EAP). This projection is defined as:

$$R = 2 \cdot r \cdot sin\left(\frac{x}{2}\right)$$

where: R…distance of the projected point from the optical centre in the image plane; r…relative radius of the imaged hemisphere (given by the dimensions of the image); x…angular distance of the imaged object from the optical axis.

The border of the circular field of view corresponds to x = 90°. This border also corresponds to R = 1100 pixels in case of the used Canon EOS 400D camera providing the image size of 3888 x 2592 pixels. Therefore r value can be defined as:

$$r = \frac{R}{2 \cdot sin\left(\frac{x}{2}\right)} = \frac{1100}{2 \cdot \sin(45°)} \cong 777.8175$$

Now it is possible to define the projection function for the Canon EOS 400D + Sigma 4.5 mm F 2.8 DC HSM configuration as:

$$x = 2 \cdot arcsin\left(\frac{R}{2r}\right)$$

This function can be approximated by 3rd degree polynom for R (0, 1100):

$$x = 0.00000001R^3 - 0.00000557R^2 + 0.07521179R$$

As both empirical projection functions EPF_1 and EPF_2 somehow differ from the EAP function, EAP function was finally used for the digital hemispherical image processing (see Figure 3.5).

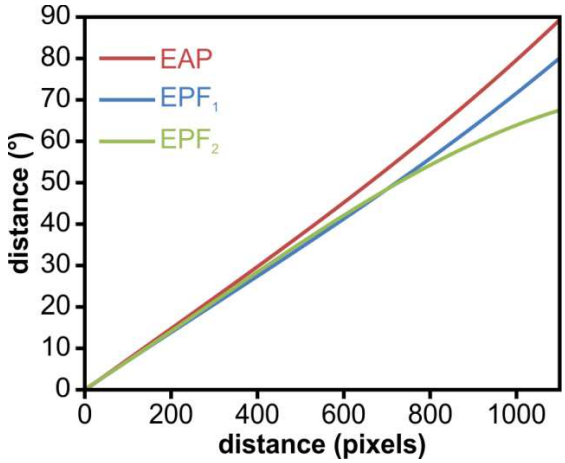

Figure 3.5: *Comparison of the both EPF_1 and EPF_2 empirical projection functions with the Equisolid Angle Projection function (EAP) for the Canon EOS 400D + Sigma 4.5 mm fisheye lens configuration.*

3.2.2 Sampling design of biophysical and structural parameters estimation

Digital hemispherical photographs were taken at the Norway spruce stands where the needle sampling had been conducted during the field campaigns. Moreover additional measurements were performed at other stands to cover the gradients of biophysical and structural parameters. These localities were carefully selected using the forest stand maps (1: 10 000). The aim was to take measurements at all age classes of Norway spruce stands. Finally, 18 localities (including the 4 needle sampling stands) were selected for biophysical and structural parameters estimation (see Figure 2.5 and Table 2.1).

The digital hemispherical photographs were taken using the C_{12} sampling design described in Majasalmi et al. (2012). This sampling design is easy to define in the field and it is also recommended as the elementary sampling unit (ESU) by the VALERI network (Majasalmi et al. 2012). However, regarding the spatial resolution of the HyMap data the size of C_{12} sampling design was somehow modified. The hemispherical photography were taken with 10 m spacing so the entire sampling design covered the 60 × 60 m square (see Figure 3.6). The coordinates of the central point of each sampling was measured using Trimble Nomad field GPS receiver.

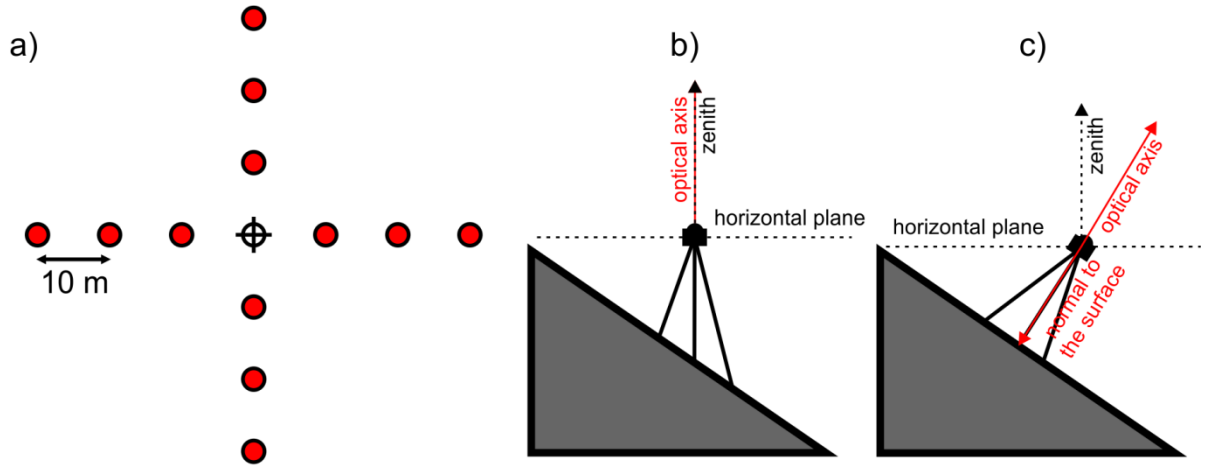

Figure 3.6: *Modified design C_{12} by Majasalmi et al. (2012) used for DHP data acquisition (a). Levelled (b) and tilted (c) designs for DHP data acquisition by Gonsamo and Pelikka (2008).*

The orientation of the sampling design was determined using the compass integrated into the Trimble Nomad field computer. The camera was oriented to the north in terms of the azimuthal orientation. The proper vertical orientation was achieved using two bull-eye levels integrated onto the used photographic tripod. The zenith direction was then defined using the vertical scale of the used tripod (see Figure 3.7). Note that all measurements were performed using the levelled acquisition described by Gonsamo and Pelikka (2008) so all the image are taken in the local zenith direction perpendicular to the horizontal plane. Three images differing by exposure compensation (-1 EV, 0 EV and +1 EV) were taken at each sampling point.

Figure 3.7: *Azimuthal and vertical orientation of the digital hemispherical photography acquisition.*

3.2.3 Processing of digital hemispherical photography

The acquired digital hemispherical photography was processed using the CanEye software (http://www6.paca.inra.fr/can-eye). The calculation of biophysical and structural parameters is based on gap fraction probability estimation. One of the first pre-processing steps is classification of the hemispherical images to distinguish the sky and vegetation. This classification is based on thresholding the three parameters: brightness, greenness and brownness. However, the results of this classification (integrated into the CanEye software) was found rather unsatisfactory as the setting of optimal threshold values is very subjective. Due to that high inconsistency was found

between the results of particular image classification. The image classification was therefore performed by alternative unified workflow outside of the CanEye environment.

The images were processed using the GIMP 2.8 (www.gimp.org) software. First, the image contrast was optimized using the contrast enhancement tool. The areas representing the sky were selected by the select by colour tool. The selected areas were filled by white colour. The selection was then inverted using the invert selection tool. These areas representing the sky obscured by vegetation were then filled by black colour. Finally, the 8-bit RGB image was transformed into the form of binary mask and saved (see Figure 3.8). These binary files were then loaded into the CanEye to perform the biophysical parameters calculation. The following biophysical and structural parameters were estimated:

- **LAI_e:** effective LAI (PAI)
- **LAI:** true LAI (PAI)
- **ALA:** Average Leaf inclination Angle
- **fCOVER:** fraction of canopy cover
- **fAPAR:** fraction of absorbed photosynthetic active radiation (both black-sky and white-sky fAPAR calculated)

The acquisition of digital hemispherical photography as well as its processing and biophysical/structural parameters calculation was designed and practically performed by the author.

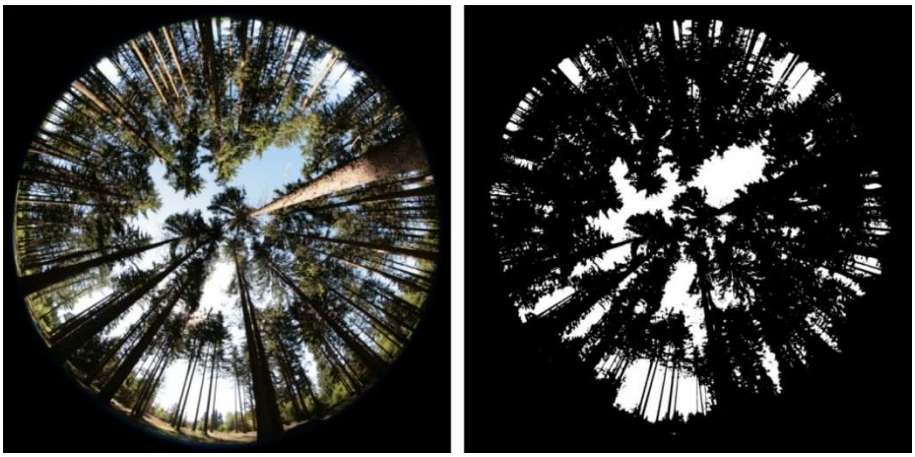

Figure 3.8: *Original hemispherical photography of Norway spruce forest stand (left) and the corresponding binary mask (right).*

3.3 Soil sampling and sample processing

Soil sampling was conducted at the four primary Norway spruce stands. Several representative soil probes were dug at each Norway spruce stand (6 at H_3, 4 at E_3, 5 at M_{5a} and 4 at S_3) during the 2009 field campaign. Material was collected from four horizons: two organic (h_1 and h_2) and two mineral (h_3 and h_4) – see Kopačková et al. 2014a, b. The collected material was transferred to laboratory analyses to determine exchangeable acidity (TEA) and exchangeable cations of Al^{3+}, Mg^{2+}, Ca^{2+}, Na^{+} and K^{+} (0.1 M $BaCl_2$ extracts analysed by FAAS method). Soil pH was

determined in distilled water and 1M KCl. In addition, relative nitrogen (N) and carbon (C) content as well as the C/N ratio were also determined (using Carlo-Erba Fissionas analyzer). Finally, the content of Cu, Zn, As and Zn was performed using the portable XRF spectrometer. The laboratory analyses of the collected soil samples were processed by the laboratories of the Czech Geological Survey and are described in details in Kopačková et al. 2014a, b.

In the next step, the exchangeable cations concentrations (originally expressed in mg/kg or g/kg) were transformed into mmol/kg using the molar masses of the particular elements (Al, Mg, Ca, Na and K). These values were then used to calculate three other soil characteristics: Basic Exchangeable Cations (BCE), Cation Exchange Capacity (CEC) and Base Saturation (BS) where:

$$BCE = Mg^{2+}_{[mmol/kg]} + Ca^{2+}_{[mmol/kg]} + Na^{+}_{[mmol/kg]} + K^{+}_{[mmol/kg]}$$

$$CEC = BCE + TEA$$

$$BS = \frac{BCE \cdot 100}{CEC}$$

3.4 Acquisition of reference field spectroscopy data

Ground spectral measurements essential for successful pre-processing of the airborne hyperspectral data in terms of calibration and atmospheric correction were performed during the supportive field campaigns organized simultaneously with the airborne data acquisition (i.e. 27th July 2009 and 21st August 2010). The field spectral measurements were conducted on the reference targets meeting the following conditions:

1) spatial homogeneity for the area equivalent to at least 5×5 pixels of the image data
2) natural or artificial lambertian (or near-lambertian) surfaces preferably with constant reflectance within the entire spectral range with no absorption features

As a result, following targets were chosen for acquisition of field spectra: 2× asphalt area, 1× beach volleyball court (sand), 1× concrete area, 1× artificial grass, 1× water pool.

The hemispherical-conical reflectance factor (HCRF) (Schaepman-Strub et al. 2006) was measured by the means of ASD Fieldspec-3 spectroradiometer for each reference target. All the targets were measured twice and the closest measurement to the time of overflight was used for further processing. Raw spectroradiometric data were transformed into HCRF using the calibrated Spectralon panel. Acquisition of the field spectra was performed partially by the CzechGlobe team and partially by the DLR team with the active contribution of the author.

3.5 Acquisition and pre-processing of HyMap airborne hyperspectral data

3.5.1 HyMap sensor

HyMap (Hyperspectral Mapper) is a whiskbroom airborne hyperspectral sensor developed and manufactured by Integrated Spectronics Ltd., Australia. It is designed to acquire

hyperspectral image data in 126 spectral bands covering the spectral range 450 – 2500 nm with the spectral resolution ranging from 15 to 20 nm (sampling interval 13 – 17 nm). The sensor is mounted on a gyro-stabilized platform which is equipped by GPS/IMU unit to monitor aircraft pitch, roll and heading motions. HyMap is a wide-FOV sensor (FOV = 63.3°). On one hand the covered swath is generally wider in compare with narrow-FOV systems, but on the other hand the data are affected by cross-track illumination (BRDF) effects. Regarding the FOV, scanning frequency and the aircraft speed, the HyMap sensor is usually operated in higher altitudes in compare with other systems, which is resulting in spatial resolution ranging from 5 – 10 m (related to flight altitude). For more technical specifications of the HyMap sensor see Cocks et al. (1998).

3.5.2 HyMap data acquisition

The first HyMap dataset was acquired on 27th July 2009 during the HyEUROPE 2009 campaign. The instrument was flown over the Sokolov area of interest between 10:45 – 12:03 UTC (12:45 – 14:03 CEST) at the average altitude 2570 m above the ground level. The flight campaign finished by obtaining 9 cloud-free flight lines oriented in NE-SW direction (geographic azimuth 70°/250°, sun-relative azimuth 114°/66°, solar zenith angle 33°). The resulting ground spatial resolution of the image data was 5 m.

The second HyMap dataset was acquired on 21st August 2010 during the HyEUROPE 2010 campaign. The sensor was flown over the area of interest at the average altitude 2475 m above the ground level. The flight campaign finished by obtaining 7 almost cloud-free flight lines oriented in NE-SW direction (geographic azimuth 40°/221°, sun-relative azimuth 126°/55°, solar zenith angle 39°). The resulting spatial resolution of the image data was 4 m.

3.5.3 HyMap data pre-processing

The inflight recorded DN data were corrected by DLR for dark current/electronic offset and then converged to at-sensor radiance [$\mu W/cm^2 \cdot sr \cdot nm$] using laboratory radiometric calibration information and in-flight measurements of the on-board calibration lamp. The data calibration is described in more details in Weide (2009) and Weide (2010).

Several atmospheric correction workflows were applied on the HyMap data. The performance of these workflows were tested focusing on the effects of the applied atmospheric correction on utilization of the data in quantitative vegetation studies. The results of this testing see in Mišurec (2014). The data used within the framework of this thesis were corrected by the workflow proposed by the CzechGlobe and University of Zürich teams as it was found to be the most appropriate in case of vegetation studies (Mišurec 2014).

The atmospheric correction was performed in ATCOR-4 software package using the flat terrain module. There are two essential parameters influencing the atmospheric correction results: a) aerosol type and b) visibility. Visibility was estimated using the Microtops II SunPhotometer measurements performed during the data acquisition. Aerosol type was selected as rural regarding the dominant character of the landscape in the area of interest. Reflectance of

the selected reference targets measured by ASD Fieldsopec-3 spectroradiometers (see 3.4) was used to final tuning of the atmospheric correction. Bands 22, 31-38, 45-52, 63-69 and 93-96 were interpolated due to strong oxygen and water vapour absorption. The final at-surface reflectance was finally multiplied by the factor of 10 000 to allow saving the data as integer values. This part of the atmospheric correction was performed by the CzechGlobe team.

The HyMap data suffered by strong cross-track illumination (BRDF) effects due to wide FOV and not optimal sun-relative azimuth. The BRDF effect was minimized by the means of semi-empirical nadir normalization using the Ross-Li kernel approach (Schaaf et al. 2002). The surface was divided into four land cover classes using Spectral Angle Mapper (SAM) classification: a) dark green (forest) vegetation, 2) bright green (grass) vegetation, 3) bare soil, 4) bright sand/gravel/clay. The Ross-Li model was parameterized regarding this land cover classification and then inverted to gain nadir-BRDF adjusted reflectance values. This part of the atmospheric correction was performed by University of Zürich.

The ortho-georectification of the HyMap 2009 data was performed by the CzechGlobe team using the PARGE software. Data from the on-board inertial unit and 10 m spatial resolution digital elevation model (DEM) were used as the inputs for the parametric ortho-georectification. The used DEM was created by merging two datasets: a) up-to date DEM with spatial resolution 10 m covering the mining areas provided by Geodis Inc. and b) DEM derived from digital topographic database DMU-25 with contour interval 5 m for the rest area. The HyMap data were georeferenced to the UTM 33N (WGS-84) coordinate system. The HyMap 2010 dataset was ortho-georectified by the DLR team using the Ortho software. The workflow was similar as in case of the HyMap 2009 data.

The ortorectified HyMap 2009 product was compared with very high resolution aerial ortophotos (0.5 m spatial resolution) to assess its final geometrical accuracy. The total position error was calculated using 20 GCPs resulting in the RMSE = 2.7 m.

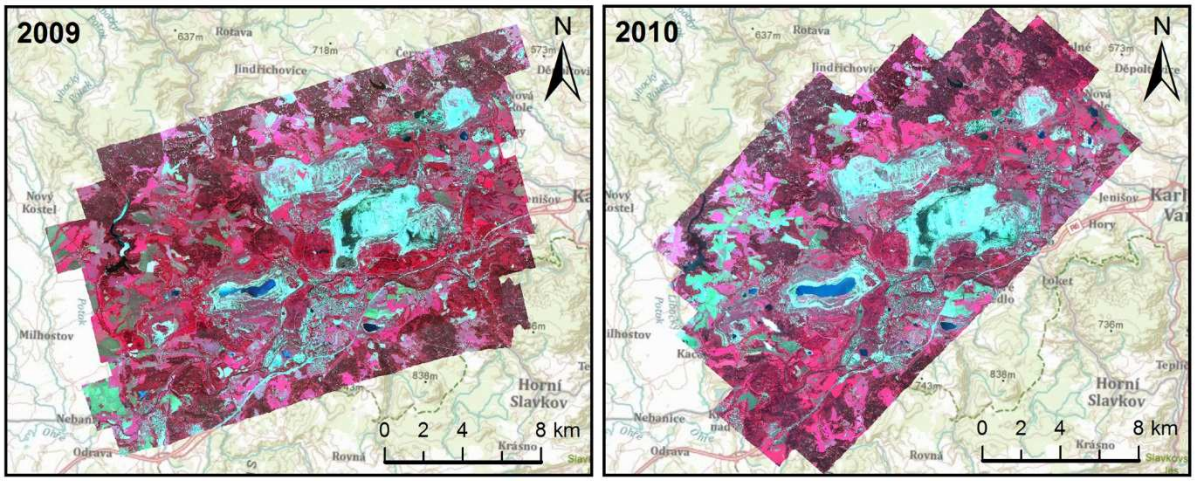

Figure 3.9: *CIR colour compositions of the HyMap 2009 and 2010 datasets*

Chapter 4: Performance of PROSPECT and LIBERTY Leaf level Radiative transfer Models for Coniferous Tree Species

The chapter focuses on the problematics of simulating optical/spectral properties of vegetation at leaf level. First, it provides a brief introduction of the two leaf level radiative transfer models – PROSPECT-5 and LIBERTY, which are used for the further analysis. Parameterization of the both models is described in the next part meaning the process of finding the most optimal setting of the model input parameters for getting the best possible fit between model simumations and the corresponding reference spectra. The part focusing on parameterization of the PROSPECT-5 model includes description of the concept of using so called infinite recletance instead of single leaf reflectance for model parameterization. This step seems to be crucial in case when the reference needle spectra are measured by contact probe instaed of using integration sphere. In addition, forward simulations of the both models and creating a simulated leaf level spectra database covering the defined ranges of needle biochemical parameters are described as well. Finally, up-scaling of the simulated leaf level spectra to shoot level using the spectral invariants theory is described at the end of the chapter.

4.1 Introduction of PROSPECT and LIBERTY leaf level radiative transfer models

PROSPECT model, introduced by Jacquemoud and Baret (1990) is currently one of the most frequently used leaf level radiative transfer model. It is based on the Allen's plate theory (Allen et al. 1969) considering leaf internal structure a pile of parallel semi-transparent layers (plates) characterized by absorption and refracting indexes. The number of these plates is defined by the structural parameter N. Furthermore, the initial version of the model has three more inputs related to leaf biochemistry/biophysics: total chlorophyll content (C_{ab}), water content (C_w) and dry matter content (C_m). In the most recent version PROSPECT-5 (Feret et al. 2008), two additional parameters were introduced: total carotenoids content (C_x) and brown pigments content (C_b).

PROSPECT model is very popular due its simplicity, relatively low number of inputs and thus good inversion ability. It has been used in many studies on broadleaved as well as coniferous vegetation (e.g. Zarco-Tejada et al. 2004; Zhang et al, 2008; Moorthy et al. 2008; Hernandéz-Clemente et al. 2012), although Malenovský et al. (2006) highlighted the fact, that original PROSPECT model is not fully applicable to coniferous vegetation as the considered internal leaf structure does not correspond with real internal structure of needle-shaped leaves.

As the plate models were not optimized for simulating optical properties of non-flat (e.g. needle shaped) leaves, compact spherical particle models have been developed. In this case the leaf/needle internal structure is considered to be a mixture of uniform compact layers of spherical particles and air spaces through which the light propagates. One example of such model is LIBERTY introduced in Dawson et al. (1998). The model includes nine input parameters regarding leaf structure and biochemistry/biophysics. The considered internal leaf structure better fits the real structure of needles. However, due to higher number of the input parameters (compared to models like PROSPECT), the parameterization and inversion of LIBERTY is far more complex.

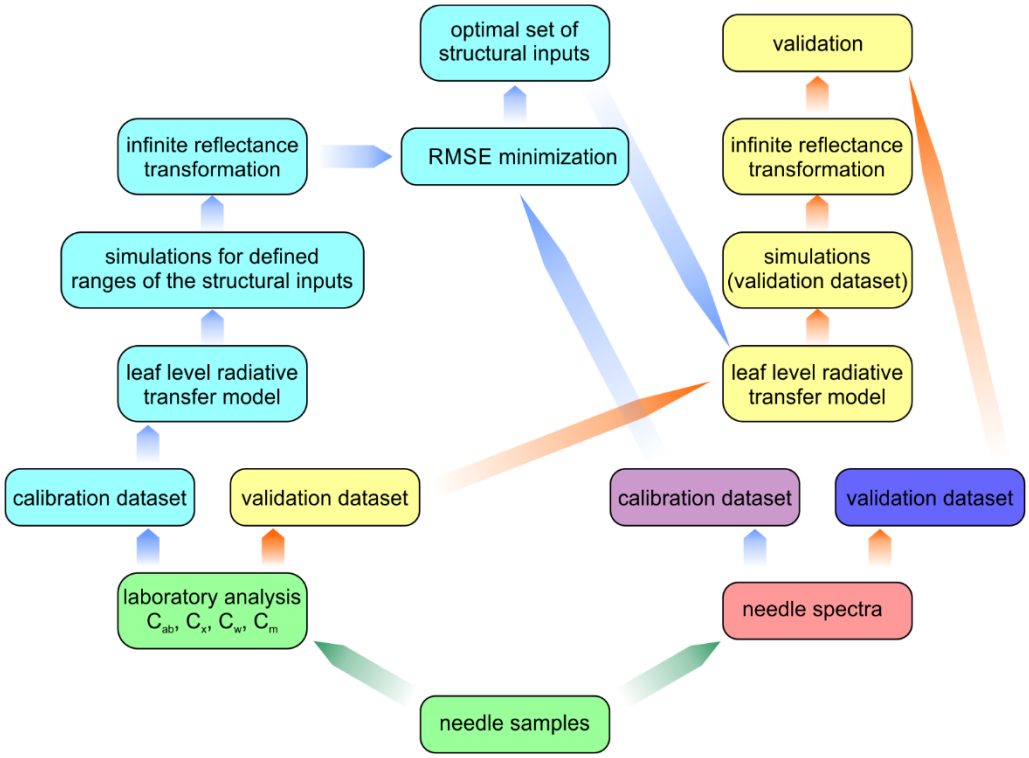

Figure 4.1: *Workflow scheme describing parameterization of the leaf level radiative transfer models (PROSPECT-5 and LIBERTY) and validation of the leaf level reflectance simulations.*

4.2 Parameterization of PROSPECT model

Parameterization of the both PROSPECT-5 and LIBERTY models was based on the needle samples collected during the HyMap 2010 flight campaign (see part 3.1). The original datasets (including 50 samples of U_1 level needles and 50 L_1 level needles) were first divided into two sub-datasets. Calibration dataset (containing 30 samples) was used for parameterization of PROSPECT-5 and LIBERTY models. Validation dataset (containing 20 samples) was used for validation of the simulations performed by the parameterized models (i.e. it was not used for model parameterization).

PROSPECT-5 requires several input parameters related to leaf internal structure (structural parameter N) and biochemistry (C_{ab}, C_x, C_w and C_m). The inputs regarding leaf biochemistry were obtained from the laboratory analyses of the collected samples (see part 3.1). The PROSPECT-5 was run in the forward mode with C_{ab}, C_x, C_w and C_m values fixed as an a-priori

laboratory determined values, whereas N was ranging from 1.0 to 5.0 (in 0.1 step). The obtained simulated single-leaf reflectance R was then compared with the ASD measured reflectance (R_{ASD}). The most appropriate N value was finally found using minimization of the merit function describing the RMSE between simulated and measured spectra:

$$RMSE = \sqrt{\frac{\sum(R_\lambda - R_{ASD\lambda})^2}{n}}$$

where: R_λ…simulated single-leaf reflectance at wavelength λ, $R_{ASD\lambda}$…ASD measured reflectance at wavelength λ, n…number of wavelengths λ.

This parameterization is called "R approach" in the further text.

However, regarding the design of needle spectra measurement, the obtained ASD outputs have rather character of so called infinite reflectance (R_∞) defined as reflectance of leaf stack where the effects of multiple scattering are taken into account. The simulated single-leaf reflectance spectra (R) were therefore transformed onto the level of infinite reflectance (R_∞) using the equation described in Zarco-Tejada et al. (1999):

$$R_{\infty\lambda} = \frac{R_\lambda}{1 - T_\lambda^2}$$

where: $R_{\infty\lambda}$…simulated infinite reflectance at wavelength λ; R_λ…simulated single-leaf reflectance at wavelength λ; T_λ…simulated single leaf transmittance.

The R_∞ values were finally used for searching the most appropriate N value using the merit function minimization in the similar way as in case of the single leaf spectra simulations:

$$RMSE = \sqrt{\frac{\sum(R_{\infty\lambda} - R_{ASD\lambda})^2}{n}}$$

where: $R_{\infty\lambda}$…simulated infinite reflectance at wavelength λ, $R_{ASD\lambda}$…ASD measured reflectance at wavelength λ, n…number of wavelengths λ.

This parameterization is called "R_∞ approach" in the further text.

The merit functions used for searching the most optimal N values for both described approaches see in Figure 4.2.

4.3 Parameterization of LIBERTY model

Compared to PROSPECT-5 model, parameterization of LIBERTY is considerably challenging due to higher number of model inputs. There are five input parameters except the ones regarding leaf biochemistry. These are: average cell diameter, intercellular air space, needle thickness, baseline absorption and needle absorption. Since it was not possible to optimize all the input parameters at once (to too many combinations increasing ambiguity of model inversion), the parameterization was performed in so-called stepwise mode fixing some of the input parameters while changing the others.

The parameterization was performed using merit function minimization technique in a similar way as in case of PROSPECT-5 model. The first input parameter was taken and optimized while the other inputs were fixed on their default values. The optimal value was then fixed and the model was run again while varying the next parameter. This process was repeated until all the parameters were optimized.

The parameterization of LIBERTY model was performed using the R as well as R_∞ approaches. Note that infinite reflectance R_∞ is a standard part of the LIBERTY output, so there is no need to upscale single leaf reflectance to infinite reflectance as in case of PROSPECT-5 model.

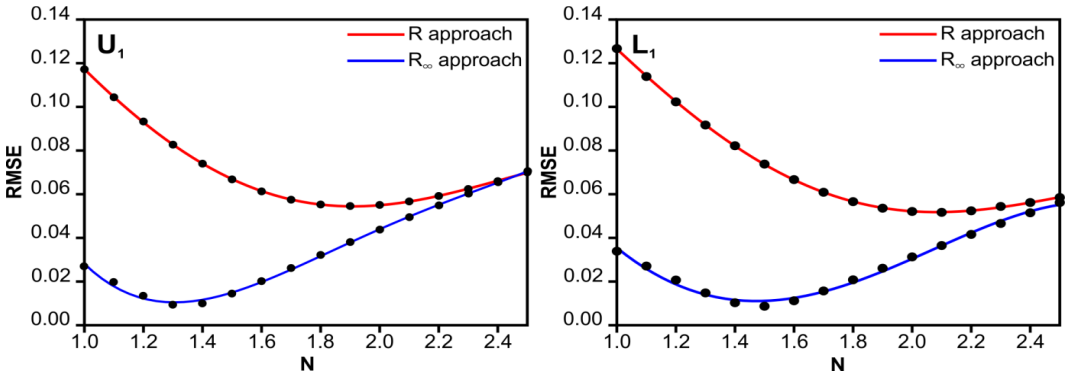

Figure 4.2: *Merit functions used to find the optimal value of the structural parameter N in PROSPECT-5 model: RMSE between simulated R resp. R_∞ and the ASD measured reflectance (R_{ASD}).*

4.4 Forward simulations using PROSPECT and LIBERTY models

Both PROSPECT-5 and LIBERTY radiative transfer models were run in the forward mode with the laboratory measured C_{ab}, C_x, C_w and C_m (validation dataset) values as the inputs. One needle spectrum was thus simulated for each validation dataset sample by each model. The simulations were then compared to the corresponding ASD measured spectra to assess reliability and stability of the performed parameterizations. The goodness of fit between simulated and measured spectra was assessed using three statistical indicators: total root mean squared error (RMSE), systematic ($RMSE_S$) and random ($RMSE_R$) components of the RMSE as defined in Willmott (1981).

An ordinary linear regression was set up first between the simulated ($R_{\infty\lambda}$) and measured ($R_{ASD\lambda}$) reflectance:

$$R_{\infty\lambda} = aR_{\mathrm{ASD}\lambda} + b$$

The regression coefficients a and b were then used to predict theoretical values of $R'_{\infty\lambda}$ free of random error:

$$R'_{\infty\lambda} = aR_{\mathrm{ASD}\lambda} + b$$

The systematic component of the RMSE ($RMSE_S$) is then calculated using the difference of theoretically predicted $R'_{\infty\lambda}$ and measured $R_{ASD\lambda}$ values:

$$RMSE_S = \sqrt{\frac{\sum(R'_{\infty\lambda} - R_{\mathrm{ASD}\lambda})^2}{n}}$$

The random component of the RMSE ($RMSE_R$) is then calculated using the difference of the theoretical random error free $R'_{\infty\lambda}$ and model simulated $R_{\infty\lambda}$ values:

$$RMSE_R = \sqrt{\frac{\sum(R'_{\infty\lambda} - R_{\infty\lambda})^2}{n}}$$

The total RMSE as well as the $RMSE_S$ and $RMSE_R$ were calculated for each particular wavelength λ and then averaged across three spectral domains: VIS (400 – 750 nm), NIR (750 – 1200 nm) and SWIR (1200 – 2500 nm). The values for the entire spectral range (400 – 2500 nm) were also calculated. Note that $RMSE_S$ and $RMSE_R$ are related to RMSE as: $RMSE^2 = RMSE_S^2 + RMSE_R^2$. The difference between simulated single-leaf (R) and infinite (R_∞) as well as ASD measured (R_{ASD}) reflectance spectra is illustrated in the Figure 4.3.

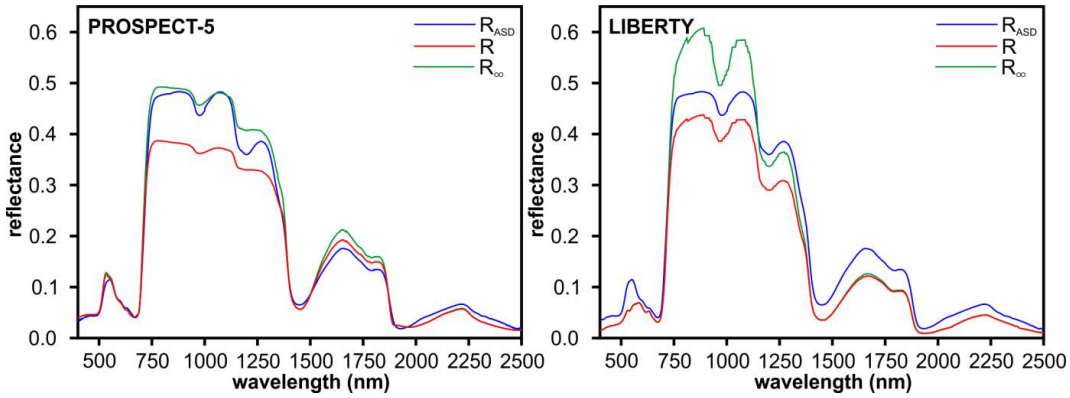

Figure 4.3: *Measured ASD reflectance (R_{ASD}) with the corresponding simulated single-leaf (R) and infinite reflectance (R_∞) spectra for one randomly selected sample of the validation dataset.*

4.5 Up-scaling to shoot level

The simulated single leaf spectra were finally up-scaled to the shoot level to take into account mutual shading of the needles on tree shoots. The shoot level upscaling was performed by the application of spectral invariants theory using the procedure described in Rautiainen et al. (2012) with the specie specific recollision probability (p) set to 0.356. The comparison of single leaf spectrum simulation and the corresponding shoot level spectrum see in Figure 4.4. The shoot level spectra were then used into FRT canopy level radiative transfer model (see Chapter 5).

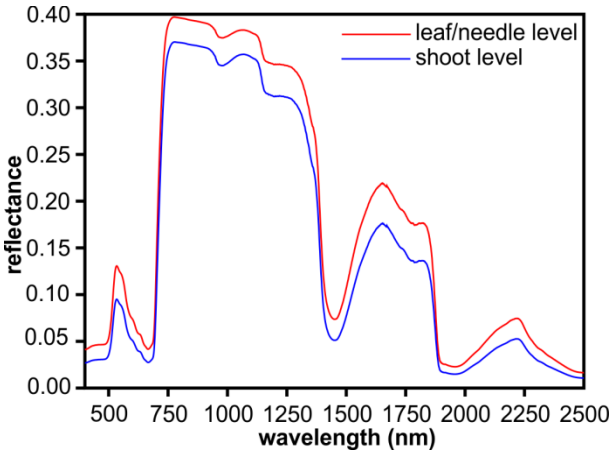

Figure 4.4: *Single leaf reflectance spectrum (R) simulated by the PROSPECT-5 model and the corresponding shoot level spectrum up-scaled by the application of spectral invariants theory.*

Chapter 5: Simulating spectral properties of Norway spruce coniferous forests using radiative transfer approach

The chapter includes detailed description of the simulated leaf/shoot level spectra upscaling onto the canopy level using the FRT radiative transfer model. Therefore, this chapter represents direct continuation of the issues described in the previous chapter. Brief description of the main characteristics of the FRT radiative transfer model is provided at the beginning followed by detailed workflow of the model parameterization based on a combination of in-situ canopy structure measurements (based on digital hemispherical photography), application of allometric relationships and expert estimations. The workflow includes definition of basic tree canopy architecture, estimation of crown closure and amount of biomass followed by definition of effective leaf area index and shoot shading.

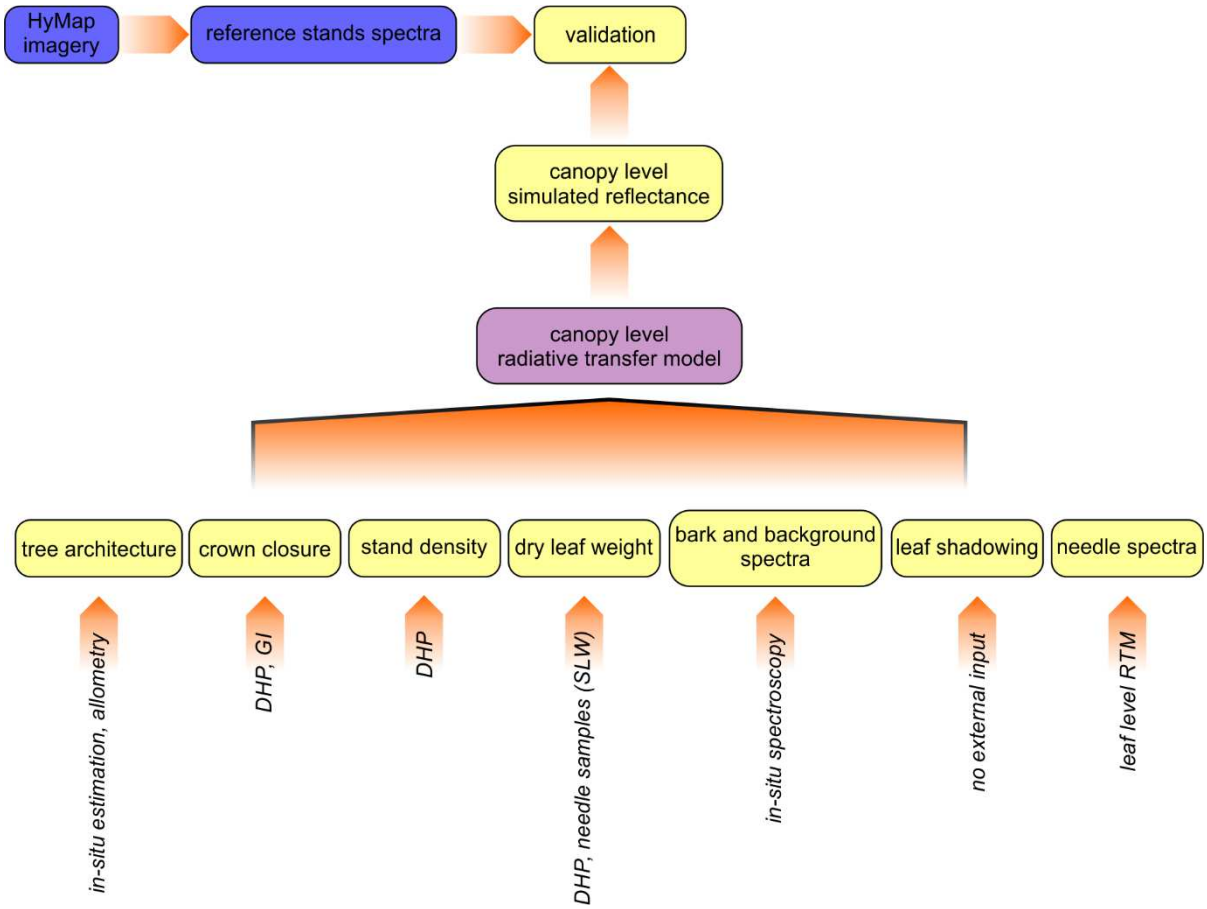

Figure 5.1: *Workflow describing parameterization and validation of the canopy level radiative transfer model (FRT).*

5.1 Introduction of FRT canopy level radiative transfer model

The FRT (Forest Reflectance and Transmittance) canopy level model has been developed by Andres Kuusk and Tiit Nilson at Tartu Observatory, Estonia (Kuusk and Nilson 2000). It can be classified as a hybrid-type model including geometrical as well as numerical radiative transfer concepts. Tree crowns are considered as simple ellipsoidal, conical or cylindrical envelopes. Tree architecture and morphology is then defined by several parameters such as tree height, crown height, crown radius or trunk diameter that can be relatively easily taken from forest inventories databases. The optical/spectral properties of foliage can be simulated by the built-in PROSPECT and LIBERTY models or can be defined by an external file. Spectra of wooden parts (trunk and branches) as well as a background spectrum are required as well. The amount of biomass within the tree crowns can be defined by the dry leaf weight parameter. The FRT model simulates the forest spectral properties at stand level rather than the level of individual tree crowns. Therefore the tree spatial pattern within the modelled stand is also taken into account.

5.2 Parameterization of the FRT model

The appropriate simulations of the PROSPECT-5 and LIBERTY leaf level models transformed onto the shoot level were used to define spectral properties of trees foliage. As no information about green biomass distribution was available, the U_1 and L_1 shoot level spectra were averaged to produce one shoot level spectrum for each sampled tree. Then the mean shoot level spectrum was determined for each particular modelled forest stand. These spectra were finally used in the FRT model.

In-situ samples of Norway spruce bark collected from tree branches and trunk were used to determine spectral properties of the wooden parts of the modelled trees. The spectra were measured by the portable Spectral Evolution SR-2500 spectroradiometer using the High Intensity contact probe. In addition, samples of dry Norway spruce litterfall were collected as it covers the major parts of the surface at the modelled forest stands. The samples were placed into glass Petri dish coated by matt-black colour and their spectra were measured using the SR-2500 spectroradiometer. The Norway spruce litterfall spectrum was considered as the background spectrum in case of the FRT model. The measured trunk and branch bark as well as dry litterfall spectra see in Figure 5.2.

As mentioned above, the FRT model was optimized to be parameterized using common forest inventory databases. However, these data are not always available. Therefore an alternative workflow for the FRT model parameterization was developed within this study for the cases when no forest inventory data are available. This workflow is based on the information extracted from in-situ acquired digital hemispherical photography in combination with expert estimations and allometric modelling. The workflow consist of the following steps:

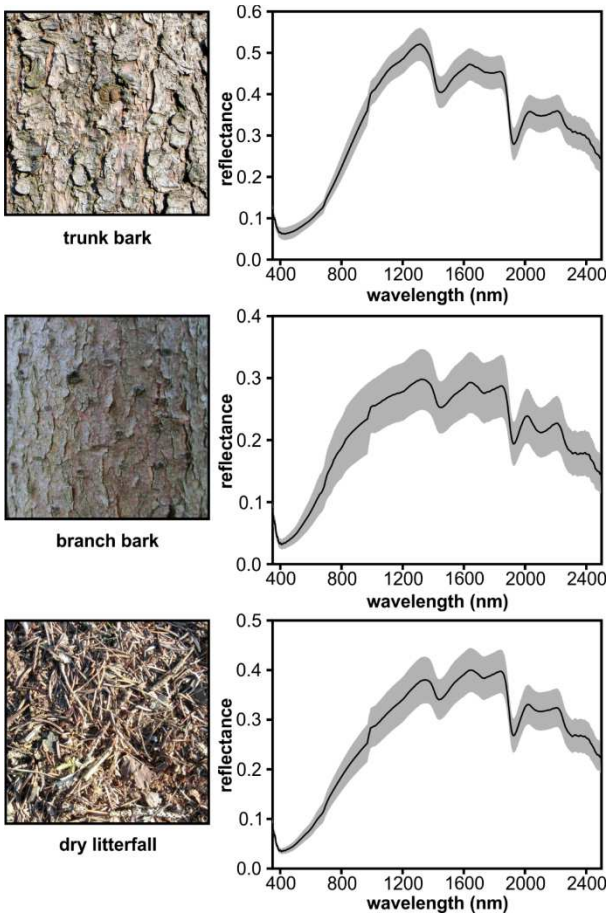

Figure 5.2: *The reflectance spectra (mean ± std.) of Norway spruce trunk bark, branch bark and dry litterfall measured by the SR-2500 spectroradiometer.*

Step 1 – Basic tree architecture:

In the first step, the appropriate values of trunk diameter (DBH), tree height (h), crown height (h_c) and crown diameter (R_c) were defined to describe the basic architecture and morphology of the trees considered in the FRT canopy level model. The DBH value was in-situ estimated during the ground campaigns. The h, and R_c values were derived using the allometric relationships from Widlowski et al. (2003):

$$h = 1.3 + \left(\frac{DBH^2}{0.0317DBH^2 + 0.131DBH + 6.22}\right)$$

$$R_c = \frac{1}{2} \cdot exp\left(0.2195 + 0.2545\ ln(DBH) + 0.009h - 0.6735\ ln\left(\frac{h}{DBH}\right)\right)$$

where: DBH…trunk diameter [cm] and h…tree height [m].

Finally, the following values were considered for the next work: DBH = 30 cm, h = 24 m and R_c = 2.5 m. The crown height was in-situ estimated as 12 m (to be 50 % of the total tree height).

Step 2 – Crown closure:

Crown closure (CRC) is determined from the canopy cover (CAC) value and tree distribution parameter (TDP) using the following formula (Nilson 1999):

$$CRC = \frac{-ln(1 - CAC)}{TDP}$$

where: CRC…crown closure; CAC…canopy cover; TDP…tree distribution parameter.

While the CAC value can be easily derived from the processing of digital hemispherical photography (as in case of this study), tree distribution parameter (TDP) usually remains unknown. The TDP value is closely connected with the Fisher's grouping index – GI (Fisher et al. 1922) describing the spatial tree pattern at the given stand. The GI is calculated as the ratio of the variance of the tree number in a sub-area of a certain size and the average number of trees within this sub-area (Pukkala 1988). Regular tree distribution is represented by GI < 1 while clumped distribution is represented by GI > 1 (Pukkala 1988; Nilson 1999). The influence of the spatial tree patterns on the GI and TDP values can be demonstrated by Figure 5.3.

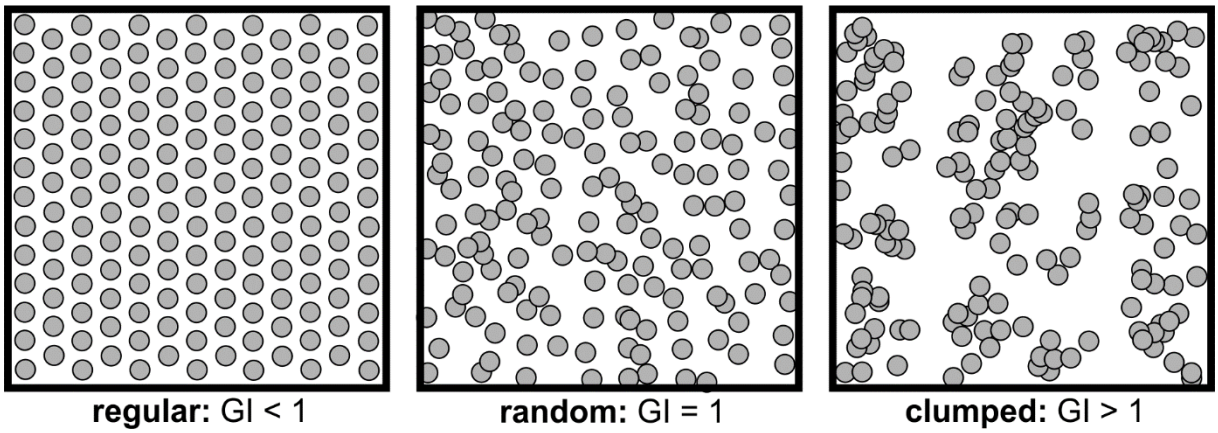

Figure 5.3: *Influence of tree spatial pattern on the Fisher's grouping index (GI). Each of the showed plot consist of 163 trees, however these trees are distributed in different spatial patterns. The left plot represents regular pattern with GI < 1, whereas the right plot shows clumped pattern with GI > 1. The central plot represents random tree pattern that is considered to have GI = 1.*

The TDP is then calculated as (Nilson 1999):

$$TDP = \frac{-\ln(GI)}{1 - GI}$$

Using this formula, it can be demonstrated that TDP > 1 in case of GI < 1 while TDP < 1 in case of GI > 1 (Figure 6.3).

Three scenarios of the FRT model parameterization using different values of tree distribution parameter (TDP = 0.7, TDP = 1.0 and TDP = 1.5) were empirically tested within this study as no exact estimation of the GI value was performed. The best results in terms of the fit between simulated and image-derived spectra was obtained for TDP = 1.5. This value was therefore used for further processing.

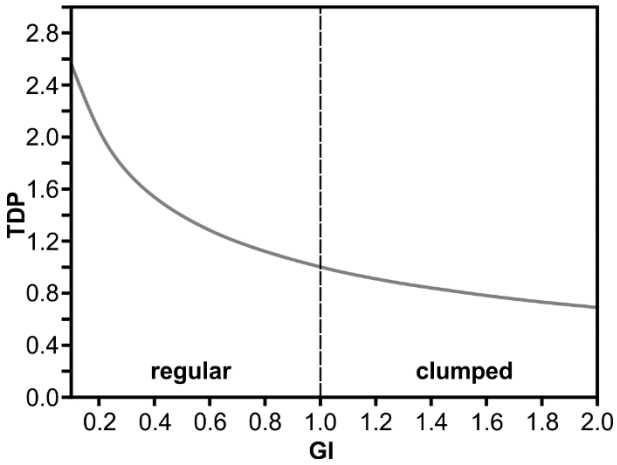

Figure 5.4: *Relationship of the Fisher's grouping index (GI) and tree distribution parameter (TDP) values.*

Step 3 – Stand density:

Vertical crown projections can be considered as circular. The stand density (number of trees per the unit area) can be thus calculated by the following formula using the CRC value determined in the step 1:

$$DEN = \frac{CRC}{\pi R_c^2}$$

where: DEN…stand density [trees/m^2]; CRC…crown closure; R_c…crown diameter [m].

Step 4 – Dry leaf weight:

Dry leaf weight (DLW) defines the total dry leaf biomass weight per tree [kg/tree]. It can be also expressed as:

$$DLW = \frac{LAI \cdot SLW}{DEN \cdot 1000}$$

where: DLW…dry leaf weight [kg/tree]; LAI…leaf area index; SLW…specific leaf weight [g/m^2]; DEN…stand density [trees/m^2].

In case of this study, LAI value was determined from the processing of digital hemispherical photography (DHP) and SLW was measured during the laboratory processing of the collected needle samples (as SLW = 1/SLA). The DEN value was derived in the step 3.

Step 5 – Effective LAI:

In this step, the FRT model was repeatedly run in the forward mode for varying BAI/LAI ratio values (and with fixed values of others parameters). The effective LAI (LAI_e) values obtained as the FRT model output were compared with the LAI_e values extracted from the processing of

DHP for each run to find the most optimal BAI/LAI value producing the LAI_e values with the best fit with the DHP-derived LAI_e. The most optimal solution was found for BAI/LAI = 0.15.

Step 6 – Shoot shading coefficient:

In the last step, the FRT model was repeatedly run in the forward mode with the varying value of the shoot shading coefficient (SSC). The output canopy level simulated spectra were compared with the spectra of the coresponding forest stands derived from the HyMap image datasets. The RMSE between the FRT simulated and HyMap image-derived spectra was calculated for each run. The merit function minimization approach was used to find the most appropriate SSC value (Figure 5.5). The most optimal solution was obtained for SSC = 0.2653 (2009) resp. SSC = 0.2605 (2010). The rounded value SSC = 0.3 was thus used for the further processing.

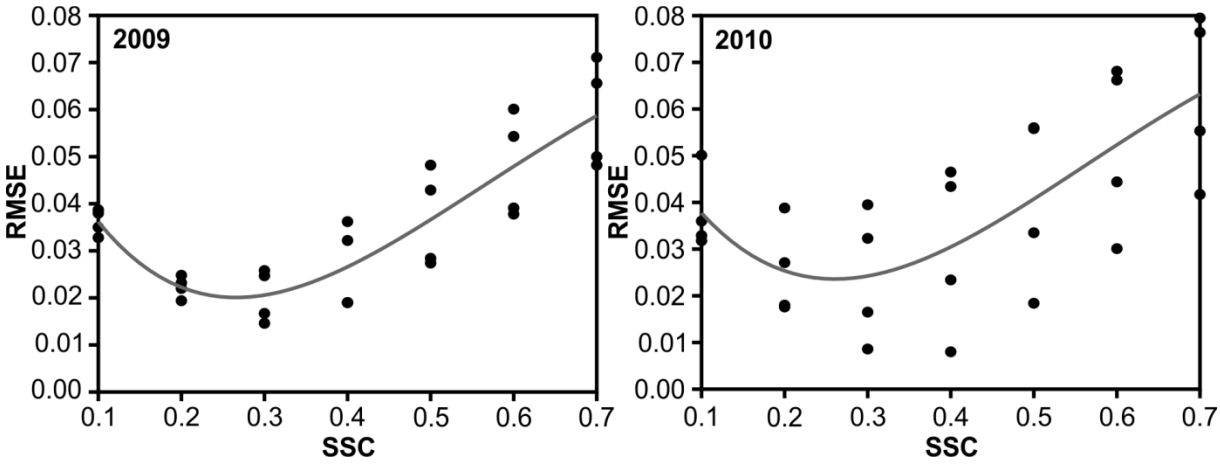

Figure 5.5: *Merit function describing the RMSE between FRT simulated canopy level spectra and HyMap image-derived spectra used to find the most optimal value of the shoot shading coefficient (SSC).*

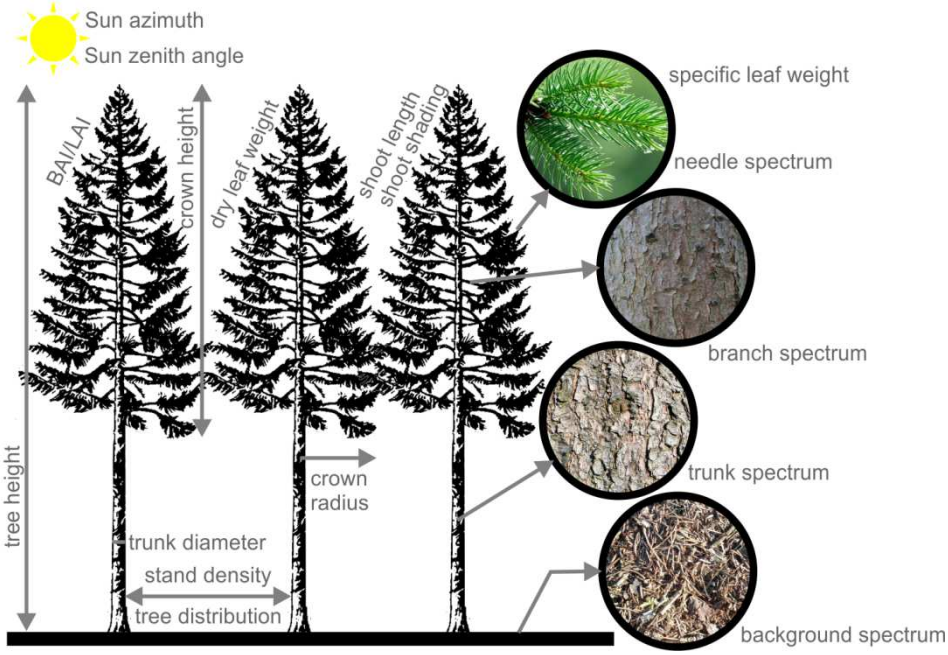

Figure 5.6: *General scheme of the tree/stand parameters used for the FRT model parameterization.*

Table 5.1.: *Parameterization of the FRT canopy level model (FRT input parameters)*

parameter	Erika	Habartov	Studenec	Mezihorská
stand density (DEN) [trees/m^2]	0.0450	0.0436	0.0379	0.0366
tree height (h) [m]	24.0	24.0	24.0	24.0
crown height (h_c) [m]	12.0	12.0	12.0	12.0
crown radius (R_c) [m]	2.5	2.5	2.5	2.5
trunk diameter (DBH) [cm]	30	30	30	30
dry leaf weight (DLW) [kg/tree]	22.19	21.46	29.79	26.30
specific leaf weight SLW [g/m^2]	200	200	200	200
BAI/LAI	0.15	0.15	0.15	0.15
tree distribution parameter (TDP)	1.5	1.5	1.5	1.5
shoot shading coefficient (SSC)	0.3	0.3	0.3	0.3
shoot length (SHL) [m]	0.1	0.1	0.1	0.1
Sun azimuth (A) [°]	66° (2009) 55°(2010)	66° (2009) 55°(2010)	66° (2009) 55°(2010)	66° (2009) 55°(2010)
Sun zenith angle (Z) [°]	33° (2009) 39° (2010)	33° (2009) 39° (2010)	33° (2009) 39° (2010)	33° (2009) 39° (2010)

5.3 Forward FRT simulations

Two version of the canopy level simulation procedure were developed within this study differing by the used leaf level radiative transfer model. The first one using the coupling of the PROSPECT-5 and FRT models was called PRO-FRT whereas the second one, based on coupling of the LIBERTY and FRT models, was called LIB-FRT. Both versions were optimized by the same procedure as described above and then used to simulate the canopy level spectrum for each studied forest stand for both years (2009 and 2010). Note that sun azimuth and zenith angle were set to the values representing real position of the Sun in the time of HyMap data acquisition.

The obtained simulations were resampled into the spectral resolution of the HyMap image data (original spectral resolution of the simulations was 5 nm). The canopy level simulations were finally compared with the HyMap image-derived spectra extracted for the corresponding tree stands by the means of RMSE, $RMSE_S$ and $RMSE_R$ in the similar way as in case of the leaf level simulations assessment (see 4.4).

Chapter 6: Retrieval of semi-quantitative indices of Norway spruce forests from HyMap airborne hyperspectral data

Classification of the HyMap airborne hyperspectral data resulting in a binary mask of mature Norway spruce forests is described first. The main part of this chapter is devoted to retrieval of quantitative and semi-quantitative indices of Norway spruce forests biochemistry and biophysics based on the HyMap airborne hyperspectral imagery using the databases of the simulated canopy level spectra whose preparation was described in the previous two chapters. Sensitivity analysis of the canopy spectral signatures to leaf area index, foliar pigments and water contents is described at the beginning. Quantitative estimation of leaf area index and chlorophyll content is then described and further followed by definition of functional relationships of the selected vegetation indices to chlorophyll content, relative amount of carotenoids and water content. Finally, concept of a statistical model for forest health status assessment is provided. The concept is based on classification of the selected forest characteristics (chlorophyll, relative carotenoids and water contents) relative to the most common values of the given area of interest. This approach is used instead of using any fixed threshold whose definition might be misleading.

6.1 Classification of the HyMap airborne data

Both HyMap 2009 and 2010 datasets were classified to get a mature Norway spruce forests mask. The classification was performed using a hybrid approach including object as well as pixel classification techniques. The classification process consisted of the following steps:

- **Step 1:** HyMap data segmentation using mean-shift segmentation algorithm (mean-shift segmentation of the HyMap imagery was performed in the open-source Monteverdi 2 software based on Orfeo Toolbox). As the segmentation is computationally highly demanding process, only 6 bands of the original dataset were used for segmentation (ca. 450, 550, 650, 800, 1650 and 2200 nm).
- **Step 2:** The segmented image was classified using ten different supervised classification algorithms: ANN-BP-GA (Artificial Neural Network with backpropagation training and Gaussian activation function), ANN-BP-SS (Artificial Neural Network with backpropagation training and Symetrical Sigmoid activation function), ANN-RPROP-SS (Artificial Neural Network with RPROP training and Symetrical Sigmoid activation function), DT (Decision Tree), GBT (Gradient Boosted Tree), KNN (K-nearest neighbours), NB (Normal Bayes), RF (Random Forests), SVM-L (Support Vector Machine with linear kernel) and SVM-P (Support Vector Machine with polynomial kernel). These classifiers

were used to distinguish between vegetated and non-vegetated surface. The given segment was considered as vegetated once it was classified as vegetation in at least 8/10 cases (as ten classification algorithms was used in total). Image classifications were performed in the Monteverdi 2 software.

- **Step 3:** PCA transformation of the original HyMap dataset was performed under the vegetated pixels mask to enhance the spectral differences of particular vegetation types and species. The statistics for PCA calculation were calculated only from vegetated pixels. Note that only first five components (PC_1 – PC_5) were used in the further processing.
- **Step 4:** The PCA transformed image was segmented using the segments defined in step 1. Note that only those segments classified as vegetated were used.
- **Step 5:** The segmented PCA image was classified by the same ten supervised classifiers mentioned in step 2 to separate mature Norway spruce forests from other types/species of vegetation (e.g. young spruce forests, deciduous forests, grass etc.). The given segment was taken into account once it was classified as Norway spruce forest by in at least 6/10 cases. The training data used for the described supervised image classification were based partially on visual interpretation of the HyMap source imagery and high resolution airborne ortophotos as well as on information collected during fieldworks.
- **step 6:** The segments classified as mature Norway spruce forests consisted of both sunlit as well as shadowed pixels. Therefore removal of the shadowed pixels (on pixel-per-pixel classification basis) was performed using a simple maximum likelihood (MLC) classification.

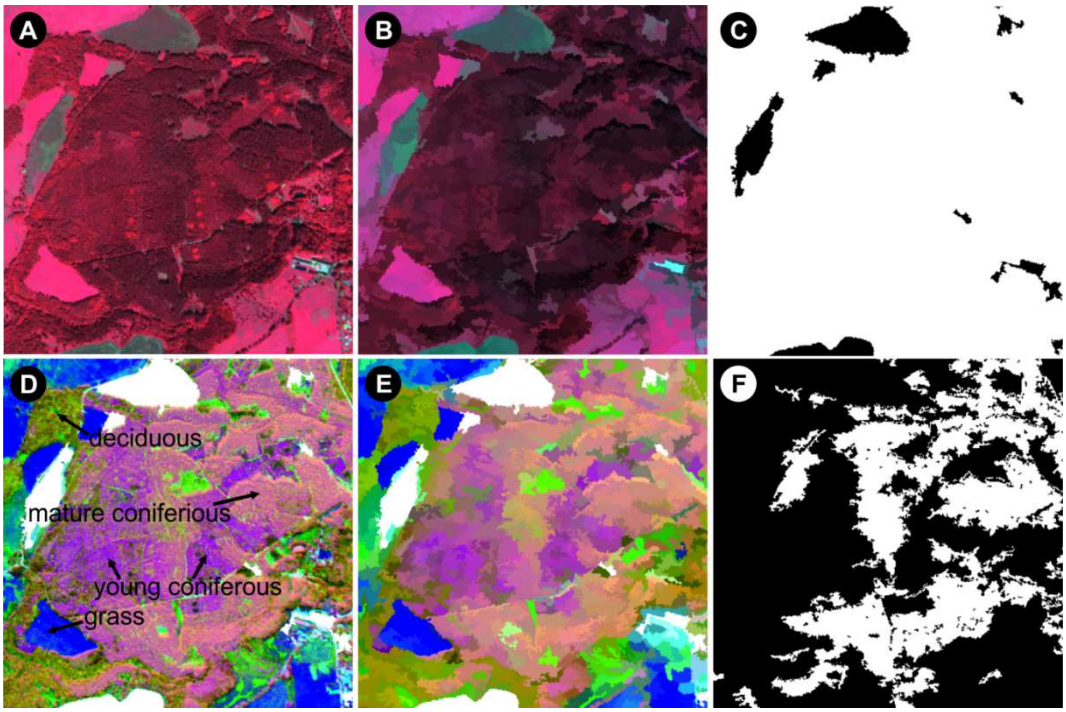

Figure 6.1: *Classification scheme of the HyMap data: original HyMap dataset (A); segmented HyMap dataset (B); vegetation mask (C); PCA calculated from the vegetated pixels (D); segmentation of the PCA transformed image (E); final Norway spruce mask after removal of shadowed pixels (F).*

6.2 Sensitivity analysis

Selection of the most appropriate indicators of vegetation variables of interest was based on sensitivity analysis describing how much is reflectance (resp. its derivatives) in the given spectral band sensitive to variations of the variables of interest.

Sensitivity of canopy level spectrum on variations of the given vegetation parameter was expressed by a simple **sensitivity index (SE)** defined by the following formula (example for LAI):

$$SE_\lambda = \frac{|R_{\lambda\ LAI\ MAX} - R_{\lambda\ LAI\ MIN}|}{LAI_{max} - LAI_{min}}$$

where: SE_λ...sensitivity index for wavelength λ; $R_{\lambda\ LAI\ MAX}$...reflectance at wavelength λ simulated for maximal considered LAI value; $R_{\lambda\ LAI\ MIN}$...reflectance at wavelength λ simulated for minimal considered LAI value; LAI_{max}...maximal considered LAI value; LAI_{min}...minimal considered LAI value.

The sensitivity index values were then relativized to the maximal SE value (SE_{max}) representing the highest sensitive spectral band. **Relative sensitivity index (rSE)** was thus defined as:

$$rSE_\lambda = \frac{SE_\lambda}{SE_{max}}$$

where: rSE_λ...relative sensitivity index for wavelength λ; SE_λ...sensitivity index for wavelength λ; SE_{max}...maximal value of sensitivity index.

The values of relative sensitivity index for the four variables of interest (LAI, C_{ab}, $C_x/(C_x+C_{ab})$ and C_w) are shown in the Figure 6.2.

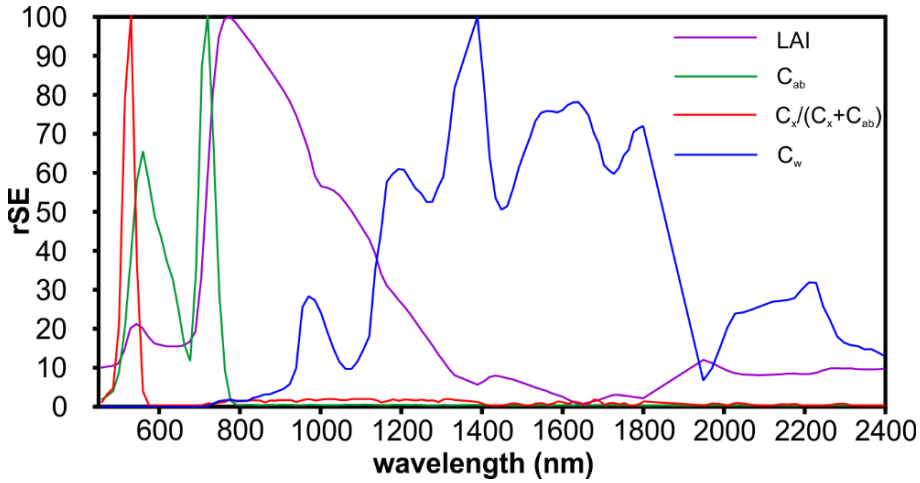

Figure 6.2: *Relative sensitivity index (rSE) calculated from simulated canopy level reflectance for the four vegetation variables of interest (LAI, C_{ab}, $C_x/(C_x+C_{ab})$ and C_w). rSE value of 100 occurs at the band which is the most sensitive to changes in the given vegetation parameter. Sensitivity of all other bands are relativized against the most sensitive one.*

6.3 Leaf Area Index (LAI)

6.3.1 Simulation of the LAI look-up table

Parameterized FRT model (see Chapter 5) was used to simulate canopy level reflectance spectra for various combinations of dry leaf weight (DLW) and tree density (DEN) defining the leaf area index (LAI) to create LAI look-up table (LUT). The relationship of LAI, DLW and DEN see in the part 5.2. The DLW-DEN combinations with the corresponding LAI values used for the FRT simulations see in Table 6.1. Note that all simulations were performed with the fixed leaf/shoot level spectrum on the input which was simulated by the parameterized PROSPECT-5 model (see Chapter 4) using the mean C_{ab}, C_x, C_w and C_m values calculated from the all needle samples collected in the given year. The leaf level PROSPECT-5 simulation was then up-scaled to the shoot level by the procedure described in the part 4.5.

Table 6.1: *LAI values defined as combination of dry leaf weight (DLW) and stand density (DEN) values used for canopy spectra simulation.*

DLW [kg/tree]	DEN [trees/m^2]				
	0.0300	0.0400	0.0500	0.0600	0.0700
10				3.00	3.50
15		3.00	3.75	4.50	5.25
20	3.00	4.00	5.00	6.00	7.00
25	3.75	5.00	6.25	7.50	8.75
30	4.50	6.00	7.50	9.00	10.50

6.3.2 LAI sensitive vegetation indices and LAI estimation

LAI estimation was generally based on derivative analysis. It can be clearly seen that four major peaks of rSE (indicating high sensitivity of spectrum on LAI changes) can be found in simulated derivative canopy level simulated: A (490 – 550 nm), B (645 – 805 nm), C (1270 – 1450 nm) and D (1830 – 1930 nm) – see Figure 6.3. Nevertheless, the D peak was excluded from the further processing as there are no spectral bands in this part of spectrum in case of real HyMap datasets. As so, the four ratios were selected as potential LAI indicators:

$$\frac{D_{529}}{D_{544}}; \frac{D_{733}}{D_{805}}; \frac{D_{748}}{D_{805}}; \frac{D_{1419}}{D_{1290}}$$

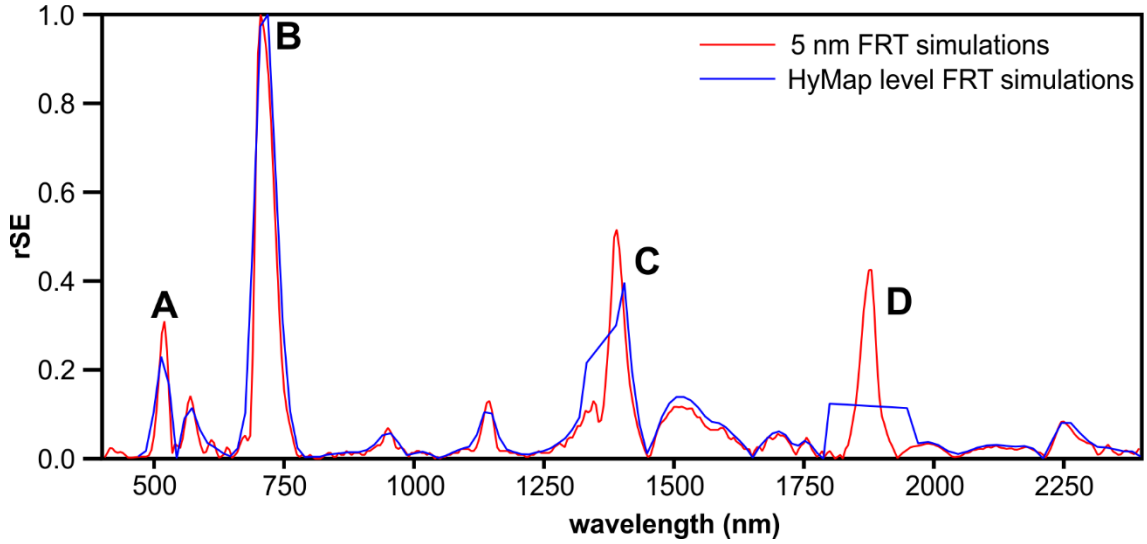

Figure 6.3: *Sensitivity of canopy level spectra to LAI expressed by relative sensitivity index (rSE) for original FRT simulations (5 nm spectral resolution) and FRT simulations transformed to the spectral resolution of HyMap datasets.*

These ratios were calculated from each simulated canopy level spectrum included in the used LUT. Regression models linking the values of the given ratios and the corresponding LAI values were then constructed. D_{733}/D_{805} and D_{748}/D_{805} ratios were finally selected as the most promising LAI indicators due to the highest values of coefficient of determination (R^2). The regression between LAI and D_{733}/D_{805} resp. D_{748}/D_{805} ratios see in Figure 6.4.

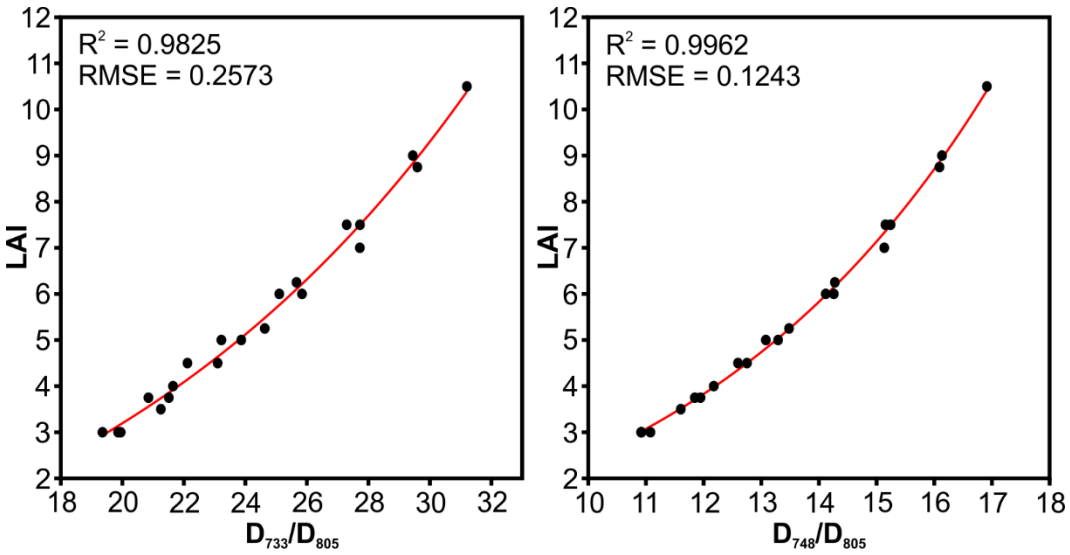

Figure 6.4: *Statistical regressions between the PRO-FRT simulated values of D_{733}/D_{805} and D_{748}/D_{805} indices and LAI values.*

The developed retrieval models were applied on the real HyMap 2009 and 2010 data. However, the D_{733}/D_{805} resp. D_{748}/D_{805} values calculated from the HyMap imagery were not exactly fitting the corresponding values extracted from the PRO-FRT simulations. This was most probably due to a) inaccuracies in spectra simulations (either on leaf or on canopy level) and b) the fact that the values extracted from DHPs (LAI_{DHP}) were considered as true LAI, although they in fact represents plant area index (PAI) values. The predicted LAI_{FRT} values obtained by the

described retrieval models applied on the real HyMap data were therefore underestimated compared to the corresponding in-situ measured LAI_{DHP} values. Thus an empirical transformation was performed to improve the fit between the predicted LAI_{FRT} and measured LAI_{DHP} values.

The performed empirical transformation was based on the assumption that the LAI_{DHP} and LAI_{FRT} values are differing by some systematic offset b as follows:

$$LAI_{DHP} = LAI_{FRT} + b$$

LAI_{FRT} can be then substituted using its relationships to D_{733}/D_{705} and D_{748}/D_{805} indices:

$$LAI_{DHP} = 0.3806e^{0.1074 \cdot D733/D805} + b_1$$

$$LAI_{DHP} = 0.3147e^{0.2080 \cdot D748/D805} + b_2$$

The in-situ LAI measurements were performed in total at 19 stands (see part 2.2). These stands were divided into calibration stands (9: E_1, E_3, H_3, M_1, M_3, M_{5a}, S_1, S_3 and S_5) and validation stands (10: E_2, E_4, E_6, M_2, M_4, M_{5b}, M_6, S_2, S_4 and S_6). The previously mentioned equations were applied for each calibration stand using D_{733}/D_{805} and D_{748}/D_{805} values extracted from real HyMap imagery for b_1 and b_2 varying between 2.0 to 5.0 (0.02 step). The RMSE between the predicted LAI value and the in-situ measured LAI_{DHP} value was calculated for each considered b_1 (resp. b_2) value. The most optimal b_1 and b_2 values were then found using the merit function minimization technique (see Figure 6.5). The LAI retrieval models were thus finally defined by the following formulas using the optimized b_1 and b_2 values:

$$LAI = 0.3806e^{0.1074 \cdot D733/D805} + 3.44 \text{ (2009)}$$

$$LAI = 0.3806e^{0.1074 \cdot D733/D805} + 3.70 \text{ (2010)}$$

$$LAI = 0.3147e^{0.2080 \cdot D748/D805} + 3.80 \text{ (2009)}$$

$$LAI = 0.3147e^{0.2080 \cdot D748/D805} + 3.78 \text{ (2010)}$$

The optimized retrieval models were finally applied on the real HyMap data and the estimated LAI values were compared with the in-situ measured LAI_{DHP} values for the validation stands.

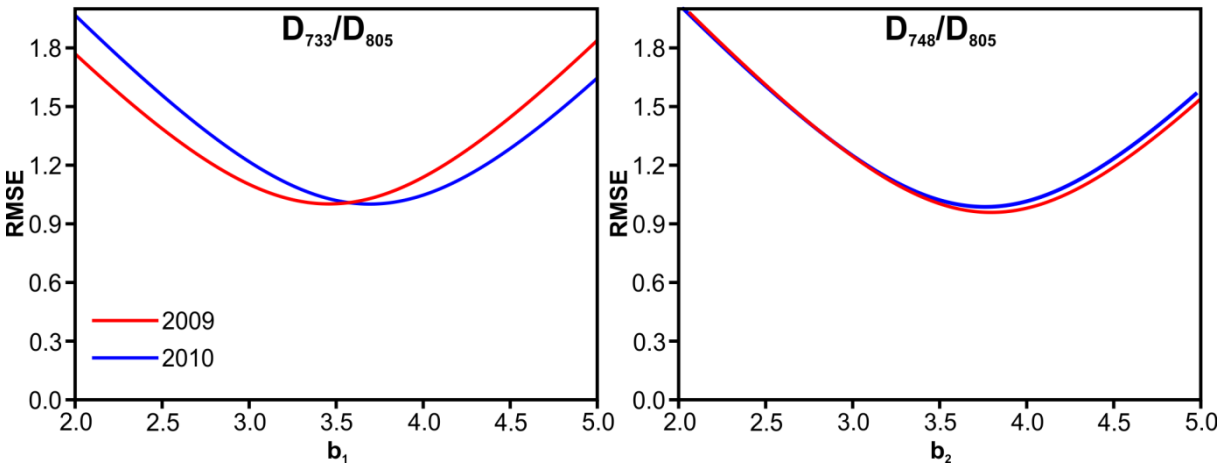

Figure 6.5: *Merit functions used to find the most appropriate b_1 and b_2 values used for the LAI retrieval models optimization.*

6.4 Total chlorophyll content (C_{ab})

6.4.1 Simulation of the C_{ab} look-up-table

The parameterized PROSPECT-5 model (see Chapter 4) was used to simulate spectral properties of Norway spruce needles with C_{ab} ranging from 20 to 80 µg/cm² (step 10 µg/cm²). The other input parameters regarding needle biochemistry were fixed as C_x = 7.0 µg/cm²; C_w = 0.0250 cm and C_m = 0.0200 g/cm². These needle level simulations were transformed to the shoot level using the procedure described in the part 4.5. The shoot level spectra were then up-scaled to canopy level using the FRT model (see Chapter 5). The canopy level simulations were performed with varying DEN and DLW values resulting in different LAI of the simulated forest stands. All the combinations mentioned in Table 6.1 were used resulting in 147 canopy level simulations. The simulated canopy level spectra were finally resampled from the original 5 nm spectral resolution to the spectral resolution of the HyMap datasets.

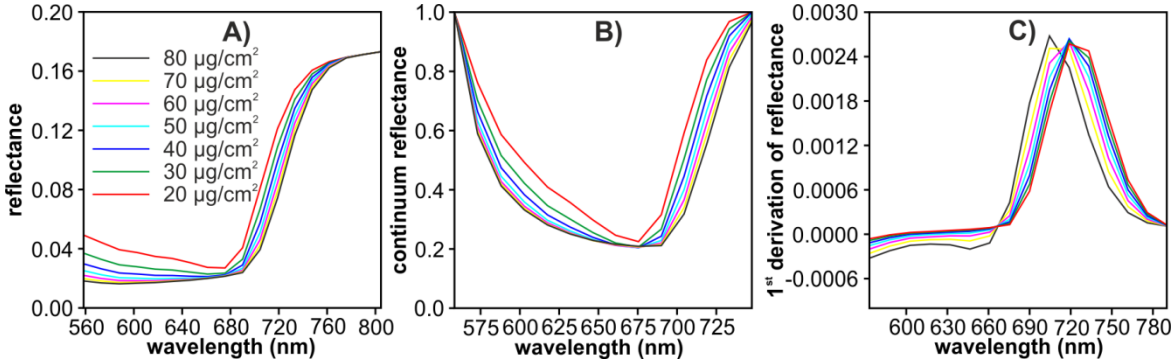

Figure 6.6: *Relationship of the canopy spectral properties (simulated by the PRO-FRT model) and chlorophyll content: A) reflectance, B) continuum removal reflectance, C) 1st derivative of reflectance.*

6.4.2 Chlorophyll sensitive vegetation indices calculated from the simulated reflectance data

The canopy level reflectance spectra simulated for various chlorophyll content values were used to calculate a set of traditional vegetation indices used as chlorophyll content indicators. The calculated values of the vegetation indices were linked with the appropriate chlorophyll content values to construct predictive formulas. As the vegetation indices are calculated mainly from the spectral bands of the red edge region, it should not be forgotten that their values are influenced not only by chlorophyll content itself but also by vegetation structure (e.g. Asner 1998). Therefore a sensitivity analysis of the all considered vegetation indices was performed to select the ones whose sensitivity to changes in vegetation structure (described via LAI) is as minimal as possible. Finally, eight vegetation indices were selected as the most promising chlorophyll content indicators:

Modified Chlorophyll Absorption Reflectance Index/Optimized Soil Adjusted Vegetation Index – MCARI/OSAVI (Haboudane et al. 2002):

$$\frac{MCARI}{OSAVI} = \frac{[(R_{700} - R_{670}) - 0.2(R_{700} - R_{550})] \cdot (R_{700}/R_{670})}{[1.16 \cdot (R_{800} - R_{675})]/[R_{800} + R_{675} + 0.16]}$$

Transformed Chlorophyll Absorption Reflectance Index/Optimized Soil Adjusted Vegetation Index – TCARI/OSAVI (Haboudane et al. 2002):

$$\frac{TCARI}{OSAVI} = \frac{3 \cdot [(R_{700} - R_{670}) - 0.2(R_{700} - R_{550}) \cdot (R_{700}/R_{670})]}{[1.16 \cdot (R_{800} - R_{675})]/[R_{800} + R_{675} + 0.16]}$$

Modified Red Edge Normalized Difference Vegetation Index – mRENDVI (Datt 1999; Sims and Gamon 2002):

$$mRENDVI = \frac{R_{750} - R_{705}}{R_{750} + R_{705} - 2R_{450}}$$

Modified Red Edge Simple Ratio – mRESR (Datt 1999; Sims and Gamon 2002):

$$mRESR = \frac{R_{750} - R_{450}}{R_{705} - R_{450}}$$

Vogelmann Red Edge Index 1 – VOG_1 (Vogelmann et al. 1993):

$$VOG_1 = \frac{R_{740}}{R_{720}}$$

Normalized Reflectance at 718 nm – N_{718} (Campbell et al. 2004):

$$N_{718} = \frac{R_{718} - R_{675}}{R_{747} - R_{675}}$$

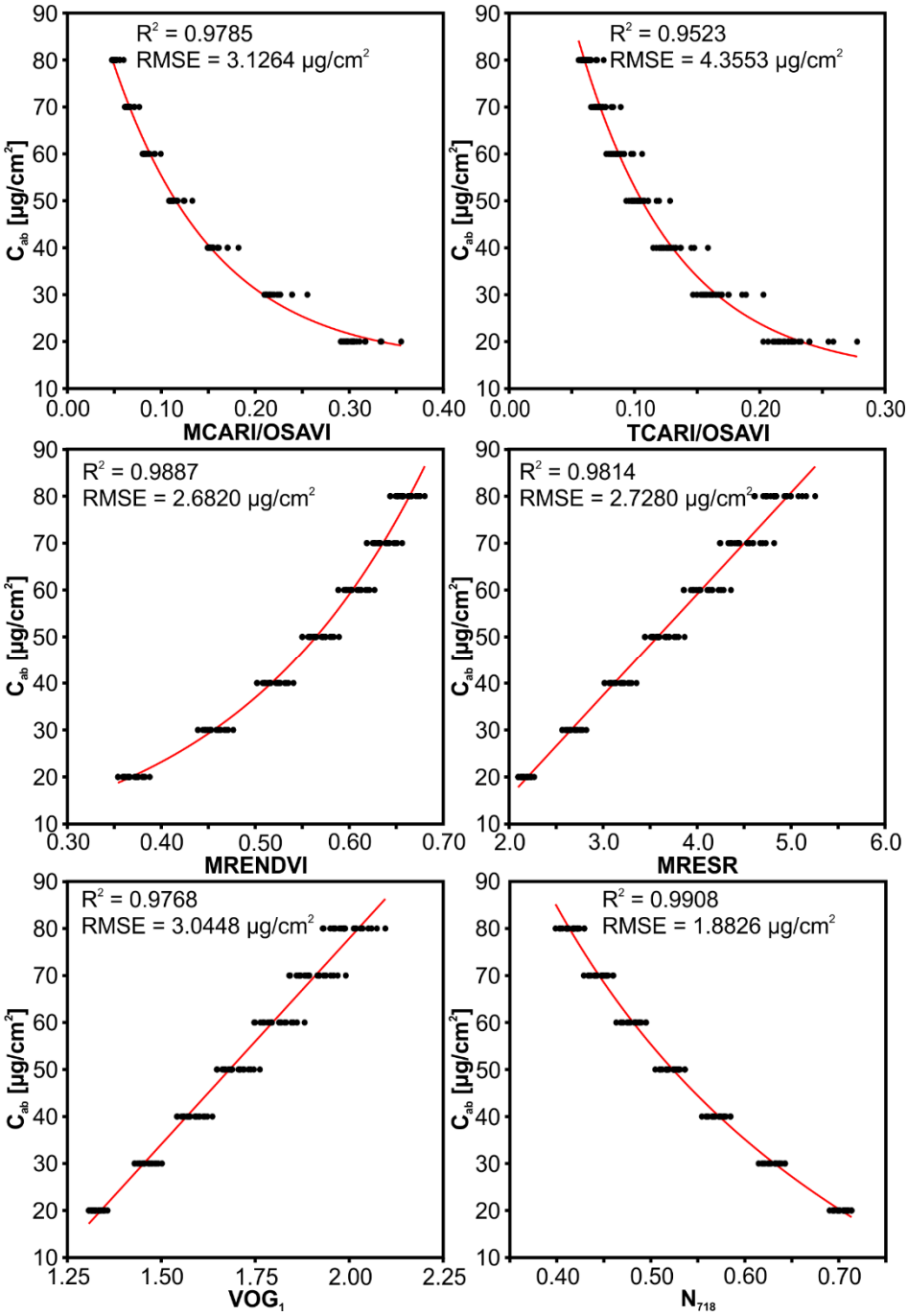

Figure 6.7: *Statistical regressions between the PRO-FRT simulated values of the six chosen vegetation indices (MCARI/OSAVI, TCARI/OSAVI, MRENDVI, MRESR, VOG_1 and N_{718}) and C_{ab} values.*

6.4.3 Chlorophyll sensitive vegetation indices calculated from the simulated continuum removal reflectance data

In addition to the traditional chlorophyll sensitive vegetation indices two measures of chlorophyll absorption feature were extracted from simulated continuum removed canopy level spectra. Absorption feature can be described either by its depth or by the area under the continuum removed reflectance curve (e.g. Kokaly et al. 2009). Both of these measures should generally increase with rising concentration of the absorbing matter. However, as it was reported

by Malenovský et al. (2006), the area under continuum removed curve becomes saturated at chlorophyll content concentration of approximately 60 µg/cm² while the feature depth starts systematically decrease above this C_{ab} concentration value. As so, the authors recommended a new index defined as the chlorophyll content absorption feature area normalized by maximal chlorophyll absorption depth (Area under curve normalized to maximal chlorophyll absorption between 650 – 720 nm: $ANCB_{650-720}$). The index is defined by the following equation:

$$ANCB_{650-720} = \frac{0.5 \cdot \sum(\lambda_{j+1}\lambda_j) \cdot (BD_{j+1} + BD_j)}{BD_{675}}$$

where: λ_j and λ_{j+1}…wavelengths of j-th and j+1th spectral bands; BD_j and BD_{j+1}…band depths of j-th and j+1th bands (as $BD_j = 1 - CR_j$); BD_{675}…band depth at the maximal chlorophyll absorption at 675 nm.

Two versions of this index were used within this study: first calculated from 6 HyMap spectral bands between 647 and 718 nm and second one calculated from 14 HyMap bands between 558 and 747 nm including broader neighbourhood of the core chlorophyll absorption feature. Both indices were then linked with the appropriate chlorophyll content values using exponential regression models (see Figure 6.8)

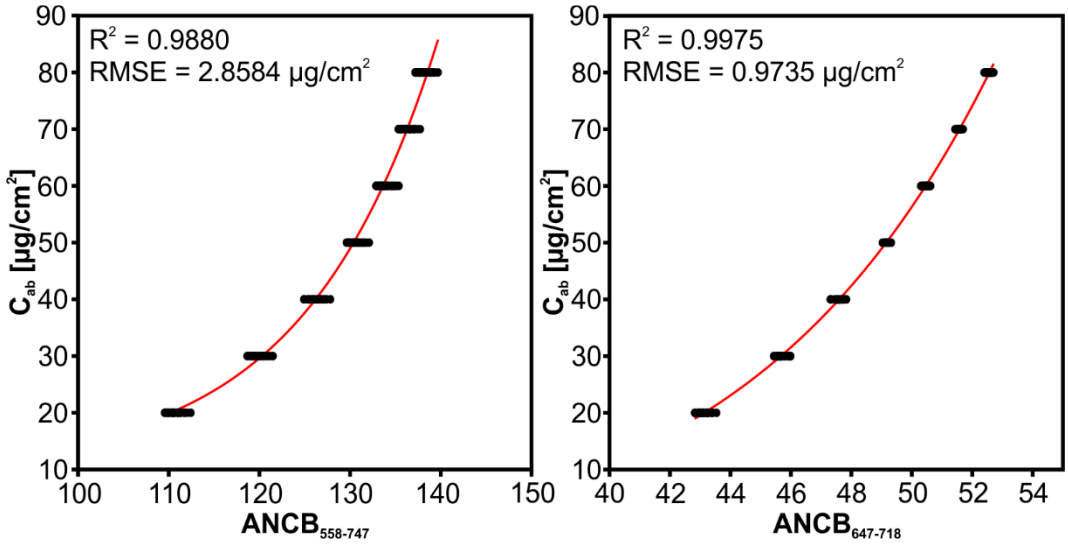

Figure 6.8: *Statistical regressions between the PRO-FRT simulated values of $ANCB_{558-747}$ (left) and $ANCB_{647-718}$ (right) indices and C_{ab} values.*

6.4.4 Chlorophyll sensitive vegetation indices calculated from the simulated 1st derivative of reflectance

Two more vegetation indices were calculated from the 1st derivative of the simulated canopy level spectra:

$$\frac{D_{718}}{D_{704}}; \frac{D_{733}}{D_{675}}$$

The D_{718}/D_{704} index was proposed in Campbell et al. (2004) and its ability to be used as chlorophyll content indicator has been proven many times (e.g. Mišurec et al. 2012; Kopačková et al. 2014; Mišurec 2014). The D_{733}/D_{675} index was defined based on the results of the sensitivity analysis

performed within this study. Relationship of these two indices and chlorophyll content is shown in Figure 6.9.

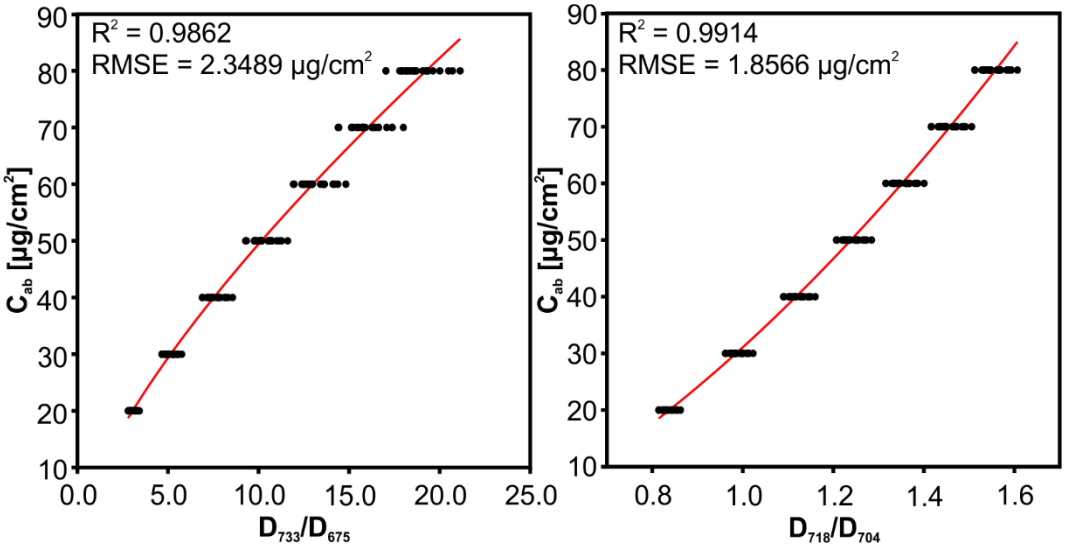

Figure 6.9: *Statistical regressions between the PRO-FRT simulated values of D_{733}/D_{675} (left) and D_{718}/D_{704} (right) indices and C_{ab} values.*

6.5 Relative carotenoids content (C_x/C_x+C_{ab})

6.5.1 Simulation of the C_x/C_x+C_{ab} look-up-table

Similarly as in case of the chlorophyll LUT, the parameterized PROSPECT-5 model was used to simulate needle level spectra. However, in this case two input parameters (C_{ab} and C_x) were changing instead of only one in case of C_{ab} and C_w LUTs preparation. Note that in this case the primary interest is in relative proportion of carotenoids (C_x) on the total amount of foliar pigments (C_x + C_{ab}) rather than in absolute C_x values. This is due to fact that it is quite difficult to strictly separate influence of carotenoids and chlorophylls on the resulting vegetation reflectance in the appropriate spectral domain (mostly VIS-B and VIS-G). Four levels of chlorophyll content were considered: C_{ab} = 20, 40, 60 and 80 µg/cm². For each C_{ab} level the following C_x values were taken into account: C_x = 2, 4, 6 and 8 µg/cm². These combinations of C_{ab} and C_x values cover relative C_x amount ranging from 0.0244 to 0.3333. The two other parameters regarding needle biochemistry remained fixed as C_w = 0.0250 cm and C_m = 0.0200 g/cm². The needle level simulations were transformed to shoot level and then up-scaled to canopy level using the FRT model. Five levels of LAI were considered in this case: LAI = 3.0, 4.0, 5.0, 6.0 and 7.0 which resulted in total in 100 canopy level simulations. The canopy level simulations were finally resampled to the spectral resolution of the HyMap datasets.

6.5.2 Carotenoids sensitive vegetation indices calculated from the simulated reflectance data

Regarding to the results of the performed sensitivity analysis, four indices based on ratio of canopy level reflectance were developed and further tested as the potential $C_x/(C_{ab}+C_x)$ indicators:

$$\frac{R_{558}}{R_{529}}; \frac{R_{558}}{R_{514}}; \frac{R_{573}}{R_{514}}; \frac{R_{573}}{R_{529}}$$

These indices were also tested in normalized difference version:

$$\frac{R_{558}-R_{529}}{R_{558}+R_{529}}; \frac{R_{558}-R_{514}}{R_{558}+R_{514}}; \frac{R_{573}-R_{514}}{R_{573}+R_{514}}; \frac{R_{573}-R_{529}}{R_{573}+R_{529}}$$

Relationship of these vegetation indices and relative carotenoids amount (as simulated by the PRO-FRT model coupling) is shown in Figures 6.10 and 6.11.

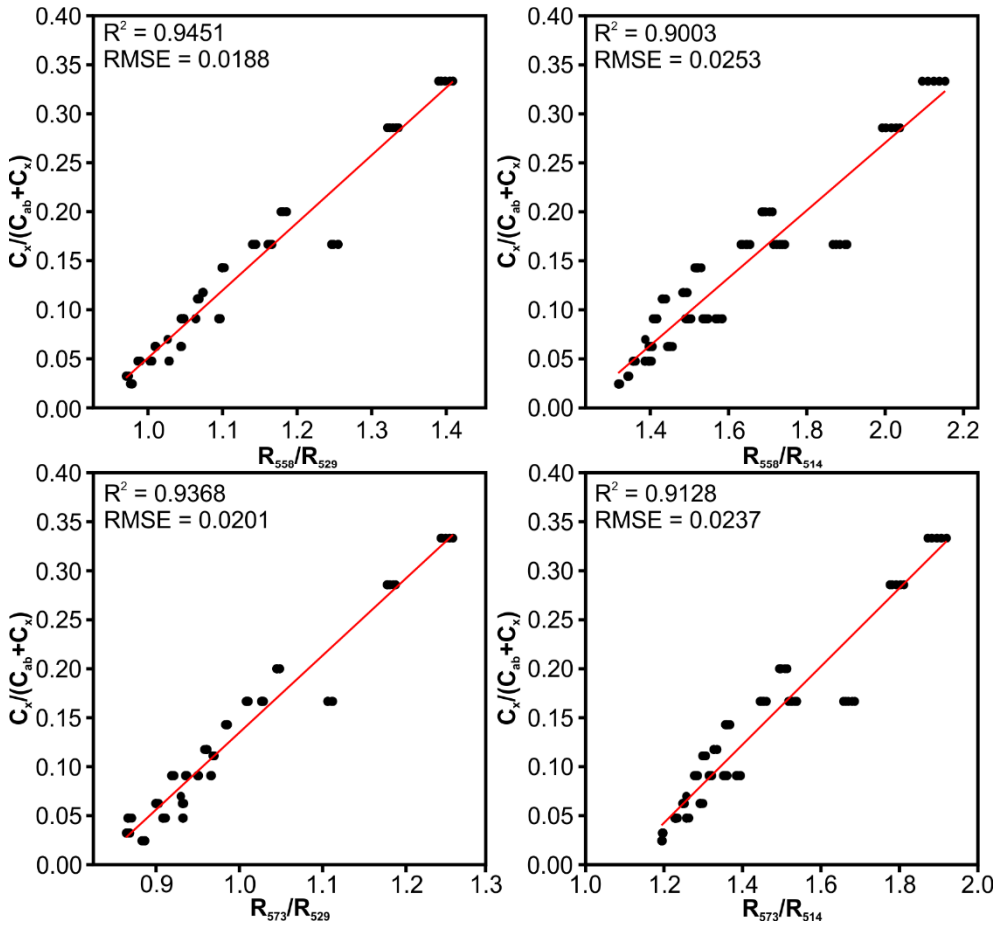

Figure 6.10: *Statistical regression between the PRO-FRT simulated values of the four simple ratio indices and $C_x/(C_{ab}+C_x)$ values.*

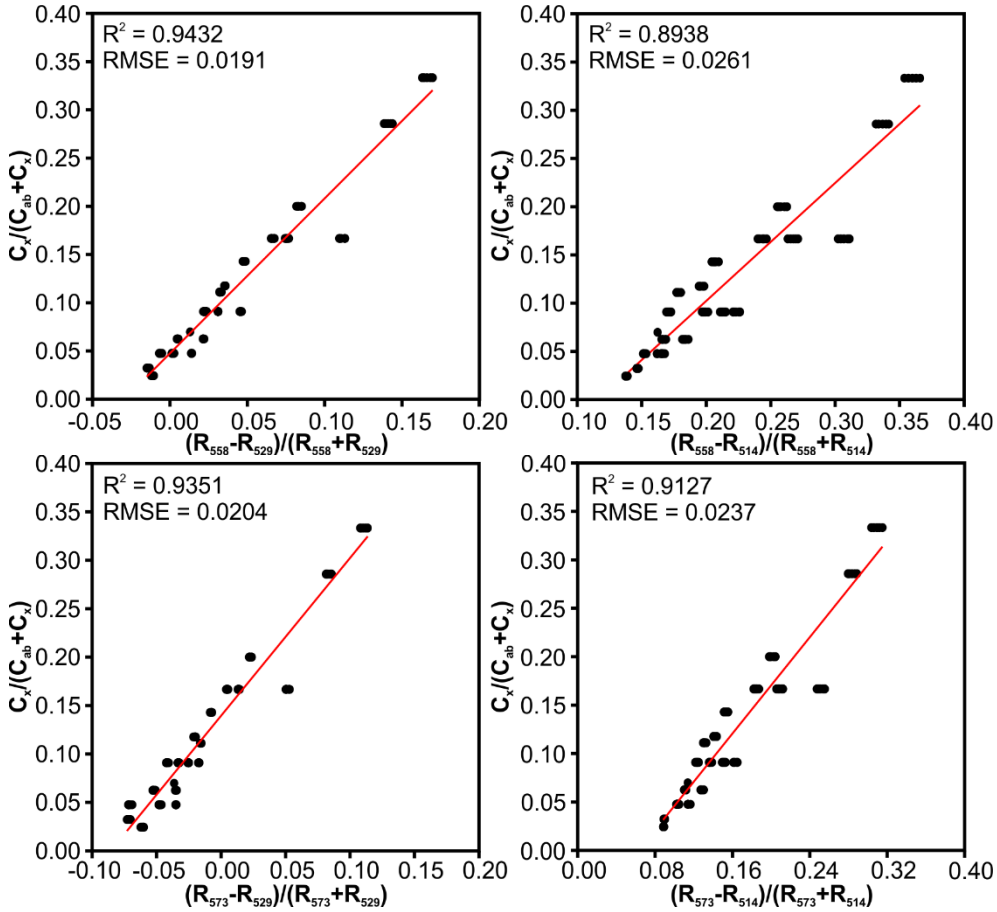

Figure 6.11: *Statistical regression between the PRO-FRT simulated values of the four normalized difference indices and $C_x/(C_{ab}+C_x)$ values.*

6.5.3 Carotenoids sensitive vegetation indices calculated from the simulated 1st derivative of reflectance

Two other carotenoids sensitive vegetation indices based on 1st derivative of canopy level reflectance were developed in addition to those based on simple reflectance ratios (see 6.5.2). The design of these two indices originates in the performed sensitivity analysis (in the same way as in case of the reflectance-based indices). The two derivative-based indices are defined by the following formulas:

$$\frac{D_{514}}{D_{529}}; \frac{D_{514}-D_{529}}{D_{514}+D_{529}}$$

Relationship of these two indices and the relative carotenoids amount ($C_x/C_{ab}+C_x$) as simulated by the PRO-FRT models coupling can be seen in Figure 6.12.

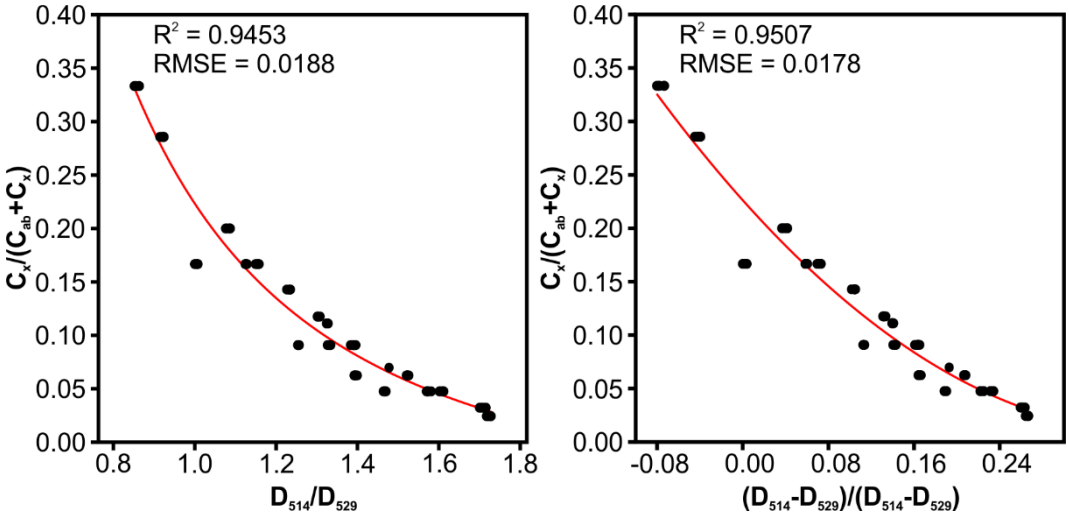

Figure 6.12: *Statistical regressions between the PRO-FRT simulated values of the vegetation indices based on the 1st derivative of canopy level reflectance and $C_x/(C_{ab}+C_x)$ values.*

6.6 Total water content (C_w)

6.6.1 Simulation of the C_w look-up-table

The parameterized PROSPECT-5 model was used to simulate spectral signatures of Norway spruce needles with C_w ranging from 0.0100 to 0.0500 cm (step 0.0050 cm) with fixed values of the all other parameters (C_{ab} = 50 µg/cm², C_x = 7.0 µg/cm² and C_m = 0.0200 g/cm²). The simulated leaf-level spectra were then transformed onto the shoot level and finally up-scaled to canopy level using the parameterized FRT model. The canopy level simulations were performed with varying DEN and DLW parameters (resulting in varying scene LAI). All the combinations mentioned in Table 6.1 were used resulting in 189 canopy level simulations. The simulated spectra were finally resampled to the spectral resolution of the HyMap sensor.

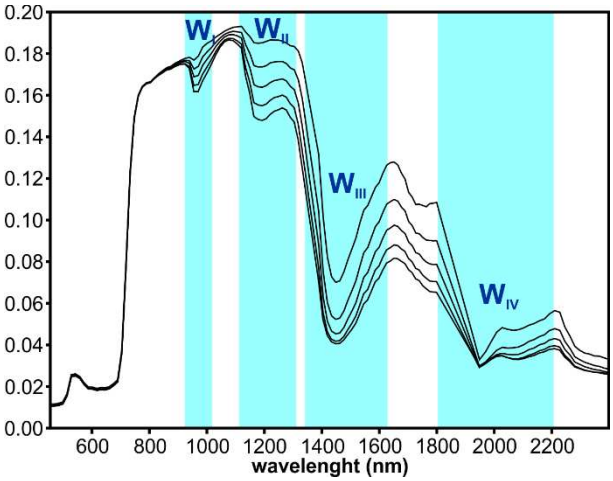

Figure 6.13: *Canopy level reflectance spectrum simulated by the PRO-FRT model coupling for C_w ranging from 0.0100 – 0.0500 cm. Four main water absorption features W_I – W_{IV} are highlighted in blue.*

6.6.2 Water sensitive vegetation indices calculated from the simulated reflectance data

A set of six water sensitive vegetation indices was calculated from the simulated canopy level spectra. This set included the following indices whose relationship to water content is shown in Figure 6.14:

Moisture Stress Index – MSI (Hunt and Rock 1989; Ceccato et al. 2001):

$$MSI = \frac{R_{1600}}{R_{820}}$$

Normalized Difference Infrared Index – NDII (Jackson et al. 2004):

$$NDII = \frac{R_{820} - R_{1650}}{R_{820} + R_{1650}}$$

Normalized Difference Water Index – NDWI (Gao 1996; Chen et al. 2005)[1]:

$$NDWI_{1640} = \frac{R_{860} - R_{1640}}{R_{860} + R_{1640}}$$

Normalized Multiband Drought Index – NMDI (Wang and Qu 2007):

$$NMDI = \frac{R_{860} - (R_{1640} - R_{2130})}{R_{860} + (R_{1640} - R_{2130})}$$

Simple Ratio Water Index – SRWI (Zarco-Tejada and Ustin, 2001):

$$SRWI = \frac{R_{860}}{R_{1240}}$$

Water Band Index – WBI (Peñuelas et al. 1993):

$$WBI = \frac{R_{970}}{R_{900}}$$

[1] Three versions of the NDWI index differing by the used water absorption feature (at 1240, 1640 and 2140 nm) were used.

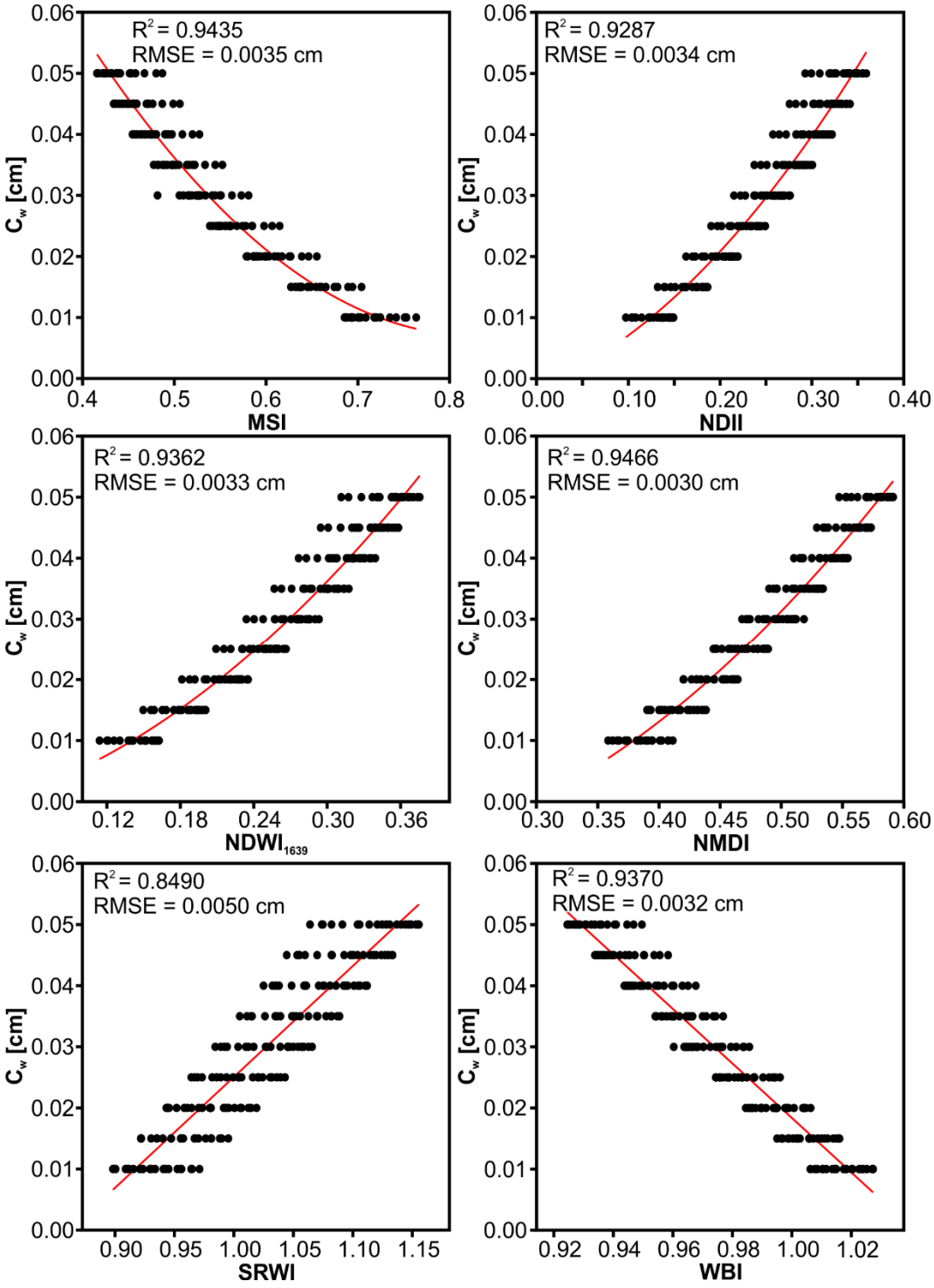

Figure 6.14: *Statistical regressions between the PRO-FRT simulated values of the reflectance vegetation indices and C_w values.*

6.6.3 Water sensitive vegetation indices calculated from the simulated continuum removal reflectance data

As mentioned in theoretical introduction (see part 1.3.1), there are four main water absorption features in the NIR and SWIR domains. These features were labelled as follows: W_I

(920 – 1040 nm), W_{II} (1120 – 1270 nm), W_{III} (1300 – 1650 nm) and W_{IV} (1800 – 2230 nm) – see Figure 6.13. Note that the real HyMap data contain no spectral band between 1799 and 1948 nm, so the W_{IV} feature cannot be used for water content analysis. Behaviour of canopy level spectra in the W_I – W_{III} was tested in detail. First, area of the particular absorption feature (FA) as well as its maximal depth (BD) were calculated and linked to the leaf water content C_w. Strong linear relationship was detected between absorption feature area and C_w as well as between absorption feature maximal depth and C_w in case of W_I and W_{II} absorption features. However, the relationship between absorption feature maximal band depth and leaf water content C_w become saturated for approx. C_w = 0.0300 cm in case of the W_{III} absorption feature. The relationship between W_{III} feature area and C_w have non-linear character showing no signs of saturation until the C_w = 0.0500 cm (higher water content was not simulated). Absorption feature areas were finally normalized by the maximal feature depths, using the same concept as the chlorophyll-sensitive indices $ANCB_{558\text{-}747}$ resp. $ANCB_{647\text{-}718}$. The indices are called as FA/BD W_I, FA/BD W_{II} and FA/BD W_{III}. Relationships of these indices and the C_w have non-linear exponential character showing no signs of saturation (see Figure 6.15)

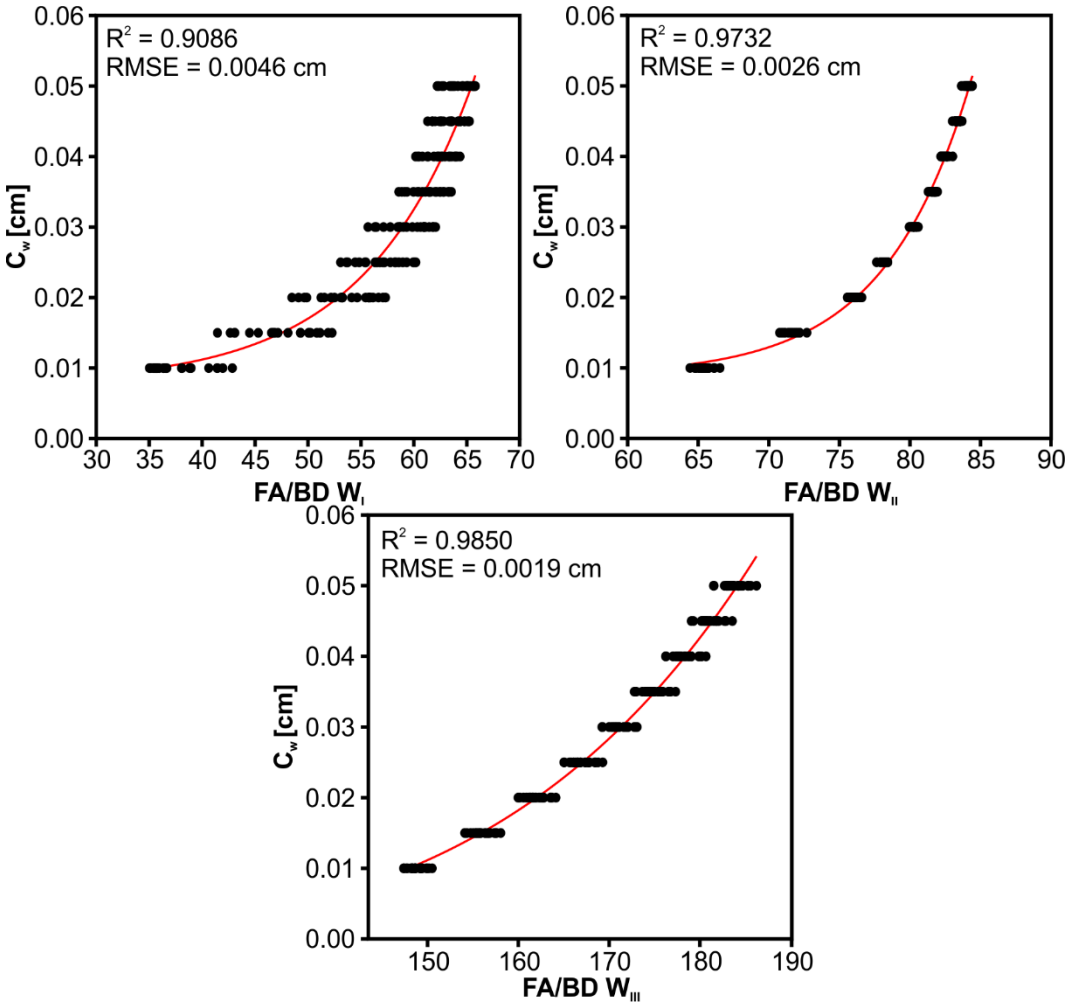

Figure 6.15: *Statistical regressions between the PRO-FRT simulated values of the absorption feature area normalized by its maximal depth calculated for W_I, W_{II} and W_{III} water absorption features and leaf water content C_w.*

6.6.4 Water sensitive vegetation indices calculated from the simulated 1st derivative of reflectance

A set of two ratio indices was calculated from the 1st derivative of the simulated canopy level spectra:

$$\frac{D_{1318}}{D_{1389}}; \frac{D_{1405}}{D_{1389}}$$

The definition of these indices originates in the results of the sensitivity analysis performed within this study. Relationship of these indices and water content is shown in Figure 6.16.

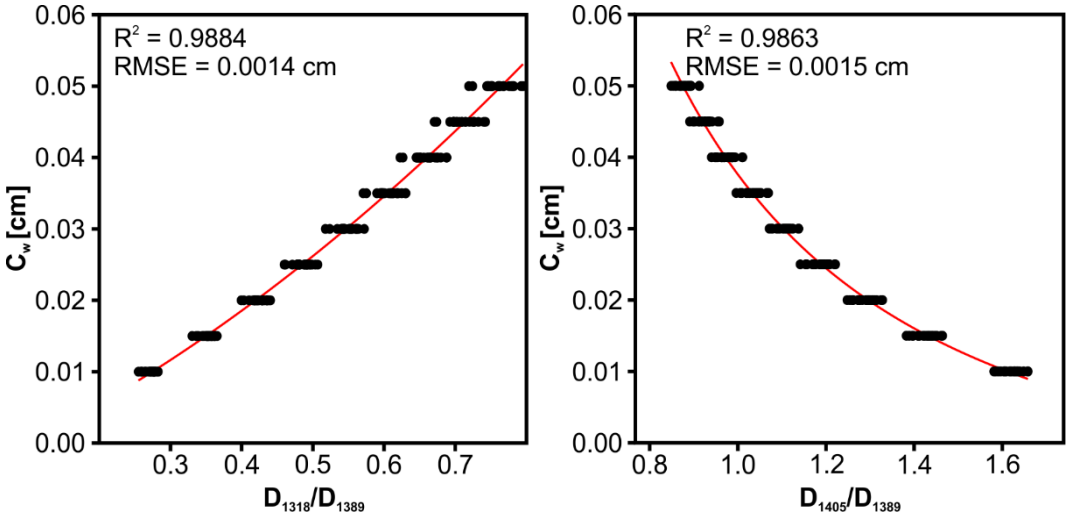

Figure 6.16: *Statistical regression between the PRO-FRT simulated values of the vegetation indices based on the 1st derivative of canopy level reflectance and C_w values.*

6.7 Forest health classification model

The three biochemical parameters (C_{ab}, $C_x/(C_x+C_{ab})$ and C_w) whose relationship to forest canopy reflectance was simulated by the PRO-FRT radiative transfer models coupling were considered as indicators of forest health status. The aim is to develop statistical model allowing complex assessment of the three biophysical parameters instead of analysing them separately. The proposed model should result into a relative classification of forest health status based on the three indicators – i.e. with no use of any fixed thresholds of C_{ab}, $C_x/(C_x+C_{ab})$ and C_w indices.

As it was mentioned in Chapter 1, finding of any "universal" threshold values of the mentioned biochemical parameters indicating vegetation stress is rather complicated as these threshold values are somehow related to the local environmental conditions. In other words, one given value of C_{ab} should indicate vegetation stress in case of one particular stand whereas the same value can be relatively common in case of another locality with different environmental conditions.

In the first step, one spectral indicator (vegetation index) must be selected for each biochemical parameter. Selection of the most appropriate vegetation indices should be based on how tight is the functional relationship between the index and the related biochemical parameter.

The prepared RTM simulations are very helpful for this as they allow simulating relationship of the given index and the related biochemical parameter for sufficient range of values (in contrast with empirical modelling). The R^2 and RMSE values of these simulated relationships can be then used as the indicators of tightness of the relationship between the given index and biochemical parameter (see parts 6.4 – 6.6). It is clear that in case of ideal relationship (i.e. the value of the given vegetation index is determined only by the related biochemical parameter) would be the $R^2 = 1.0$ and RMSE = 0.0. In reality, however, the value of any vegetation index is determined by the related biochemical parameter, but also by the influence of other disturbing factors (like for example LAI, biomass amount, stand density etc.). It could be therefore mentioned that the lowest R^2 and highest RMSE, the strongest influence of the disturbing factors meaning the less suitability of the index for health status assessment. This is also the main reason why the relationships to leaf biochemistry were simulated for relatively high number of indices. There was also another condition for vegetation index selection as the all three vegetation indices entering the forest health status classification model had to be based on the same spectral transformation technique. In other words, when for example the D_{718}/D_{704} vegetation index is chosen as the C_{ab} indicator, then the indices for $C_x/(C_x+C_{ab})$ and C_w have to be selected only from those indices based on the 1st spectral derivative (and not for example on continuum removal transformation).

The selected vegetation indices were transformed from the original values to secure linear relationship between the transformed vegetation indices values and the related biochemical parameters. It also secures that all transformed indices correlate with the related biochemical parameter in positive direction – i.e. the high values of the index represent high values of the biochemical parameter and vice-versa. The RTM simulated relationships were used for the linearization step again. Of course the original values of the selected vegetation indices could be assessed as well, but as it can be seen in the parts 6.4 – 6.6, vast majority of the vegetation indices are related non-linearly to the corresponding biochemical parameters. Moreover, some of the indices correlated in negative direction (high index values represent low values of the corresponding biochemical parameter – for example TCARI/OSAVI, MCARI/OSAVI, MSI, WBI etc.). These two factors could cause difficulties in the following interpretation of the results which is the reason why the described linearization was applied.

The linearized values of the vegetation indices were then normalized into so called Z-scores (or standard scores) to ensure their comparability and independence of their physical dimensions/units.

$$z = \frac{X - \mu}{\sigma}$$

Where: X…given value, μ…mean, σ…standard deviation

Z-scores generally express how far from the mean (μ) the given values is compared to the standard deviation (σ) of the dataset (i.e. z = 2.0 means that the given value is 2σ above the mean).

The values of each particular C_{ab}, $C_x/(C_x+C_{ab})$ and C_w related index were then classified into five classes using the following thresholds: -1.0σ, -0.5σ. +0.5σ and +1.0σ. Very important thing must be highlighted at this point. The C_{ab} and C_w values (and thus the C_{ab} and C_w indicators values

as well[2]) are correlated to the vegetation health status in positive way as high chlorophyll and water contents are usually typical for healthy and prospering vegetation and on the other hand low chlorophyll and water content are typical for damaged vegetation. However, the $C_x/(C_x+C_{ab})$ ratio is correlated with the vegetation health status in negative way – i.e. high $C_x/(C_x+C_{ab})$ values are indicating vegetation stress whereas low $C_x/(C_x+C_{ab})$ indicate non-disturbed vegetation. This fact must be taken into account for classification of the $C_x/(C_x+C_{ab})$ indicators values which must be performed in the reverse direction in comparison with the classification of the C_{ab} and C_w related indices. In other words, Class 1 (representing the values indicating the worst vegetation health status) includes low values of C_{ab} and C_w related indices but high values of $C_x/(C_x+C_{ab})$ related index while Class 5 (representing the values indicating the best vegetation health status) includes high C_{ab} and C_w related indices and low $C_x/(C_x+C_{ab})$ related index. The described classification method can be seen on the scheme illustrated in the Figure 6.17.

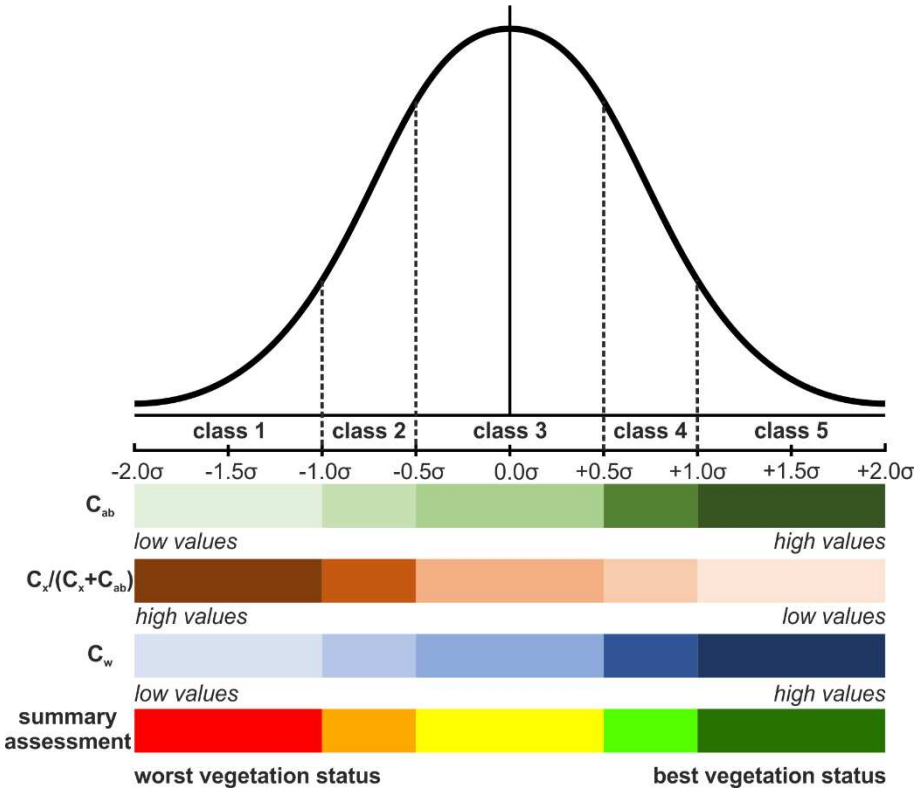

Figure 6.17: *Scheme showing the concept of the proposed health status classification method based on summarization of the particular classifications of the C_{ab}, $C_x/(C_x+C_{ab})$ and C_w related vegetation indices (resp. z-scores calculated from the linearized versions of these indices).*

The classified rasters (ranging from 1 to 5) created by the particular classifications of C_{ab}, $C_x/(C_x+C_{ab})$ and C_w related indices calculated from the real HyMap image data were then summarized to obtain complex information about the vegetation health status. It is assumed that if there are low grades in C_{ab}, $C_x/(C_x+C_{ab})$ and C_w, then the sum of these grades will be also low and vice-versa. The summarized raster values originally ranged between 3 (when C_{ab} grade is 1, $C_x/(C_x+C_{ab})$ grade is 1 and C_w grade is 1) and 15 (when C_{ab} grade is 5, $C_x/(C_x+C_{ab})$ grade is 5 and C_w

[2] The positive direction of the relationship between biochemical parameters and the corresponding indices were secured in the linearization step.

grade is 5). These values were finally linearly rescaled back to the range 1 – 5. The value 1 in the summarized raster thus represents pixels for which there are low values of C_{ab} and C_w related indices and high values of $C_x/(C_x+C_{ab})$ related index. As so, it indicate the worst vegetation health status. On the other hand, the value 5 in the summarized raster represents the pixels for which there are high values of C_{ab} and C_w related indices and low values of $C_x/(C_x+C_{ab})$ related index. Therefore the value 5 indicate the best vegetation health status. The whole workflow can be seen in Figure 6.18.

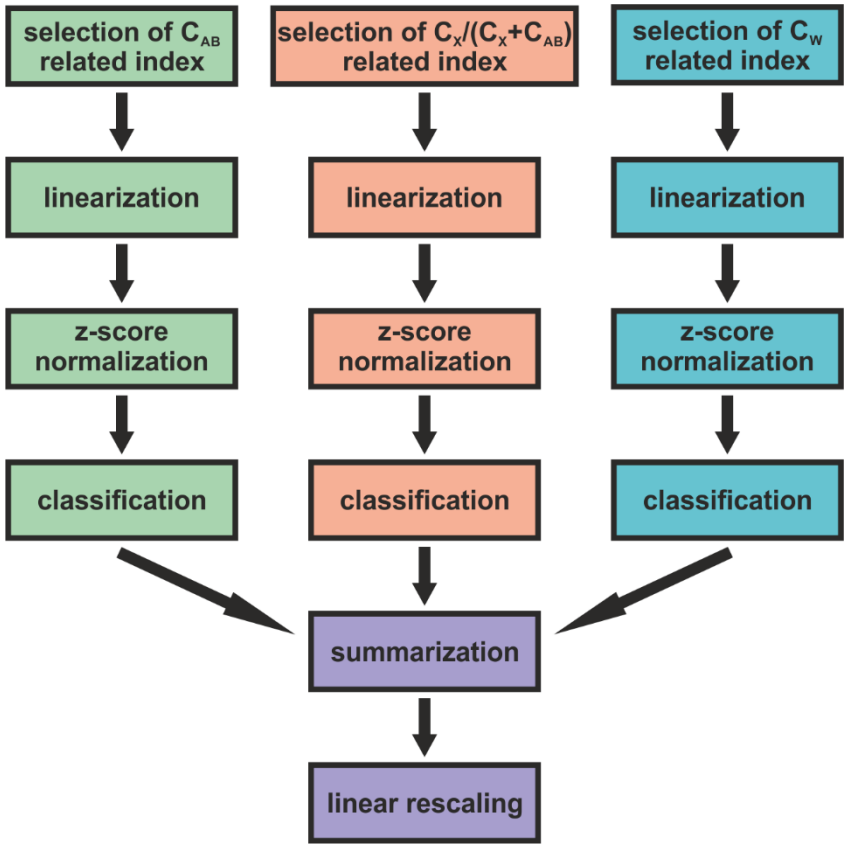

Figure 6.18: *Complete scheme of the proposed forest health status classification based on classification of three vegetation indices related to three vegetation biochemical parameters:* C_{ab}, $C_x/(C_x+C_{ab})$ *and* C_w.

Chapter 7: Results

The chapter provides complete summary of the results obtained from the analyses performed within this study. First, results of laboratory determination of needle biochemistry (foliar pigments and water contents) are described with testing statistical significancy of the differences in needle biochemistry between the particular sampling localities. Next, results of laboratory determination of the selected chemical elements contents in Norway spruce foliage are provided comparing the observed values with the plausible limits reported by the ICP Forests Manual. Results of the collected soil samples laboratory analysis are summarized in the next part of the chapter. The observed soil characteristics are then compared with the values reported by the methodology used for forest soil conditions assessment in the Czech Republic. In addition, the chapter also notices potential linkages between some of the soil variables (e.g. relationship between soil acidity and base cations content or link between soil acidity and mobile aluminium cations etc.). Potential links between soil characteristics and the observed needle chemistry are highlighted as well. Results of the leaf level radiative transfer models parameterization are reported with main focus on potential differences in the optimal values of the models inputs obtained for different needle age classes. Differences in the results of the models parameterization using concept of infinite reflectance instead of single leaf reflectance are also reported. This part is followed by the results of the FRT canopy level radiative transfer model parameterization showing the fit between model simulations and the corresponding HyMap image-extracted spectral signatures of mature Norway spruce forests. The results and validation of leaf area index and chlorophyll content quantitative estimation are reported in the next part of the chapter followed by definition of functional relationships between the selected spectral indices and the corresponsing vegetation biochemical/biophysical variables. The use of these relationships is then demonstrated for assessment of the forest health status using the proposed statistical model. Finally, testing the influence of other factors (like stand elevation, terrain orientation or tree age) on the results of forest health status classification is mentioned at the end of the chapter.

7.1 Leaf biochemical parameters assessment and its relationship to soil chemistry

7.1.1 Biochemical analysis of the collected Norway spruce samples

The Norway spruce needle samples collected during the field campaigns at the reference stands were laboratory analysed to determine the basic biochemical variables: chlorophylls and carotenoids content as well as water content. The samples were collected for two crown levels: upper (U) and lower (L) part of the sunlit crown and two needle age classes: current (1) and current + 2 years (3). Finally, four levels of the Norway spruce needles were distinguished: U_1, U_3, L_1 and L_3. In addition, mean values of U_1, U_3, L_1 and L_3 samples were also taken into account. For details see the section 3.1.

Mean value ± standard deviation was calculated for each sample level and reference stand for both years 2009 and 2010. For each sampled tree, average of the U_1, U_3, L_1 and L_3 samples was also calculated whose means and standard deviations were then added into the analysis (see Table 7.1). Kruskal-Wallis test was applied to the original values to explore whether there are statistically significant differences in needle biochemistry amongst the reference stands. The Kruskal-Wallis test was used because it has no a-priori assumptions on the input data in contrast with ANOVA (assuming normal distribution of the values and the same variance of the values at the compared stands). To avoid problems arising from not complying of these assumptions, the Kruskal-Wallis test was used for the analysis. Results of this test were expressed in the form of the p-value.

As it can be seen in the Table 7.1 the question of possible differences in needle biochemistry amongst the reference stand cannot be clearly answered as for some sample levels significant differences were detected whereas no significant differences were detected for others. Boxplot charts for the MEAN values (mean of the U_1, U_3, L_1, L_3 sample levels) were constructed to help interpretation of the results (see Figure 7.1).

No statistically significant differences in chlorophyll content were found for the samples collected in 2009. However, this result is primarily caused by the high variability of the values observed at Erika stand which is more than twice higher in comparison with the other stands. The median values were almost the same for Erika and Habartov stands. The median of Studenec is very slightly above the level of these two stands whereas Mezihorská show the lowest value. Very similar pattern can be seen in 2010 where Erika and Habartov are quite similar (median of Habartov is a bit higher) with remarkably lower value for Mezihorská and the highest value for Studenec. In contrast with 2009, the observed differences are statistically significant in 2010 – mostly due to the fact that variances of the values are much similar in this case then they were in 2009.

Similar patterns for 2009 and 2010 can be seen also for the relative carotenoids content which is generally highest at the Erika stand whereas the lowest median values can be observed for the Studenec site. Habartov and Mezihorská are quite similar with slightly higher value for Mezihorská stand (this is more remarkable in case of 2010). Water content seems to be the biochemical variable most susceptible to inter-annual changes as the pattern observed in 2009 is seriously different from that observed in 2010. In 2009, Mezihorská stand showed significantly higher needle water content whether the lowest median value was observed in case of Studenec. Erika and Habartov showed similar values (slightly higher for Erika) between the levels for Mezihorská and Studenec. Nevertheless, in 2010, two couples of sites with similar values can be observed. Erika and Studenec are on practically equal level which is higher than the level observed in case of Mezihorská and Habartov stands.

Table 7.1: *Summary of the laboratory biochemical analysis of the collected Norway spruce samples. Four levels of samples were analysed: U_1, U_3, L_1 and L_3 with taking into account also the mean across these four sample levels (MEAN). Mean ± std. were calculated for each reference stand (Erika, Habartov, Mezihorská and Studenec) for both years 2009 and 2010. The original values of the biochemical variables of interest were compared using the Kruskal-Wallis test to explore statistical significance of possible differences between the reference stands. Results of this test is expressed by the p-value. The cases where statistically significant difference was observed are in bold (for 95% significance level).*

Parameter	Needle age class	Year	p-value	Erika	Habartov	Mezihorská	Studenec
C_{ab} [µg/cm^2]	U_1	2009	0.3127	29.72±12.37	33.21±5.75	29.18±5.09	30.98±5.02
		2010	**0.0209**	32.30±6.39	36.57±6.88	29.49±5.10	35.78±5.04
	U_3	2009	0.0505	62.55±28.04	58.41±14.88	47.44±10.36	61.26±6.94
		2010	**0.0276**	58.91±9.99	58.14±13.00	50.04±7.33	61.67±9.24
	L_1	2009	0.5558	47.47±27.06	39.58±11.02	34.23±10.18	40.56±6.51
		2010	**0.0003**	39.83±5.22	43.66±6.88	33.38±4.96	46.48±12.07
	L_3	2009	0.4835	68.36±18.68	69.92±18.15	62.64±10.80	65.09±11.87
		2010	**0.0011**	61.93±13.47	63.85±12.35	52.06±7.53	67.37±6.53
	MEAN	2009	0.0723	52.61±16.64	50.68±12.30	43.23±4.93	49.47±4.73
		2010	**<0.0001**	48.24±7.37	50.55±8.01	41.10±4.26	52.82±5.60
$C_x/(C_x+C_{ab})$	U_1	2009	0.1957	0.1258±0.0092	0.1186±0.0042	0.1189±0.0067	0.1175±0.0051
		2010	0.4338	0.1374±0.0111	0.1362±0.0090	0.1377±0.0087	0.1319±0.0101
	U_3	2009	**0.0119**	0.1269±0.0058	0.1256±0.0072	0.1275±0.0067	0.1184±0.0066
		2010	**0.0032**	0.1367±0.0065	0.1310±0.0088	0.1320±0.0067	0.1244±0.0037
	L_1	2009	0.1208	0.1232±0.0072	0.1158±0.0062	0.1179±0.0096	0.1147±0.0050
		2010	**0.0104**	0.1334±0.0039	0.1323±0.0074	0.1389±0.0084	0.1285±0.0070
	L_3	2009	**0.0142**	0.1245±0.0029	0.1215±0.0055	0.1229±0.0058	0.1182±0.0034
		2010	**0.0002**	0.1364±0.0051	0.1253±0.0076	0.1313±0.0074	0.1218±0.0060
	MEAN	2009	**0.0097**	0.1252±0.0054	0.1206±0.0043	0.1216±0.0055	0.1172±0.0038
		2010	**0.0027**	0.1360±0.0059	0.1312±0.0053	0.1351±0.0063	0.1267±0.0048
C_w [cm]	U_1	2009	**0.0025**	0.0211±0.0024	0.0216±0.0015	0.0237±0.0028	0.0204±0.0025
		2010	0.7232	0.0253±0.0006	0.0251±0.0006	0.0251±0.0009	0.0253±0.0009
	U_3	2009	**0.0223**	0.0217±0.0016	0.0218±0.0017	0.0235±0.0017	0.0216±0.0018
		2010	**0.0063**	0.0259±0.0008	0.0249±0.0011	0.0256±0.0010	0.0264±0.0007
	L_1	2009	**0.0071**	0.0225±0.0039	0.0238±0.0033	0.0269±0.0036	0.0223±0.0029
		2010	0.2735	0.0290±0.0007	0.0284±0.0005	0.0284±0.0010	0.0283±0.0013
	L_3	2009	0.1224	0.0250±0.0031	0.0240±0.0027	0.0262±0.0044	0.0226±0.0034
		2010	0.4234	0.0264±0.0010	0.0260±0.0010	0.0262±0.0013	0.0268±0.0013
	MEAN	2009	**0.0045**	0.0226±0.0023	0.0228±0.0016	0.0251±0.0025	0.0217±0.0017
		2010	0.0739	0.0266±0.0006	0.0261±0.0005	0.0263±0.0008	0.0267±0.0006

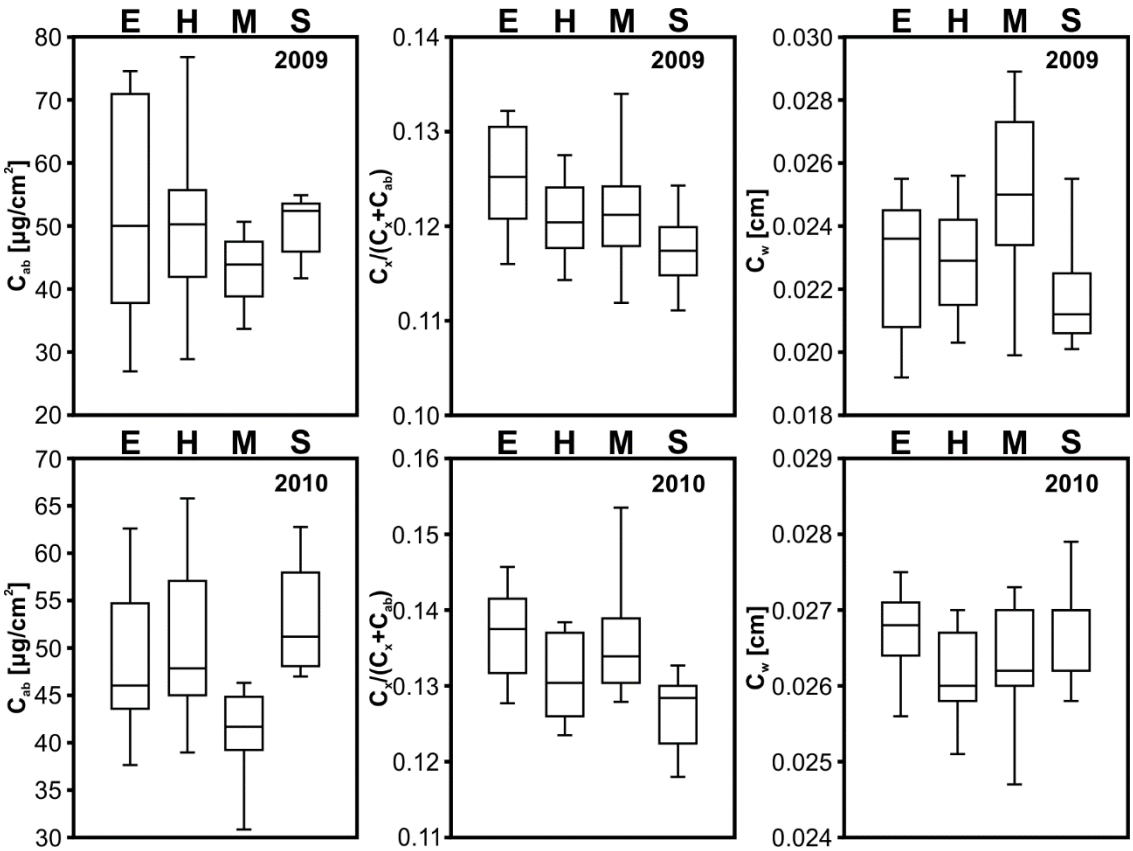

Figure 7.1: *Boxplots for the means of U_1, U_3, L_1 and L_3 sample levels constructed for the biochemical variables of interest (C_{ab}, $C_x/(C_{ab}+C_x)$ and C_w) for both years 2009 and 2010. E – Erika, H – Habartov, M – Mezihorská, S – Studenec.*

7.1.2 Element analysis of the collected Norway spruce needle samples

Foliar analysis was conducted for the collected Norway spruce needle samples in addition to biochemical analysis (see 7.1.1) to determine concentration of certain chemical elements. Selected nutrient elements (Mg, Ca, Na and K) were analysed together with heavy metals (Cu, Zn and Hg) and Aluminium (Al). Mean ± standard deviation was calculated for each element and stand for both years 2009 and 2010 (see Table 7.2).

The values observed for the samples collected at the reference stands were then compared with the limits defined within the framework of the ICP Forests programme (ICP Forests Manual, Part XII: Sampling and analysis of needles and leaves). Nevertheless, these limits are defined as 5 and 95 percentiles of the values determined from samples collected across all Europe having no direct link to vegetation health/damage. Since that, the values outside these limits can be understood as "very unusual", which does not automatically mean that vegetation is damaged. Low needle contents of the nutrient elements can be an indicator of inadequate mineral nutrition which can finally lead to weakening of vegetation against external stressors like imissions etc. On the other hand, high contents of some elements can be indicator of intoxication by the given element or show influence of imission load. Note that ICP limits determined specifically for Norway spruce (current needle age class) were taken into account for this analysis. In addition, boxplots were constructed for those elements for which the ICP limits have been referred (i.e. Cu,

Zn, Mg, Ca and K) together with Al (see Figure 7.2). Such in case of leaf biochemistry, Kruskal-Wallis test was applied to prove statistical significance of possible differences in foliar elements content between the sampled reference stands. The reason of using the Kruskal-Wallis test instead on ANOVA is the same as in the previous analysis – i.e. no a-priory assumptions on statistical distribution and variance of the data (which might not to be fulfilled in some cases).

First, the main problem related to the obtained results of foliar element content is the fact that there are quite high inter-annual changes between 2009 and 2010. This can be observed especially in case of Zn, Mg and Ca. The reason of these inter-annual changes are unknown to the author, but they generally complicate interpretation of the results. On the other hand, concentrations of some other elements were stable, such as in case of Cu which stayed within the interval defined by the ICP limits for all time. Relatively highest values were observed for Studenec, whereas the lowest values occurred at Mezihorská. Zn exhibits the mentioned high inter-annual changes where the observations from 2010 are generally lower than the ones from 2009. Nevertheless, the relative pattern of the reference stands remained the same with the highest values at Studenec and lowest values at Mezihorská. The majority of the measurements from 2009 exceeded the ICP limits in case of Studenec whereas some of the measurements from Erika and Mezihorská were below the limit in 2010. No ICP limits heve been defined for Al, however, regarding the results of soil analyses it is considered as an important element. It can be seen that the reference stands are divided into two groups regarding the Al foliar content where significantly higher values can be seen at Erika and Habartov sites whereas lower contents are observed in case of Mezihorská and Studenec. This pattern was the same for both years 2009 and 2010. Mg is another element where high inter-annual changes of the observed values can be observed. The mean values were very similar in 2009 (no statistically significant differences were detected) with remarkably higher variability of the values for Habartov site (almost twice higher than in case of the other stands). The values in 2010 dropped in compare with the 2009 level. Erika, Habartov and Studenec sites remained similar in relative comparison whereas Mezihorská site exhibited significantly lower values (some samples of Mezihorská and Studenec showed below-limit values). The most confusing situation can be registered in case of Ca where dramatic inter-annual values changes can be seen. Generally, the lowest Ca content was observed in case of Erika and Mezihorská (with significant majority of below-limit measurements in 2010), whereas the highest Ca content values were observed at Habartov in 2009 (with some over-limit values). However, the values dropped significantly in 2010 and became comparable with the level observed at Studenec. On the other hand, stable pattern can be seen in case of K content which remained very similar in both years with slightly lower values in case of the Mezihorská stand (in relative comparison with the other stands). However, the K content values exhibited remarkably high variability covering almost entire interval defined by the ICP limits (with some over- and below-limit measurements).

Table 7.2: *Results of laboratory chemical element analysis of the Norway spruce samples collected at the reference stands Erika, Habartov, Mezihorská and Studenec. Limit refers to the low and high limit values referred by the ICP Forests programme. Significance of possible differences amongst the reference stands was tested using the Kruskal-Wallis test (p-value). Cases where significant difference was detected are in bold.*

Element	Limit	Year	p-value	Erika	Habartov	Mezihorská	Studenec
Cu	1.41	2009	**0.0411**	3.10±0.42	3.16±0.36	2.86±0.27	3.35±0.43
[mg/kg]	5.94	2010	**<0.0001**	2.75±0.30	3.11±0.38	2.50±0.22	3.15±0.29
Zn	16.0	2009	**<0.0001**	30.38±7.35	39.75±8.45	27.81±6.78	50.04±5.10
[mg/kg]	47.0	2010	**<0.0001**	22.70±6.57	31.80±6.78	18.43±4.42	39.80±5.90
Al		2009	**<0.0001**	96.20±12.26	110.07±23.57	74.40±16.31	70.90±15.90
[mg/kg]		2010	**<0.0001**	84.03±10.21	96.30±14.26	64.99±8.14	65.20±17.60
Mg	650	2009	0.2111	1160.00±92.95	1210.00±191.76	1112.00±114.74	1088.00±110.80
[g/kg]	1560	2010	**0.0026**	792.00±105.43	860.00±156.50	664.29±130.15	828.00±123.60
Ca	1830	2009	**<0.0001**	2555.00±795.74	5708.00±1124.80	2767.33±890.23	4305.00±758.37
[g/kg]	7010	2010	**<0.0001**	1446.00±468.43	3530.00±726.31	1525.71±485.63	2827.00±383.98
Na		2009	0.0754	21.40±12.49	17.00±9.80	13.67±11.65	22.80±12.64
[mg/kg]		2010	**<0.0001**	46.30±5.35	40.03±1.74	44.30±2.86	39.69±2.73
K	3650	2009	0.1749	6323.00±1232.92	5994.67±1276.30	5194.00±1184.17	5923.00±944.31
[g/kg]	8360	2010	**0.0034**	6370.00±783.63	6003.33±1397.06	4763.57±994.93	5548.00±873.85
Hg		2009	**0.0005**	0.0187±0.0053	0.0191±0.0033	0.0219±0.0082	0.0257±0.0021
[ppm]		2010	0.0715	0.0173±0.0024	0.0181±0.0033	0.0154±0.0020	0.0185±0.0035

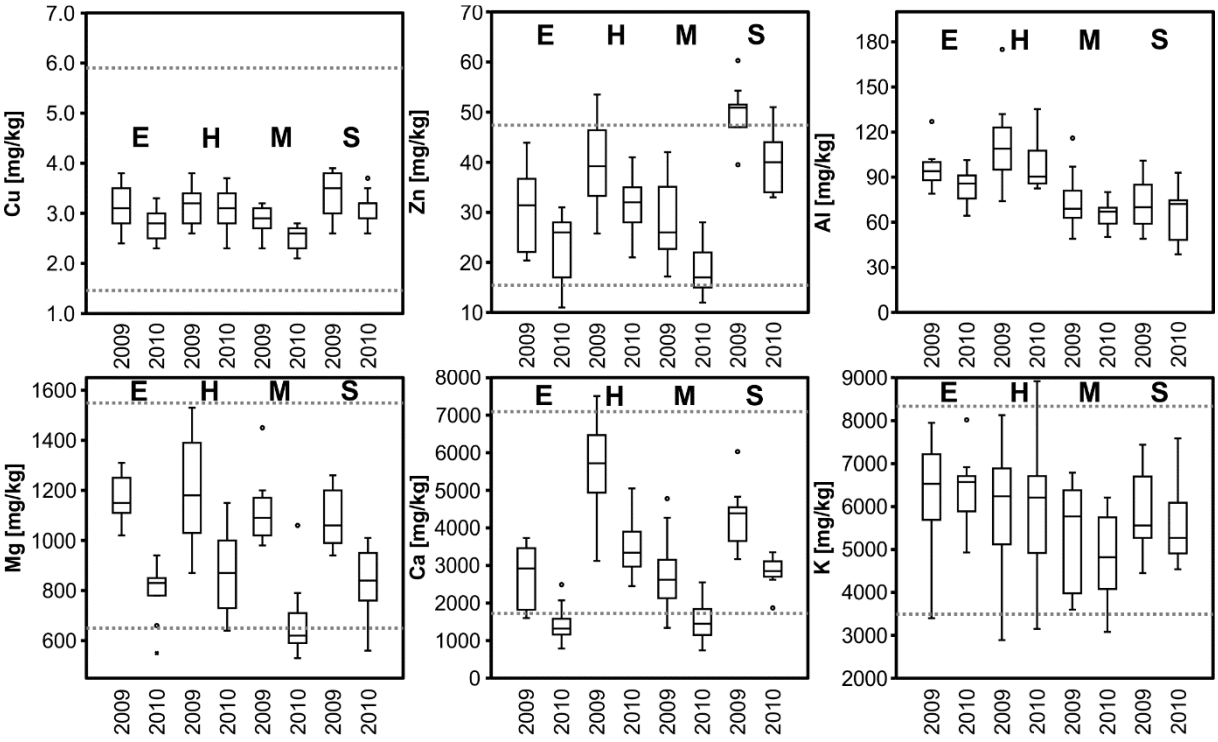

Figure 7.2: *Boxplots of the concentrations of Cu, Zn, Al, Mg, Ca and K observed in the Norway spruce needle samples collected at the reference Norway spruce stands in 2009 and 2010. Dotted lines represent limit values reported by the ICP Forests programme. E – Erika, H – Habartov, M – Mezihorská, S – Studenec.*

7.1.3 Analysis of the collected soil samples

Several soil samples were collected at each reference Norway spruce stand (see part 3.3). These samples then went under laboratory processing to determine exchangeable base cations (Mg^{2+}, Ca^{2+}, Na^{+} and K^{+}) and Al^{3+} cations, exchangeable acidity (TEA), exchangeable pH, organic carbon (C) and nitrogen (N) and content of selected heavy metals (As, Cu and Zn). The contents of base cations were further transformed from the original values (mg/kg or g/kg) to mmol/kg to determine basic exchangeable cations (BCE), cation exchangeable capacity (CEC) and base saturation (BS). The obtained values of the selected soil indicators were compared with limit values reported in Fabiánek et al. (2004) resp. the results of Second European Forest Soil Survey (de Vos and Cools, 2011). The mean ± std. values calculated for all considered soil parameters can be seen in Tables 7.3 and 7.4.

Regarding the obtained results of soil samples analysis it can be declared that soil substrate is very acidic in case of the all reference Norway spruce stands while exchangeable pH is lower than the limit value (pH = 3.5) referred in Fabiánek et al. 2004 for both organic horizons (h_1 and h_2)as well as for the upper mineral horizon. The only exception is the lower mineral horizon (h_4) where above-limit values can be seen in case of the all stands except of Habartov (h_4: 3.39±0.07). In terms of relative stand comparison, remarkably lower pH values can be observed in case of Erika and Mezihorská stands (h_1: 2.55±0.14 and 2.87±0.14 resp. h_2: 2.50±0.01 and 2.76±0.12), whereas higher values can be seen in case of Habartov and Studenec (h_1: 3.18±0.16 and 3.33±0.11 resp. h_2: 3.43±0.07 and 2.99±0.13). Significantly lower pH values can be seen only for Erika site in case of the upper mineral horizon (h_3). The results see in Figure 7.3.

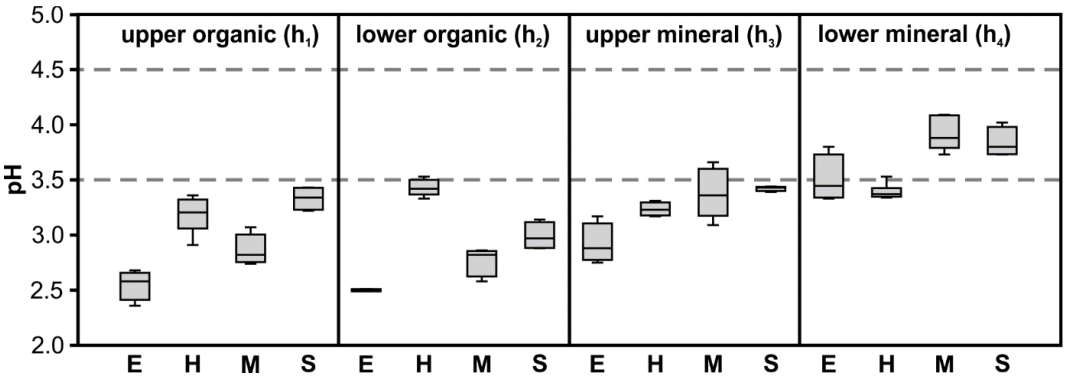

Figure 7.3: *Soil exchangeable pH values measured at the four reference Norway spruce stands: Erika (E), Habartov (H), Mezihorská (M) and Studenec (S). The dashed lines represents lower and upper limit values regarding Fabiánek et al. 2004.*

Exchangeable pH (not to be confused with active pH) refers on acidification level of soil and stock of H^{+} cations. If exchangeable pH < 3.5, saturation of soil sorption complex by base cations is usually less than 20 %. This results in low availability for these cations for forest vegetation. On the other hand, if exchangeable pH > 4.5, base saturation is higher than 50 % for mineral horizons and up to 90 % for organic horizons respectively (Fabiánek et al. 2004). This is in full accordance with the observed exchangeable base cation concentrations which are below limits in most cases for both mineral and organic soil horizons. Clear relationship can be observed

especially between the content of Ca^{2+} cations and exchangeable pH for organic horizons (i.e. lower Ca^{2+} concentration for the stands with lower pH values and vice-versa). The same pattern is evident also in case of BCE (sum of Ca^{2+}, Mg^{2+}, K^{+} and Na^{+}) and BS (percentage of sorption complex capacity occupied by base cations) which are again lower in case of the localities exhibiting lower pH values (i.e. Erika and Mezihorská) and vice-versa. See the results in Figure 7.4.

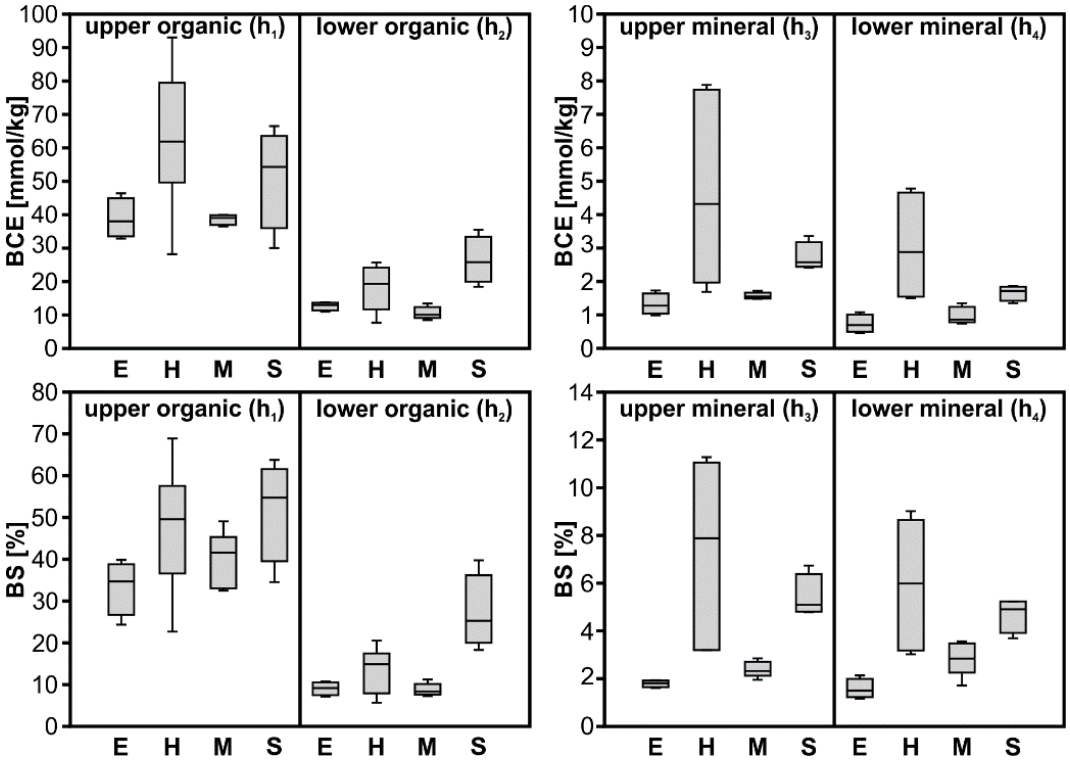

Figure 7.4: *Base Exchangeable Cations (BCE) and Base Saturation (BS) measured at the reference Norway spruce stands Erika (E), Habartov (H), Mezihorská (M) and Studenec (S).*

In general, mobility of metallic elements increases with lower soil pH (e.g. Rieuwerts et al. 1998). As so, an obvious relationship can be seen between Total Exchangeable Acidity – TEA (capacity of the acidic H^{+} and Al^{3+} cations) and concentration of exchangeable Al^{3+} cations. This relationship was expressed by the means of Pearson's correlation coefficient (r_P) which was equal to 0.78 (h_1), 0.88 (h_2), 0.96 (h_3) and 0.99 (h_4). In this point of view, Studenec is the locality exhibiting the lowest TEA and thus also exchangeable Al^{3+} in all cases. See the results in Figure 7.5.

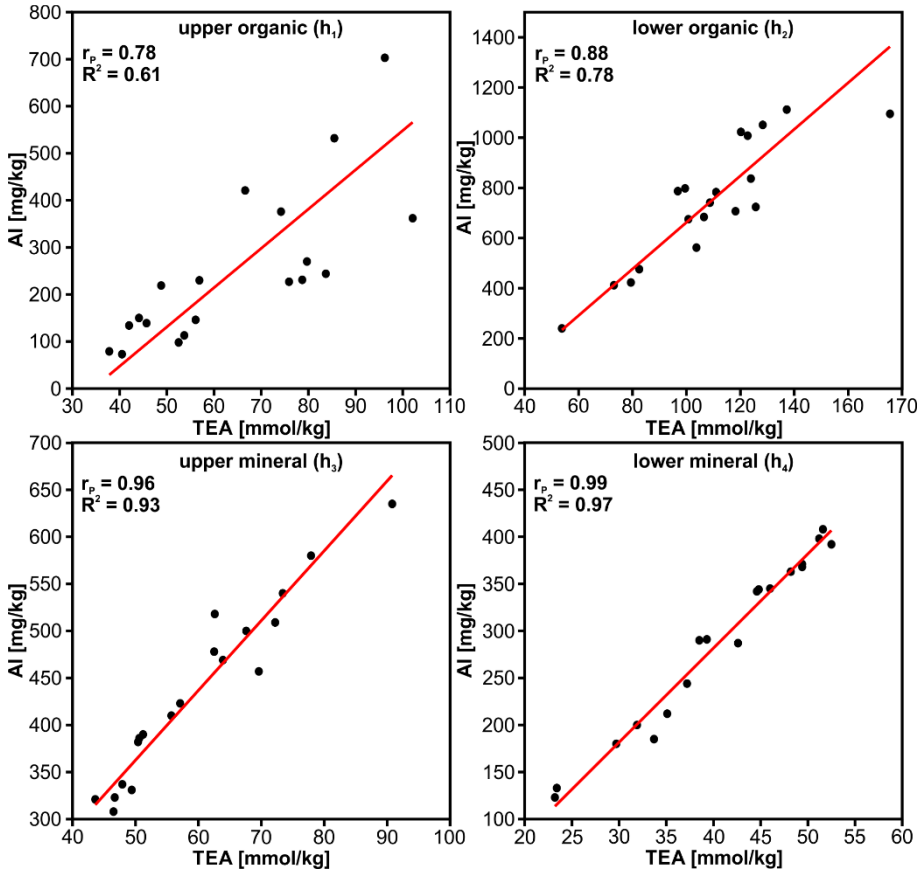

Figure 7.5: *Relationship of Total Exchangeable Acidity (TEA) and exchangeable Al^{3+} cations observed retrieved from the soil samples collected at the four reference Norway spruce stands. r_P stands for Pearson's correlation coefficient, R^2 is coefficient of determination.*

Fabiánek et al. 2004 refers also limit values for two heavy metallic elements – copper (Cu) and zinc (Zn). The lower limits are defined as values typical for soils not influenced by immission loads, whereas the upper limits are defined with respect to toxicity of the given metallic element to plants (Fabiánek et al. 2004). The concentration of Cu is very similar at all reference stands in both mineral horizons. This similarity can be seen also at the level of organic horizons with exception of Habartov site where significantly higher values can be observed. In fact, all the values (organic horizons) exceeded the referred upper limit of 20 mg/kg as the Cu concentration was approximately 30 mg/kg for Erika, Mezihorská and Studenec stands and approximately 95 mg/kg (h_1) resp. 165 mg/kg (h_2) for Habartov. In addition, the same pattern can be seen in case of arsenic (As) concentration. Unfortunately, no official limit values for forest soils were known to the author. Therefore, the observed soil As content values were compared with the value 30 mg/kg (30 ppm) recommended by the Guideline of the Ministry of Agriculture of the Czech Republic (see in Rotter et al. 2013). The observed As contents are quite close to this value in most cases. The content significantly exceeding this recommended value can be seen only in case of the lower organic horizon at Erika a Habartov sites (53 ppm resp. 84 ppm) as well as in case of the upper organic horizon at Habartov 69 ppm. Zinc concentrations are within the interval defined by the lower and upper limits in all cases. However, the Zn concentrations for Erika, Habartov and Mezihorská are relatively similar and close to the lower limit (35 mg/kg), the values for Studenec

are generally almost 3× higher (approx. 60 – 70 mg/kg for Erika, Habartov and Mezihorská whereas more than 200 mg/kg for Studenec) and quite close to the upper limit (300 mg/kg). See the results in Figure 7.6.

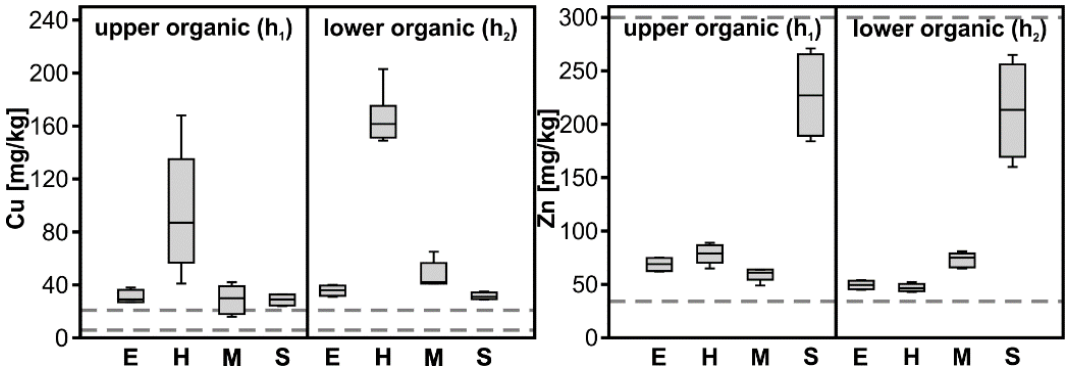

Figure 7.6: *Copper (Cu) and zinc (Zn) contents measured at the reference Norway spruce stands Erika (E), Habartov (H), Mezihorská (M) and Studenec (S). The dashed lines represents limit values referred by Fabiánek et al. (2004).*

Attention was payed also to ratio of organic carbon (C) and nitrogen (N). The observed values of the C/N ratio were very similar in both organic horizons with no statistically significant differences amongst the reference stands. Note that the C/N ratio was analysed only for organic soil horizons. Fabiánek at al. 2004 refers the optimal values as between 15 and 25. C/N < 15 signalizes too rapid decomposition of organic material with leading to nutrient loss. On the other hand, C/N > 25 signalizes too slow decomposition leading to nutrient deficiency. The C/N values observed at the reference stands are in general slightly above the upper limit (up to 30). See the results in Figure 7.7.

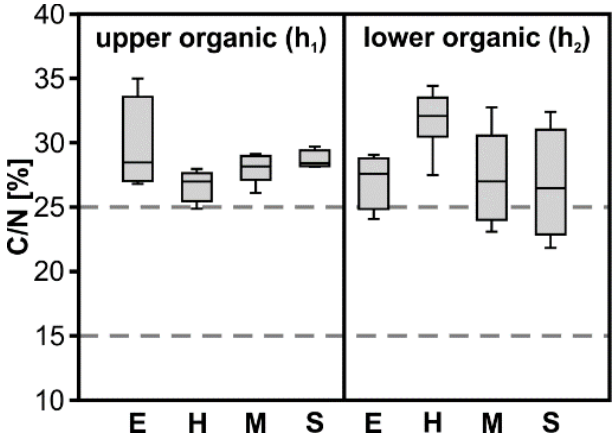

Figure 7.7: *Ratio of soil organic carbon to organic nitrogen (C/N) measured at the reference Norway spruce stands Erika (E), Habartov (H), Mezihorská (M) and Studenec (S). The dashed lines represents limit values referred by Fabiánek et al. (2004).*

Table 7.3: *Results of laboratory analysis of the soil samples collected at the reference Norway spruce stands Erika, Habartov, Mezihorská and Studenec.*

Soil parameter	Horizon	Limit	p-value	Erika	Habartov	Mezihorská	Studenec
pH	1	3.5 – 4.5	**0.0019**	2.55±0.14	3.18±0.16	2.87±0.14	3.33±0.11
	2	3.5 – 4.5	**0.0008**	2.50±0.01	3.43±0.07	2.76±0.12	2.99±0.13
	3	3.5 – 4.5	**0.0086**	2.92±0.18	3.24±0.06	3.38±0.23	3.42±0.02
	4	3.5 – 4.5	**0.0067**	3.51±0.21	3.39±0.07	3.93±0.16	3.84±0.14
Al^{3+} [mg/kg]	1	n.a.	0.0906	247.25±102.82	397.50±206.75	155.00±72.48	149.50±62.08
	2	n.a.	**0.0008**	772.00±227.27	963.17±136.95	744.00±68.08	387.75±102.39
	3	n.a.	**0.0329**	502.75±97.00	427.00±73.39	485.00±81.74	324.75±12.55
	4	n.a.	**0.0310**	336.75±92.96	354.83±39.49	235.80±101.10	205.25±29.41
Mg^{2+} [mg/kg]	1	500 – 2500	0.4914	164.00±23.14	147.00±51.13	139.00±16.45	154.00±47.38
	2	500 – 2500	**0.0088**	63.25±9.78	43.33±12.69	51.80±5.97	99.00±26.09
	3	20 – 60	0.0701	7.00±2.94	13.00±9.27	8.40±2.07	13.00±0.82
	4	20 – 60	**0.0126**	2.75±1.26	9.00±5.51	3.40±1.67	6.00±0.82
Ca^{2+} [mg/kg]	1	2000 – 10000	**0.0104**	870±136.38	1990±680.79	760±76.16	1405±466.08
	2	2000 – 10000	**0.0029**	190±60.55	515±274.14	92±20.49	725±228.69
	3	140 – 500	**0,0016**	10±0.00	128.33±107.78	10±0.00	45±10.00
	4	140 – 500	**0.0164**	10±0.00	75±57.18	10±0.00	28±5.00
Na^{+} [mg/kg]	1	n.a.	**0.0078**	18.00±4.90	26.83±8.01	16.20±3.70	11.00±0.82
	2	n.a.	**0.0189**	20.00±6.38	30.00±16.33	24.80±4.87	11.25±2.22
	3	n.a.	0.0997	6.50±2.38	11.33±6.06	10.00±1.87	6.25±2.63
	4	n.a.	0.5177	5.75±1.50	8.00±2.83	6.60±1.95	6.25±2.22
K^{+} [mg/kg]	1	400 – 2000	**0.0047**	375.25±93.03	231.67±103.59	513.80±67.57	368.00±76.82
	2	400 – 2000	**0.0070**	174.00±61.99	85.00±22.08	199.00±48.97	146.00±17.61
	3	30 – 100	**0.0432**	19.50±4.51	16.83±4.79	21.20±3.96	31.25±10.56
	4	30 - 100	**0.0421**	12.00±2.83	17.33±3.27	13.80±5.45	17.75±2.22
C:N	1	15 – 25	0.0507	29.68±3.69	26.67±1.19	28.07±1.18	28.66±0.71
	2	15 – 25	0.0836	27.08±2.14	31.79±2.38	27.23±3.68	26.78±4.34
As [ppm]	1	n.a.	**0.0015**	29.75±6.64	68.83±18.51	12.60±3.36	31.00±10.17
	2	n.a.	**0.0016**	53.25±4.57	83.67±5.28	37.60±6.27	36.25±3.77
	3	n.a.	**0.0124**	27.25±3.20	18.83±4.62	20.80±6.14	39.75±9.54
	4	n.a.	**0.0036**	18.25±2.50	10.83±3.87	14.00±3.54	31.25±7.89
Cu [ppm]	1	5 - 20	**0.0106**	30.75±5.19	94.83±46.51	28.80±10.83	28.75±4.43
	2	5 - 20	**0.0010**	35.75±4.03	165.50±19.52	47.40±10.26	31.50±2.65
	3	n.a.	0.1448	23.00±4.58	23.00±3.46	18.00±0.00	33.25±13.91
	4	n.a.	**0.0499**	25.33±2.08	20.67±1.15	23.00±2.83	29.00±5.03
Zn [ppm]	1	35 – 300	**0.0019**	68.75±6.70	78.33±8.87	59.60±6.19	227.25±39.80
	2	35 – 300	**0.0016**	49.50±4.20	47.00±3.46	73.00±6.78	213.00±44.70
	3	n.a.	**0.0010**	37.75±7.89	25.33±5.96	107.20±7.76	477.00±190.75
	4	n.a.	**0.0019**	68.75±6.70	78.33±8.87	59.60±6.19	227.25±39.80

Table 7.4: *Results of laboratory analysis of the soil samples collected at the reference Norway spruce stands Erika, Habartov, Mezihorská and Studenec.*

Soil parameter	Horizon	Limit	p-value	Erika	Habartov	Mezihorská	Studenec
TEA [mmol/kg]	1		0.1054	79.80±19.95	68.88±20.89	60.74±16.21	46.13±7.95
	2		**0.0204**	130.78±31.18	117.45±16.07	110.16±8.58	72.20±12.88
	3		**0.0190**	72.08±14.43	55.73±8.41	65.28±11.39	47.63±1.34
	4		**0.0474**	45.58±9.18	46.63±5.13	34.90±10.85	33.93±3.16
BCE [mmol/kg]	1		0.1405	38.84±5.96	62.79±21.47	38.53±1.51	51.28±15.31
	2		**0.0166**	12.66±1.24	18.11±7.03	10.61±1.88	26.39±7.06
	3		**0.0054**	1.32±0.32	4.66±2.98	1.57±0.10	2.73±0.43
	4		**0.0030**	0.73±0.26	3.03±1.64	0.98±0.25	1.66±0.23
CEC [mmol/kg]	1		**0.0202**	118.64±20.52	131.68±15.77	99.27±16.06	97.41±7.47
	2		**0.0110**	143.44±31.80	135.56±14.16	120.77±8.98	98.59±7.19
	3		**0.0419**	73.39±14.73	60.39±10.25	66.85±11.46	50.35±1.13
	4		**0.0341**	46.31±9.34	49.67±6.01	35.88±10.99	35.58±3.18
BS [%]	1		0.1177	33.39±6.55	47.63±15.25	39.66±6.79	51.95±12.36
	2		**0.0162**	9.05±1.59	13.50±5.43	8.79±1.51	27.14±9.03
	3		**0.0019**	1.79±0.14	7.40±4.06	2.40±0.33	5.43±0.90
	4		**0.0049**	1.57±0.41	5.96±2.86	2.86±0.72	4.69±0.73

7.1.4 Relationship between soil chemistry and Norway spruce foliage characteristics

Soil properties measured at the reference Norway spruce stands were related to the properties of Norway spruce foliage properties in terms of biochemistry (foliar pigments and water content) and content of the selected chemical elements. In this case, the main problematic issue is that the soil samples were collected randomly across the reference Norway spruce stands and thus there was no direct link between the soil samples and the collected Norway spruce trees (e.g. one soil sample collected within the neighbourhood of the each collected tree etc.). As so, it was not possible to link soil and foliage properties in 1:1 basis, but instead it was necessary to work only with the values integrated across the whole sampling stands (i.e. mean value per one sampling site). These values were used to check a potential relationship between soil and foliar properties by the mean of Pearson's correlation coefficient (r_P). The following relationships were tested: soil Cu content/needle Cu content, soil Zn content/needle Zn content, soil exchangeable Al^{3+} cations/needle Al content, soil exchangeable Mg^{2+} cations/needle Mg content, soil exchangeable Ca^{2+} cations/needle Ca content, soil Na^{+} exchangeable cations/needle Na content and soil K^{+} exchangeable cations/needle K content. Clear relationship between soil and foliar properties were discovered for zinc, aluminium and calcium in the all four soil horizons (h_1 – h_4): Zn 0.90 (h_1), 0.80 (h_2), 0.78 (h_3), 0.90 (h_4); Al 0.97 (h_1), 0.83 (h_2), 0.35 (h_3), 0.97 (h_4); Ca 0.99 (h_1), 0.75 (h_2), 0.97 (h_3), 0.80 (h_4). Nevertheless, since it was necessary to use the values aggregated across the sampling stands, the analysis has rather informative character (whether the mean needle content of the given element has similar pattern as its content in soil), but it cannot be understood as the key for quantitative prediction of the foliar characteristics based on soil properties. It should be mentioned, that the described analysis was based only on the needle samples collected in 2009 as the soil samples were collected in 2009 as well and no further soil sampling was conducted in 2010 (when the needle samples were collected again).

The reference stands were divided into two groups based on the results of soil sample analysis to those, which are considered to have worse soil conditions (lower pH, BCE and BS) and

the others, which seem to have more favourable soil conditions. The first group was represented by Erika and Mezihorská stands whereas Habartov and Studenec belong to the second group. A statistical analysis was performed to prove whether there are significant differences in foliar biochemistry (C_{ab}, C_x/C_x+C_{ab} and C_w) between these two groups. The C_{ab}, C_x/C_x+C_{ab} and C_w values were used at the level of individual trees (i.e. means of the U_1, U_3, L_1 and L_3 needle age classes calculated for each sampled Norway spruce tree were taken into account as these values were further used in the all analyses related to hyperspectral image data products). Student's two samples t-test was used for the described analysis where the values related to the trees growing at Erika and Mezihorská were understood as one sample whereas values related to the trees from Habartov and Studenec were considered as the second sample. The test showed that chlorophylls content is slightly higher at the stands considered as those with the more favourable conditions, but the difference from the other stands is small and not statistically significant ($p = 0.3017$). Statistically significant ($p = 0.0104$) difference can be seen in case of $C_x/(C_x+C_{ab})$ values which are higher at Erika and Mezihorská site group, which is in full accordance with theory described in literature. On the other hand, significant difference can be found in case of C_w as well ($p = 0.0083$). However, lower values can be seen at the Erika and Mezihorská stands in compare with Habartov and Studenec, which is opposite to the theoretical assumptions. As so, it seems that needle C_w values are rather not affected by soil characteristics in contrast with foliar pigments.

7.2 Leaf level radiative transfer simulations

The input parameters of the two used leaf level radiative transfer models (PROSPECT-5 and LIBERTY) required for forward leaf spectra simulations were optimized using reference spectra measured by ASD Fieldspec-3 spectroradiometer equipped by contact probe. Two different approaches were used for the models parameterization. Single leaf reflectance (R) generated by the PROSPECT-5 and LIBERTY models was compared with the corresponding ASD Fieldspec measured spectra in case of so called R approach. In the second case, simulated infinite reflectance (R_∞) was used instead of the single leaf reflectance R. Note, that R_∞ is a standard part of the LIBERTY output, but in case of the PROSPECT-5 model it has to be calculated from the single leaf reflectance R using the appropriate transforming formula (see part 4.2). At this point, it has to be highlighted that the R_∞ approach describes the real setup of the reference spectra measurement much better than the R approach since reflectance of needle stack of measured by the used contact probe instead of measuring spectra of individual needles. In such case, effects of multiple scattering has to be taken into account which is secured by the use of R_∞. The optimal values of each input parameter were determined using minimization of the merit function describing the goodness of fitting (RMSE) between the model simulations and reference calibration dataset. The optimized values of the input parameters obtained by the use of both R as well as R_∞ approach can be seen in the Table 7.5.

Table 7.5: *Optimized values of the input parameters of the PROSPECT-5 and LIBERTY leaf level radiative transfer models obtained by R and R_∞ parameterization approaches.*

parameter	parameterization	U_1	L_1
N (PROSPECT-5)	R approach	1.9196	2.0944
	R_∞ approach	1.3053	1.4717
Thickness (LIBERTY)	R approach	2.1961	2.2669
	R_∞ approach	1.3053	1.4717
Cell diameter (LIBERTY)	R approach	35.8844	34.3970
	R_∞ approach	46.6647	44.1458
Air space (LIBERTY)	R approach	0.04535	0.04558
	R_∞ approach	0.04603	0.04622
Baseline absorption (LIBERTY)	R approach	0.0005694	0.0006071
	R_∞ approach	0.0005757	0.0005833
Albino absorption (LIBERTY)	R approach	1.4239	1.3699
	R_∞ approach	1.3494	1.5965

Reliability of the models parameterizations was assessed using independent validation datasets (i.e. sets of the reference ASD measured spectra which were not used for the model parameterization). Absolute accuracy of the model simulations was expressed by the total RMSE. The RMSE was calculated for each particular wavelength λ and then averaged across the VIS (400 – 750 nm), NIR (750 – 1200 nm) and SWIR (1200 – 2500 nm) domains as well as across the entire spectral range (400 – 2500 nm). The RMSE values were calculated for both R and R_∞ parameterization approaches (see Table 7.6).

Table 7.6: *Validation of the forward PROSPECT-5 and LIBERTY simulations for both R and R_∞ parameterization approaches: average RMSE ± std. between simulated and ASD measured reflectance.*

spectral domain	parameterization	PROSPECT-5		LIBERTY	
		U_1	L_1	U_1	L_1
ALL (400 – 2500 nm)	R approach	0.0456 ± 0.0306	0.0417 ± 0.0310	0.0289 ± 0.0305	0.0307 ± 0.0298
	R_∞ approach	0.0324 ± 0.0252	0.0318 ± 0.0278	0.0423 ± 0.0190	0.0390 ± 0.0175
VIS (400 – 750 nm)	R approach	0.0335 ± 0.0204	0.0287 ± 0.0186	0.0238 ± 0.0122	0.0258 ± 0.0115
	R_∞ approach	0.0185 ± 0.0111	0.0177 ± 0.0102	0.0310 ± 0.0142	0.0287 ± 0.0127
NIR (750 – 1200 nm)	R approach	0.0817 ± 0.0191	0.0817 ± 0.0246	0.0490 ± 0.0047	0.0419 ± 0.0090
	R_∞ approach	0.0756 ± 0.0163	0.0794 ± 0.0220	0.0576 ± 0.0071	0.0466 ± 0.0090
SWIR (1200 – 2500 nm)	R approach	0.0359 ± 0.0234	0.0314 ± 0.0234	0.0234 ± 0.0358	0.0287 ± 0.0369
	R_∞ approach	0.0212 ± 0.0088	0.0191 ± 0.0073	0.0401 ± 0.0198	0.0392 ± 0.0194

In addition, systematic ($RMSE_S$) and random ($RMSE_R$) components of the total RMSE were calculated according Willmott (1981) to decide about the character of the observed differences between the simulated and measured leaf level reflectance (see Table 7.7).

Table 7.7: *RMSE, $RMSE_S$ and $RMSE_R$ calculated for the PROSPECT-5 and LIBERTY leaf level radiative transfer models. The values correspond to R_∞ parameterization approach.*

PROSPECT-5						
Spectral domain	U_1			L_1		
	RMSE	$RMSE_S$	$RMSE_R$	RMSE	$RMSE_S$	$RMSE_R$
ALL (400 – 2500 nm)	0.0324	0.0317	0.0036	0.0318	0.0312	0.0040
VIS (400 – 750 nm)	0.0185	0.0148	0.0087	0.0177	0.0151	0.0078
NIR (750 – 1200 nm)	0.0756	0.0755	0.0047	0.0794	0.0790	0.0070
SWIR (1200 – 2500 nm)	0.0212	0.0211	0.0018	0.0191	0.0190	0.0020
LIBERTY						
Spectral domain	U_1			L_1		
	RMSE	$RMSE_S$	$RMSE_R$	RMSE	$RMSE_S$	$RMSE_R$
ALL (400 – 2500 nm)	0.0423	0.0421	0.0029	0.0390	0.0387	0.0031
VIS (400 – 750 nm)	0.0310	0.0298	0.0072	0.0287	0.0270	0.0082
NIR (750 – 1200 nm)	0.0576	0.0576	0.0020	0.0466	0.0465	0.0020
SWIR (1200 – 2500 nm)	0.0401	0.0401	0.0021	0.0392	0.0391	0.0021

Looking on the values in the Table 7.5 it can be seen that the differences of the optimized values of the models input parameters are very small comparing the U_1 and L_1 sample levels. On the other hand there are quite high differences of the optimized models inputs comparing the values obtained by the R and R_∞ parameterization approaches.

In case of the PROSPECT-5 model, an improvement in the simulation fitting can be seen in the all spectral domains when R_∞ parameterization approach is used instead of using R approach. The highest influence of using the R_∞ parameterization approach can be seen in the green peak part of spectra (ca. 550 nm) and then in the SWIR domain close to 1380 nm and especially between 1450 – 1900 nm where the RMSE dropped from approximately 0.08 (R approach) to 0.03 (R_∞ approach). As so, it can be concluded that the R_∞ parameterization approach provides much better results compared to those obtained by the use of the R parameterization approach.

The simulated R_∞ generally fitted well to the ASD measurements in the VIS domain not only in terms of spectra shape, but also in terms of absolute reflectance (average RMSE less than 0.02). The spectra matched well up to approx. 800 nm. However, significant variability between the simulated and measured spectra can be observed in the NIR domain (average RMSE ca. 0.08). There was also a mismatch between simulations and reference data close to the water absorption feature near 1250 nm with the significant difference between the U_1 and L_1 datasets. The SWIR domain is comparable with the VIS domain in terms of the total RMSE which is approximately 0.02.

The character of the observed differences between PROSPECT-5 simulated and measured spectra was assessed according Willmott (1981) using the $RMSE_R^2/RMSE^2$ ratio describing the

relative contribution of the random component to the total RMSE. From this perspective, VIS domain surprisingly seems to be the most affected by the random component whereas it has weak influence in NIR and SWIR domains (U_1: VIS = 33.7 %, NIR = 0.4 %, SWIR = 0.9 %; L_1: VIS = 23.1 %, NIR = 0.9 %, SWIR = 1.4 %).

In case of the LIBERTY model, situation is not as clear as in case of the PROSPECT-5. The ASD measured reflectance falls between the simulated R and R_∞. Nevertheless, the results obtained by the R_∞ parameterization approach are still slightly better when compared to those obtained by the R approach.

Certain distortions of the LIBERTY simulated spectra shape was observed in the VIS domain. The simulated reflectance was underestimated up to approx. 600 nm. On the other hand there was relatively high agreement of the simulations around the chlorophyll absorption region (near 670 nm). Nevertheless the total RMSE is generally higher (approx. 0.03) compared to the values obtained by the use of the PROSPECT-5 model simulations. In the NIR domain, R_∞ is generally overestimated compared to R_{ASD}, but the total RMSE is still lower compared to the PROSPECT-5 simulations (approx. 0.05 instead of 0.08). In addition, the shape of the R_{ASD} spectra match better with the single leaf R simulations than the R_∞ in NIR. Still, the shape of the simulated spectra matched better in case of the LIBERTY model compared to PROSPECT-5. Simulated spectra fitted well in the SWIR domain, however, reflectance was slightly underestimated compared to the ASD measured values (RMSE approx. 0.04).

The character of the observed differences between the LIBERTY simulations and ASD measured reflectance is similar as in case of the PROSPECT-5 model. The $RMSE_R^2/RMSE^2$ ratio was generally highest in the VIS domain whereas in the NIR and SWIR domains it had relative small influence (U_1: VIS = 10.7 %, NIR = 0.2 %, SWIR = 0.2 %; L_1: VIS = 19.1 %, NIR = 0.3 %, SWIR = 0.2 %).

The differences between the simulated R resp. R_∞ and the measured R_{ASD} can be seen in Figures 7.8 and 7.9.

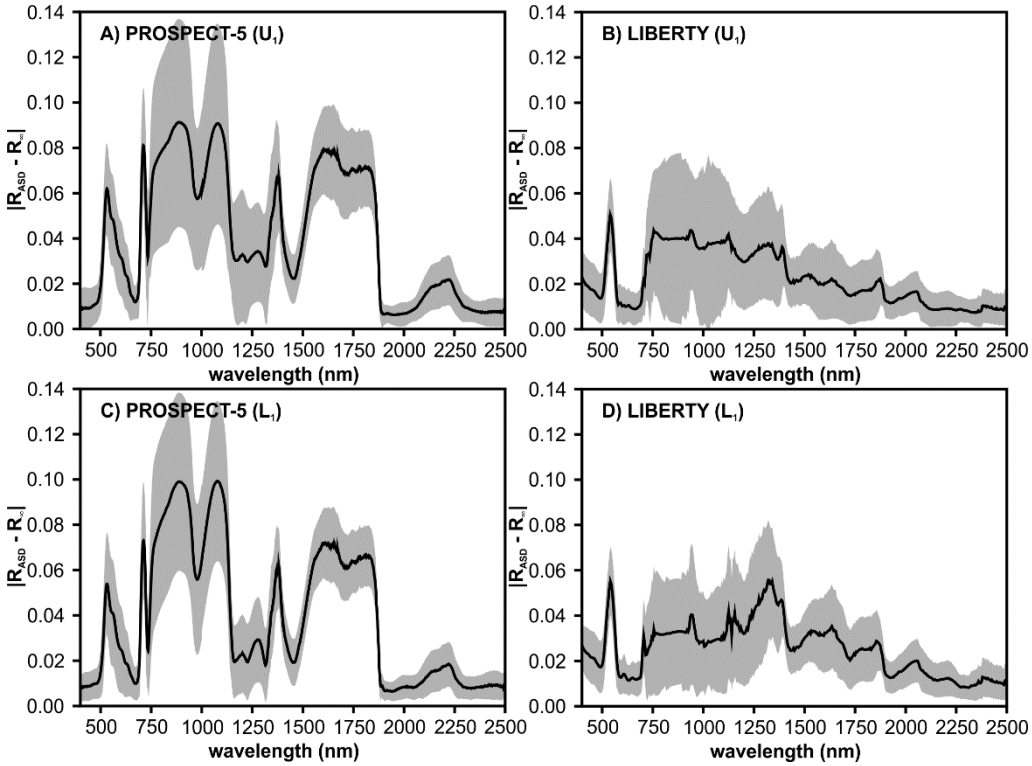

Figure 7.8: *Difference (mean ± std.) between measured R_{ASD} and single-leaf R simulated by PROSPECT-5 (left) and LIBERTY (right) models for U_1 (upper) and L_1 (bottom) needle levels.*

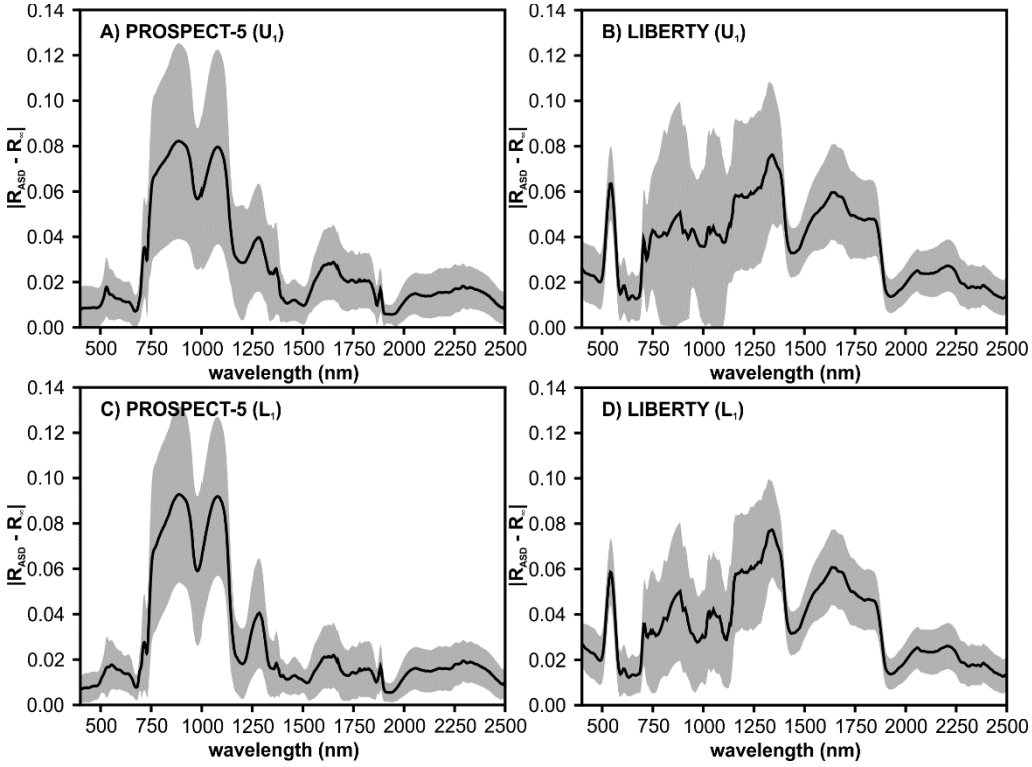

Figure 7.9: *Difference (mean ± std.) between measured R_{ASD} and R_∞ simulated by PROSPECT-5 (left) and LIBERTY (right) models for U_1 (upper) and L_1 (bottom) needle levels.*

7.3 Canopy level radiative transfer simulations

Single-leaf reflectance (R) and transmittance (T) simulations obtained from the parameterized PROSPECT-5 and LIBERTY models were transformed onto shoot level reflectance using the spectral invariants theory first. These shoot level spectra were then up-scaled to the canopy level using the FRT whose parameterization was based on the use of digital hemispherical photographs (DHPs), in-situ expert estimations and allometric relationships.

Two different scenarios were used based on the used leaf-level model. The coupling of PROSPECT-5 and FRT models was called "PRO-FRT", whereas the combination of LIBERTY and FRT was called as "LIB-FRT"[3].

Canopy level simulations were generated for each sampling plot (E_3, H_3, M_{5a} and S_3) specifically for each year 2009 and 2010 as the needle biochemistry (C_{ab}, C_x, C_w and C_m) required for needle level modelling was determined during both sampling campaigns. The canopy level spectra obtained from the PRO-FRT and LIB-FRT models couplings were resampled from original 5 nm spectral resolution according to spectral characteristics of the HyMap sensor (having spectral resolution between 10 and 15 nm). Finally, these simulations were compared with the corresponding HyMap image-extracted spectra calculated as the mean of the all pixels within the particular stand (see Figure 7.10). Total RMSE as well its systematic ($RMSE_S$) and random ($RMSE_R$) components were calculated in the same manner as in case of leaf level spectra assessment. All the indicators were calculated for each particular spectral domain (VIS, NIR and SWIR) as well as for the entire spectral range 400 – 2500 nm see in Table 7.8).

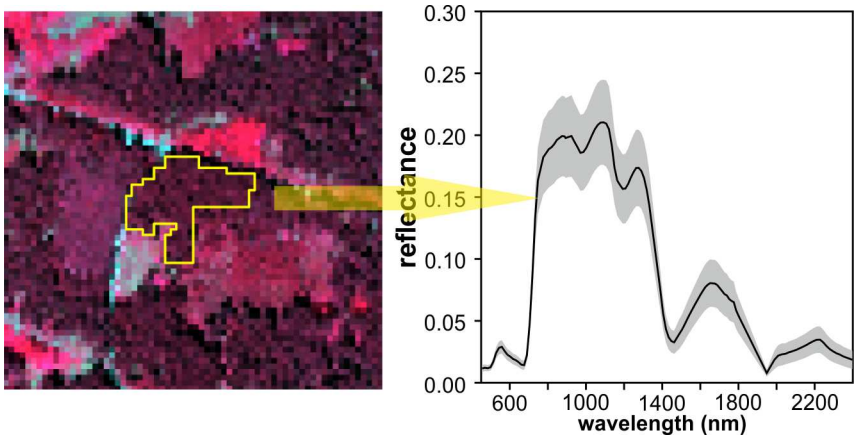

Figure 7.10: *Calculation of mean ± std. image-extracted spectra.*

[3] The used designations of the used radiative transfer models couplings PRO-FRT and LIB-FRT were established just for the needs of this thesis and as so they are not official terms.

Table 7.8: *Total (RMSE), systematic ($RMSE_S$) and random ($RMSE_R$) root mean squared error calculated between model predicted (PRO-FRT and LIB-FRT) and HyMap image-extracted canopy level reflectance spectra.*

PRO-FRT						
Spectral domain	2009			2010		
	RMSE	$RMSE_S$	$RMSE_R$	RMSE	$RMSE_S$	$RMSE_R$
ALL (400 – 2500 nm)	0.0198	0.0197	0.0019	0.0230	0.0229	0.0008
VIS (400 – 750 nm)	0.0076	0.0074	0.0013	0.0095	0.0093	0.0018
NIR (750 – 1200 nm)	0.0226	0.0224	0.0025	0.0310	0.0309	0.0012
SWIR (1200 – 2500 nm)	0.0223	0.0222	0.0018	0.0235	0.0235	0.0002
LIB-FRT						
Spectral domain	2009			2010		
	RMSE	$RMSE_S$	$RMSE_R$	RMSE	$RMSE_S$	$RMSE_R$
ALL (400 – 2500 nm)	0.0145	0.0144	0.0012	0.0244	0.0241	0.0035
VIS (400 – 750 nm)	0.0057	0.0057	0.0004	0.0107	0.0107	0.0011
NIR (750 – 1200 nm)	0.0187	0.0187	0.0010	0.0348	0.0343	0.0058
SWIR (1200 – 2500 nm)	0.0153	0.0152	0.0015	0.0238	0.0235	0.0033

The best performance of the two tested models (PRO-FRT and LIB-FRT) was observed in VIS domain in terms of the lowest RMSE values: PRO-FRT 0.0076 (2009) resp. 0.0095 (2010), LIB-FRT 0.0057 (2009) resp. 0.0107 (2010). However, a serious distortion of spectra shape can be seen in case of the LIB-FRT simulations in VIS. On the other hand, the LIB-FRT model provided slightly better results than the PRO-FRT in NIR domain in terms of the simulated spectra shape, which was fitting better the HyMap image-extracted spectra than the PRO-FRT simulations. Nevertheless, both models generally tended to overestimate reflectance in NIR domain. The RMSE for PRO-FRT simulations was 0.0226 (2009) resp. 0.0310 (2010), whereas for LIB-FRT 0.0187 (2009) resp. 0.0348 (2010). Overestimation of reflectance can be seen also in SWIR domain where the RMSE values were generally similar as in NIR domain: PRO-FRT 0.0223 (2009) resp. 0.0235 (2010), LIB-FRT 0.0153 (2009) resp. 0.0238 (2010).

Systematics/randomness of the observed differences between the models simulations and image-extracted reference spectra were assessed again using $RMSE_R^2/RMSE^2$ ratio. The situation was similar such as in case of leaf level modelling as the random component had the highest influence in the VIS domain whereas in NIR and SWIR domains was much weaker. The influence of the random component on the observed RMSE is expressed as percentage fraction of the total RMSE ($100 \cdot RMSE_R^2/RMSE^2$). PRO-FRT: 4.9 % (2009) resp. 6.5 % (2010), NIR = 1.4 % (2009) resp. 0.2 % (2010), SWIR 0.7 % (2009) resp. less than 0.1 % (2010). LIB-FRT: VIS = 1.1 % (2009) resp. 0.9 % (2010), NIR = 0.7 % (2009) resp. 3.0 % (2010), SWIR = 1.8 % (2009) 2.8 % (2010). The PRO-FRT and LIB-FRT simulations as well as the reference image-extracted spectra for each sampling stand are shown in Figures 7.11 and 7.12.

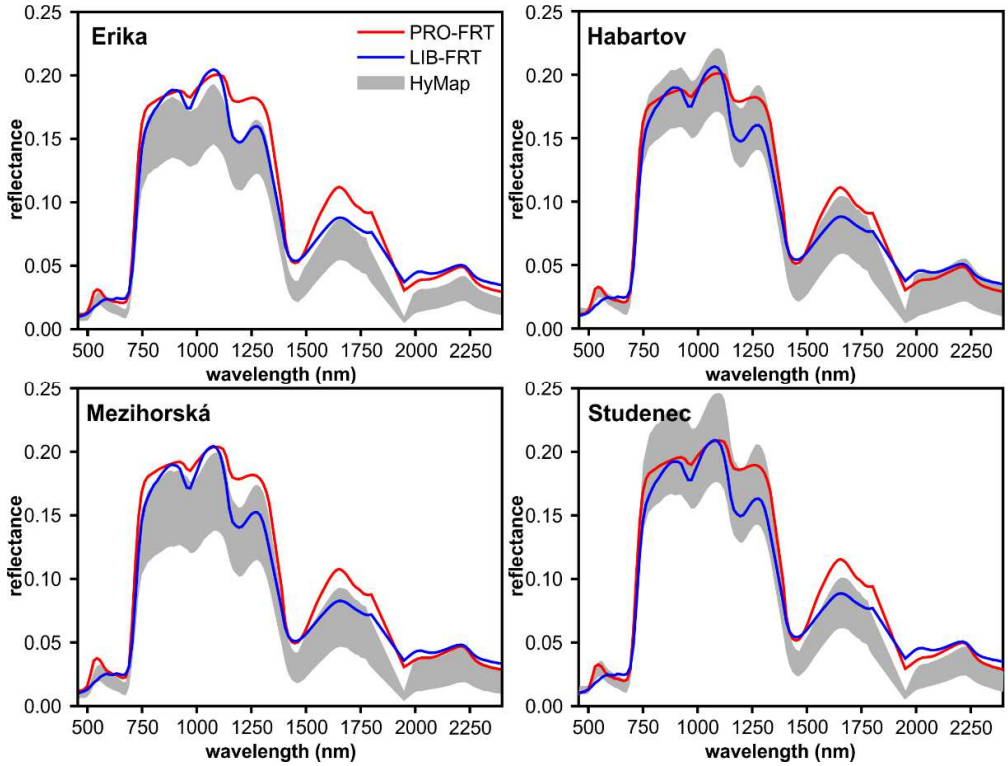

Figure 7.11: *Comparison of canopy reflectance spectra extracted from the HyMap 2009 dataset for the particular sampling stands (mean ± std.) and the corresponding simulations obtained by PRO-FRT and LIB-FRT models. Erika (E_3), Habartov (H_3), Mezihorská (M_{5a}), Studenec (S_3).*

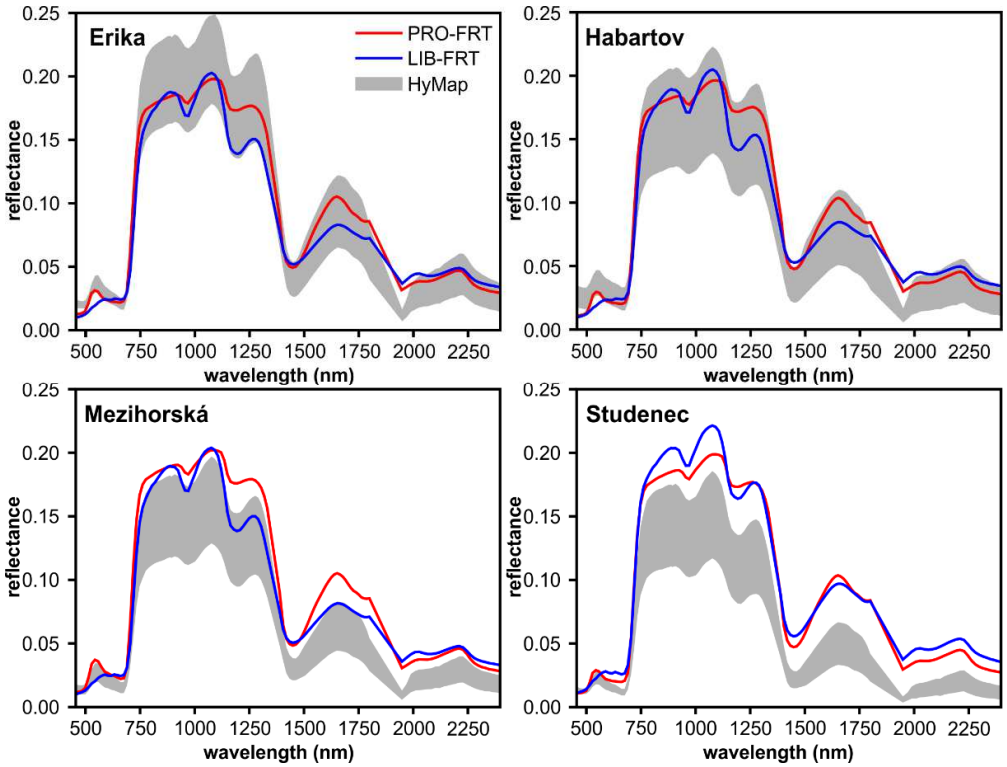

Figure 7.12: *Comparison of canopy reflectance spectra extracted from the HyMap 2010 dataset for the particular sampling stands (mean ± std.) and the corresponding simulations obtained by PRO-FRT and LIB-FRT models. Erika (E_3), Habartov (H_3), Mezihorská (M_{5a}), Studenec (S_3).*

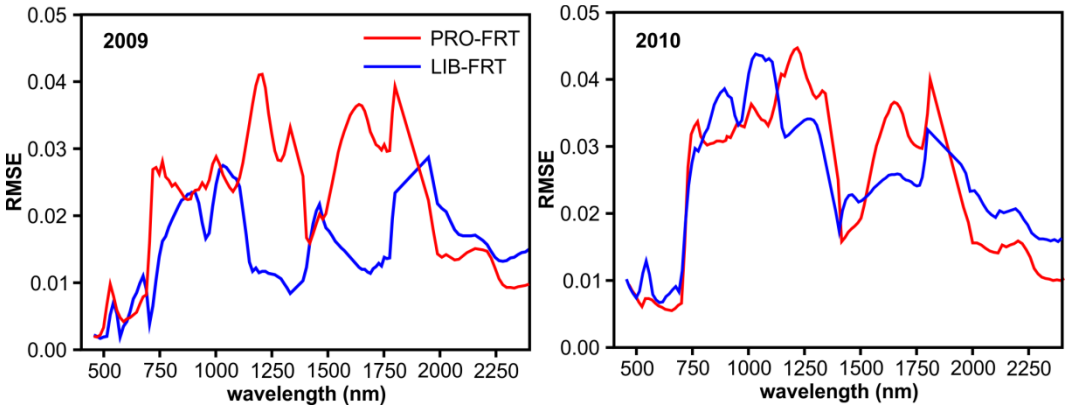

Figure 7.13.: *RMSE between the canopy level simulations and the HyMap image-derived spectra.*

7.4 Retrieval of semi-quantitative indices

7.4.1 Leaf Area Index (LAI)

Parameterized PRO-FRT radiative transfer models coupling was used to simulate LAI LUT for 21 combinations of DLW and DEN values (DLW ranged from 10 – 30 kg, step 5 kg; DEN ranged between 0.0100 – 0.0700 trees/m^2, step 0.0100 trees/m^2). Regarding the performed sensitivity analysis (described in part 6.2), two vegetation indices based on 1st derivative of reflectance were selected as the most promising LAI predictors. The exponential regression models were defined to describe relationships between the used vegetation indices and the corresponding LAI values. Both of these models exhibited very high coefficient of determination and low RMSE of the LAI prediction such as R^2 = 0.9825, RMSE = 0.2575 (D_{733}/D_{805}) resp. R^2 = 0.9962, RMSE = 0.1243 (D_{748}/D_{805}) – see 6.3.2.

As the LAI values predicted by the original regression models were generally underestimated in compare to the in-situ measured ones, empirical correction of the predictive formulas was performed (see part 6.3.2) to minimize the RMSE between the predicted and measured LAI values. The corrected predictive formulas were than applied again on the real HyMap data.

The predicted LAI values were extracted from both HyMap 2009 and HyMap 2010 datasets for the 10 validation sites. Note that in-situ LAI estimation (using DHP technique) was performed here, but the stands were used neither for the FRT model parameterization nor for empirical transformation of the LAI predictive formulas. The predicted LAI values were compared with the in-situ measured ones to assess absolute and relative accuracy of the performed LAI estimation based RMSE calculation. In addition, relative RMSE (RRMSE) was calculated as the RMSE normalized by the range of the measured LAI values. Comparison of the in-situ measured and HyMap predicted LAI values see in Table 7.9 and Figures 7.14 and 7.15.

Table 7.9: *Comparison of the predicted LAI values (extracted from the HyMap datasets using D_{733}/D_{805} and D_{748}/D_{805} vegetation indices as LAI predictors) and the in-situ measured values (based on DHP technique).*

Stand	D_{733}/D_{805} (2009)		D_{733}/D_{805} (2010)		D_{748}/D_{805} (2009)		D_{748}/D_{805} (2010)	
	Predicted	Measured	Predicted	Measured	Predicted	Measured	Predicted	Measured
E_2	5,75	4,94	5,67	4,94	5,61	4,94	5,55	4,94
E_4	5,46	5,46	5,34	5,46	5,43	5,46	5,23	5,46
E_6	5,10	4,29	4,96	4,29	5,10	4,29	4,84	4,29
M_2	5,07	5,93	5,12	5,93	5,13	5,93	5,08	5,93
M_4	5,04	5,90	5,10	5,90	5,05	5,90	5,04	5,90
M_{5b}	5,07	5,18	5,08	5,18	5,07	5,18	5,03	5,18
M_6	5,14	5,20	5,19	5,20	5,10	5,20	5,11	5,20
S_2	5,06	4,51	5,05	4,51	5,24	4,51	5,14	4,51
S_4	5,07	4,65	5,25	4,65	5,11	4,65	5,18	4,65
S_6	4,95	3,35	5,24	3,35	5,02	3,35	5,20	3,35
RMSE	0.77		0.80		0.77		0.79	
RRMSE	30 %		31 %		30 %		31 %	

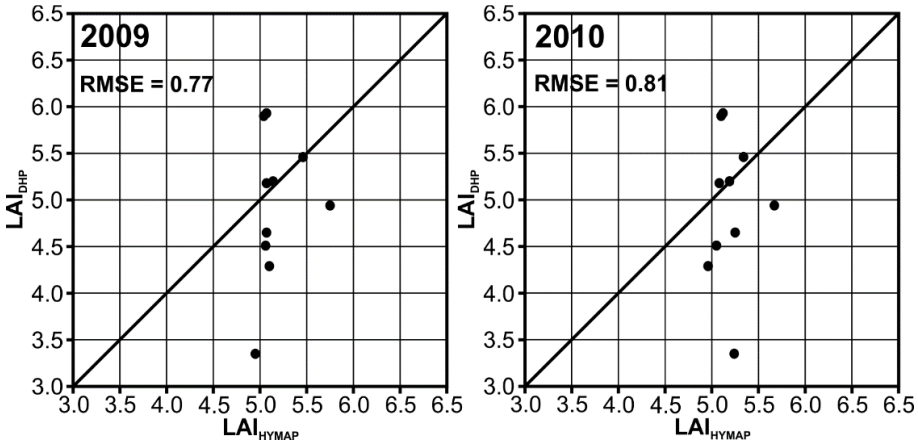

Figure 7.14: *Scatterplots of the predicted (LAI_{HYMAP}) vs. measured (LAI_{DHP}) leaf area index values. The LAI estimation was performed using the D_{733}/D_{805} vegetation index.*

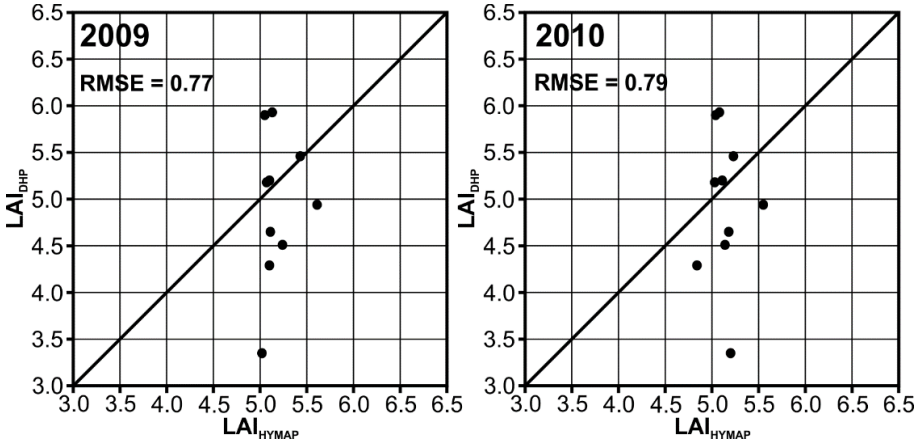

Figure 7.15: *Scatterplots of the predicted (LAI_{HYMAP}) vs. measured (LAI_{DHP}) leaf area index values. The LAI estimation was performed using the D_{748}/D_{805} vegetation index.*

Regarding the obtained results of LAI estimation validation, several fact should be mentioned. Relatively good fit between the predicted and measured values can be observed in terms of absolute accuracy assessment as the RMSE is approximately 0.7 meaning the RRMSE equal to ca. 30 %. Very comparable results can be observed for both tested vegetation indices (D_{733}/D_{805} and D_{748}/D_{805}) in both years 2009 and 2010. It should be also highlighted that the same number of measurements is located above and below the 1:1 line. This means that the numbers of under- and overestimated values are the same within the validation dataset. Unfortunately, the situation is much complicated in terms of the relative accuracy as the coefficient of determination (R^2) is very low indicating that there is almost no systematic relationship between the predicted and measured LAI values. The possible reasons of this situation are discussed further (see chapter 8 - Discussion).

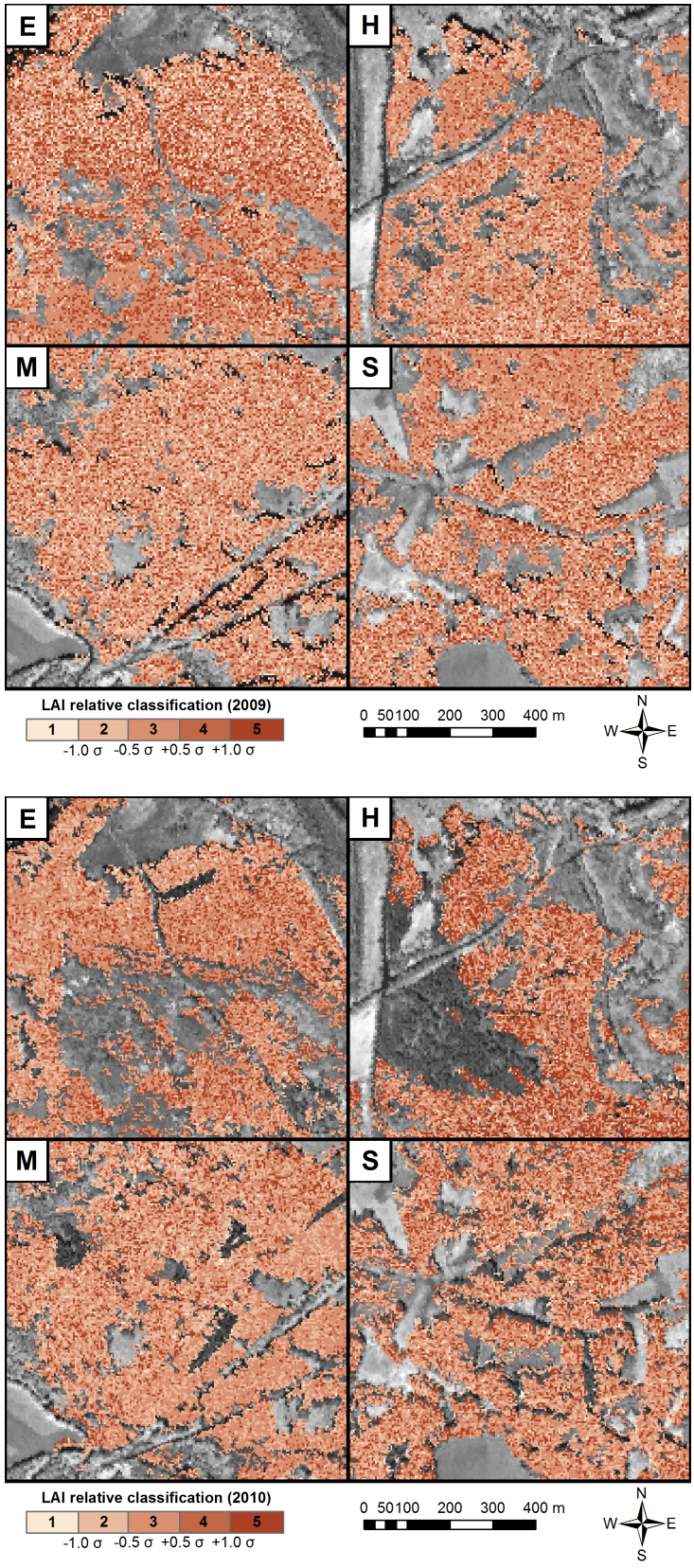

Figure 7.16: *Example of the relative classification of LAI based on D_{733}/D_{805} vegetation index applied on the HyMap 2009 (upper) and 2010 (lower) dataset (E – Erika, H – Habartov, M – Mezihorská, S - Studenec).*

7.4.2 Chlorophyll content (C_{ab})

The parameterized PRO-FRT was used to simulate C_{ab} LUT for 7 different levels of leaf chlorophyll content (20 – 80 µg/cm^2, step 10 µg/cm^2) and LAI ranging from 3.0 to 10.5 (various combinations of DLW and DEN). In total, 147 simulations were included in the C_{ab} LUT. Statistical regression models were established between the leaf chlorophyll content and vegetation indices calculated from the corresponding PRO-FRT simulated spectra. Six indices based on canopy reflectance were used together with two models based on continuum removal spectra and two other based on 1st derivative of canopy level reflectance. Quality of these models were assessed by coefficient of determination R^2 (ranging from ca. 0.95 to more than 0.99) and root mean squared error of the C_{ab} prediction RMSE (ranging from ca. 0.97 µg/cm^2 to 4.36 µg/cm^2) – see Table 7.10. These models were then applied on the values of the same vegetation indices extracted from both HyMap 2009 and 2010 datasets to map spatial variability of chlorophyll content.

Table 7.10: *Overview of the statistical regression models established between the leaf chlorophyll content and vegetation indices calculated from the PRO-FRT simulated spectra. Quality of the models is described by coefficient of determination (R^2) and root mean squared error of the C_{ab} prediction (RMSE).*

Vegetation index	Predictive equation	R^2	RMSE [µg/cm^2]
Canopy reflectance			
MCARI/OSAVI	$C_{ab} = 95.6035e^{-5.2091(MCARI/OSAVI)}$	0.9785	3.1264
TCARI/OSAVI	$C_{ab} = 121.2985e^{-8.0638(TCARI/OSAVI)}$	0.9523	4.3553
mRENDVI	$C_{ab} = 3.5792e^{4.6708MRENDVI}$	0.9887	2.6820
mRESR	$C_{ab} = 21.6731MRESR - 27.6001$	0.9814	2.7280
VOG_1	$C_{ab} = 87.6084VOG_1 - 97.3329$	0.9768	3.0448
N_{718}	$C_{ab} = 580.8505e^{-4.7304N718}$	0.9908	1.8826
Continuum removal			
$ANCB_{558-747}$	$C_{ab} = 0.0803e^{0.0495(ANCB558-747)}$	0.9880	2.8584
$ANCB_{647-718}$	$C_{ab} = 0.0371e^{0.1463(ANCB647-718)}$	0.9975	0.9732
1st Derivative			
D_{733}/D_{675}	$C_{ab} = -0.0599(D_{733}/D_{675})^2 + 4.9321(D_{733}/D_{675}) + 5.7940$	0.9862	2.3489
D_{718}/D_{704}	$C_{ab} = 26.7761(D_{718}/D_{704})^2 + 19.1502(D_{718}/D_{704}) - 14.8400$	0.9914	1.8566

Note that in contrast to the two other modelled biochemical variables ($C_x/(C_{ab}+C_x)$ and C_w) both relative (spatial differences in chlorophyll content in relative scale) as well as absolute (absolute chlorophyll level in physical units of µg/cm^2) chlorophyll content layers were produced in this case. The relative product was then used as one of the inputs of the developed forest health classification model whereas the absolute chlorophyll content product was handled as a separate output independent of the results of the forest health model classification.

To check its quality, the absolute chlorophyll content map went under validation against the ground truth values originating from the laboratory analysis of the collected Norway spruce needle samples. The collected needles originate from ten clusters of Norway spruce trees (labelled A - J) where each cluster includes five trees. The predicted C_{ab} values were extracted only from those pixels within the least circumscribed polygons around the sampling trees (see Figure 7.17).

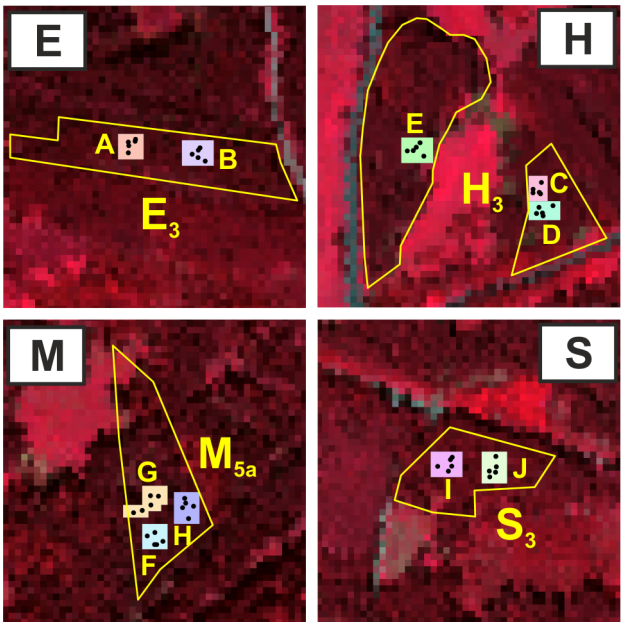

***Figure 7.17**: Tree clusters (A – J) used for the validation of chlorophyll content estimation defined within the validation Norway spruce stands E_3, H_3, M_{5a} and S_3 (whose borders are marked by yellow polygons). Each cluster includes five sampling trees (black dots).*

Mean value was calculated from these pixels for each tree cluster A - J. These values were compared with those originating from laboratory measurements. In that case, mean value of U_1, U_3, L_1 and L_3 chlorophyll content values was calculated for each sampled tree and these values were then averaged across the particular tree clusters. RMSE and R^2 were calculated for predicted (image extracted) vs. measured (laboratory analysis) values. The obtained results were summarized in Table 7.11.

***Table 7.11:** Ground truth validation of the chlorophyll content predicted by the 10 models based on different chlorophyll-sensitive vegetation indices. RMSE and R^2 were calculated from the predicted (image extracted) chlorophyll content values and the corresponding laboratory values.*

indicator	2009		2010	
	RMSE (µg/cm²)	R^2	RMSE (µg/cm²)	R^2
Reflectance vegetation indices				
MCARI/OSAVI	12.55	0.79	6.03	0.49
TCARI/OSAVI	5.23	0.20	8.74	0.06
mRENDVI	7.94	0.58	15.97	0.76
mRESR	7.95	0.58	16.09	0.76
VOG_1	12.19	0.48	8.26	0.22
N_{718}	4.83	0.57	4.53	0.48
Continuum removal vegetation indices				
$ANCB_{558-747}$	12.41	0.43	15.43	0.10
$ANCB_{647-718}$	21.40	0.65	20.90	0.53
1st derivative vegetation indices				
D_{733}/D_{675}	5.88	0.58	12.61	0.52
D_{718}/D_{704}	4.98	0.54	5.88	0.48

RMSE gives an information about absolute accuracy of the obtained chlorophyll content prediction (in comparison to the reference validation dataset), whereas R^2 describes character of the differences observed between predicted and measured values. RMSE was ranging from 4.83 µg/cm² (N_{718}) to 12.55 µg/cm² (MCARI/OSAVI) for HyMap 2009 and from 4.53 µg/cm² (N_{718}) to 16.09 µg/cm² (mRESR) in case of HyMap 2010 dataset. From this point of view, N_{718} and D_{718}/D_{704} seem to be the most reliable C_{ab} predictors (N_{718}: $RMSE_{2009}$ = 4.83 µg/cm², R^2_{2009} = 0.57; $RMSE_{2010}$ = 4.53, µg/cm² R^2_{2010} = 0.48; D_{718}/D_{704}: $RMSE_{2009}$ = 4.98 µg/cm², R^2_{2009} = 0.54; $RMSE_{2010}$ = 5.88 µg/cm², R^2_{2010} = 0.48) as the obtained results are stable when comparing 2009 and 2010 datasets. Quite low RMSE values can be observed also in case of the models based on TCARI/OSAVI index. However, in this case the corresponding R^2 values are very low (R^2_{2009} = 0.20; R^2_{2010} = 0.06). Comparison of the predicted and measured chlorophyll content values can be also seen in Figures 7.18 and 7.19.

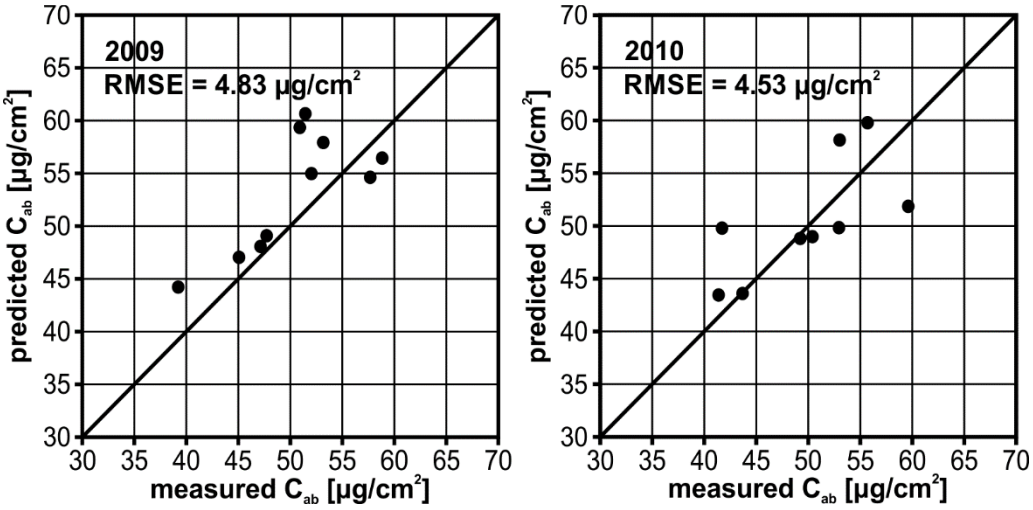

Figure 7.18: *Comparison of the predicted (HyMap image extracted) and measured (laboratory) values of chlorophyll content. N_{718} vegetation index was used as the chlorophyll content predictor.*

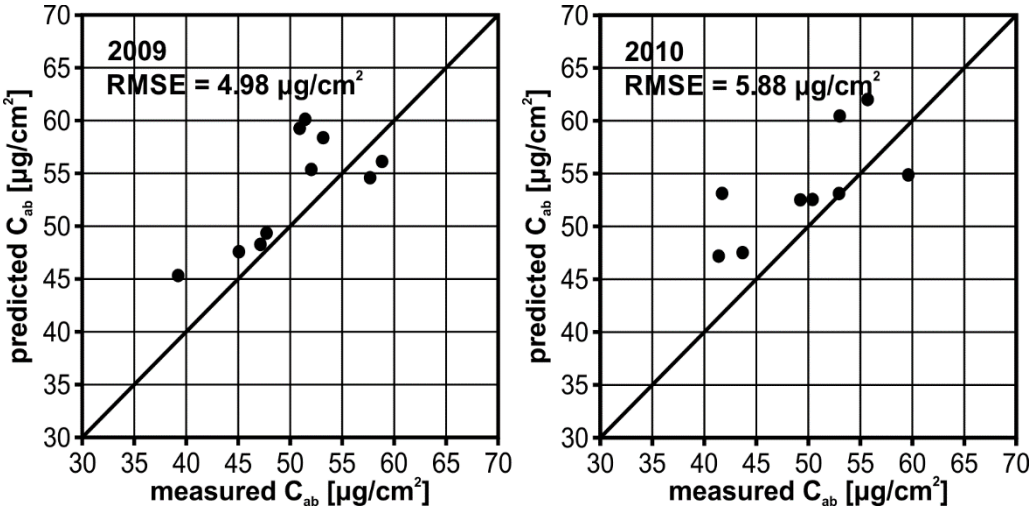

Figure 7.19: *Comparison of the predicted (HyMap image extracted) and measured (laboratory) values of chlorophyll content. D_{718}/D_{704} vegetation index was used as the chlorophyll content predictor.*

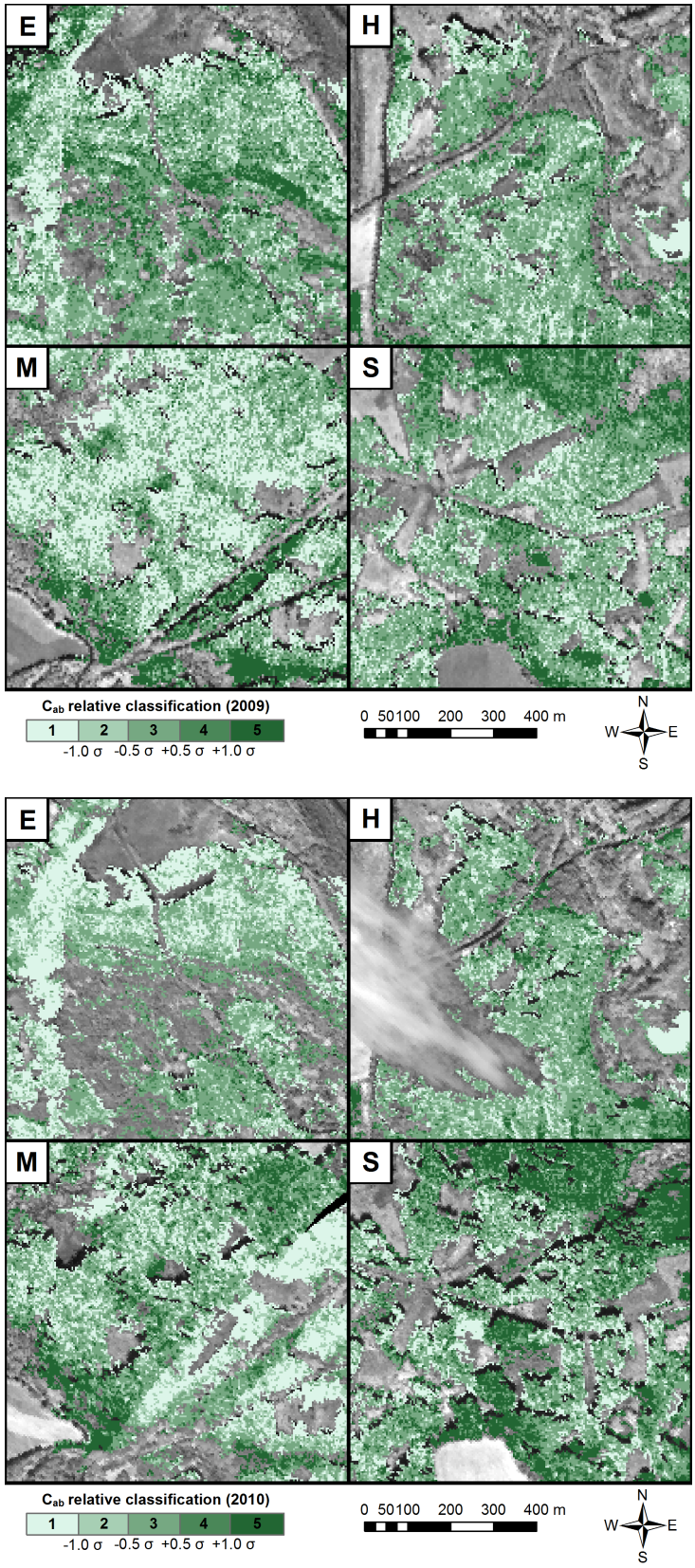

Figure 7.20: *Example of the relative classification of C_{ab} based on N_{718} vegetation index applied on the HyMap 2009 (upper) and 2010 (lower) dataset (E – Erika, H – Habartov, M – Mezihorská, S - Studenec).*

7.4.3 Relative carotenoids content ($C_x/(C_x+C_{ab})$)

In addition to chlorophyll content products, various models describing relationship of relative carotenoids content and carotenoids-sensitive vegetation indices were established using the relative carotenoids content LUT simulated by the PRO-FRT radiative transfer models coupling. Eight models were based on vegetation indices based on either simple ratios or normalized differences of appropriate spectral bands sensitive to changes in relative carotenoids content. Appropriateness of these bands were checked by the performed sensitivity analysis. Two other models were based on ratios of 1st derivatives of the original spectral bands.

Quality of the produced models was assessed in the same style as in case of chlorophyll content – i.e. using RMSE of $C_x/(C_x+C_{ab})$ prediction and R^2 to check the residual variability of the used vegetation indices (i.e. variability not related by changes of $C_x/(C_x+C_{ab})$). The coefficient of determination (R^2) was ranging from ca. 0.89 to 0.95 whereas RMSE ranged between 0.0178 and 0.0253 (see Table 7.12). All the models were then applied on the values of the same vegetation indices extracted from both HyMap 2009 and 2010 datasets. These layers further served as inputs of the developed forest health classification.

Table 7.12: *Overview of the statistical regression models established between the relative carotenoids content and vegetation indices calculated from the PRO-FRT simulated spectra. Quality of the models is described by coefficient of determination (R^2) and root mean squared error of the prediction (RMSE).*

Vegetation index	Predictive equation	R^2	RMSE
Canopy reflectance			
R_{558}/R_{529}	$C_x/(C_x+C_{ab}) = 0.6897(R_{558}/R_{529}) - 0.6389$	0.9451	0.0188
R_{558}/R_{514}	$C_x/(C_x+C_{ab}) = 0.3446(R_{558}/R_{514}) - 0.4188$	0.9003	0.0253
R_{573}/R_{514}	$C_x/(C_x+C_{ab}) = 0.3991(R_{573}/R_{514}) - 0.4662$	0.9128	0.0237
R_{573}/R_{529}	$C_x/(C_x+C_{ab}) = 0.7868(R_{573}/R_{529}) - 0.6519$	0.9368	0.0201
$(R_{558}-R_{529})/(R_{558}+R_{529})$	$C_x/(C_x+C_{ab}) = 1.6070((R_{558}-R_{529})/(R_{558}+R_{529})) + 0.0475$	0.9432	0.0191
$(R_{558}-R_{514})/(R_{558}+R_{514})$	$C_x/(C_x+C_{ab}) = 1.2233(R_{558}-R_{514})/(R_{558}+R_{514})) - 0.1423$	0.8938	0.0261
$(R_{573}-R_{514})/(R_{573}+R_{514})$	$C_x/(C_x+C_{ab}) = 1.2439((R_{573}-R_{514})/(R_{573}+R_{514})) - 0.0784$	0.9127	0.0237
$(R_{573}-R_{529})/(R_{573}+R_{529})$	$C_x/(C_x+C_{ab}) = 1.6290((R_{573}-R_{529})/(R_{573}+R_{529})) + 0.1395$	0.9351	0.0204
1st Derivative			
D_{514}/D_{529}	$C_x/(C_x+C_{ab}) = 0.3461(D_{514}/D_{529})^2 - 1.2131(D_{514}/D_{529}) + 1.0971$	0.9453	0.0188
$(D_{514}-D_{529})/(D_{514}+D_{529})$	$C_x/(C_x+C_{ab}) = 1.4502((D_{514}-D_{529})/(D_{514}+D_{529}))^2 - 1.1218((D_{514}-D_{529})/(D_{514}+D_{529})) + 0.2262$	0.9507	0.0178

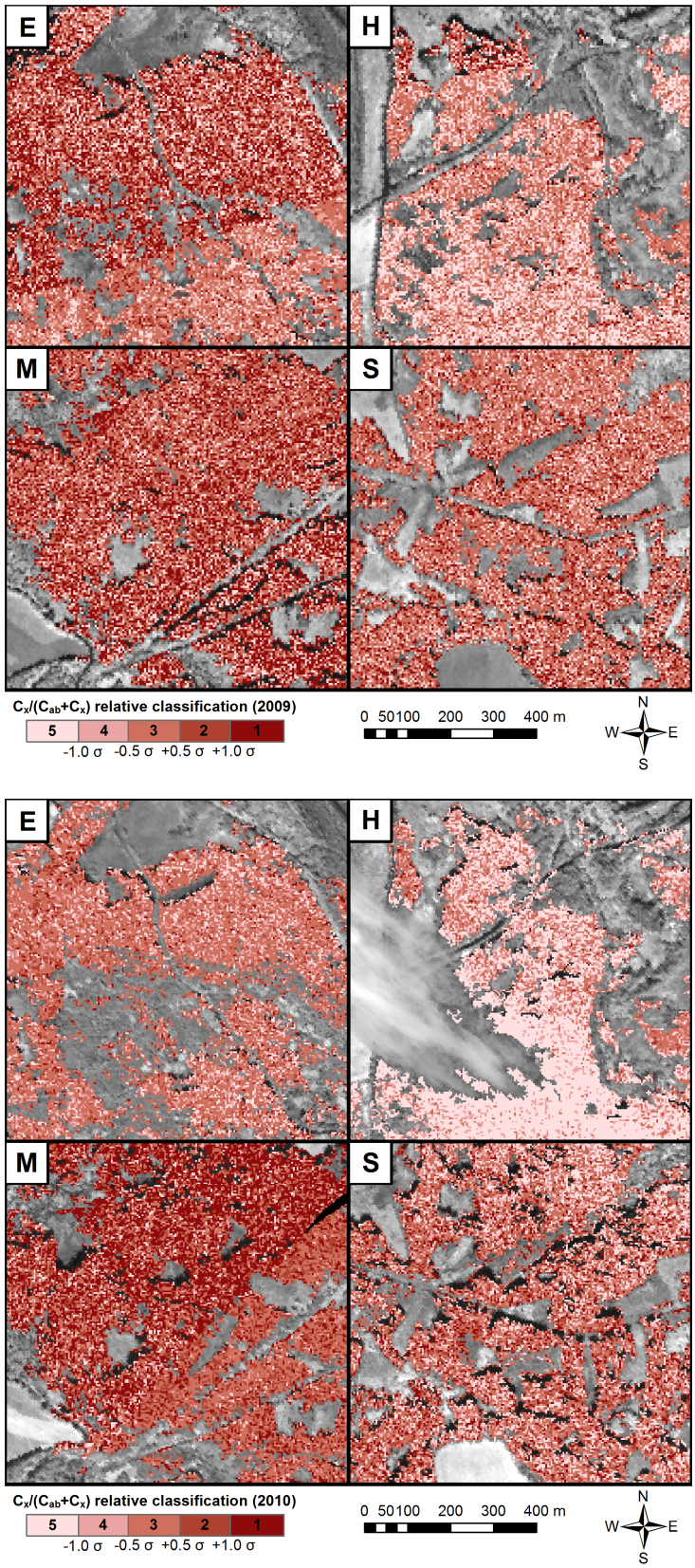

Figure 7.21: *Example of the relative classification of $C_x/(C_x+C_{ab})$ based on R_{558}/R_{529} vegetation index applied on the HyMap 2009 (upper) and 2010 (lower) dataset (E – Erika, H – Habartov, M – Mezihorská, S - Studenec).*

7.4.4 Water content (C_w)

Water content was the third biochemical variable considered for forest health status classification. Six classical water-sensitive vegetation indices based either on simple ratios or normalized differences of appropriate spectral bands were used as the vegetation water content predictors. In addition, vegetation index calculated as the area of water absorption feature normalized by its maximal depth was calculated for each water absorption feature W_I (920 – 1040 nm), W_{II} (1120 – 1270 nm) and W_{III} (1300 – 1650 nm). Finally, two other indices were based on simple ratios of the 1st derivatives of the original spectral bands. The bands used to construct these indices were based on the performed sensitivity analysis.

Quality of the models established to describe relationship between the chosen vegetation indices and water content were assessed in the same way as in case of chlorophyll and relative carotenoids contents using RMSE of water content prediction and R^2. The coefficient of determination ranged from ca 0.84 to 0.98 with RMSE between 0.0014 – 0.0090 cm (see Table 7.13). All the models were then applied on the values of the same vegetation indices extracted from both HyMap 2009 and 2010 datasets. These layers further served as inputs of the developed forest health classification.

Table 7.13: *Overview of the statistical regression models established between the water content content and vegetation indices calculated from the PRO-FRT simulated spectra. Quality of the models is described by coefficient of determination (R^2) and root mean squared error of the prediction (RMSE).*

Vegetation index	Predictive equation	R^2	RMSE [cm]
Canopy reflectance			
MSI	$C_w = 0.5568e^{-5.5094WBI}$	0.9435	0.0034
NDII	$C_w = 0.2596NDII^2 + 0.0597NDII - 0.0016$	0.9287	0.0090
NMDI	$C_w = 0.2676NMDI^2 - 0.0588NMDI - 0.0062$	0.9466	0.0030
$NDWI_{1639}$	$C_w = 0.2739NDWI_{1639}^2 + 0.0437NDWI_{1639} - 0.0016$	0.9362	0.0048
SRWI	$C_w = 0.1815SRWI - 0.1565$	0.8490	0.0060
WBI	$C_w = -0.4461WBI - 0.4645$	0.9370	0.0025
Continuum removal			
FA/BD W_I	$C_w = 0.001125e^{0.05629(FA/BD\ WI)}$	0.9086	0.0046
FA/BD W_{II}	$C_w = 0.000034975e^{0.08499(FA/BD\ WII)}$	0.9732	0.0026
FA/BD W_{III}	$C_w = 0.00014165e^{0.04457(FA/BD\ WIII)}$	0.9850	0.0019
1st Derivative			
D_{1318}/D_{1389}	$C_w = 0.03705(D_{1318}/D_{1389})^2 + 0.04314(D_{1318}/D_{1389}) - 0.00464$	0.9884	0.0014
D_{1405}/D_{1389}	$C_w = 0.05850(D_{1405}/D_{1389})^2 - 0.1980(D_{1405}/D_{1389}) - 0.1777$	0.9863	0.0015

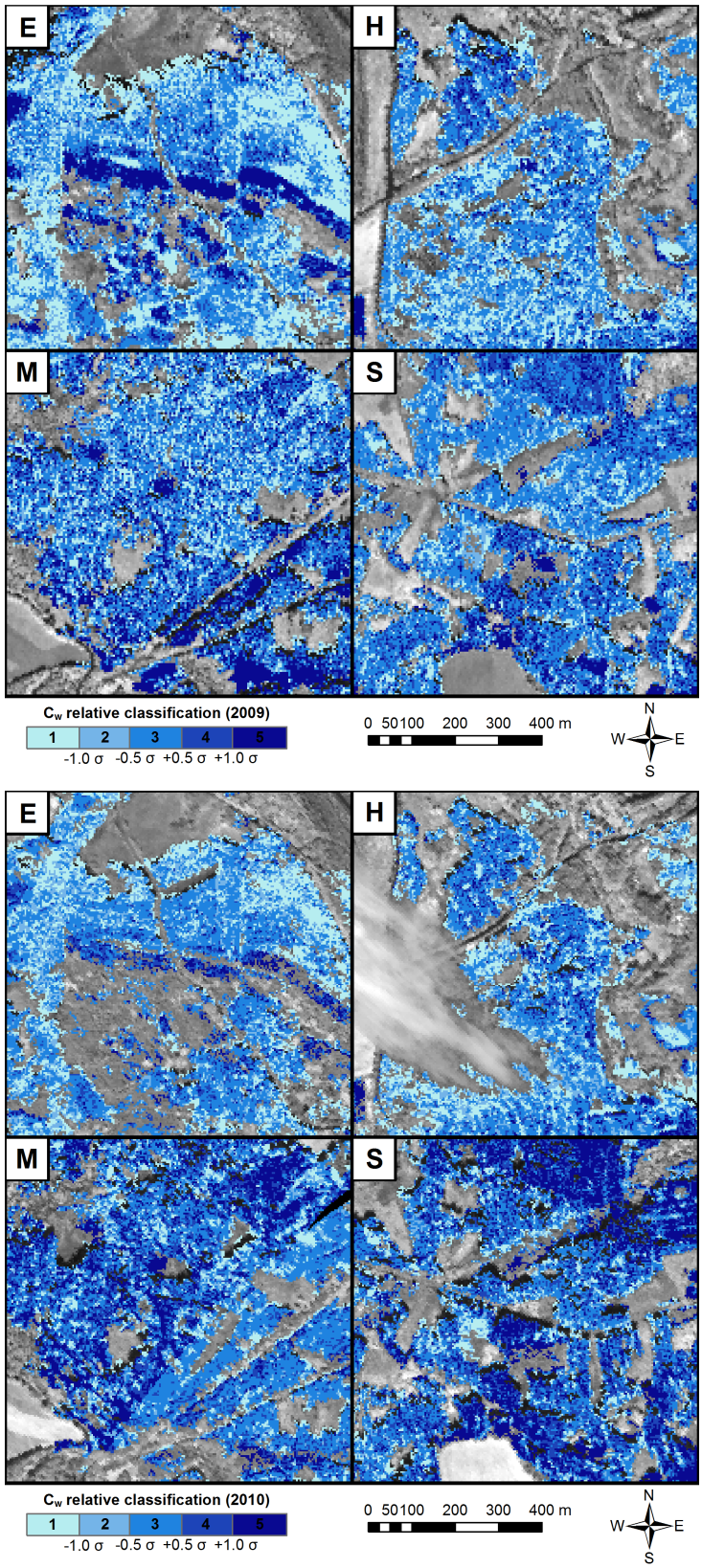

Figure 7.22: *Example of the relative classification of C_w based on NMDI vegetation index applied on the HyMap 2009 (upper) and 2010 (lower) dataset (E – Erika, H – Habartov, M – Mezihorská, S - Studenec).*

7.5 Classification of forest health status using the statistical model

The developed model assess forest health status in terms of three vegetation biochemical variables: chlorophyll content (C_{ab}), relative carotenoids content ($C_x/(C_x+C_{ab})$) and water content (C_w). It is based on assumption that low C_{ab} and C_w values and high $C_x/(C_x+C_{ab})$ indicate worse health status of vegetation in contrast with situations when high C_{ab} and C_w together with low $C_x/(C_x+C_{ab})$. However, primary problem lies in the definition of "high" and "low" values which can be differentiate either by some fixed threshold values or as a result of statistical analysis. In case of the developed model, the second possibility has been applied as the definition of fixed threshold values of the mentioned biochemical variables is almost impossible.

Each of the three considered biochemical variables is described by spectral indicator (vegetation index) which has been proved as sensitive to that variable. Relationships of various vegetation indices with the biochemical variables of interest were simulated using the PRO-FRT radiative transfer coupling. The functional dependence of a particular index with the corresponding biochemical parameter was then used to calculate score values whose relationship to the given biochemical parameter is linear.

In total, 10 chlorophyll sensitive, 10 carotenoids sensitive and 11 water sensitive vegetation indices have been tested within this work. All of them were found to be enough sensitive to be used as the inputs for the developed classification model. A basic principle was applied for selection of the indices used as the inputs for classification: all three used indices must be based on the same level of data transformation (i.e. using of indices based on for example continuum removal transformation together with indices based on reflectance derivative was not possible). The indices were then selected according to the highest R^2 values (indicating the tightest possible relationship to the biochemical variable of interest) and lowest RMSE values (indicating that the influence of other vegetation variables on the relationship to the biochemical variable of interest is as lowest as possible) respectively. Since the N_{718} was found to be the best chlorophyll content indicator (R^2 = 0.99; RMSE = 1.88 μg/cm^2) two other inputs had to be selected from the indices based on TOC reflectance (without any further transformation). Finally, these two indices were selected: R_{558}/R_{529} (R^2 = 0.95; RMSE = 0.0188) as the $C_x/(C_{ab}+C_x)$ indicator and NMDI (R^2 = 0.95; RMSE = 0.0030 cm).

The classification scheme described in the section 6.8 was then applied on these three input layers resulting in one raster layer whose values were ranging from 1 (representing the worst forest health status) to 5 (representing the best forest health status). An example of visualization of these classification layers both for HyMap 2009 and HyMap 2010 datasets can be seen in the Figure 7.23.

Looking on the results of the particular classifications (C_{ab}, $C_x/(C_x+C_{ab})$ and C_w) in Figures 7.20 to 7.22 as well as the results of the summary classification (Figure 7.23) we can see, that except the $C_x/(C_x+C_{ab})$ one there are similar spatial patterns of the values in 2009 and 2010. This indicates that 1) no dramatic changes of the forest health statues occurred between 2009 and 2010 and 2) the proposed classification approach is able to provide stable results.

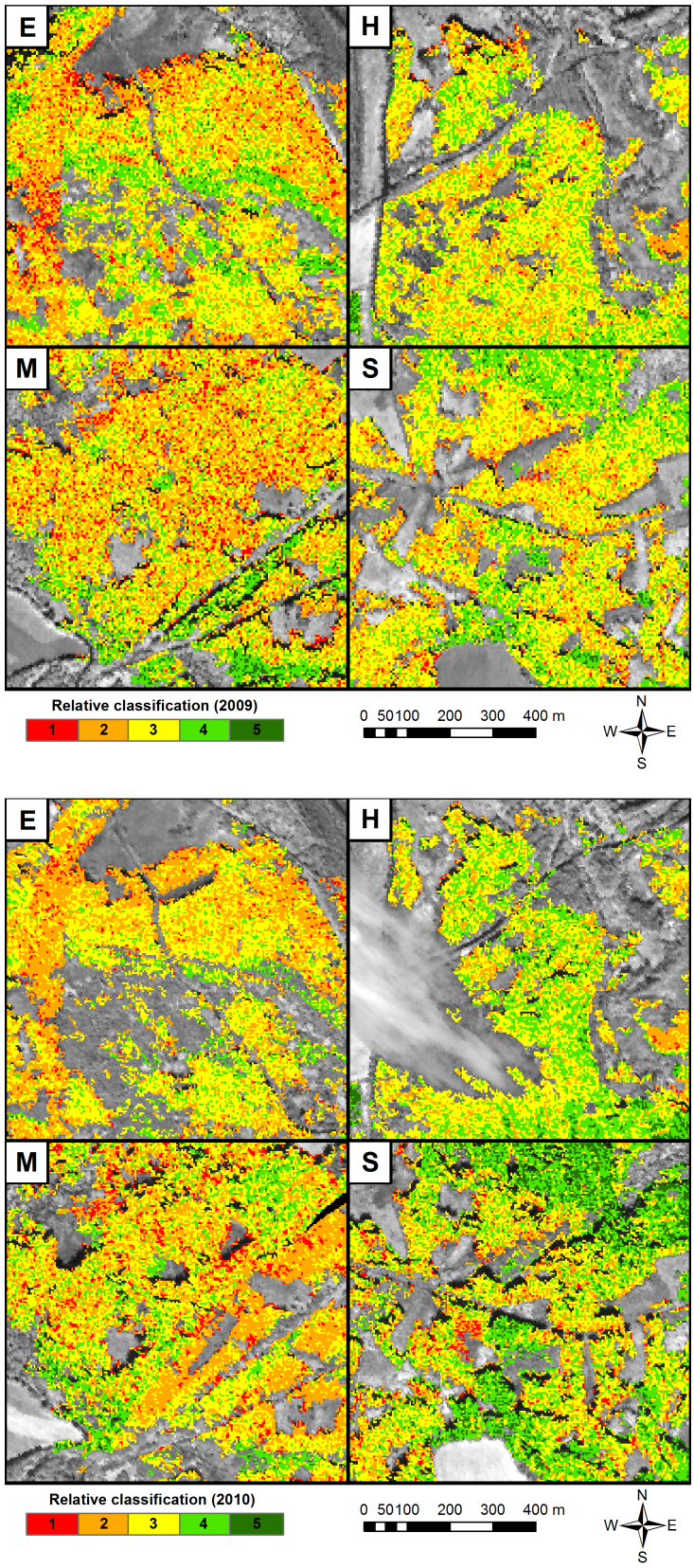

Figure 7.23: *Example of the relative forest health status classification based on the proposed classification scheme using the N_{718} (C_{ab}), R_{558}/R_{529} ($C_x/(C_x+C_{ab})$) and NMDI (C_w) as the inputs. HyMap 2009 (upper), HyMap 2010 (bottom). E – Erika, H – Habartov, M – Mezihorská, S – Studenec.*

Assessment of the performed classifications results was based on analysing relative frequencies of the particular classes 1 – 5. The results of the summary classification based on the all three input layers (C_{ab}, $C_x/(C_x+C_{ab})$ and C_w scores) were compared with the results of classification based on the same principle, but using only C_{ab} scores on the input (C_{ab} scores were calculated using the same vegetation index N_{718} as the summary classification). First, relative frequencies of the particular classes were calculated from the all pixels under the Norway spruce mask (see 6.1). As it can be seen in the Figure 7.24, distribution of the classes calculated for all Norway spruce pixels is very symmetric – i.e. the negative classes 1 and 2 have very similar frequencies as the positive ones (classes 4 and 5). The only difference between the summary classification and purely chlorophyll classification is that more values falls into the neutral class 3 and slightly negative (class 2) resp. slightly positive (class 4) classes, so the most extreme classes 1 and 5 are much less frequent than in case of the pure chlorophyll classification.

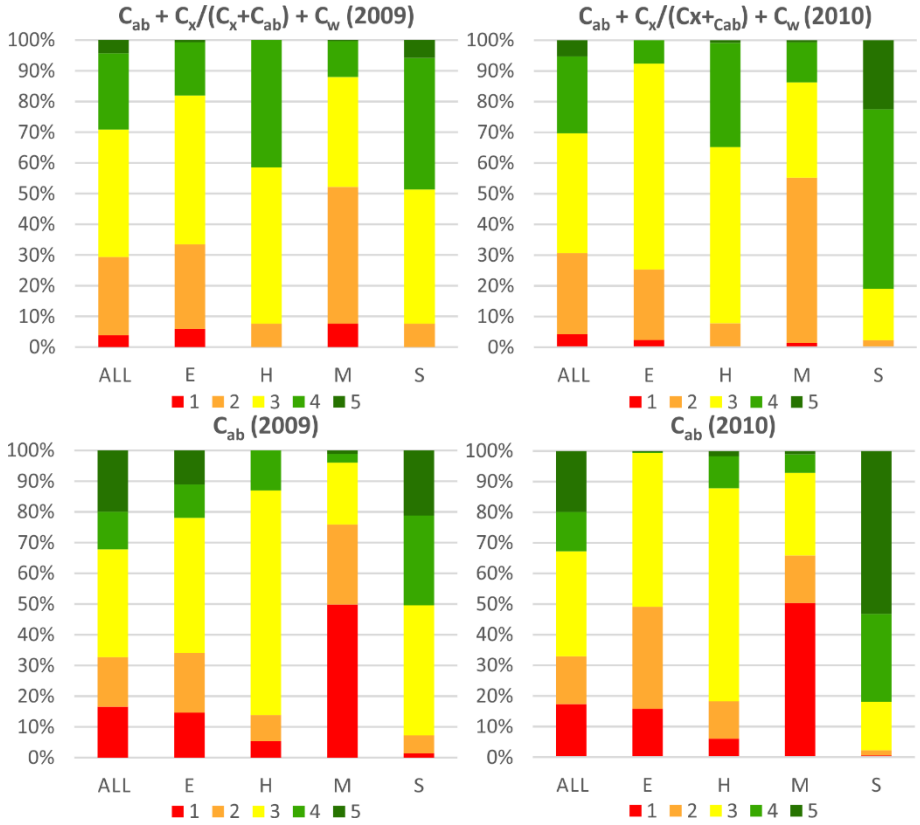

Figure 7.24: *Relative frequencies of the classes 1 – 5 resulting from the performed summary classification (C_{ab} + $C_x/(C_x+C_{ab})$ + C_w) as well as from classification based purely on chlorophyll content scores (C_{ab}). Both classifications were performed for both HyMap 2009 and 2010 datasets. Relative frequencies of the particular classes were calculated for the all Norway spruce pixels (ALL) as well as for the reference locations of interest Erika (E), Habartov (H), Mezihorská (M) and Studenec (S).*

In the next step, class frequencies were calculated also for the all four reference localities Erika (E), Habartov (H), Mezihorská (M) and Studenec (S). In this case we can observe significant asymmetries. Neutral class 3 significantly dominates in case of the Erika site with slight asymmetry to negative values. Strong asymmetry to the negative values can be seen in case of the Mezihorská site where class 4 significantly dominates in the summary classification. In case of the

chlorophyll classification, the most extreme (negative) class 1 dominates at this site. Opposite situation occurs for the Studenec site where the two positive classes (4 and 5) have the highest frequencies. The Habartov site shows domination of the neutral class 3, but class 2 has also quite high frequencies (higher than in case Erika and Mezihorská sites). It should be also noted that the frequencies patterns observed in 2009 dataset are very similar to those observed in 2010 dataset. As so, it proves stability of the results (i.e. the results are not changing randomly).

In addition, class frequencies were analysed also in the link with other factors, namely elevation, aspect (terrain orientation) and stand age. First, the stand age was taken into account. As for the forest inventory practice, forest stands are divided into the following eight classes by age: 1 – 20 years, 21 – 40 years, 41 – 60 years, 61 – 80 years, 81 – 100 years, 101 – 120 years, 121 – 140 years and 140+ years. Fifteen different stands were found for each age class except of the 140+ class which had to be excluded from the analysis as there were no enough pure Norway spruce stand of such age within the Sokolov basin area. As so, in total 105 Norway spruce stands entered the age class analysis for which frequencies of the health status classes were calculated (both for the summary classification $C_{ab} + C_x/(C_x+C_{ab}) + C_w$ as well as for the pure C_{ab} classification). The results can be seen in the Figure 7.25.

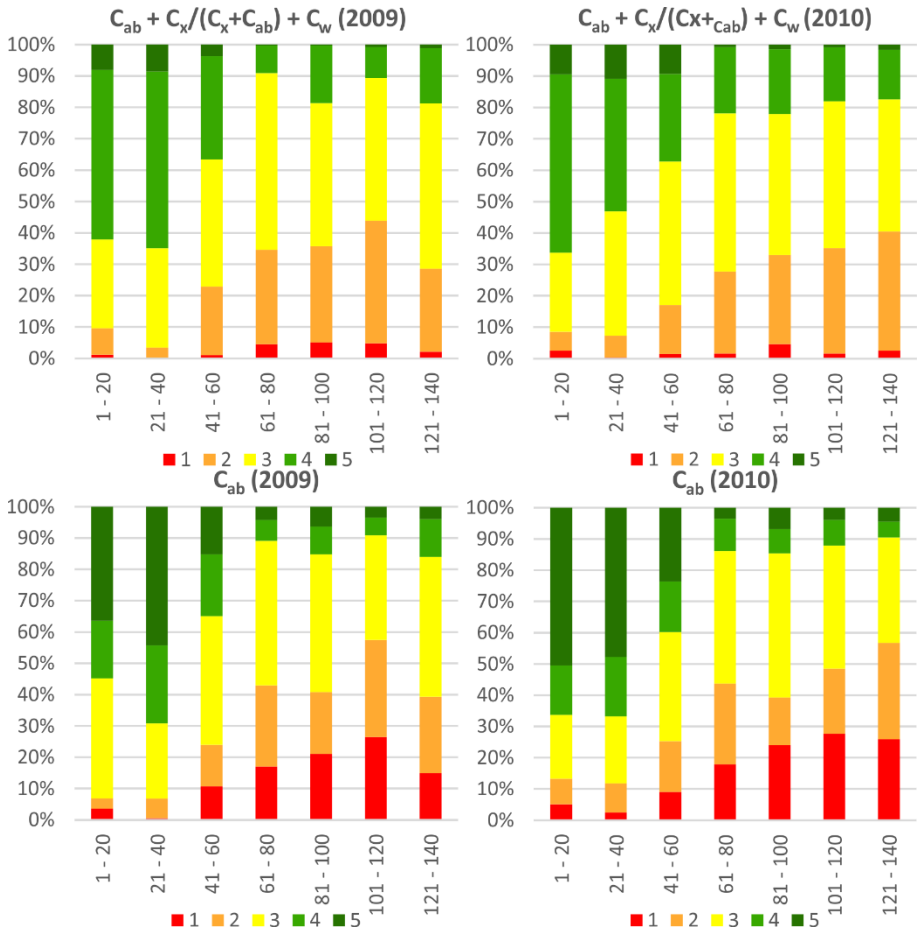

Figure 7.25: *Frequencies of the forest health status classes (both $C_{ab} + C_x/(C_x+C_{ab}) + C_w$ as well as C_{ab} classification calculated for different tree stands age classes.*

It is evident that frequencies of both classifications are related to stand age. In case of two youngest ages classes (1 – 20 and 21 – 40 years) there is clear domination of the two positive

classes (4 and 5) with no or very rare occurrence of the two negative classes (1 and 2). Since the age of 40 years, frequency of the neutral class 3 became relatively stable. Nevertheless, frequencies of the classes 1 and 2 gradually increase while frequencies of the classes 4 and 5 decrease. This trend can be seen in case of the both classification schemes as well as in the both years 2009 and 2010. These results also explain why the age of 40 years is considered as the border between young and mature Norway spruce stands.

The classification results were also tested in relationship with topographic properties of the stands – namely their elevation and aspect. The area of interest was divided into four elevation zones: 375 – 450 m, 450 – 550 m, 550 – 650 m and 650 – 750 m above the sea level. Frequencies of both summary and chlorophyll classifications were calculated for each of these zones (only Norway spruce pixels were taken into the analysis). From the Figure 7.26 it can be seen that frequency of the neutral class 3 stay stable in all four zones, but proportion of the negative classes 1 and 2 increases to the detriment of proportion of the positive classes 4 and 5 with the increasing elevation. This trend can be seen in case of both compared classification and was observed in the both years 2009 and 2010.

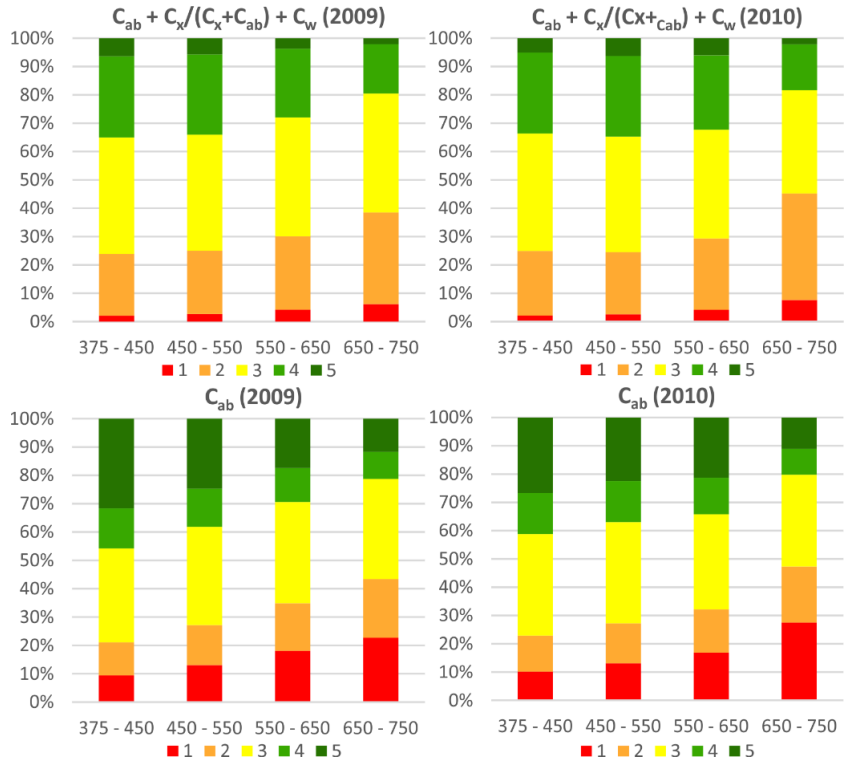

Figure 7.26: *Frequencies of the forest health status classes (both C_{ab} + $C_x/(C_x+C_{ab})$ + C_w as well as C_{ab} classification calculated for different elevation ranges (meters above the sea level).*

Influence of the stand aspect was also investigated within this analysis. The Norway spruce pixels were divided into three groups by their aspect: north facing (azimuth 0 – 45° and 315 – 360°), south facing (135 – 225°) and west and east facing (45 – 135° and 225° – 315°). The west and east orientation was taken together because they are equal in terms of sun illumination. The class frequencies were calculated for these three aspect zones in the same style as in case of elevation or age classes. However, in this case no significant differences were found neither in

summary nor in chlorophyll classification. This is the same in both years 2009 and 2010 (see Figure 7.27).

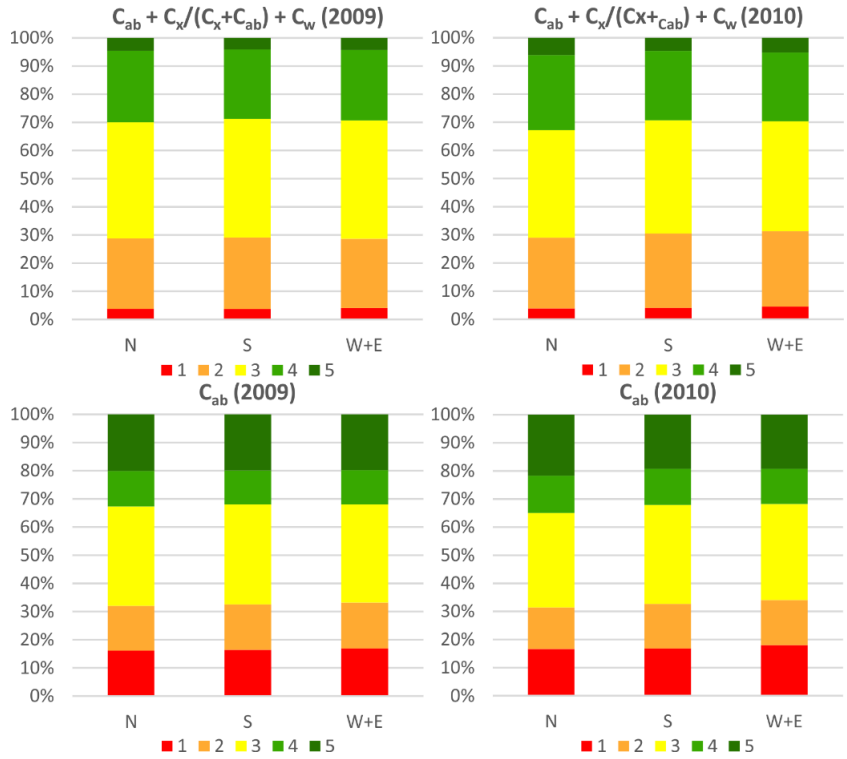

Figure 7.27: *Frequencies of the forest health status classes (both $C_{ab} + C_x/(C_x+C_{ab}) + C_w$ as well as C_{ab} classification calculated for different terrain orientations.*

Based on the obtained results of the forest health status classification it can be seen that there is remarkable similarity with the results of soil and needle sample analyses in terms of dividing the reference Norway spruce stands to those with less favourable soil conditions (Erika and Mezihorská) and the others with better soil conditions (Habartov and Studenec). Nevertheless, the soil conditions are for sure just one of several factors affecting the obtained results of forest health classification. As it can be seen, the results are also somehow affected by stand elevation and age. In this case it should be reminded that the trees growing at the Mezihorská site are a bit older than those at the other stands (81 – 100 years vs. 41 – 60 years). As it was demonstrated, older stands naturally tend to have higher frequency of negative classes in compare with younger stands. Real influence of elevation is questionable in case of the reference Norway spruce stands. It was demonstrated that higher elevated stands have generally higher frequency of negative classes compared to lower elevated ones. However, in case of the four selected reference stands the worst health status was classified at Mezihorská with located at 674 m a.s.l., whereas the best status was found at Studenec located at 662 m a.s.l. while the two other stands classified relatively close to average forest health class are located at much lower elevation (501 and 459 m a.s.l.). Therefore, probably the most correct conclusion is, that all the mentioned effects (soil properties, elevation, tree age etc.) have influence on the results of the forest health classification and since that it is not possible to take into account only one of them with ignoring the others.

Chapter 8: Discussion

The chapter provides discussion on the results obtained by the performed data analyses, their interpretation and practical consequences. At the beginning, the four reference Norway spruce forest localities are mutually compared in terms of their local environmental conditions, soil characteristics, foliage biochemistry and content of the selected chemical elements. This part is then followed by discussing on the results of the leaf level radiative transfer models parameterization including comparison of the obtained results with the results reported by other authors. Advantages and pitfalls of replacing optical properties measured in an integration sphere by measurements acquired by the use of a contact probe are discussed as well. The section contains also discussion on suitability of the both compared models for simulating optical properties of needles. Next, parameterization of the FRT canopy level radiative transfer model is discussed focusing mainly on potential source of inacurracies in model setting originating from the use of digital hemispherical photohraphy for extracting canopy architecture characteristics. Results of leaf area index estimation are discussed in the next section. The main attention is paid to reasons which might explain relatively poor quality of the LAI estimation. This topic is followed by evaluation of the chlorophyll content estimation comparing the obtained results with the outcomes of similar analyses reported by other authors. Importance of the need to optimize validation protocols taking into account influence of the different needle age classes on the overall tree spectral signature and thus on the results of chlorophyll content estimation is mentioned in the next section. The observed chlorophyll needle content is also confronted with chlorophyll content ranges repoted for healthy mature Norway spruce trees by other authors. Discussion on the results of the performed forest health status classification is provided at the final section of the chapter including also potential linkage between the patterns of the forest health classes and soil characteristics.

8.1 Comparison of local conditions of the Norway spruce stands of interest

The study demonstrated within this thesis was focused on potential of hyperspectral remote sensing to describe actual vegetation health status and detect possible vegetation damage/stress before any visual symptoms are observable. Norway spruce forests located in the Sokolov lignite basin were selected as the test area as the local growing conditions were supposed to be affected by long term open-pit coal mining and presence of several heavy industrial facilities (coal powerplants, chemical facility etc.). Therefore it was assumed that vegetation health status would show high spatial variability. Four localities (Erika, Habartov, Mezihorská and Studenec) were selected as the reference areas where collection of samples needed for current health status assessment was performed in 2009 and 2010.

Results of the laboratory analysis of needle foliar pigments and water content were assessed first. Trees growing at the Studenec site show highest needle chlorophyll content whereas the lowest values can be found at Mezihorská. Erika and Habartov sites are very similar

in terms of needle chlorophyll content with very slightly lower values in case of Erika. The basic problem is that the differences observed between these four localities were not statistically significant in case of 2009 dataset (mainly due to unequal variabilities of the C_{ab} content values at the particular sites). In fact, this has one very important consequence. It is evident that analysis aiming on general assessment of forest health status cannot be based only on chlorophyll content in such case. Other additional biochemical/biophysical vegetation parameters thus have to be taken into account.

One of the additional biochemical parameter was relative proportion of carotenoids on total foliar pigments content $C_x/(C_x+C_{ab})$. As it is reported by literature, relative proportion of carotenoids is higher in case of stressed vegetation (e.g. Demming-Adams and Adams (1996); Young and Britton (1990)). In case of the four reference stands used in this study, the lowest values were found at Studenec, whereas the highest values were found at Erika. In contrast with needle chlorophyll content, relative differences between the particular stands were found to be statistically significant.

Relative differences between the reference stands were similar in terms of both C_{ab} and $C_x/(C_x+C_{ab})$ parameters comparing two years 2009 and 2010. However, quite different situation was found in case of needle water content (C_w) as the pattern of water content values in 2009 differed from the one detected in 2010. It was also assumed that vegetation with worse health status will show lower water content in comparison with unstressed vegetation. This was found to be not truth as the highest water content values were found at Mezihorská (in 2009) which was generally considered as the site with the worst vegetation health status. This suggests that the actual needle water content is more related for example to amount of precipitation in the actual vegetation season then to be directly linked with influence of long-term vegetation stress.

The relative differences in foliar pigments observed between the four reference Norway spruce stands remarkably correspond with differences in soil substrate characteristics on these sites. This is most obvious in case of the parameters describing acidity of the soil environment such as exchangeable pH, exchangeable base cations (BCE) or base saturation (BS) where soil substrate at Erika and Mezihorská is significantly more acid than at Studenec and Habartov. This can be observed also on other related indicators as lack of the Ca^{2+} cations at the sites with lower pH or relationship of exchangeable soil acidity (TEA) with concentration of Al^{3+} cations (mobile aluminium is one of vegetation stressing factor).

On the other hand, situation in terms of the effect of soil heavy metals content on vegetation health status is far from being clear. Significantly higher concentrations of Cu and Zn were detected in soil substrate at Habartov and Studenec respectively. However, both of these sites show rather good vegetation conditions both in terms of laboratory analysis of the collected needle samples as well as the results of hyperspectral imagery analysis. It is remarkable that high soil Cu content was not propagated into the needle Cu content but in case of Zn high soil Zn level resulted in significantly higher content of Zn detected in the collected needles. Similarly, lack of soil Ca^{2+} cations was related in lower needle Ca content compared with other localities with higher soil pH.

Based on the obtained results it can be concluded that none of the reference Norway spruce stand can be classified as significantly damaged and others as totally undamaged. All reference stands grow in conditions which cannot be declared as optimal on one hand, but on the other hand, they are still far to be considered as critical. Nevertheless, particular differences in local conditions could be seen between the four reference sites. The effects of these differences in local conditions on vegetation biochemical and biophysical characteristics can be also observed. In relation to this, localities Studenec and Habartov can be considered as those with relatively good and average-to-good health status, whereas Mezihorská and Erika represents sites with relatively worse or average-to worse forest health status.

8.2 Leaf level spectra modelling

Leaf level spectra modelling was performed using the PROSPECT-5 and LIBERTY radiative transfer models. Both models were parameterized first using the calibration dataset containing measured values of C_{ab}, C_x, C_w and C_m together with ASD Fieldspec-3 spectrum for each particular sample used as the reference.

Better results were obtained using the PROSPECT-5 model as the average RMSE between simulated and measured spectra was generally lower in comparison with the LIBERTY model, especially in VIS and SWIR domains. The highest difference between the models can be seen in NIR domain where performance of LIBERTY is slightly better, but the observed RMSE was still quite high. This mismatch has probably two main reasons. First one is related to the fact that reflectance in NIR domain is mostly affected by internal structure of leaf/needle. (e.g. Slaton et al. 2001). PROSPECT model considers the leaf internal structure as a stack of N parallel plates divided by air gaps. This structure is typical for dorsiventral leaf which is typical for broadleaved vegetation, but is far different from the internal structure of needles where mesophyll cells are not arranged into parallel layers, but are concentrically surrounding central cylinder with vascular bundle (Lhotáková et al., 2008). This structure is far more similar to the concept of the LIBERTY model. The observed mismatch in reflectance within NIR domain might be thus caused by the fact that real structure of needles does not correspond with that structure which is considered by the used models. Different mesophyll structure then leads to different environment for radiation scattering in NIR domain (Kivimäenpääa and Sutinen, 2007). The second reason of the observed differences in NIR domain might be related to instability of reflectance measurement when a contact probe has been used for acquisition of the needle spectra. This instability affects mostly the NIR region (see further).

The obtained results were compared with the results of Yañez-Rausell et al. (2010) comparing performance of the original PROSPECT model with the results obtained by corrected versions of this model optimized for simulating needle spectra. This comparison can be seen in Table 8.1. It can be observed that some level of correction is required in case of the PROSPECT model to be fully applicable to coniferous tree species. On the other hand, the RMSE values obtained from original (i.e. uncorrected) PROSPECT-5 model are significantly lower in comparison with the values reported by Yañez-Rausell et al. (2010) for the uncorrected versions PROSPECT-3.01 and PROSPECT-4.

Table 8.1: *RMSE of the simulated vs. measured reflectance averaged for the spectral ranges of 450 – 1600 nm and 750 – 1600 nm calculated for various versions of the PROSPECT model. The results reported by Yañez-Rausell et al. (2010) are compared with the results obtained in this study. All measurements were performed on Norway spruce needles. The versions of PROSPECT model using an optimization for simulation Norway spruce spectra are marked by asterisk (*).*

author	Leaf level RTM model	RMSE [%] (450 – 1600 nm)	RMSE [%] (750 – 1600 nm)
Yañez-Rausell et al. (2010)	PROSPECT-3.01	6.35	7.10
	PROSPECT-3.01S*	2.33	3.93
	PROSPECT-4	7.01	7.98
	PROSPECT-4.01*	3.83	4.64
	PROSPECT-4.02*	2.98	3.52
This study	PROSPECT-5	4.39 (U_1) 4.39 (L_1)	5.26 (U_1) 5.28 (L_1)
	LIBERTY	5.10 (U_1) 4.54 (L_1)	5.79 (U_1) 4.65 (L_1)

Several problematic aspects related to the acquisition of Norway spruce needles spectra were identified during this study. These aspects should be mentioned and discussed as they might have influence on the obtained results.

First, acquisition of Norway spruce needles spectra was performed using an ASD Fieldspec radiometer equipped by high intensity contact probe (CP). Spectra of needle stacks were measured instead of measuring spectra of individual needles. As so, the resulting spectra have character of infinite reflectance (R_∞) rather than character of single-leaf reflectance. Leaf level spectra simulated by PROSPECT-5 model (representing single-leaf reflectance) had to be transformed to the level of infinite reflectance before considering it for model parameterization. In fact both approaches (i.e. model parameterization with and without considering infinite reflectance transformation) were carried out. It can be seen that consideration of infinite reflectance has strong influence on model parameterization as the optimal values of the N parameter obtained with consideration of the infinite reflectance transformation are highly different from those without consideration of such transformation. As the overall accuracy of the performed parameterization was much lower in case of using the infinite reflectance transformation, this setup was chosen for further analysis. Note, that infinite reflectance is a standard part of the output simulation in case of the LIBERTY model, so no transformation has to be performed in such case.

In addition, since the needle spectra were acquired using a contact probe, only reflectance has been measured. Therefore there was no information about needle transmittance. Due to that, the best possible fit between simulated and measured reflectance was looked for while ignoring fit between simulated and reference transmittance. Thus the performed model parameterization might have resulted into situation when there is very low error in simulated reflectance at the

cost of high error in simulated transmittance (which cannot be assessed in any way as there were no reference values).

The described problems with the need of infinite reflectance transformation and missing reference for leaf transmittance are directly related to the used method of needle spectra acquisition using a contact probe. An alternative way of needle spectra acquisition is using an integration sphere. A quick analysis was performed to compare these two approaches to see their potential advantages and drawbacks. Spectra of the same needle samples were measured both using contact probe (CP) and integration sphere (IS). Five spectra were measured for each sample. The results can be seen in Figure 8.1. It can be seen that the main problem of the measurement using a contact probe is instability of the measured reflectance values especially in the NIR domain (the measured reflectance fluctuated in approximately 10 % range in NIR). On the other hand, stability of the measured reflectance values is almost ideal in case of using integration sphere. However, the measured spectra are strongly affected by high level of noise, especially in the SWIR domain. From practical point of view, acquisition using a contact probe is far quicker and generally simpler than using an integration sphere. Especially setting the measured needle sample into the sphere in correct way is very time consuming. In addition, gap fraction measurement has to be performed for each measured sample to perform a necessary correction to get correct reflectance and transmittance values. On the other hand, reflectance measured by the use of integration sphere are much closer to single-leaf reflectance, so there is no further need of infinite reflectance transformation during model parameterization. Advantages and disadvantages of both approaches are summarized in Table 8.2.

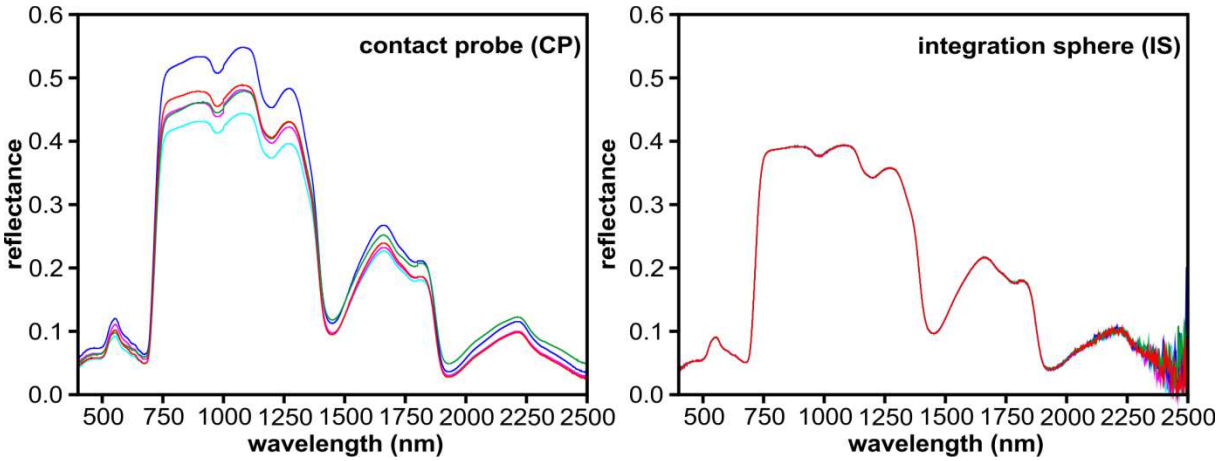

Figure 8.1: *Reflectance of the one particular needle sample measured five times by contact probe (left) and integration sphere (right).*

Table 8.2: *Summary of advantages and disadvantages of using contact probe (CP) and integration sphere (IS) for acquisition of needle spectra.*

Contact probe (CP)	Integration sphere (IS)
• suffering by instability of the measured reflectance in NIR • low level of noise in the data (compared with IS) • clusters of needles are measured instead of measuring spectra of single needles; measured reflectance is thus affected by multiple reflections of radiation – the result has thus rather character of infinite reflectance than single leaf reflectance • measurement is easy and quick	• high stability of the measured reflectance and transmittance values • suffering by high level of noise especially in SWIR • need for gap fraction correction to get correct reflectance and transmittance values (in case of measuring needle spectra) • setting of the measured sample into the sphere is difficult and time demanding (in case of measuring needle spectra) • measured output has character of single leaf reflectance/transmittance so no further transformations (taking into account needle clumping) is required

8.3 Canopy level spectra modelling

A simple workflow based on combination of DHP processing, application of allometric relationships and in-situ expert estimation was used for parameterization of the FRT canopy level radiative transfer model. The proposed method could be useful, especially when no forest inventory data are available for the model parameterization.

Use of allometric equations for the canopy level model parameterization is not ideal as there are usually no a-priori information on parameters of the stands (e.g. age, location etc.) used for development of such allometric relationships. On the other hand parameters such as tree height or crown diameter have relatively limited influence on the stand spectral signature, so the mismatch of the simulated and measured spectra rising from character of the used allometric equations is not dramatic. Nevertheless, in-situ measured values are still preferred if available.

Amount of foliage biomass (defined by DLW in case of the FRT model) has much larger impact on stand spectral signature. The DLW (dry leaf weight) was determined using the relationship of SLW (specific leaf weight), LAI (leaf area index) and DEN (tree density) parameters. SLW was determined with reasonable accuracy using the collected Norway spruce needle samples, but both LAI and DEN were estimated indirectly using DHPs. Errors of LAI and DEN estimations are thus propagated into DLW calculation and finally may influence the stand spectral signature. In this case, LAI derived from DHP processing was considered as correct and error-free value. However, as digital hemispherical photography is only an indirect method for LAI estimation, there is some level of error in fact. As so, it would be correct to verify the LAI values extracted by DHP processing with results of some other LAI estimation method. In addition, it should not be forgotten that the values obtained from DHP processing (as well as from all other indirect methods including canopy plant analysers) refers in fact not to LAI (leaf area index) but to PAI (plant area index). One possible solution could be based on measurement of WAI (wood

area index) which could be than used to transform PAI values to LAI. Measurement of WAI can be performed in case of broadleaf trees, but is very problematic for evergreen coniferous vegetation.

The observed differences between canopy model simulated and hyperspectral image-extracted forest stands spectra may have origin in inaccuracies of canopy model parameterization as well as in the level of generalization of canopy structure, but they are also caused by propagation of the error of leaf level simulation. Discrepancies may also rise from the fact that only current age class needles were used for leaf level model parameterization whereas in real canopy there are several needle age classes present. In addition, the used FRT canopy level model cannot handle more than one type of needles within one tree crown. Still, the current year needles are most exposed ones and thus should have the biggest contribution in forming the TOC reflectance.

Indeed, quality of hyperspectral image data calibration and pre-processing should also not to be forgotten. In case of this study all pre-processing chains were justified using in-situ reference data. From this point of view, better results were obtained for the dataset acquired in 2009 compared to the 2010 dataset. This is somewhat surprising as the pre-processing chain was the same for both datasets but the sun-sensor orientation was less optimal in 2009 (55°) than in 2010 (66°) resulting in stronger influence of cross-track illumination effects. The reason of such result might be explained by the different timing of ground campaigns associated with both hyperspectral data acquisitions. Collection of the reference Norway spruce needle samples was conducted simultaneously with the HyMap data acquisition in 2009 (resp. in the day of data acquisition and the following day). However, the samples were collected 12 days after the flight campaign in 2010 as heavy rains started shortly after the HyMap data acquisition. This highlights the importance of simultaneous airborne and field data collection.

8.4 Retrieval of semi-quantitative indicators of forest health status and its classification

Four layers describing forest biochemistry and biophysics were generated from the source HyMap hyperspectral imagery: leaf area index (LAI), chlorophyll content (C_{ab}), carotenoids-to-foliar pigments ratio ($C_x/(C_x+C_{ab})$) and water content (C_w). A sensitivity analysis was performed first to check which of the HyMap imagery bands are the most sensitive to changes in these biochemical/biophysical parameters. The results of this analysis were used to define several new vegetation indices that seemed to be optimal in case of using HyMap imagery. These newly developed indices were used in addition with other indices reported by various authors.

Leaf area index layer was produced first. The very basic problem was that none of the vegetation indices reported by literature as good LAI indicators was highly sensitive to changes in LAI on one hand and totally insensitive to changes in leaf chlorophyll content on the other hand. In fact, the values of such indices were found to be influenced both by LAI as well as by C_{ab}. Range of the wavelengths where high sensitivity of reflectance to changes in LAI can be observed is quite broad and thus covering also the wavelengths where high sensitivity to changes in chlorophyll occurs. Vegetation indices based on the 1st derivative of reflectance were finally found as much

better option for retrieval of LAI as the wavelengths where maximum sensitivity to changes in LAI occurs are relatively clearly separated from those with maximal sensitivity to leaf chlorophyll content. As a result two derivative-based vegetation indices D_{733}/D_{805} and D_{748}/D_{805} were used as the LAI spectral indicators. Functional relationship between these indices and leaf area index was simulated using the PRO-FRT ratiative transfer model coupling. The predictive regression formulas were then inversely applied on the values of these indices calculated from the source HyMap imagery to obtain the LAI layers.

The LAI values retrieved from HyMap imagery were then compared with the values obtained by the processing of digital hemispherical photography. The HyMap based LAI values were found to be underestimated in comparison with the DHP based ones and a simple linear empirical correction was applied to minimize difference between DHP and HyMap based values. It should be noted that the parameters of this empirical correction were calculated using different DHP dataset than the one used for validation. The corrected values were compared with the validation dataset again resulting in RMSE of 0.77 (both D_{733}/D_{805} and D_{748}/D_{805} in 2009) and 0.80 (D_{733}/D_{805}; 2010) resp. 0.79 (D_{748}/D_{805}; 2010). This represents relative RMSE (RRMSE) of approximately 30 %. Moreover, the observed differences between image-extracted LAI and the reference values seem to have character of random error rather than a systematic offset. A positive thing is that the number of overestimated values is similar as the number of underestimated values.

These errors in LAI estimation might have several reasons. First, LAI values determined from DHP were considered as fully correct reference. However, DHPs are also an indirect technique for LAI estimation as well as spectral analysis of hyperspectral data. Thus there is no guarantee that the DHP-derived LAI values are totally error-free. In addition, all values based on DHP (or any other indirect gap distribution method) refer in fact to Plant Area Index (PAI) rather than LAI. This means that the whole area of plant is taken into consideration instead of green foliage only. A species-specific transformation coefficient has to be known to be able to transform PAI to true LAI. This can be relatively easily obtained for broadleaved trees where the transformation coefficient is calculated as the difference of PAI calculated from DHPs acquired in full vegetation season and PAI calculated from the DHPs of the same stand acquired during winter (after leaf fall). However, this method cannot be applied on coniferous trees species as there is no leaf fall (with exception of larch).

The second reason of the observed error in LAI estimations might be caused by incorrect parameterization of the FRT canopy level radiative transfer model. This is primarily related to the clumping index whose values were not a-priori known for the reference stands and thus had to be estimated. Due to these findings, the LAI data layers were finally not used for the further statistical forest health classification.

Chlorophyll content layers were produced in the next phase. In total, 10 vegetation indices were taken into consideration as the chlorophyll content spectral indicators. Functional relationships of these indices to chlorophyll content were simulated using the PRO-FRT models coupling. The obtained predictive regression formulas were inversely applied on the values of these indices extracted from HyMap imagery. The estimated chlorophyll content values were then compared with the ground truth values based on laboratory analysis of the collected Norway

spruce needle samples. The best results were obtained for N_{718} (2009: RMSE = 4.83 μg/cm^2, R^2 = 0.57; 2010: RMSE = 4.53 μg/cm^2, R^2 = 0.48) and D_{718}/D_{704} (2009: RMSE = 4.98 μg/cm^2, R^2 = 0.54; 2010: RMSE = 5.88 μg/cm^2, R^2 = 0.49). These results are in good correspondence with the previous work of the author (e.g. Mišurec et al. 2012 or Kopačková et al. 2014) where different chlorophyll content estimation techniques were used. The radiative transfer modelling approach was applied in Mišurec (2014) where PROSPECT and DART models were used for Norway spruce chlorophyll estimation resulting in RMSE = 5.82 μg/cm^2, R^2 = 0.39.

The obtained results were compared with the results reported by other authors. Zarco-Tejada et al. (2004) performed chlorophyll content estimation for five stands of Jack Pine (*Pinus banksiana*) based on coupling of PROSPECT and SPRINT radiative transfer models. Chlorophyll content values were retrieved from CASI airborne hyperspectral imagery using R_{750}/R_{710} vegetation index as the chlorophyll content indicator. The final RMSE of the chlorophyll content estimation was 8.1 μg/cm^2. Both needle as well as canopy level chlorophyll content estimation was performed also by Moorthy et al. (2008) using LIBERTY and SAILH radiative transfer models. Canopy chlorophyll content values were extracted from CASI imagery using again the R_{750}/R_{710} vegetation index as the chlorophyll content indicator with the final RMSE of 5.3 μg/cm^2 (the study was performed again for Jack Pine). Malenovský et al. (2013) performed chlorophyll content estimations for Norway spruce located at Bílý Kříž (Moravian-Silesian Beskids, North-east Moravia) using coupling of PROSPECT and DART models. Chlorophyll content retrieval was performed using Artificial Neural Network technique (ANN) with the final RMSE = 2.18 μg/cm^2 as well as four vegetation indices: $ANCB_{650\text{-}720}$ (RMSE = 2.27 μg/cm^2), $ND_{925/710}$ (9.07 μg/cm^2), $R_{750/R710}$ (RMSE = 4.16 μg/cm^2) and TCARI/OSAVI (12.30 μg/cm^2).

Nevertheless, the final results of the chlorophyll content estimation validation is strongly related to the setup of the used validation protocol. Although not much attention is usually payed to this topic, it should be discussed. The given forest stand (used for validation) is represented by a group of pixels in case of hyperspectral imagery. Since it is not possible to distinguish individual trees in case of the HyMap imagery, overall value for the entire stand has to be taken into consideration. This overall value can be calculated as mean (such as in case of this study) of the all pixel values representing the given stand. Median could be alternatively used as well. This mean (or median) value has to be compared with the results of the laboratory analysis of the collected needle samples. However, there are separate chlorophyll content values for particular needle age classes and crown positions (U_1, U_3, L_1 and L_3) for each individual tree. These values have to be first somehow merged together to get one value per one sampled tree which are then merged across the given stand. The question is how to merge U_1, U_3, L_1 and L_3 levels chlorophyll content values into one "whole tree" value. Simple mean of the U_1, U_3, L_1 and L_3 values was used in case of this study. This means that each needle level had the same influence on the final "whole tree" value. However, this is not corresponding with reality at least because the following reasons:

- There is generally higher amount of older needles (represented by U_3 and L_3 classes) within the tree crown in comparison with the amount of the current year needles (U_1 and L_1). However, the older needles are hidden inside the crown whereas the current needles make an outer crown layer. The current year needles thus should

have higher influence on the overall spectral signature of the tree crown than the hidden older needles.

- Transitional part (represented by L_1 and L_3) includes major amount of foliage within the crown. However, the part of crown which is visible in case of nadir view sensing is represented mostly by the topmost juvenile part of the crown (needle classes U_1 and U_3). Therefore, needles from the juvenile part of the crown should have higher influence on the crown spectral signature than the needles from transitional part of the crown.

It can be seen that the relationships between needle age/crown position and crown spectral signature are far from being easily defined. But it is also clear that some kind of weighting of the particular needle sample classes should be applied before calculating the "whole tree" reference value that is used for further validation. This system of weights calculated for different needle age/crown positions were developed and described by Lukeš et al. 2011. Unfortunately, these weights were developed for young Norway spruce trees whose crown geometry is significantly different from the geometry of mature trees. Moreover, three crown position levels and three needle age classes were defined within this study. As a result, it was not possible to use this weighting system for the purpose of the study described in this thesis.

Both LAI and C_{ab} data layers were designed as absolute values estimations. In contrast to that, the two other data layers: $C_x/(C_x+C_{ab})$ and C_w were designed as relative indicators describing spatial patterns of these two parameters. This was done by transformation of the original vegetation indices into scores with clearly defined functional relationship to these two biochemical variables. This functional relationship was again modelled using the PRO-FRT radiative transfer models coupling. The C_{ab} layer was finally generated in relative version as well and was used together with the two other layers ($C_x/(C_x+C_{ab})$ ans C_w as the inputs for statistical forest health classification model.

8.5 Statistical forest health classification model

Health status of the Norway spruce forests located within the area of interest was assessed using three spectral indicators related to forest biochemistry and biophysics. These spectral indicators were defined as vegetation indices whose functional relationship to vegetation biochemistry/biophysics was modelled using the PROSPECT+FRT radiative transfer models coupling. These indicators were: N_{718} (indicator of C_{ab}), R_{558}/R_{529} (indicator of $C_x/(C_x+C_{ab})$) and NMDI (indicator of C_w) These vegetation indices were extracted from the two HyMap datasets acquired over the area on interest in 2009 and 2010.

Forest health status classification is naturally complicated by the fact that it is not possible to define fixed threshold values of vegetation biochemical/biophysical parameters clearly dividing health and damaged (stressed) vegetation. For example, Siefermannharms (1994) reports range of needle chlorophyll content for 60 years old healthy Norway spruces growing at 840 m above sea level to 2.2 – 2.7 mg/g (meaning 40.0 – 49.1 μg/cm^2 in case of taking into consideration SLA = 55 g/cm^2 for Norway spruce needles). Schlerf et al. (2010) report the range of needle chlorophyll content for healthy mature Norway spruces growing in altitude 400 m a.s.l.

as 3.21 ± 0.30 mg/g (i.e. 52.9 – 63.8 μg/cm^2), whereas 4.30 ± 1.06 mg/g (i.e. 58.9 – 97.5 μg/cm^2) is reported by Atzberger and Werner (1998) for spruces located at 700 m a.s.l. It can be thus seen that the limit values defining "common" (or undisturbed) status are strongly site specific and thus no "general" values can be found.

If there had been clearly defined damaged and healthy Norway spruce stands within the area of interest, then it would have been possible to define such local threshold values on empirical basis. However, none of the reference Norway spruce stands could be classified either as seriously damaged or fully undamaged. Therefore, the described statistical approach was applied in case of this study. Statistical distributions of the values of the four spectral indicators of forest biophysics and biochemistry were used to define the most common values (mean μ). The threshold values defining the particular forest health classes were then defined using multiples of the measure of values variability (standard deviation σ) after filtering out out-layer values (further than ±2σ from μ). Nevertheless, it has to be clearly stated that this method represents classification of the actual values relative to the most common ones. For example, if there would be only damaged stands within the area of interest, then mean and standard deviation of the indicator values can be definitely calculated, but classification results have to be understood as differentiation of "more damaged" and "less damaged" stands rather than differentiation of "damaged" and "undamaged" stands. In other words, result of the proposed classification (and its interpretation) is always related to the actual situation within the area of interest. However, this can be seen as advantage since it is not requiring definition of any fixed threshold values.

Frequencies of the particular forest health classes of the proposed classification scheme were then further assessed to see what is the effect of such factors as elevation, terrain orientation and stand age structure. Finally, influence on the classification results was found in case of elevation and age structure (the higher elevation or older trees, the higher frequency of negative forest health classes). Some of these influences might affect the results of forest health classification of the used reference stands. In general, Mezihorská site was found as the stand with the relatively worst health status, whereas the best forest conditions were found in case of Studenec stand. Erika and Habartov are somewhere in the middle between these two stands, but the results indicate that tree health status at Erika is slightly worse in comparison with Habartov. The worst forest health status at Mezihorská might be explained by the fact that it is the site with the highest elevation (674 m) and the highest tree age. However, Studenec is the site with the second highest elevation (662 m) and the local forest health status was classified as the best one. So elevation itself cannot fully explain the observed pattern. Moreover, the age structure of the Studenec stand is the same as in case of the site Erika and Habartov.

Correspondence of the observed forest health status patterns with the results of needle biochemistry and soil substrate analysis become evident in more detailed view on the data. The best forest health status, observed as the result of the proposed classification scheme at Studenec, corresponds with the highest needle chlorophyll content and lowest carotenoids-to-foliar pigments ratio determined by laboratory analysis of the collected needle samples. On the other hand, lowest chlorophyll content and relatively higher carotenoids-to-foliar pigments ratio was found at Mezihorská.

A link can be also found between the observed forest health status pattern and the soil substrate properties related to soil acidity. The two stands showing relatively worse forest health status (Mezihorská and Erika) represents places with significantly lower soil pH (organic horizons) in comparison with the stands showing relatively better health status (Habartov and Studenec). The same pattern can be then found in case of both Base Exchangeable Cations (BCE) and Base Saturation (BC). The lack of soil base cations can be further documented by significantly lower content of Ca^{2+} cations in more acidic conditions of the Mezihorská and Erika sites. In addition, the lack of soil calcium cations propagated to needle calcium content, which is here significantly lower in compare with the values observed at Studenec and Habartov sites. On the other hand, influence of the presence of heavy metals in soil was found to be unclear. Over limit soil copper (Cu) content values were detected at Habartov in comparison with the other reference stands. However, high soil copper content was surprisingly not propagated into the needle copper content, which was very similar to the values observed for all other stands with much less soil Cu content. On the other hand, high soil zinc values were found at Studenec (much higher than in case of the other stands, very close to upper limit). In this case, high soil zinc content resulted in higher needle zinc content. Although significantly higher soil zinc content values were detected at the Studenec site, the local Norway spruce forest shows the better vitality. Therefore it seems that presence of the observed levels of soil zinc and copper is not the main driving force of the observed forest health status as it is more likely determined by soil acidity as the main factor. In addition, no significant differences between the reference stands were observed in terms of other soil parameters such as organic material decomposition indicated by the C/N ratio etc.

Chapter 9: Synthesis and Conclusion

The final chapter of the thesis provides overall synthesis of the results obtained by the performed analyses followed by conclusions and practical consequences that might help with implementation of the proposed forest health classification concept. Finally, several issues having strong potential for improvements are proposed for a further research.

The main objective of the performed study was to develop methodology for forest health status assessment based on analysis of airborne hyperspectral data supported by ground data collection. Performance of the developed methodology was practically demonstrated on the Norway spruce forests growing within the Sokolov lignite basin. These Norway spruce forests were not directly affected by mining activities as they are located outside the mining areas. However, there was still assumed indirect influence including mainly dust imisions and fallout as well as soil acidification linked to emission of gases such as sulphur dioxide (SO_2) and nitrogen oxides (NO_x) originating from local coal power-plants and heavy industry facilities.

Four reference localities were selected for this study: Erika, Habartov, Mezihorská and Studenec where ground data were collected for calibration and validation purposes. In total, 19 Norway spruce stands were taken into account for collection of ground reference data. Needle sampling was performed at four of these stands (50 sampled mature Norway spruce trees) to analyse foliage biochemistry. In addition, data for describing stand biophysics and structure were collected at the all stands using primarily digital hemispherical photography technique.

None of the reference locality can be considered as significantly damaged in terms of forest health status as no symptoms of vegetation damage were observed during the ground data collection. Nevertheless, relative differences in forest biochemical and biophysical properties were found. However, it is not possible to set any general threshold values of parameters such as foliar pigments content or leaf area index clearly differentiating damaged and undamaged stands. Such threshold values are strongly site specific and usually there is not sharp boundary of what is considered as “damaged” and “undamaged” forest. Therefore, a statistical approach was used for the developed method as it is related to statistical distribution of the selected forest health biophysical and biochemical indicators values described by corresponding vegetation indices extracted from airborne hyperspectral data. The most common values are found first and relative classification based on the variability measures is then applied. At this point it has to be highlighted, that such classification has relative character – i.e. it describes what is the current status of the given stand in relative comparison with the most common values occurring within the given area. On one hand, this approach is able to describe spatial patterns of the particular biochemical/biophysical variables and general forest health status. In case of this study, it was tested whether the spatial pattern of the observed forest health status corresponds with characteristics of soil substrate. On the other hand, it is unable to provide any information on vegetation characteristics in absolute level. As so, it is not suitable for comparing forest status at several areas far away from each other and differing in local environmental conditions as this will result in differences in statistical distributions of the forest parameters of interest.

Functional relationships between the biochemical/biophysical parameters of interest (C_{ab}, $C_x/(C_x+C_{ab})$, C_w and LAI) were modelled using combination of two radiative transfer models: PROSPECT-5 (needle level) and FRT (canopy level). On needle level, performance of the PROSPECT-5 radiative transfer model was compared with the results obtained by the use of the LIBERTY radiative transfer model. Although the PROSPECT model was originally developed for simulating optical properties of dorsiventral leaves, the obtained results were found slightly better corresponding to the reference dataset than the simulations provided by the LIBERTY model, which was originally developed for simulating optical properties of needle-leaved vegetation. From technological point of view, parameterization of the both models was performed using reference needle spectra acquired by ASD Fieldspec-3 spectroradiometer equipped by contact probe. This workflow is much easier and far less time consuming than using an integration sphere. However, there are also several disadvantages. First, there is no information about leaf/needle transmittance in contrast with using an integration sphere. As so, the leaf level models were calibrated to provide reflectance corresponding as much as possible to the reference spectra regardless possible errors in simulated transmittance. Second, spectra of needle stacks or clusters were measured by the contact probe in contrast with using an integration sphere where the result can be understood as single-leaf reflectance. Infinite reflectance transformation thus has to be taken into account when the spectra acquired by contact probe are used.

Database of needle optical properties were created using the parameterized PROPECT-5 model for defined ranges of leaf chlorophyll, carotenoids and water contents. These databases were then up-scaled to canopy level using the FRT radiative transfer model. This model combines geometrical properties of forest stand with numerical solution of radiative transfer. The FRT model is quite highly generalized and can be used on the level of forest stands (i.e. not for simulation of spectral signature for individual tree crowns). However, this was not perceived as disadvantage in case of this study because the simulations obtained by the FRT modelling were finally applied on HyMap airborne hyperspectral data whose spatial resolution did not allow distinguishing of individual trees in the imagery and thus all the analyses were performed on stand level. On the other hand, simplicity of the FRT model was understood as the most important advantage of this model as only relatively simple tools and methods need to be used for the model parametrization in comparison with such complex and thus complicated models like for example DART. The FRT model can be parameterized using just the information from forest inventory data. The workflow demonstrated in this thesis shows an alternative way of the FRT model parameterization in case when forest inventory data are not available.

Combination of the PROSPECT-5 leaf level model and FRT canopy level model was used to produce database of canopy level spectral signatures for various levels of the biochemical parameters of interest (C_{ab}, $C_x/(C_x+C_{ab})$ and C_w) and canopy structure (LAI described by stand density – DEN and dry leaf weight – DLW). Sensitivity analysis was performed first to find the most appropriate wavelengths (corresponding to bands of the HyMap imagery) for definition of functional relationships between spectral signature and forest biochemistry and biophysics.

Leaf area index (LAI) was estimated first using two newly developed vegetation indices based on 1st derivative of canopy reflectance. The original estimations (based just on PRO-FRT modelling) were found to be significantly underestimated. This was most probably due to use of

DHPs as the source of reference LAI values as this technique provides in fact values of PAI rather than LAI. Moreover, there was no exact information on foliage clumping which had to be estimated. As so, the original values were further transformed using an empirical correction. However, estimation of LAI was considered as not very successful as the observed differences between reference and estimated values had random character, although there were similar number of under- and overestimated values. LAI estimation was thus finally not included into the developed forest health classification model due to these reasons.

Absolute estimation of chlorophyll content was performed in the next phase. Performance of 10 chlorophyll-sensitive vegetation indices was assessed first resulting in selection of the N_{718} index as the most appropriate chlorophyll indicator. In contrast with LAI, accuracy of the chlorophyll content estimation was considered as good as RMSE of the estimation was relatively low and the relationship of the estimated and reference values relatively well followed the 1:1 line. However, it was concluded that great attention should be paid to the validation protocol in terms of handling with the foliage samples corresponding to different age classes and crown positions. Influence of each age class/crown position on the overall spectral signature of the given crown should be defined as there could be significant differences between the particular sample levels in this point of view. This issue can then affect the results of validation procedure.

Chlorophyll content data layer was produced in a relative version as well, together with layers describing spatial patterns of the other biochemical parameters ($C_x/(C_{ab}+C_x)$ and C_w). Since no fixed absolute levels of these parameters are defined for distinguishing damaged and healthy forest stands, there is no reason for absolute quantitative estimations of these parameters for analysing spatial patterns of forest conditions. Only relative estimations were thus used for the developed health classification model. This means that the functional relationships between the selected vegetation indices and the considered vegetation parameters were first defined using radiative transfer modelling. The original values of these indices were then transformed to relative scores linearly corresponding with the given biochemical parameters. This is considered as a crucial step as majority of the vegetation indices are correlated with vegetation biochemistry and biophysics in non-linear way. Forest health classification and the following interpretation of the results would be thus much complicated in case of using the original values of such indices in comparison with considering linear relationships.

The selected indices were then calculated form the source HyMap imagery followed by the application of the same transformation as defined by the radiative transfer modelling simulations. Classification of the actual forest health status was then based on statistical basis. Statistical distributions of the scores values (related to forest biochemistry) were analysed first. Relative distance from the most common values was then calculated for each pixel classified as “Norway spruce forest”. Break values defining the particular forest health classes were then defined taking into account variability of the source values. This classification was performed separately for each vegetation parameter of interest which were then merged into one general classification. Health status of any given forest stand was then assessed by asymmetries in relative frequencies of the particular forest health classes.

Classification performed in the described way showed differences between the reference Norway spruce stands. Two of them (Studenec and Habartov) were then considered as having

good or average-to-good health status, whereas two others (Mezihorská and Erika) showed health status assessed as worse or average-to-worse. These results corresponded well with the outcomes of laboratory analyses of the collected needle samples (e.g. highest chlorophyll content level at Studenec and lowest at Mezihorská, higher level of carotenoids-to-foliar pigments ratio at Erika etc.) with exception of water content which did not agree the original assumptions (in contrast with the two other parameters). The same results (in terms of relative comparison of the four reference localities) were obtained in both years 2009 and 2010. This indicate that a) no significant changes in forest health status occurred between 2009 and 2010 and b) the performance of the described model is consistent in time.

Influence of other factors (such as stand age, terrain orientation or elevation) was also assessed. Elevation and stand age were found as the factors having some influence on the results of the developed forest health classification model. However, only these two factor cannot explain the observed differences between the reference stands – i.e. the observed differences are caused by real variability in vegetation status, although there might be some minor influence of the differences in elevation (e.g. Studenec and Mezihorská vs. Erika and Habartov) or tree age (81 – 100 at Mezihorská vs. 41 – 60 at other localities).

The observed differences in forest health status were then linked to the differences in soil substrate characteristics. Differentiation of the four reference stands by the health status classified by the developed model was found remarkably well corresponding with the differences in soil substrate characteristics related to soil acidity which was found higher at Erika and Mezihorská sites compared to Studenec and Habartov stands. On the other hand, relationship to the content of heavy metals in soil was found to be not clear.

The developed and demonstrated forest health classification approach has all the properties defined at the beginning of this thesis. It is semi-empirical as it includes application of radiative transfer modelling to describe functional relationships between forest biochemistry/biophysics and its spectral properties where parameterization of the used radiative transfer models was performed on empirical basis using the collected ground in-situ data. It is semi-quantitative as it is based on quantitative variables describing forest conditions instead of using qualitative categorical values. The used quantitative indicators are used only for relative comparison of the different localities within the given area and description of spatial patterns of the selected vegetation variables instead of any analysis in absolute level. The developed classification approach proved its ability to provide temporally stable and consistent results corresponding with the collected ground truth data and detect differences in forest health status related to character of soil substrate. Therefore it is possible to conclude that despite partial problems all the goals defined at the beginning of this thesis were achieved, although there are still issues which might be the focus of a further research (e.g. finding the most optimal way of simulation of optical properties of needle-leaved vegetation, further development in the methods of reference data acquisition including measurement of needle spectra as well as description of forest stand structure characteristics, weightening of the influence of different needle age classes on the spectral signature of the whole tree crown etc.).

Reference

Chapter 1:

ALLEN, W.A., GAUSMAN, H.W., RICHARDSON A.J. (1970): Mean effective optical contents of cotton leaves, *Journal of Optical society of America*, 60, 542-547.

ARDÖ J. (1998): Remote sensing of forest decline in the Czech Republic, Doctoral thesis, Lund University, Department of Physical Geography, Sweden, 47 p.

ASNER G.P. (1998): Biophysical and biochemical sources of variability in canopy reflectance, *Remote Sensing of Environment*, 64(3), 234-253, DOI: 10.1016/S0034-4257(98)00014-5.

BOLSTAD, P.V., GOWER, S.T. (1990): Estimation of leaf area index in fourteen southern Wisconsin forest stands using a portable radiometer, *Tree Physiology*, 7(1-4), 115-124.

BONAN G.B. (2008): Forest and climate change: forcing, feedbacks and their climate benefits of forests, *Science*, 320, 1444-1449.

BRÉDA, N.J.J. (2003): Ground-based measurements of leaf area index: A review of methods, instruments and current controversies, *Journal of Experimental Botany*, 54(392), 2403-2417, DOI: 10.1093/jxb/erg263.

BROCKHAUS, J.A., KHORRAM, S. (1992): A Comparison of SPOT and Landsat-TM data for use in conducting inventories of forest resources, *International Journal of Remote Sensing*, 13(16), 3035-3043.

BROGE, N.H., LEBLANC, E. (2001): Comparing prediction power and stability of broadband and hyperspectral vegetation indices for estimation of green leaf area index and canopy chlorophyll density, *Remote Sensing of Environment*, 76(2), 156-172, DOI: 10.1016/S0034-4257(00)00197-8.

BUTERA, M.K. (1986): A Correlation and regression analysis of percent canopy closure versus TMs spectral response for selected forest sites in the San Juan National Forest, *IEEE Transactions on Geoscience and Remote Sensing*, 24(1), 122-129, DOI: 10.1109/TGRS.1986.289693

CALDWELL, M.M., HELMAIER, G., LANGE, O.L., MOONEY, H.A., SCHULTZE, E.D., SOMMER, U. (1997): Forest decline and ozone: a comparison of controlled chamber and field experiments, Berlin, Springer Verlag.

CAMPBELL, P.K.E., ROCK, B.N., MARTIN, M.E., NEEFUS, C.D., IRONS, J.R., MIDDLETON, E.M., ALBRECHTOVÁ, J. (2004): Detection of initial damage in Norway spruce canopies using hyperspectral airborne data, *International Journal of Remote Sensing*, 25(24), 5557-5583, DOI: 10.1080/01431160410001726058.

CHADWICK, M.J., HUTTON, M. (1991): Acid depositions in Europe, Oxford, Stockholm Environmental Institute.

CHEN, J.M., BLACK, T.A., ADAMS, R.S. (1991): Evaluation of hemispherical photography for determining plant-area index and geometry of a forest stand, *Agricultural and Forest Meteorology*, 56(1-2), 129-143, DOI: 10.1019/0168-1923(91)90108-3.

CHEN, J.M., BLACK, T.A. (1992): Defining leaf area index for non-flat leaves, *Plant Cell and Environment*, 15(4), 421-429, DOI: 10.1111/j.1365-3040.1992.tb00992.x.

CHEN, J.M., RICH, P.M., GOWER, S.T., NORMAN, J.M., PLUMMER, S. (1997): Leaf area index of boreal forests: Theory, techniques and measurements, *Journal of Geophysical Research-Atmospheres*, 102(D24), 29429-29443, DOI: 10.1029/97JD01107.

CHENG, Y.B., ZARCO-TEJADA, P.J., RIANO, D., RUEDA, C.A., USTIN, S.L. (2006): Estimating vegetation water content with hyperspectral data for different canopy scenarios: Relationship between AVIRIS and MODIS indexes, *Remote Sensing of Environment*, 105(4), 354-366, DOI: 10.1016/j.rse.2006.07.005.

CHIANUCCI F., CUTTINI, A. (2013): Estimation of canopy properties in deciduous forest with digital hemispherical and cover photography, *Agricultural and Forest Meteorology*, 168, 130-139, DOI: 10.1016/j.agrformet.2012.09.002.

CLEVERS, J.G.P.W., KOOISTRA, L., SCHAEPMAN, M.E. (2010): Estimating canopy water content using hyperspectral remote sensing data, *International Journal of Applied Earth Observation and Geoinformation*, 12(2), 119-125, 10.1016/j.jag.2010.01.007.

COULSON, R.N., STEPHEN, F.M. (2008): Impacts of insects in forest landscapes: Implications for forest health management, In: Paine, T.D. (Ed.) Invasive Forest Insects, Introduced Trees and Altered Ecosystems, Springer, 101-125, ISBN 978-1-4020-9290-9.

DARVISHZADEH, R., SKIDMORE, A., SCHLERF, M., ATZBERGER, C., CORSI, F., CHO, M. (2008): LAI and chlorophyll estimation for a heterogeneous grassland using hyperspectral measurements, *ISPRS Journal of Photogrammetry and Remote Sensing*, 63(4), 409-426, DOI: 10.1016/j.isprsjprs.2008.01.001.

DATT, B. (1998): Remote Sensing of chlorophyll-a, chlorophyll-b, chlorophyll-a+b and total carotenoid content in Eucalyptus leaves, *Remote Sensing of Environment*, 66(2), 111-121, 10.1016/S0034-4257(98)00046-7.

DAWSON, T.P., CURRAN, P.J., PLUMMER, S.E. (1998): LIBERTY – Modelling the effects of leaf biochemical concentration on reflectance spectra, *Remote Sensing of Environment*, 65(1), 50-60, DOI: 10.1016/S0034-4257(98)00007-8.

DEMAREZ, V., DUTHOIT, S., BARET, F., WEISS, M., DEDIEU, G. (2008): Estimation of leaf area and clumping indexes of crops with hemispherical photographs, *Agricultural and Forest Meteorology*, 148(4), 644-655, DOI: 10.1016/j.agrformet.2007.11.015.

D'URSO, G., DINI, L., VUOLO, F., ALONSO, L., GUANTER, L. (2004): Retrival of leaf area index by inverting hyperspectral multiangular CHRIS/PROBA data from SPARC 2003, *Proceedings of the 2nd CHRIS/PROBA Workshop*, ESA/ESRIN, Frascati, Italy, 28-30th April 2004, 6 pp.

GANAPOL, B.D., JOHNSON, B.D., HAMMER, P.D. (1998): LEAFMOD: A new within-leaf radiative transfer model, *Remote Sensing of Environment*, 63(2), 182-193, DOI: 10.1016/S0034-4257(97)00134-X

GARRIGUES, S., SHABANOV, N.V., SWANSON, K., MORISETTE, J.T., BARET, F., MYNENI, R.B. (2008): Intercomparison and sensitivity analysis of leaf area index retrievals from LAI-2000, AccuPAR and digital hemispherical photography over croplands, *Agricultural and Forest Meteorology*, 148(8-9), 1193-1209, DOI: 10.1016/j.agrformet.2008.02.014.

GASTELLU-ETCHEGORRY, J.P., MARTIM, E., GASCON, F. (2004): DART: A 3D model for simulating satellite images and studying surface radiation budget, *International Journal of Remote Sensing*, 25(1), 73-96, DOI: 10.1080/0143116031000115166.

GATES, D.M., KEEGAN, H.J., SCHLETER, J.C., WEIDNER, V.R., (1965): Spectral properties of plants, *Applied Optics*, 4, 11 – 20.

GAUSMAN H.W., ALLEN, W.A. (1973): Optical parameters of leaves of 30 plant species, *Plant Physiology*, 52, 57-62.

GITELSON, A.A., CHIVKUNOVA, O.B., MERZLYAK, M.N. (2002): Assessing carotenoid content in plant leaves with reflectance spectroscopy*, Photochemistry and Photobiology*, 75(3), 272-281, DOI: 10.1562/0031-8655(2002)075

GOEL, N.S., THOMPSON, R.L. (2000): A snapshot of canopy reflectance models and a universal model for the radiation regime, *Remote Sensing Reviews*, 18(2-4), 197-225, DOI: 10.1080/02757250009532390.

GONG, P., RUILIANG, P., BIGING, G.S., LARRIEU, M.R. (2003): Estimation of forest leaf area index using vegetation indices derived from Hyperion hyperspectral data*, IEEE Transactions on Geoscience and Remote Sensing*, 41(6), 1355-1362, DOI: 10.1109/TGRS.2003.812910.

GONSAMO A., PELIKKA, P. (2009): The computation of foliage clumping index using hemispherical photography, *Agricultural and Forest Meteorology*, 149(10), 1781-1787, DOI: 10.1016/j.agrformet.2009.06.001.

GOVAERTS, Y.M., JACQUEMOUD, S., VERSTRAETE, M.M., USTIN, S.L. (1996): Three-dimensional radiative transfer modelling in a dicotyledon leaf, *Applied Optics*, 35, 6585-6598, DOI: 0003-6935/96/06585-14$10.00/0.

GOWER, S.T., KUCHARIK, C.J., NORMAN, J.M. (1999): Direct and indirect estimation of leaf area index, fAPAR and net primary production of terrestrial ecosystems, *Remote Sensing of Environment*, 70(1), 29-51, DOI: 10.1016/S0034-4257(99)00056-5.

GUEVARA-ESCOBAR, A., TELLEZ, J., GONZALES-SOSA, E. (2005): Use of digital photography for analysis of canopy closure, *Agroforestry Systems*, 65(3), 175-185, DOI: 10.1007/s10457-005-0504-y.

GUYOT, G., GUYON, D., RIOM, J. (1989): Factors affecting the spectral responses of forest canopies: a review, *Geocarto International*, 4(3), 3-18, DOI: 10.1080/10106048909354217

HABOUDANE, D., MILLER, J.R., PATTEY, E., ZARCO-TEJADA, P.J., STRACHAN, I.B. (2004): Hyperspectral vegetation indices and novel algorithms for predicting green LAI of crop canopies: Modelling and validation in the context of precision agriculture, *Remote Sensing of Environment*, 90(3), 337-352, DOI: 10.1016/j.rse.2003.12.013.

HERNÁNDEZ-CLEMENTE, R., NAVARRO-CERRILLO, R.M., ZARCO-TEJADA, P.J. (2013): Carotenoid content estimation in a heterogeneous conifer forest using narrow-band indices and PROSPECT+DART simulations, Remote Sensing of Environment, 127, 298-315, DOI: 10.1016/j.rse.2012.09.014.

HOQUE, E., HUTZLER, P.J.S., SIEDLITZ, H.K. (1988): Relationship between discoloration and histological changes in leaves of trees affected by forest decline, *Remote Sensing of Environment*, 26(2), 171-184.

HUANG, Z., TURNER, B.J., DURY, S.J., WALLIS, I.R., FOLEY, W.J. (2004): Estimating foliar nitrogen concentration from HyMap data using continuum removal analysis, *Remote Sensing of Environment*, 93(1-2), 18-29, DOI: 10.1016/j.rse.2004.06.008.

HUBER, S., KNEUBUHLER, M., PSOMAS, A., ITTEN, K., ZIMMERMANN, N.E. (2008): Estimating foliar biochemistry from hyperspectral data in mixed forest canopy, *Forest Ecology and Management*, 256(3), 491-501, DOI: 10.1016/f.foreco.2008.05.011.

HUEMMRICH, K.F. (2001): The GeoSail model: a simple addition to the SAIL model to describe discontinuous canopy reflectance, *Remote Sensing of Environment*, 75(3), 423-431, DOI: 10.1016/S0034-4257(00)00184-X.

HÜTTL, R.F., SCHAAF, W. (1997): Magnesium deficiency in forest ecosystems, Dordrecht, Kluwer Academic Publishers.

JACKSON, R.B., RANDERSON, J.T., CANADELL, J.G., ANDERSON R.G., AVISSAR, R., BALDOCCHI, D.D., BONAN, G.B., CALDEIRA, K., DIFFENBAUGH, N.S., FIELD, C.B., HUNGATE, B.A., JOBBÁGY, E.G., KUEPPERS, L.M., NOSETTO, M.D., PATAKI, D.E. (2008): Protecting climate with forests, *Environmental Research Letters*, 3 (4), 5 pp.

JACQUEMOUD, S., BARET, F. (1990): PROSPECT – A model of leaf optical properties spectra, *Remote Sensing of Environment*, 34(2), 75-91, DOI: 10.1016/0034-4257(90)90100-Z

JENNINGS, S.B., BROWN, N.D., SHEIL, D. (1999): Assessing forest canopies and understorey illumination: canopy closure, canopy cover and other measures, *Forestry*, 71(1), 59-73, DOI: 10.1093/forestry/72.1.59.

JONCKHEERE, I., FLECK, S., NACKAERTS, K., MUYS, B., COPPIN, P., WEISS, M., BARET, F. (2004): Review of methods for in-situ leaf area index determination – part I.: Theories, sensors and hemispherical photography, *Agricultural and Forest Meteorology*, 121(1-2), 19-35, DOI: 10.1016/j.agrformet.2003.08.027.

JONES, H.G., VAUGHAN, R.A. (2010): Remote Sensing of Vegetation: Principles, Techniques and Applications, New York, Oxford University Press, 2010, ISBN: 978-0-19-920779-4

KLEMAN, J. (1986): The Spectral reflectance of stands of Norway spruce and Scotch pine measured from a helicopter, *Remote Sensing of Environment*, 20(3), 253-265, DOI: 10.1016/0034-4257(86)90046-5

KOCH, B., AMMER, U., SCHNEIDER, T., WITTMEIER, H. (1990): Spectroradiometer measurements in the laboratory and in the field to analyse the influence of different damage symptoms on the reflection spectra of forest trees, *International Journal of Remote Sensing*, 11(7), 1145-1163.

KOKALY, R.F., CLARK, R.N. (1999): Spectroscopic determination of leaf biochemistry using band-depth analysis of absorption features and stepwise multiple linear regression, *Remote Sensing of Environment*, 67(3), 267-287, DOI: 10.1016/S0034-4257(98)00084-4.

KOKALY, R.F., ASNER, G.P., OLLINGER, S.V., MARTIN, M.E., WESSMAN, C.A. (2009): Characterizing canopy biochemistry from imaging spectroscopy and its application to ecosystem studies, *Remote Sensing of Environment*, 113, S78-S91, DOI: 10.1016/j.rse.2008.10.018

KOLB, T.E., WAGNER, M.R., COVINGTON, W.W. (1994): Forest health from different perspectives, *Proceedings of the 1995 national silvaculture workshop*, 5-13.

KORHONEN, L., KORHONEN, K.T., RAUTIAINEN, M., STENBERG, P. (2006): Estimation of forest canopy cover: A comparison of field measurement techniques, *Silva Fennica*, 40(4), 577-588.

KUUSK, A., NILSON, T. (2000): A directional multispectral forest reflectance model, *Remote Sensing of Environment*, 72(2), 244-252, DOI: 10.1016/S0034-4257(99)00111-X.

LANG, A.R.G., MVCMURTRIE, R.E., BENSON, M.L. (1991): Validity of surface-area indexes of Pinus radiate estimated from transmittance of the suns beam, *Agricultural and Forest Meteorology*, 57(1-3), 157-170, DOI: 10.1016/0168-1923(91)90084-4.

LARSEN, J.B. (1995): Ecological stability of forests and sustainable silviculture, Forest Ecology and Management, 73(1 - 3), 85 – 96, DOI: 10.1016/0378-1127(94)03501-M.

LEOPOLD, A. (1949): A Sand County Almanac and Sketches Here and There, Oxford University Press, New Your, USA, 240 pp., ISBN 0-19-500777-8.

LICHTENTHALER, H. (1988): In vivo chlorophyll fluorescence as a tool for stress detection in plants In: Lichtenthaler, H. (Eds): Applications of chlorophyll fluorescence, Kluwer Academic Publishers, 1988, 129-142.

LU, X., HU, Z., GUO, L. (2009): Quantitative inverse modelling of nitrogen content from Hyperion data under stress of exhausted coal mining sites, *Mining Science and Technology*, 19, 31-35.

MAIER, S.W., LUDEKER, W., GUNTER, K.P. (1999): SLOP: A revised version of the stochastic model for leaf optical properties, *Remote Sensing of Environment*, 68(3), 273-280, DOI: 10.1016/S0034-4257(98)00118-7.

MALENOVSKÝ, Z., BARTHOLOMEUS, H.M., ACERBI-JUNIOR, F.W., SCHOPFER, J.T., PAINTER, T.H., EPEMA, G.F., BREGT, A.K. (2007): Scaling dimensions in spectroscopy of soil and vegetation, *International Journal of Applied Earth Observation and Geoinformation*, 9(2), 137-164, DOI: 10.1016/j.jag.2006.08.003

MALENOVSKÝ, Z., HOMOLOVÁ, L., ZURITA-MILLA, R., LUKEŠ, P., KAPLAN, V., HANUŠ, J., GASTELLU-ETCHEGORRY, J.P., SCHAEPMAN, M.E. (2013): Retrival of spruce leaf chlorophyll content from airborne image data using continuum removal and radiative transfer, *Remote Sensing of Environment*, 131, 85-102, DOI: 10.1016/j.rse.2012.12.015.

MANION, P.D. (1991): Tree disease concept, 2nd Edition, New Jersey, Prantice Hall Career and Technology, ISBN 0-12-929423-6.

MONNIG, E., BYLER, J. (1992): Forest health and ecological integrity in the Northern Rockies, U.S. Department of Agriculture, Forest Service, Northern Region, 16 pp.

MOORTHY, I., MILLER, J.R., NOLAND, T.L. (2008): Estimating chlorophyll concentration in conifer needles with hyperspectral data: An assessment at the needle and canopy level. *Remote Sensing of Environment*, 112(6), 2824-2838, DOI: 10.1016/j.rse.2008.01.013.

MOSSOR-PIETRASZEWSKA, T. (2001): Effect of aluminium on plant growth and metabolism, *Acta Biologica Polonica*, 48(3), 673-686.

NAGAI, S., INOUE, T., OHTSUKA, T., KOBAYASHI, H., KURUMADO, K., MURAOKA, H., NASAHARA, K.N. (2014): Relationship between spatio-temporal characteristics of leaf fall phenology and seasonal variations in near surface- and satellite observed vegetation indices in a cool-temperate deciduous broad-leaved forest in Japan, *International Journal of Remote Sensing*, 35(10), 3520-3536, DOI: 10.1080/01434161.2014.907937

NEUMANN, H.H., DENHARTOG, G., SHAW, R.H. (1989): Leaf area measurements based on hemispheric photographs and leaf litter collection in a deciduous forest during autumn leaf fall, *Agricultural and Forest Meteorology*, 45(3-4), 325-345, DOI: 10.1016/0168-1923(089)90052-X.

NORTH, P. (1996): Three-dimensional forest light interaction model using a Monte-Carlo method, *IEEE Transactions on Geoscience and Remote Sensing*, 34(4), 946-956, DOI: 10.1109/36.508411.

O'LAUGHLIN, J., LIVINGSTONE, R., THEIR, R., THORNTON, J., TOWEIL, D.E., MORLAN, L. (1994): Defining and measuring forest health, *Journal of Sustainable Forestry*, 2 (1-2), 65-85.

PALETTO, A., TOSSI, V. (2009): Forest canopy cover and canopy closure: comparison of assessment techniques, *European Journal of Forest Research*, 128(3), 265-272, DOI: 10.1007/s10342-009-0262-x.

PFANZ, H., BEYCHLAG, W. (1993): Photosynthetic performance and nutrient status of Norway spruce (Picea abies L. Karst.) at forest sites in Ore Mountains (Erzgebirge), *Trees*, 7, 115-122.

POSO, S., PAANEN, R., SIMILÄ, M. (1997): Forest inventory by compartments using satellite imagery, Silva Fennica, 13, 3035-3043.

RAUTIAINEN, M., STENBERG, P., NILSON, T., KUUSK, A. (2004): The Effect of crown shape on the reflectance of coniferous stands, *Remote Sensing of Environment*, 89(1), 41-52, DOI: 10.1016/j.rse.2003.10.001.

RICH, P.M. (1990): Characterizing plant canopies with hemispherical photographs, *Remote Sensing Reviews*, 5(1), 13-29, DOI: 10.1080/02757259009532119.

ROCK, B.N., HOSHIZAKI, T., MILLER, J.R. (1988): Comparison of in-situ and airborne spectral measurements of the blue shift associated with forest decline, *Remote Sensing of Environment*, 24(1), 109-127, DOI: 10.1016/0034-4257(88)90008-9

ROCK, B.N., ARDÖ, J. (1993): The use of satellite remote sensing to monitor forest decline in the United States and Europe, Proceedings of International Conference on Opticas Within Life Sciences: Optics for Protection of Man and Environment against natural and technological disasters, Elsevier Science Publishers, 49-58.

SCHLERF, M., ATZBERGER, C., HILL, J. (2005): Remote sensing of forest biophysical variables using HyMap imaging spectrometer data, *Remote Sensing of Environment*, 95(2), DOI: 10.1016/j.rse.2004.12.016.

SCHLERF, M., ATZBERGER, C., HILL, J., BUDENBAUM, H., WERNER, W., SCHÜLER, G. (2010): Retrieval of chlorophyll and nitrogen in Norway spruce (Picea abiel L. Karst) using imaging spectroscopy, *International Journal of Applied Earth Observation and Geoinformation*, 12(1), 17-26, DOI: 10.1016/j.jag.2009.08.006.

SEIDEL, D., FLECK, S., LEUSCHNER, C. (2012): Analyzing forest canopies with ground-based laser scanning: A comparison with hemispherical photography, *Agricultural and Forest Meteorology*, 154, 1-8, DOI: 10.1016/j.agrformet.2011.10.006.

SIMS, D.A., GAMON, J.A. (2002): Relationships between leaf pigment content and spectral reflectance across a wide range of species, leaf structures and developmental stages, *Remote Sensing of Environment*, 81(2-3), 337-354, DOI: 10.1016/S0034-4257(02)00010-X.

SLOVIK, S., SIEGMUND A., KINDERMANN, G., REIBLING, R., BALÁZ, Á. (1995): Stomatal SO_2 uptake and sulphate accumulation in needles of Norway spruce stands (Picea abies) in central Europe, *Plant and Soil*, 168-169, 405-419.

SMITH, N.J. (1991): Predicting radiation attenuation in stands of Douglas fir, *Forest Science*, 37(5), 1213-1223.

SOLBERG, S. (1999): Forest health monitoring: Evaluation of methods, trends and causes based on a Norwegian nationwide set of monitoring plots, Norwegian Forest Research Institute, Oslo, Norway, ISBN 82-7169-897-4.

SPANNER, M.A., PIERCE, L.L., PETERSON, D.L., RUNNING, S.W. (1990): Remote sensing of temperate coniferous forest leaf area index: the influence of canopy closure, understory vegetation and background reflectance, *International Journal of Remote Sensing*, 11(1), 95-111.

The Manual on methods and criteria for harmozized sampling, assessment, monitoring and analysis of the effects of air pollution on forests (ICP Manual), International Co-operative Programme on Assessment and Monitoring of Air Pollution Effects on Forests, [on-line]: http://icp-forests.net/page/icp-forests-manual (cit. 23.4. 2017)

THOMAS, J.R., NAMKEN, L.M., OERTHER, G.F., BROWN, R.G. (1971): Estimating leaf water content by reflectance, *Agronomy Journal*, 63(6), 845

TUOMINEN, J., LIPPING, T., KUOSMANEN, V., HAAPANEN, R. (2009): Remote Sensing of Forest Health, In: PEI-GEE, P.H. (Ed.), *Geoscience and Remote Sensing*, InTech, 26 pp., ISBN 978-953-307-003-2.

ULRICH B. (1991): Introducing to acidic deposition effects – critical deposition rates and emission densities, In: Acid Depositions in Europe, Chadwick, M.J. and Hutton, M. (Eds.), Stockholm Environmental Institute, Oxford, pp. 1-15.

VAN GARDINGEN, P.R., JACKSON, G.E., HERNANDEZ-DAUMAS, S., RUSSELL, G., SHARP, L. (1999): Leaf area index estimates obtained from clumped canopies using hemispherical photography, *Agricultural and Forest Meteorology*, 94(3-4), 243-257, DOI: 10.1016/S0168-1923(99)00018-0.

VERRELST, J., ALONSO, L., CAMPS-VALLS, DELEGIDO, J., MORENO, J. (2012): Retrieval of vegetation biophysical parameters using Gaussian process techniques, *IEEE Transactions on Geoscience and Remote sensing*, 50(5), 1832-1843, DOI: 10.1109/TGRS.2011.2168962.

WALKER D.J., KENKEL, N.C., 2000: The adaptive geometry of boreal conifers, *Community Ecology*, 1, 13-23.

WANG, Q., ADIKU, S., TENHUNEN, J., GRANIER, A. (2005): On the relationship of NDVI with leaf area index in deciduous forest site, *Remote Sensing of Environment*, 94(2), 244-255. DOI: 10.1015/j.rse.2004.10.006

WATSON, D.J. (1947): Comparative physiological studies on the growth of field crops: I. Variation in net assimilation rate and leaf area between species and varieties and within and between years, *Annals of Botany*, 11(41), 41-76.

WARING, R.H., RUNNING, S.W., (2010): Forest Ecosystems: Analysis at Multiple Scales (3rd edition), Elsevier Academic Press, San Diego, California, USA, 440 p., ISBN 978-0-12-370605-8.

WELLES, J.M., NORMAN, J.M. (1991): Instrument for indirect measurement of canopy architecture, *Agronomy Journal*, 83(5), 818-825.

WELLES, J.M., COHEN, S. (1996): Canopy structure measurement by gap fraction analysis using commercial instrumentation, *Journal of Experimental Botany*, 47(302), 1335-1342, DOI: 10.1093/jxb/47.9.1335.

WOOLEY, J.T. (1971): Reflectance and transmittance of light by leaves, *Plant Physiology*, 47, 556-662.

WULFF, S., (2011): Monitoring Forest Damage: Methods and Development in Sweden, Doctoral Thesis, Swedish University of Agricultural Sciences, Umea, 2011, 66 pp., ISBN 978-91-576-7641-2.

ZARCO-TEJADA, P.J., MILLER, J.R., HARRON, J., HU, B.X., NOLAND, T.L., GOEL, N., MOHAMMED, G.H., SAMPSON, P. (2004): Needle chlorophyll content estimation through model inversion using hyperspectral data from boreal conifer forest canopies, *Remote Sensing of Environment*, 89(2), 189-199, DOI: 10.1016/j.rse.2002.06.002.

ZHAO, F., YANG, X.F., SCHULL, M.A., ROMAN-COLON, M.O., YAO, T., WANG, Z.S., ZHAN, Q.L., JUPP, D.L.B., LOWELL, J.L., CULVENOR, D.S., NEWNHAM, G.J., RICHARDSON, A.D., NI-MEINSTER, W., SCHAAF, C.L., WOODCOCK, C.E., STRAHLER, A.H. (2011): Measuring effective leaf area index, foliage profile and stand height in New England forest stands using full-waveform ground-based lidar, *Remote Sensing of Environment*, 115(11), 2954-2964, DOI: 10.1016/j.rse.2010.08.030.

ZHANG, Y.Q., CHEN, J.M., MILLER, J.R. (2005): Determining hemispherical photograph exposure for leaf area index estimation, *Agricultural and Forest Meteorology*, 133(1-4), 166-181, DOI: 10.1016/j.agrformet.2005.09.009.

ZHANG, Y.Q., CHEN, J.M., MILLER, J.R., NOLAND, T.L. (2008): Leaf chlorophyll content retrieval from airborne hyperspectral remote sensing imagery, *Remote Sensing of Environment*, 112(7), 3234-3247, DOI: 10.1016/j.rse.2008.04.005.

Zpráva o stavu lesa a lesního hospodářství České republiky v roce 2012, Ministerstvo zemědělství České republiky, Praha, 2013, 134 pp., ISBN 978-80-7434-112-0.

Chapter 2:

BOUŠKA, V., PEŠEK, J. (1999): Quality parameters of lignite in the North Bohemian Basin in the Czech Republic in comparison with the world average lignite, *International Journal of Coal Geology*, 40(2-3), 211-235, DOI: 10.1016/s0166-5162(98)00070-6

Česká geologická služba (ČGS), Geologická mapa 1: 200 000

Český hydrometeorologický ústrav (ČHMÚ), Znečištění ovzduší a atmosférická depozice v datech, Česká republika, tabelární ročenky, [on-line]:

http://portal.chmi.cz/files/portal/docs/uoco/isko/tab_roc/tab_roc_CZ.html (23.1. 2016)

Český úřad zeměměřičský a katastrální (ČUZK), Základní mapa České republiky 1: 200 000, Mapová služba WMS – ZM200, [on-line]:

http://geoportal.cuzk.cz/WMS_ZM200_PUB/WMService.aspx (23.1. 2016)

Česká zemědělská univerzita (ČZU), Soil map of the Czech Republic according to WRB 2006 classification, Mapová služba WMS, [on-line]:

http://geoportal.gov.cz/arcgis/services/CENIA/cenia_typy_pud (23.1. 2016)

LHOTÁKOVÁ Z., BRODSKÝ, L., KUPKOVÁ, L., KOPAČKOVÁ, V., POTŮČKOVÁ, M., MIŠUREC, J., KLEMENT, A., KOVÁŘOVÁ, M., ALBRECHTOVÁ, J. (2013): Detection of multiple stresses in Scots pine growing at post-mining sites using visible to near-infrared spectroscopy, *Environmental Science Processes and Impacts*, 15(11), 2004-2015, DOI: 10.1039/c3em00388d.

QUITT, E. (1971): Klimatické oblasti Československa, Praha, Academia, 1971, 73 s.

ROJÍK, P. (2003): New stratigraphy subdivision of the Tertiary in the Sokolov Basin in Northwestern Bohemia, *Journal of the Czech Geological Society*, 49(3), 173-186.

YUDOVICH, Y.E., KETRIS, M.P. (2005): Arsenic in coal: a review, *International Journal of Coal Geology*, 61(3-4), 141-196, DOI: 10.1016/j.coal.2004.09.003

Chapter 3:

COCKS, T., JENSSEN, R., STEWARD, A., WILSON, I., SHIELDS, T. (1998): The HyMap hyperspectral sensor: the system, calibration and performance, *Proceedings of 1st EARSeL Workshop on Imaging Spectroscopy*, Zürich, Switzerland, 7 p.

GONSAMO, A., PELIKKA, P. (2008): Methodology comparison for slope correction in canopy leaf area index estimation using hemispherical photography, *Forest Ecology and Management*, 256(4), 749-759, DOI: 10.1016/j.foreco.2008.05.032.

HOMOLOVÁ, L., LUKEŠ, P., MALENOVSKÝ, Z., LHOTÁKOVÁ, Z., KAPLAN, V., HANUŠ, J. (2013): Measurement methods and variability assessment of the Norway spruce total leaf area: implications for remote sensing, *Trees – Structure and Function*, 27(1), 111-121, DOI: 10.1007/s00468-012-0774-8.

KOPAČKOVÁ, V., LHOTÁKOVÁ, Z., OULEHLE, F., ALBRECHTOVÁ, J. (2014a): Assessing forest health via linking the geochemical properties of a soil profile with biochemical parameters of vegetation, *International Journal of Science Technology*, 1-16, DOI: 10.1007/s13762-014-0602-3.

KOPAČKOVÁ, V., MIŠUREC, J., LHOTÁKOVÁ, Z., OULEHLE, F., ALBRECHTOVÁ, J. (2014b): Using multi-date high spectral resolution data to assess the physiological status of macroscopically undamaged foliage on a regional scale, *International Journal of Applied Earth Observation and Geoinformation*, 27, 169-186, DOI: 10.1016/j.jag.2013.09.009.

MAJASALMI, T., RAUTIAINEN, M., STENBERG, P., RITA, H. (2012): Optimizing the sampling scheme for LAI-2000 measurements in a boreal forest, *Agricultural and Forest Meteorology*, 154, 38-43, DOI: 10.1016/j.agrformet.2011.10.002.

MIŠUREC, J. (2014): Influence of atmospheric and topographic correction on the accuracy of canopy chlorophyll content estimation of Norway spruce stands, Rigorózní práce, Univerzita Karlova v Praze, Přírodovědecká fakulta, Katedra aplikované geoinformatiky a kartografie, 108 p.

PALMROTH, S., HARI, P. (2001): Evaluation of the importance of acclimation of needle structure, photosynthesis and the respiration to available photosynthetically active radiation in Scots pine canopy, *Canadian Journal of Forest Research*, 31(7), 1235-1243, DOI: 10.1139/x01-051.

PORRA, R.J., THOMPSON, W.A., KRIEDEMAN, P.E. (1989): Determination of accurate extinction coefficients and simultaneous equations for assaying chlorophyll-a and chlorophyll-b extracted with 4 different solvents – verification of the concentration of chlorophyll standards by atomic-absorption spectroscopy, *Biochimica at biophysica Acta*, 975(3), 384-394, DOI: 10.1016/S0005-2728(89)80347-0.

SCHAAF, C.B., GAO, F., STRAHLER, A.H., LUCHT, W., LI, X., TSANG, T., STRUGNELL, N.C., ZHANG, X.,JIN, Y., MULLER, J.-P., LEWIS, P., BARNSLEY, M., HOBSON, P., DISNE, M., ROBERTS, G., DUNDERDALE, M., DOLL, C., D'ENTREMONT, R.P., HU, B., LIANG, S., PRIVETTE, J.L., ROY, D. (2002): First operational BRDF, albedo nadir reflectance products from MODIS, *Remote Sensing of Environment*, 83(1-2), 135-148, DOI: 10.1016/S0034-4257(02)00091-3.

SCHAEPMAN-STRUB, G., SCHAEPMAN, M.E., PAINTER, T.H., DANGEL, S., MARTONCHIK, J.V. (2006): Reflectance quantities in optical remote sensing – definitions ad case studies, Remote Sensing of Environment, 103(1), 27-42, DOI: 10.1016/j.rse.2006.03.002.

WEIDE, S. (2009): HyEUROPE 2009 Summary report, DLR, Wessling, Germany, 15 p.

WEIDE, S. (2010): HyEUROPE 2010 Summary report, DLR, WEssling, Germany, 14 p.

WELLBURN, A.R. (1994): The spectral determination of chlorophyll-a and chlorophyll-b, as well as total catotenoids, using various solvents with spectrometers of different resolution, *Journal of Plant Physiology*, 144(3), 307-313.

Chapter 4:

ALLEN, W.A., GUSSMAN, H.W., RICHARDSON, A.J., THOMAS, J.R. (1969): Interaction of isotropic light with compact leaf, *Journal of Optical Society America*, 59(10), 1376-1379, 10.1364/JOSA.59.001376.

DAWSON, T.P., CURRAN, P.J., PLUMMER, S.E. (1998): LIBETY – Modelling the effects of biochemical concentration on reflectance spectra, Remote Sensing of Environment, 65(1), 50-60, DOI: 10.1016/S0034-4257(98)00007-8.

FERET, J.B., FRANCOIS, C., ASNER, G.P., GITELSON, A.A., MARTIN, R.E., BIDEL, L.P.R., USTIN, S.L., LE MAIRE, G., JACQUEMOUD, S. (2008): PROSPECT-4 and 5: Advances in the leaf optical properties model separating photosynthetic pigments, *Remote Sensing of Environment*, 112(6), 3030-3043, DOI: 10.1016/j.rse.2008.02.012.

HERNANDÉZ-CLEMENTE, R., NAVARRO-CERRILLO, R.M., ZARCO-TEJADA, P.J. (2012): Carotenoid content estimation in a heterogeneous coniferous forest using narrow-band indices and PROSPECT + DART simulations, *Remote Sensing of Environment*, 127, 298-315, DOI: 10.1016/j.rse.2012.09.014.

JACQUEMOUD, S., BARET, F. (1990): PROSPECT – A model of leaf optical properties spectra, *Remote Sensing of Environment*, 34(2), 75 – 91, DOI: 10.1016/0034-4257(90)90100-Z.

MALENOVSKÝ,Z., ALBRECHTOVÁ, J., LHOTÁKOVÁ, Z., ZURITA-MILLA, R., CLEVERS, J.G.P.W., SCHAEPMAN, M.E., CUDLÍN, P. (2006): Applicability of the PROSPECT model for Norway spruce needles, *International Journal of Remote Sensing*, 27(23-24), 5313-5340, DOI: 10.1080/01431160600762990.

MOORTHY, I., MILLER, J.R., NOLAND, T.L. (2008): Estimating chlorophyll concentration in conifer needles with hyperspectral data: An assessment at the needle level and canopy level. *Remote Sensing of Environment*, 112(6), 2824-2838, DOI: 10.1016/j.rse.2008.01.013.

RAUTIAINEN, M., STENBERG, P., NILSON, T., KUUSK, A. (2004): The effect of crown shape on the reflectance on coniferous stands. *Remote Sensing of Environment*, 89(1), 41-52, DOI: 10.1016/j.rse.2003.10.001.

WILLMOTT, C.J. (1981): On the validation of models, Physical Geography, 2, 184 – 194.

ZARCO-TEJADA, P.J., MILLER, J.R., MOHAMMED, G.H., NOLAND, T.L., SAMPSON, P.H. (1999): Canopy optical indices from infinite reflectance and canopy reflectance models for forest condition monitoring: Application to hyperspectral CASI data, Proceedings of the IEEE 1999

International Geoscience and Remote Sensing Symposium, IGARSS 99, Hamburg, Germany, 28.6.-2.7. 1999, 4 pp.

ZARCO-TEJADA, P., MILLER, J.R., HARRON, J., HU, B., NOLAND, T.L., GOEL, N., MOHAMMED, G.H., SAMPSON, P. (2004): Needle chlorophyll content estimation through model inversion using hyperspectral data from boreal conifer canopies, *Remote Sensing of Environment*, 89(2), 189-199, DOI: 10.1016/j.rse.2002.06.002.

ZHANG, Y., CHEN, J.M., MILLER, J.R., NOLAND, T.L. (2008): Leaf chlorophyll content retrieval from airborne hyperspectral remote sensing imagery, *Remote Sensing of Environment*, 112(7), 3243-3247, DOI: 10.1016/j.rse.2008.04.005.

Chapter 5:

DE CARVALHO, O.A., MENESES, P.R. (2000): Spectral Correlation Mapper (SCM): An improvement of the Spectral Angle Mapper (SAM), Summaries of the 9th JPL Airborne Earth Science Workshop, JPL Publication 00-18, Pasadena, CA, 9 pp.

FISHER, R.A., THORNTON, H.G., MACKENZIE, W.A. (1922): The accuracy of the planting method of estimating the density of bacterial populations with particular reference to the use of Thornton's agar medium with soil samples, *Annals of Applied Botany*, 9, 325-359.

KUUSK, A., NILSON, T. (2000): A directional multispectral reflectance model, *Remote Sensing of Environment*, 72(2), 244-252, DOI: 10.1016/S0034-4257(99)00111-X.

NILSON, T. (1999): Inversion of gap frequency data in forest stands, *Agricultural and Forest Meteorology*, 98-99, 437-448, DOI: 10.1016/S0168-1923(99)00114-8.

PUKKALA, T. (1988): Effect of spatial distribution of trees on the volume increment of a young Scots pine stand, *Silva Fennica*, 22(1), 1-17.

WIDLOWSKI, J.L., VERSTRAETE, M., PINTY, B., GOBRON, N. (2003): Allometric relationships of selected European tree species, European Commission Joint Research Centre, Ispra (VA), Italy, 74 pp.

Chapter 6:

ASNER G.P. (1998): Biophysical and biochemical sources of variability in canopy reflectance, *Remote Sensing of Environment*, 64(3), 234-253, DOI: 10.1016/S0034-4257(98)00014-5.

CAMPBELL, P.K.E., ROCK, B.N., MARTIN, M.E., NEEFUS, C.D., IRONS, J.R., MIDDLETON, E.M., ALBRECHTOVÁ, J. (2004): Detection of initial damage in Norway spruce canopies using hyperspectral airborne data, *International Journal of Remote Sensing*, 25(24), 5557-5583, DOI: 10.1080/01431160410001726058.

CECCATO, P., FLASSE, S., TARANTOLA, S., JACQUEMOUD, S., GRÉGOIRE, J.M. (2001): Detecting vegetation leaf water content using reflectance in the optical domain, *Remote Sensing of Environment*, 77, 22 – 33, DOI: 10.1016/S0034-4257(01)00191-2.

CHEN, D., HUANG, J., JACKSON, T.J. (2005): Vegetation water content estimation for corn and soybeans using spectral indices derived from MODIS near- and short-wave infrared bands, *Remote Sensing of Environment*, 98, 225 – 236, DOI: 10.1016/j.rse.2005.07.008.

DATT, B. (1999): A new reflectance index for remote sensing of chlorophyll content in higher plants: tests using Eucalyptus leaves, *Journal of Plant Physiology*, 154, 30 – 36, DOI: 10.1016/S0176-1617(99)80314-9.

GAO, B. (1996): Normalized difference water index for remote sensing of vegetation liquid water from space, *Remote Sensing of Environment*, 58(3), 257 – 266, DOI: 10.1016/S0034-4257(96)00067-3.

HABOUDANE, D., MILLER, J.R., TREMBLEY, N., ZARCO-TEJADA, P.J., DEXTRAZE, L. (2002): Integrated narrow-band vegetation indices for prediction of crop chlorophyll content for application to precision agriculture, *Remote Sensing of Environment*, 81, 416 – 426, DOI: 10.1016/S0034-4257(02)00018-4.

HUNT Jr., E., ROCK, B. (1989): Detection of changes in leaf water content using near- and middle-infrared reflectances, *Remote Sensing of Environment*, 30, 43 – 54, DOI: 10.1016/0034-4257(89)90046-1.

JACKSON, T.J., CHEN, D., COSH, M., LI, F., ANDERSON, M., WALTHALL, C., DORIASWAMY, P., HUNT, E.R. (2004): Vegetation water content mapping using Landsat data derived normalized difference water index for corn and soybeans, *Remote Sensing of Environment*, 92(4), 475 – 482, DOI: 10.1016/j.rse.2003.10.021.

KOKALY, R.F., ASNER, G.P., OLLINGER, S.V., MARTIN, M.E., WESSMAN, C.A. (2009): Characterizing canopy biochemistry from imaging spectroscopy and its application to ecosystem studies, *Remote Sensing of Environment*, 113, S78 – S 91, DOI: 10.1016/j.rse.2008.10.018.

KOPAČKOVÁ, V., MIŠUREC, J., LHOTÁKOVÁ, Z., OULEHLE, F., ALBRECHTOVÁ, J. (2014): Using multi-date high spectral resolution data to assess the physiological status of macroscopically undamaged foliage on a regional scale, *International Journal of Applied Earth Observation and Geoinformation*, 27, 169 – 186, DOI: 10.1016/j.jag.2013/09.009.

MALENOVSKÝ, Z., UFER, C., LHOTÁKOVÁ, Z., CLEVERS, J.G.P.W., SCHAEPMAN, M.E., ALBRECHTOVÁ, J., CUDLÍN, P. (2006): A new hyperspectral index for chlorophyll estimation of a forest canopy: Area under curve normalized to maximal band depth between 650 – 725 nm, *EARSeL eProceedings*, 5, 2/2006, 161 – 172, DOI: 10.5167/uzh-62112.

MIŠUREC, J., KOPAČKOVÁ, V., LHOTÁKOVÁ, Z., HANUŠ, J., WEYERMANN, J., ENTCHEVA-CAMPBELL, P., ALBRECHTOVÁ, J. (2012): Utilization of hyperspectral image optical indices to assess the Norway spruce forest health status, *Journal of Applied Remote Sensing*, 6, 25 pp., DOI: 10.117/1.JRS.6.063545.

MIŠUREC, J., (2014): Influence of atmospheric and topographic correction on the accuracy of canopy chlorophyll content estimation of Norway spruce stands, *Rigorous thesis*, Charles University in Prague, Faculty of Sciences, Department of Applied Geoinformatics and Cartography, 108 pp.

PEÑUELAS, J., FILELLA, I., BIEL, C., SERRANO, L., SAVÉ, R. (1993): The reflectance at the 950 – 970 nm region as an indicator of plant water status, *International Journal of Remote Sensing*, 14(10), 1887 – 1905, DOI: 10.1080/01431169308954010.

SIMS, D., GAMON, J. (2002): Relationship between leaf pigment content and spectral reflectance across a wide range of species, leaf structures and development stages, *Remote Sensing of Environment*, 81, 337 – 354, DOI: 10.1016/S0034-4257(02)00010-X.

VOGELMANN, J., ROCK, B., MOSS, D. (1993): Red edge spectral measurements from Sugar maple leaves, *International Journal of Remote Sensing*, 14, 1563 – 1575, DOI: 10.1080/01431169308953986.

WANG, L., QU, J. (2007): NMDI: A normalized multi-band drought index for monitoring soil and vegetation moisture with satellite remote sensing, *Geophysical Research Letters*, 34, L20405, DOI: 10.1029/2007GL031021.

ZARCO-TEJADA, P.J., USTIN, S.L. (2001): Modeling canopy water content for carbon estimates from MODIS data and land EOS validation sites, *International Geoscience and Remote Sensing Symposium 2001*, IGARSS 01, 342 – 344.

Chapter 7:

DE VOS, B., COOLS, N. (2011): Second European Forest Soil Condition Report, Volume I: Results of the BioSoil Survey, INBO.R.2011.35, Research Institute for Nature and Forest, Brussel, Belgium, 369 pp., ISSN 1782-9054.

FABIÁNEK, P. (2004): Forest Condition Monitoring in the Czech Republic 1984 – 2003, Ministry of Agriculture of the Czech Republic and Forest and Game Management Research Institute, Elan spol. s.r.o., 2004, 436 pp., ISBN 80-86461-23-8

ICP Forests Manual, Part XII: Sampling and analysis of needle and leaves, International co-operative programme on assessment and monitoring of air pollution effects on forests, [on-line]: https://www.icp-forests.org/pdf/manual/2010/Manual_2010_Foliage.pdf (cit. 23.4. 2017)

RIEUWERTS, J.S., THORNTON, I., FARAGO, M.E., ASHMORE, M.R. (1998): Factors influencing metal bioavailability in soils: preliminare investigations for the development of a critical loads approach for metals, Chemical Specification and Bioavailability, 10(2), 61 – 75, DOI: 10.3184/095422998782775835.

ROTTER, P., ŠRÁMEK, V., VÁCHA, R., BORŮVKA, L., FADRHONSOVÁ, V., SÁŇKA, M., DRÁBEK, O., VORTELOVÁ, L. (2013): Rizikové prvky v lesních půdách: Review, Zprávy lesnického výzkumu, 58, 17 – 27.

WILLMOTT, C.J. (1981): On the validation of models, Physical Geography, 2, 184 – 194.

Chapter 8:

ATZBERGER, C., WERNER, W. (1998): Needle reflectance of healthy and diseased Spruce stands, 1st EARSeL Workshop on Imaging Spectroscopy, Remote Sensing Laboratories, University of Zurich, Impression Dumas, Saint-Etiene, France, 271 – 283.

DEMMING-ADAMS, B., ADAMS, W.W. (1996): The role of xanthophyll cycle carotenoids in the protection of photosynthesis, *Trends in Plant Science*, 1(1), 21 – 26, DOI: 10.1016/S1360-1385(96)80019-7.

KIVIMÄENPÄAÄ, M., SUTINEN, S. (2007): Microscopic structure of Scots pine (Pinus sylvestris (L.)) needles during ageing and autumnal senescence, *Trees – Structure and Function*, 21(6), 646 – 659, DOI: 10.1007/s00468-007-0157-8.¨

KOPAČKOVÁ, V., MIŠUREC, J., LHOTÁKOVÁ, Z., OULEHLE, F., ALBRECHTOVÁ, J. (2014): Using multi-date high spectral resolution data to assess the physiological status of macroscopically

undamaged foliage on a regional scale, *International Journal of Applied Earth Observation and Geoinformation*, 27, 169 – 186, DOI: 10.1016/j.jag.2013/09.009.

LHOTÁKOVÁ, Z., ALBRECHTOVÁ, J., JANÁČEK, J., KUBÍNOVÁ, L. (2008): Advantages and pitfalls of using free-hand sections of frozen needles for three-dimensional analysis of mesophyll by stereology and confocal microscopy, *Journal of Microscopy*, 232(1), 56 – 63, DOI: 10.1111/j.1365-2818.2008.02079.x.

LUKEŠ, P., RAUTIAINEN, M., STENBERG, P., MALENOVSKÝ, Z. (2011): Empirical test of the spectral invariants theory using imaging spectroscopy data from a coniferous forest, *International Journal of Applied Earth Observation and Geoinformation*, 13, 668 – 675, DOI: 10.1016/j.jag.2011.004.003.

MALENOVSKÝ, Z., HOMOLOVÁ, L., ZURITA-MILLA, R., LUKEŠ, P., KAPLAN, V., HANUŠ, J., GASTELLU-ETCHEGORRY, J.P., SCHAEPMAN, M.E. (2013): Retrieval of spruce leaf chlorophyll content from airborne image data using continuum removal and radiative transfer, *Remote Sensing of Environment*, 131, 85 – 102, DOI: 10.1016./j.rse.2012.12.015.

MIŠUREC, J., KOPAČKOVÁ, V., LHOTÁKOVÁ, Z., HANUŠ, J., WEYERMANN, J., ENTCHEVA-CAMPBELL, P., ALBRECHTOVÁ, J. (2012): Utilization of hyperspectral image optical indices to assess the Norway spruce forest health status, *Journal of Applied Remote Sensing*, 6, 25 pp., DOI: 10.117/1.JRS.6.063545.

MIŠUREC, J., (2014): Influence of atmospheric and topographic correction on the accuracy of canopy chlorophyll content estimation of Norway spruce stands, *Rigorous thesis*, Charles University in Prague, Faculty of Sciences, Department of Applied Geoinformatics and Cartography, 108 pp.

MOORTHY, I., MILLER, J.R., NOLAND, T.L. (2008): Estimating chlorophyll concentration in conifer needles with hyperspectral data: An assessment at the needle and canopy level, Remote Sensing of Environment, 112, 2824 – 2838, DOI: 10.1016/j.rse.2008.01.013.

SCHLERF, M., ATZBERGER, C., HILL, J., BUDDENBAUM, H., WERNER, W., SCHÜLER, G. (2010): Retrieval of chlorophyll and nitrogen in Norway spruce (Picea abies L. Karst.) using imaging spectroscopy, *International Journal of Applied Earth Observation and Geoinformation*, 12, 17 – 26, DOI: 10.1016/j.jag.2009.08.006.

SLATON, M.R., HUNT, E.R., SMITH, W.K. (2001): Estimating near-infrared leaf reflectance from leaf structural characteristics, *American Journal of Botany*, 88(2), 278 – 284, DOI: 10.2307/2657019.

SIEFERMANNHARMS, D. (1994): Light and temperate control of season-dependent changes in alpha-carotene and beta-carotene content of spruce needles*, Journal of Plant Physiology*, 143(4 – 5), 488 – 494.

YAÑEZ-RAUSELL, L., MALENOVSKÝ, Z., CLEVERS, J., SCHAEPMAN, M.E. (2010): Performance of PROSPECT leaf radiative transfer model version 4 for Norway spruce needles, *Proceedings of the hyperspectral 2010 Workshop*, Frascati, Italy, 17-19th March 2010, 4.

YOUNG, A., BRITTON, G. (1990): Carotenoids and stress, in Alscher R.G. and Cummings, J.R. Eds., Stress Responses in Plant: Adaptation and Aclimatization Mechanisms, Willey-Liss, New York, United States of America, 87 – 112.

ZARCO-TEJADA, P.J., MILLER, J.R., HARRON, J., HU, B., NOLAND, T.L., GOEL, N., MOHAMMED, G.H., SAMPSON, P. (2004): Needle chlorophyll content estimation through model inversion using hyperspectral data from boreal conifer canopies*, Remote Sensing of Environment*, 89, 189 – 199, DOI: 10.1016/j.rse.2002.06.002.

Curriculum Vitae

Personal details:

Name: Jan Mišurec

Date and Place of Birth: 23.8. 1985 Prague, Czech Republic

Contact e-mail: jmis@volny.cz

Eduaction:

2005 – 2008	Charles University in Prague, Faculty of Science, Geography and Cartography, Thesis: Utilization of the data from NOAA polar orbiting satellites (BSc.)
2008 – 2010	Charles University in Prague, Faculty of Science, Geography and Cartography, Thesis: Retrieval of chlorphyll content from hyperspectral image data (MSc.)
2014	Charles University in Prague, Faculty of Science, Geography and Cartography, Thesis: Influence of atmodpheric and topographic correction on the accuracy of canopy chlorophyll content estimation of Norway spruce stands (Dr. Rer. Nat.)
since 2010	Charles University in Prague, Faculty of Science, Geography and Cartography, Thesis: Application of imaging spectroscopy in monitoring of vegetation stress caused by soil pollutants in the Sokolov lignite basin (Ph.D. studium)

Employment:

2010 – 2015	Czech Geological Survey, Department of Remote Sensing
since 2016	Gisat s.r.o., Department of Remote Sensing

Courses and Certificates:

2010	TerraSync 4.10 (Geotronics Praha s.r.o.)
2011	Retrieval of ecosystem variables from the remotely sensed hyperspectral data (Hyper-I-Net)
2011	Introducing to geoprocessing scripts using Python (Arcdata Praha s.r.o./ESRI)
2012	Building geodatabases (Arcdata Praha s.r.o./ESRI)
2012	Geostatistics and open-source statistical computing (ITC, Faculty of Geoinformation and Earth Observation, University of Twente, The Netherlands)
2012	First Certificate in English (FCE)

Projects participation:

GA ČR 205/09/1989: HypSo – Assessment of mining related impacts based on utilization of airborne hyperspectral sensor (team member)

EC FP7 244242: EO-MINERS – Earth observation for monitoring and observing environmental and social impacts of mineral resources exploration and exploitation (team member)

MŠMT LH12097: INMON – Innovation of the methods for monitoring health status of Norway spruce stands in the Ore Mountains using hyperspectral data (team member)

EC FP7 262371: PanGeo – A GMES-Copernicus service enabling access to geological information (team member)

CzDA-RO-ET-2012-1-74010: Capacity building in the field of environmental geology: mapping georisks including hydrogeological condition in Dila and Hosaina areas, Ethiopia (team member)

10051606-SFŽP: Re-assessment of the ground water reserves in the Czech Republic (team member)

4000115816/15/NL/US: DROMAS-2 – Agricultural drought monitoring and assessment driven by satellites (technical leader)

ETC-ULS task 1.8.1.2: Development of a new EEA indicator on phenology (project leader)

TA ČR TH0203048: Use of Copernicus satellite data for effective monitoring of a status and managements of the selected agricultural crops (project leader)

List of publications

Impac factor publications

Mišurec, J., Kopačková, V., Lhotáková, Z., Hanuš, J., Weyermann, J., Entcheva-Campbell, P., Albrechtova, J. 2012. Utilization of hyperspectral image optical indices to assess the Norway spruce forest health status. Journal of Applied Remote Sensing 6: 25 pp. DOI: 10.1117/1.JRS.6.063545

Lhotáková, Z., Brodský, L., Kupková, L., Kopačková, V., Potůčková, M., **Mišurec, J.**, Klement, A., Kovářová, M., Albrechtová J. 2013. Detection of multiple stresses in Scotch pine growing at post-mining sites using visible to near-infrared spectroscopy. Environmental Science Processes and Impacts 15 (11): 2004-2015. DOI: 10.1039/c3em00388d

Kopačková V., **Mišurec, J.**, Lhotáková, Z., Oulehle, F., Albrechtová, J. 2014. Using multi-date high spectral resolution data to assess the physiological status of macroscopically undamaged foliage on a regional scale. International Journal of Applied Earth Observation and Geoinformation 27: 169-186. DOI: 10.1016/j.jag.2013.09.009

Mišurec, J., Kopačková, V., Lhotáková, Z., Campbell, P., Albrechtová, J. 2016. Detection of spatio-temporal changes of Norway spruce forest stands in Ore Mountains using Landsat time series and airborne hyperspectral imagery. Remote sensing, 8(2), 20 pp., DOI: 10.3390/rs8020092.

Peer-reviewed and non-reviewed proceedings

Adar, S., Notesco, G., Brook, A., Livine, I., Rojík, P., Kopačková, V., Zelenková, K., **Mišurec, J.**, Bourgignon, A., Chevrel, S., Ehler, C. Fisher, C., Hanuš, J., Shkolninsky, Y., Ben-Dor, E. 2011. Change detection over Sokolov open-pit mining area, Czech Republic, using multi-temporal HyMap data (2009-2010). Proceedings of SPIE, vol. 8180, 11/2011, 9 pp. DOI: 10.1117/12.898748

Červená L., Lhotáková, Z., Kopačková, V., Kupková, L., **Mišurec, J.**, Potůčková, M., Cudlín, P., Entcheva-Campbell, P., Albrechtová, J. 2014. Temporal changes in Norway spruce physiological status using hyperspectral data: A case study of mountainous forests affected by long-term acidic depositions. EARSeL eProceedings, vol. 13 (S1): 71-75. DOI: 10.12760/02-2014-1-13

Mišurec, J., Kopačková, V., Lhotáková, Z., Campbell, P., Albrechtová, J. 2015. Detection of spatio-temporal changes of Norway spruce forest stands in Ore Mountains using Landsat time series and airborne hyperspectral imagery. Proceedings of the 1st International Electronic Conference on Remote Sensing, 22.6. – 5.7. 2015, 13 pp., DOI: 10.3390/ecrs-1-d006.

Mišurec, J., Kopačková, V., Lhotáková, Z., Albrechtová, J., Hanuš, J. 2011. An estimation of biochemical and geochemical variables in Norway spruce forest stands from hyperspectral image data. Proceedings of 7th Workshop of EARSeL SIG Imaging spectroscopy, 11.-13.4. 2011, Edinburgh, United Kingdom, 8 pp.

Chevrel, S., Kopačková, V., Fischer, C., Ben-Dor, E., Adar, S., Shkolninsky, Y., **Mišurec, J.** 2012. Mapping minerals, vegetation health and change detection over the Sokolov lignite mine using multidate hyperspectral airborne imagery, Proceedings of 1st EAGE/GRSG remote sensing workgroup "Mapping the morphology, chemistry and mineralogy of the ground surface", 3.-5.9. 2012, Paris, France, 5 pp.

Conference presentations

Mišurec, J., Lhotáková, Z., Kopačková, V., Bartáková, D., Albrechtová, J. 2010. Využití optických indexů odvozených z hyperspektrálního senzoru HyMap pro monitoring zdravotního stavu smrkových lesních porostů na Sokolovsku. 19. konference GIS ESRI v ČR, 3.-4.11. 2010, Prague, Czech Republic (poster presentation)

Mišurec, J., Kopačková, V., Lhotáková, Z., Albrechtová, J., Hanuš, J., 2011. An estimation of biochemical and geochemical variables in Norway spruce forest stands from hyperspectral image data. 7th Workshop of EARSeL SIG Imaging spectroscopy, 11.-13.4. 2011, Edinburgh, United Kingdom (poster presentation)

Mišurec, J., Kopačková, V., Lhotáková, Z., Albrechtová, J., Hanuš, J., 2011. A comparison of different approaches to empirical modelling for retrieval of leaf pigments content of Norway spruce canopies from HyMap airborne hypespectral image data. 1st EARSeL SIG Forestry workshop: Operational remote sensing in forest management, 2.-3.6. 2011, Prague, Czech Republic (poster presentation)

Mišurec, J. 2011. Klasifikace zdravotního stavu smrkových porostů Sokolovské pánve metodami obrazové spektroskopie, 20. konference GIS ESRI v ČR, 9.-10.11. 2011, Prague, Czech Republic (oral presentation)

Hanuš, J., **Mišurec, J.**, Fabiánek, T. 2013. Using FODIS atmospheric correction for chlorophyll content estimation, 8th Workshop of SIG Imaging spectroscopy, 8.-10.4. 2013, Nantes, France (co-author of oral presentation)

Mišurec, J., Kopačková, V., Jelének, J., Koucká, L. 2013. EO-MINERS: Aplikace metod pozorování Země při hodnocení dopadů povrchové těžby. 22. konference GIS ESRI v ČR, 13.-14.11. 2013, Prague, Czech Republic (poster presentation)